FAST ALGORITHMS FOR SAMPLED MULTIBAND SIGNALS

A Thesis
Presented to
The Academic Faculty

By

Santhosh Karnik

In Partial Fulfillment
of the Requirements for the Degree
Doctor of Philosophy in the
School of Electrical and Computer Engineering

Georgia Institute of Technology

August 2021

FAST ALGORITHMS FOR SAMPLED MULTIBAND SIGNALS

Approved by:

Dr. Mark Davenport, Advisor
School of Electrical and Computer Engineering
Georgia Institute of Technology

Dr. Justin Romberg
School of Electrical and Computer Engineering
Georgia Institute of Technology

Dr. James McClellan
School of Electrical and Computer Engineering
Georgia Institute of Technology

Dr. Christopher Heil
School of Mathematics
Georgia Institute of Technology

Dr. Michael Lacey
School of Mathematics
Georgia Institute of Technology

Date Approved: July 27, 2021

ACKNOWLEDGEMENTS

First, I would like to thank Mark Davenport, my advisor, for taking me on as a PhD student, giving me a great initial research topic, providing plenty of advice and encouragement, helping me improve my writing skills, obtaining the funding for me to go to conferences, and for giving me career advice. But most of all, I would like to thank him for building a friendly, close-knit research group and for creating an enjoyable, low-stress environment for doing research. My experience as a graduate student has been the complete opposite of the PHD Comics graduate student experience.

Also, I would like to thank Justin Romberg for working very closely with me over the years. He too has helped me out in many of the same ways, and he has treated me just like one of his own students.

In addition to Mark Davenport and Justin Romberg, I would like to thank my other collaborators Mike Wakin, Zhihui Zhu, Rakshith Srinivasa, Coleman DeLude, and Christopher Hood. My research would not be the same without our many research discussions.

I would also like to thank Mark Davenport, Justin Romberg, James McClellan, Christopher Heil, and Michael Lacey for taking the time to serve on my committee. Furthermore, I need to thank Mark Davenport for teaching Statistical Machine Learning, Justin Romberg for teaching Advanced Digital Signal Processing and Convex Optimization, James McClellan for teaching Intro to Signal Processing, Christopher Heil for teaching Real Analysis, and Michael Lacey for teaching Intro to Compressed Sensing. Y'all did a fantastic job teaching those courses, and the knowledge I acquired in each of those courses played a role in helping me complete this thesis.

Thanks to my Davenportmanteau labmates Michael Moore, Andrew Massimino, Liangbei Xu, Matt O'Shaughnessy, Nauman Ahad, Andrew McRae, Namrata Nadagouda, Charles Topliff, Austin Xu, Christopher Hood, and Peimeng Guan, as well as the rest of the Children of the Norm. I am truly grateful to have been a part of this research group.

Thanks to Lee Richert and Charles Topliff for being the two best randomly-assigned roommates I've had during my time at Georgia Tech. I enjoyed having many research and non-research discussions while living with each of you.

Thanks to Alexander Tarr for giving me plenty of advice when I was applying for graduate schools, and thanks to Armenak Petrosyan, Alex Townsend, Mark Iwen, and Rongrong Wang for giving me plenty of advice when I was applying for postdoc positions.

Thanks to all my friends I met at the Georgia Tech Bridge Club. There are too many to list here, but I would like to give a special shout out to Giorgio Casinovi for helping run the club, Patty Tucker for being a fantastic teacher, and Arjun Dhir, Zhuangdi Xu, Charles Wang, Richard Jeng, Cyrus Hettle, Shengding Sun, Bo Han Zhu, and Sean McNally for being awesome teammates and for winning two collegiate bridge championships with me.

Thanks to the uncountably many[1] friends I have made at Club Math over the years. I am especially grateful that y'all still made me feel welcome even while I was the only PhD student in the club.

Thanks to Jack Bross, Harrison Brown, Tom Fulton, Charles Garner, Ben Hedrick, Charles Koppelman, Adam Marcus, Deborah Poss, Steve Sigur, Carol Sikes, and Don Slater for coaching Georgia's high school state math team when I was on it. I would not be as good of a mathematician as I am today without that experience. In addition to most of those names, I would also like to thank Angelique Allen, Sema Duzyol, Miles Edwards, Jonathan Johnson, Bhanu Kumar, Jeff McCammon, Henry Oglesby, Paul Oser, and Brian Stone for coaching Georgia's high school state math team with me since I graduated. I am very grateful for the chance to help the next generation of mathematicians.

Thanks to Dwight Stewart, Robert Kinley, and Matt Rodencal, my closest friends from high school, for keeping in touch over the years.

And finally, thanks to Mr. George, my high school electronics teacher, for inspiring me to study electrical engineering in the first place.

[1] Figuratively speaking of course.

TABLE OF CONTENTS

Acknowledgments iii

List of Tables x

List of Figures xi

Summary xiv

Chapter 1: Introduction 1

Chapter 2: Background 4

2.1 Mathematical Notation 4

2.2 DPSSs, Slepian basis vectors, and PSWFs 5

2.3 Clustering Behavior of the DPSS Eigenvalues and the PSWF Eigenvalues . 12

2.4 Signal Representation with Slepian Basis Vectors 13

2.5 Thomson's Multitaper Method 14

2.6 Structured Linear Algebra 20

2.7 Compressed Sensing 23

Chapter 3: On the Eigenvalues of Discrete Prolate Spheroidal Sequences and Prolate Spheroidal Wave Functions 25

3.1 Prior results on DPSS eigenvalues 25

3.2 Prior results on PSWF eigenvalues 28

3.3 New results on DPSS eigenvalues and PSWF eigenvalues 30

3.4 Numerical Results 34

Chapter 4: Fast Computations with Slepian Basis Vectors 38

4.1 Toeplitz Plus Low Rank Approximations 38

4.2 Fast Computations 42

4.3 Applications 44

4.4 Numerical Experiments 49

Chapter 5: Thomson's Multitaper Method for Spectral Estimation 58

5.1 Statistical Properties and Spectral Leakage 58

5.2 Fast Algorithms 63

5.3 Numerical Experiments 65

Chapter 6: Nonuniform Sampling of Multiband Signals 78

6.1 Problem Formulation 78

6.2 Structured Matrices 81

6.3 Spectral Properties 83

6.4 Conjugate Gradient Descent 85

6.5 Experiments 88

Chapter 7: Compressed Sensing of Multiband Signals 91

7.1 Signal Model 91

7.2 Modulated Slepian Dictionary 92

7.3 Block-based CoSaMP 93

7.4 Fast Block-based CoSaMP for Multiband Signals 94

7.5 Numerical Experiments 96

Chapter 8: Conclusions 97

References 110

Appendix A: Proofs for Chapter 3 112

A.1 Proof of Bounds on the Number of DPSS Eigenvalues in the Transition Region (Theorems 1 and 2) 112

A.1.1 Proof overview 112

A.1.2 Constructing the sequence of matrices $\boldsymbol{X}_L$ 114

A.1.3 Proof of Theorem 1 116

A.1.4 Proof of Theorem 2 119

A.2 Proof of DPSS Eigenvalue Bounds (Corollaries 1 and 2) 126

A.2.1 Lower bounds on λ_k for $k \leq \lfloor 2NW \rfloor - 1$ 126

A.2.2 Upper bounds on λ_k for $k \geq \lceil 2NW \rceil$ 127

A.2.3 Bounds on $\sum_{k=0}^{K-1}(1-\lambda_k)$ for $K \leq \lfloor 2NW \rfloor$ 129

A.2.4 Bounds on $\sum_{k=K}^{N-1}\lambda_k$ for $K \geq \lceil 2NW \rceil$ 130

A.3 Proof of PSWF Eigenvalue Bounds 131

A.3.1 Proof of Theorem 3 131

A.3.2 Proof of PSWF eigenvalue bounds (Corollary 3) 132

A.3.3 Proof of PSWF eigenvalue sum bounds (Corollary 4) 133

Appendix B: Proofs for Chapter 4 134

B.1 Proof of Theorem 4 134

B.1.1 Proof of Theorem 4a 134

B.1.2 Proof of Theorem 4b 136

B.1.3 Proof of Theorem 4c 137

B.2 Proof of Theorem 5 139

Appendix C: Proofs for Chapter 5 149

C.1 Proof of Results in Section 5.1 149

C.1.1 Norms of Gaussian random variables 149

C.1.2 Concentration of norms of Gaussian random variables 151

C.1.3 Intermediate results 153

C.1.4 Proof of Theorem 6 158

C.1.5 Proof of Theorem 7 160

C.1.6 Proof of Theorem 8 161

C.1.7 Proof of Theorem 9 165

C.1.8 Proof of Theorem 10 168

C.2 Proof of Results in Section 5.2 169

C.2.1 Fast algorithm for computing $\Psi(f)$ at grid frequencies 170

C.2.2 Approximations for general multitaper spectral estimates 175

C.2.3 Proof of Theorem 11 177

C.2.4 Proof of Theorem 12 178

Appendix D: Proofs for Chapter 6 180

D.1 Proof of Lemma 1 . . . 180
D.1.1 Matrix concentration results . . . 180
D.1.2 Modulated Prolate Spheroidal Wave Functions . . . 182
D.1.3 Multiband Prolate Spheroidal Wave Functions . . . 183
D.1.4 Bound on 1st eigenvalue of $\mathcal{A}^*\mathcal{A}$ . . . 184
D.1.5 Bound on K_1-th eigenvalue of $\mathcal{A}^*\mathcal{A}$ . . . 186
D.1.6 Bound on K_2-th eigenvalue of $\mathcal{A}^*\mathcal{A}$ . . . 188
D.2 Proof of Lemma 2 . . . 196
D.3 Proof of Theorem 13 . . . 198

Appendix E: Miscellaneous Results . . . 200
E.1 Zolotarev numbers . . . 200
E.2 Singular values of matrices with low rank displacement . . . 202
E.3 Polynomial approximations of the sinc function . . . 204
E.4 Low rank approximation to solutions of Lyapunov equations . . . 206

LIST OF TABLES

4.1 Comparison of the eigenvalues of $\boldsymbol{B}$, $\boldsymbol{S}_K\boldsymbol{S}_K^*$, $\boldsymbol{S}_K\boldsymbol{\Lambda}_K^{-1}\boldsymbol{S}_K^*$, $\frac{1}{1+\alpha}\boldsymbol{B}$, and $(\boldsymbol{B}^2+\alpha\mathbf{I})^{-1}\boldsymbol{B}$ corresponding to the eigenvectors $\boldsymbol{s}_k$ for which $\lambda_k \notin (\epsilon, 1-\epsilon)$. 40

5.1 Table of mean logarithmic deviations (averaged across entire frequency spectrum), precomputation times, and computation times for each of the eight spectral estimation methods. 72

LIST OF FIGURES

2.1 A plot of the DPSS Eigenvalues $\{\lambda_k\}_{k=0}^{N-1}$ for $N = 1000$ and $W = \frac{1}{8}$. These eigenvalues satisfy $\lambda_{243} \approx 0.9997$ and $\lambda_{256} \approx 0.0003$. Only 12 of the 1000 DPSS eigenvalues lie in $(0.001, 0.999)$. 13

2.2 A plot of the magnitudes of the DFT coefficients (left) and the Slepian basis coefficients with $N = 100$ and $W = \frac{1}{10}$ (right) for the signal $\boldsymbol{x}_1[n]$, which is a sum of three sinusoids at grid frequencies. 14

2.3 A plot of the magnitudes of the DFT coefficients (left) and the Slepian basis coefficients with $N = 100$ and $W = \frac{1}{10}$ (right) for the signal $\boldsymbol{x}_2[n]$, which is a sum of three sinusoids at off-grid frequencies. 14

3.1 Plots of the width of the transition region of DPSS eigenvalues $\#\{k : \epsilon < \lambda_k < 1 - \epsilon\}$ vs. N where $W = \frac{1}{4}$ and $\epsilon = 10^{-3}$(blue), $\epsilon = 10^{-8}$(green), and 10^{-13}(red) are fixed. The dashed lines indicate the upper bound from Theorem 1. 34

3.2 Plots of the width of the transition region of DPSS eigenvalues $\#\{k : \epsilon < \lambda_k < 1 - \epsilon\}$ vs. W where $N = 2^{16}$ and $\epsilon = 10^{-3}$(blue), $\epsilon = 10^{-8}$(green), and 10^{-13}(red) are fixed. The dashed lines indicate the upper bound from Theorem 2. 35

3.3 Plots of the width of the transition region of PSWF eigenvalues $\#\{k : \epsilon < \widetilde{\lambda}_k < 1 - \epsilon\}$ vs. c where $\epsilon = 10^{-3}$(blue), $\epsilon = 10^{-8}$(green), and 10^{-13}(red) are fixed. The dashed lines indicate the upper bound from Theorem 3. . . . 37

4.1 *(Left) Plots of the average time needed to project a vector onto the first* $\mathrm{round}(2NW)$ *Slepian basis elements using the exact projection* $\boldsymbol{S}_K\boldsymbol{S}_K^*$ *and using the fast factorization* $\boldsymbol{T}_1\boldsymbol{T}_2^*$*. (Right) Plots of the average time needed to project a vector onto the first* $\mathrm{round}(2NW)$ *Slepian basis elements using the exact projection* $\boldsymbol{S}_K\boldsymbol{S}_K^*$ *and using the fast projection* $\boldsymbol{B} + \boldsymbol{S}_\epsilon\boldsymbol{D}_1\boldsymbol{S}_\epsilon^*$. 52

4.2 *(Left) Plots of the average precomputation time for the exact projection $\boldsymbol{S}_K\boldsymbol{S}_K^*$ and the fast factorization $\boldsymbol{T}_1\boldsymbol{T}_2^*$. (Right) Plots of the average precomputation time for the exact projection $\boldsymbol{S}_K\boldsymbol{S}_K^*$ and the fast projection $\boldsymbol{B} + \boldsymbol{S}_\epsilon\boldsymbol{D}_1\boldsymbol{S}_\epsilon^*$.* 53

4.3 *(Left) A plot of the function used in the experiments described in Section 4.4. (Right) Plots of the function, the Fourier sum approximation to $f(t)$ using 401 terms, and the Fourier extension approximation to $f(t)$ using 401 terms. Note that the Fourier sum approximation suffers from Gibbs phenomenon oscillations while the Fourier extension sum does not.* 54

4.4 *A comparison of the relative RMS error (left) and the computation time required (right) for the $2M + 1$ term truncated Fourier series as well as the $2M + 1$ term Fourier extension using both the exact and fast pseudoinverse methods. Note that the exact and fast methods are virtually indistinguishable in terms of relative RMS error.* 56

4.5 *A comparison of the relative RMS error (left) and the computation time required (right) for the $2M + 1$ term truncated Fourier series as well as the $2M + 1$ term Fourier extension using both the exact and fast Tikhonov regularization methods. Note that the exact and fast methods are virtually indistinguishable in terms of relative RMS error.* 57

5.1 Plots of the spectral windows $\psi(f)$ for $N = 2000$, $W = \frac{1}{100}$, and $K = 39$, 36, 32, and 29 tapers. (Top) A logarithmic scale plot over $f \in [-\frac{1}{2}, \frac{1}{2}]$. (Middle) A logarithmic scale plot over $f \in [-2W, 2W]$. (Bottom) A linear scale plot over $f \in [-2W, 2W]$. 67

5.2 Plots of the true power spectral density, the periodogram, the multitaper spectral estimate with $W = \frac{1}{100}$ and $K = \lfloor 2NW \rfloor - 1 = 39$, and the multitaper spectral estimate with $W = \frac{1}{100}$ and $K = 29$ tapers (chosen so $\lambda_{K-1} \geq 1 - 10^{-9}$). 69

5.3 Plots of the true spectrum (blue) and the spectral estimates (red) using each of the eight methods. 73

5.4 Plots of the empirical mean logarithmic deviation using each of the eight methods. 74

5.5 Plot of the average precomputation time vs. signal length N for the exact multitaper spectral estimate and our fast approximation for $\epsilon = 10^{-4}$, 10^{-8}, and 10^{-12}. 76

5.6 Plot of the average computation time vs. signal length N for the exact multitaper spectral estimate and our fast approximation for $\epsilon = 10^{-4}$, 10^{-8}, and 10^{-12}. 77

6.1 A plot of the eigenvalues of $\boldsymbol{G}$. The largest $2WT = 400$ eigenvalues are all between $\lambda_1(\boldsymbol{G}) \approx 11.43$ and $\lambda_{400}(\boldsymbol{G}) \approx 0.6597$. The smallest 1577 eigenvalues are all between $\lambda_{424}(\boldsymbol{G}) \approx 1.68 \times 10^{-14}$ and 0. Only 24 eigenvalues fail to fit in one of those ranges. 84

6.2 Plot of the time needed for each of the three methods to compute the reconstructed signal on a uniformly spaced grid of M points from the N nonuniformly spaced samples. 89

6.3 Plot of the relative RMS error of the reconstructed signal for each of the three methods. All three methods yield a nearly identical reconstruction error for the values of N for which all of them could be tested. 90

6.4 Plot of the number of CGD iterations needed for the first two methods versus the number of samples N. 90

7.1 Plots of the magnitude of the DTFT of the recovered signal (left) and the difference between the recovered signal and the original signal (right). . . . 96

SUMMARY

The objective of this thesis is to present a variety of fast algorithms for working with samples of multiband signals. Our algorithms revolve around the Slepian basis vectors, which are a set of timelimited signals that are each maximally concentrated in a given frequency band subject to being orthonormal. Due to these time-frequency localization properties, the Slepian basis vectors are useful in a wide variety of applications in signal processing. However, prior to our work, there were no efficient algorithms for performing computations with Slepian basis vectors. As such, practitioners often overlooked the Slepian basis vectors for more computationally efficient tools, such as the fast Fourier transform, even in problems for which the Slepian basis vectors are a more appropriate tool.

The computational complexity and memory requirements for all of the algorithms in this thesis scale roughly linearly with the number of samples to be processed. The key to these fast algorithms is exploiting the mathematical properties of the Slepian basis vectors as well as the related discrete prolate spheroidal sequences (DPSSs) and the prolate spheroidal wave functions (PSWFs). The DPSSs and PSWFs are the eigensequences and eigenfunctions respectively of a bandlimit, then timelimit, then bandlimit procedure. The eigenvalues associated with both the DPSSs and the PSWFs are all strictly between 0 and 1, and most cluster very closely around either 0 or 1. We rigorously quantify the fact that only logarithmically many of these eigenvalues are not close to either 0 or 1, and then exploit this clustering behavior to devise our fast algorithms.

The main contributions of this thesis are:

- novel non-asymptotic bounds on the eigenvalues of the discrete prolate spheroidal sequences and prolate spheroidal wave functions,
- fast algorithms for projecting a vector onto the span of the leading Slepian basis vectors, for performing dimensionality reduction with Slepian basis vectors, and for solving systems of equations involving the prolate matrix

- novel non-asymptotic bounds on the statistical properties of Thomson's multitaper spectral estimate,
- a fast algorithm for evaluating Thomson's multitaper spectral estimate on an uniformly spaced grid of frequencies,
- a fast algorithm for reconstructing a multiband signal from nonuniform samples, provided we know the active frequency bands a priori,
- a fast algorithm for recovering a multiband signal from compressed measurements which does not require knowing the active frequency bands a priori.

CHAPTER 1
INTRODUCTION

Over the past several years, computational power has grown tremendously. This has led to two trends in signal processing. First, problems in signal processing are now being posed and solved using tools from linear algebra, instead of more traditional methods such as filtering and Fourier transforms. Second, problems are dealing with increasingly large amounts of data. Many modern applications involve signals with millions of samples.

Algorithms involving low-order filters or fast Fourier transforms typically require $O(N)$ or $O(N \log N)$ operations for a signal with N samples. In contrast, general linear algebra tasks, such as a multiplying an $N \times N$ matrix by an $N \times 1$ vector, solving an $N \times N$ linear system of equations, and computing the eigendecomposition of an $N \times N$ matrix, require between $O(N^2)$ and $O(N^3)$ operations, which is typically unfeasible for signals with $N \gtrsim 10^5$ samples. Applying tools from linear algebra to large scale problems requires the problem to have some type of low-dimensional structure which can be exploited in order to perform the computations efficiently, i.e. in roughly linear time with respect to the number of samples N.

One common type of low-dimensional structure is a multiband signal model, i.e. the Fourier transform of the signal is supported only on a finite union of finite intervals. This type of structure arises naturally in signal processing problems where many transmitters are each broadcasting a signal confined to a single frequency band and a receiver observes the sum of delayed versions of the transmitted signals. Since the Fourier transform of a multiband signal is sparsely supported, a multiband signal has far fewer degrees of freedom than a signal that is bandlimited to the same maximum frequency. Transferring this low-dimensional structure from the continuous-time signal to the discrete-time samples requires care.

Naïve approaches to exploiting the low-dimensional structure of a multiband signal involve simply using the discrete Fourier transform (DFT), which has the advantage of being computationally efficient due to the fast Fourier transform (FFT), which requires $O(N \log N)$ operations to compute for a signal of length N. Unfortunately, a finite window of samples from a multiband signal rarely has a sparse DFT. Instead the DFT of a window of samples from a multiband signal typically has slowly decaying sidelobes for each active frequency band, which contain a nontrivial amount of energy. As such, the discrete Fourier transform often fails to capture the low-dimensional structure of a multiband signal.

A more suitable method to capture this low-dimensional structure involves using Slepian basis vectors, which are defined as the eigenvectors of the so-called prolate matrix. By construction, the Slepian basis vectors are timelimited signals which are each maximally concentrated in a given frequency band subject to being orthonormal. This construction allows one to capture the low-dimensional structure of a multiband signal with a dimensionality that is only slightly greater than the time-bandwidth product of the signal. However, prior to this research, no fast algorithms for working with the Slepian basis had been developed. Hence, the Slepian basis has been often overlooked in favor of the DFT, even in problems where the Slepian basis is a more appropriate choice.

In this thesis, we first study the mathematical properties of the Slepian basis, as well as the closely related discrete prolate spheroidal sequences (DPSSs) and prolate spheroidal wave functions (PSWFs). We then use these mathematical properties to develop fast algorithms for working with samples of multiband signals. The rest of this thesis is organized as follows. In Chapter 2, we present background material on some of the topics related to this thesis. In Chapter 3, we establish novel non-asymptotic bounds on the eigenvalues of the DPSSs and the PSWFs. In Chapter 4, we present our fast algorithms for projecting a vector onto the span of the leading Slepian basis vectors, for performing dimensionality reduction with Slepian basis vectors, and for solving systems of equations involving the prolate matrix. In Chapter 5, we derive non-asymptotic bounds on the statistical proper-

ties of Thomson's multitaper spectral estimate, and we present a fast algorithm for evaluating Thomson's multitaper spectral estimate at a uniformly spaced grid of frequencies. In Chapter 6, we demonstrate a fast method for reconstructing a multiband signal from nonuniformly spaced samples, provided we know the active frequency bands a priori. In Chapter 7, we demonstrate a fast method for recovering a multiband signal from compressed measurements without knowing the active frequency bands a priori. We conclude this thesis in Chapter 8 with a discussion of possible future directions of research. To improve the readability of this thesis, the proofs of each of the results in this thesis are contained in the Appendices.

CHAPTER 2

BACKGROUND

The background for this thesis draws from the areas of signal processing, spectral estimation, structured linear algebra, and compressed sensing. The goal of this research is to apply techniques from linear algebra to develop fast algorithms for working with samples of bandlimited and/or multiband signals. This survey is by no means exhaustive, but presents a broad sample of the literature which inspired the research.

2.1 Mathematical Notation

We start by reviewing some of the mathematical notation used in this thesis which may not be universally used. We use bold lowercase letters to denote finite-dimensional column vectors, bold uppercase letters to denote finite-dimensional matrices. This distinguishes them from infinite-dimensional objects, such as sequences, functions, and operators on sequence or function spaces. Unless otherwise noted, all vectors and matrices are indexed beginning at 0. For a finite-dimensional vector $\boldsymbol{x}$, we use $\boldsymbol{x}[n]$ to denote the n-th element of $\boldsymbol{x}$, $\boldsymbol{x}^T$ to denote the transpose of $\boldsymbol{x}$, and $\boldsymbol{x}^*$ to denote the conjugate transpose of $\boldsymbol{x}$. For a finite-dimensional matrix $\boldsymbol{A}$, we use $\boldsymbol{A}[m, n]$ to denote the (m, n)-th entry of $\boldsymbol{A}$, $\boldsymbol{A}^T$ to denote the transpose of $\boldsymbol{A}$, and $\boldsymbol{A}^*$ to denote the conjugate transpose of $\boldsymbol{A}$. Note that if $\boldsymbol{x}$ or $\boldsymbol{A}$ have real entries, then $\boldsymbol{A}^T = \boldsymbol{A}^*$ or $\boldsymbol{x}^T = \boldsymbol{x}^*$ respectively. For any positive integer N, we use $[N]$ to denote the set $\{0, 1, \ldots, N-1\}$. For a linear operator between vector spaces $\mathcal{A}$, we use $\mathcal{A}^*$ to denote the adjoint of $\mathcal{A}$. For a Hermitian matrix $\boldsymbol{A} \in \mathbb{C}^{N \times N}$ or a self-adjoint operator $\mathcal{A}$, we will use $\lambda_1(\boldsymbol{A}) \geq \lambda_2(\boldsymbol{A}) \geq \cdots \geq \lambda_N(\boldsymbol{A})$ or $\lambda_1(\mathcal{A}) \geq \lambda_2(\mathcal{A}) \geq \cdots$ to denote the eigenvalues of $\boldsymbol{A}$ or $\mathcal{A}$ sorted in decreasing order. Note that in order to be consistent with standard notation, the eigenvalues associated with the Slepian basis vectors, the discrete prolate spheroidal sequences, and the prolate spheroidal wave functions (which

are introduced in the next section) will be indexed starting from 0 instead of 1.

2.2 DPSSs, Slepian basis vectors, and PSWFs

A fundamental fact of Fourier analysis is that no non-zero signal can be simultaneously bandlimited and timelimited. Thus, a compactly supported non-zero function cannot have a compactly supported Fourier transform, and a non-zero function whose Fourier transform is compactly supported cannot itself be compactly supported. Between 1960 and 1978, Landau, Pollak, and Slepian published a series of seminal papers [1–5] exploring to what extent a bandlimited signal can be timelimited and to what extent a timelimited signal can be bandlimited. They formulate both of these questions as eigenproblems involving bandlimiting and timelimiting operators. In the continuous-time case, the eigenfunctions which are bandlimited to the frequency band $[-\Omega, \Omega]$ and are maximally concentrated in the time interval $[-\frac{T}{2}, \frac{T}{2}]$ are known as the prolate spheroidal wave functions (PSWFs). In the discrete-time case, the eigensequences which are bandlimited to frequencies $[-W, W]$ and are maximally concentrated in the time indices[1] $[N]$ are known as the discrete prolate spheroidal sequences (DPSSs). By truncating the DPSSs, one can form the Slepian basis vectors, which are an efficient basis for representing a window of samples from bandlimited signals [6–8]. As such, Slepian basis vectors can be used in a variety of applications. Some classic applications include prediction of bandlimited signals based on past samples [5] and Thomson's multitaper method for spectral analysis [9]. More recent applications include time-variant channel estimation [10, 11], wideband compressive radio receivers [12], compressed sensing of analog signals [6], target detection [13, 14], and a fast method [15] for computing Fourier extension series coefficients [16, 17]. In the rest of this subsection, we will define DPSSs, Slepian basis vectors, and PSWFs, as well as discuss some of their basic properties.

[1] For any positive integer N, we use the notation $[N] = \{0, 1, \ldots, N-1\}$.

Discrete-time case

For a discrete time signal $x \in \ell_2(\mathbb{Z})$, we define its discrete-time Fourier transform (DTFT) $\widehat{x} \in L_2([-\frac{1}{2}, \frac{1}{2}])$ by

$$\widehat{x}(f) = \sum_{n=-\infty}^{\infty} x[n] e^{-j2\pi fn} \quad \text{for} \quad f \in [-\tfrac{1}{2}, \tfrac{1}{2}],$$

and for any $\widehat{x} \in L_2([-\frac{1}{2}, \frac{1}{2}])$, we define its inverse DTFT by

$$x[n] = \int_{-1/2}^{1/2} \widehat{x}(f) e^{j2\pi fn} \, df \quad \text{for} \quad n \in \mathbb{Z}.$$

With these definitions, any discrete-time signals $x, x' \in \ell_2(\mathbb{Z})$ satisfy the Parseval-Plancherel identity $\langle x, x' \rangle_{\ell_2(\mathbb{Z})} = \langle \widehat{x}, \widehat{x}' \rangle_{L_2([-1/2,1/2])}$. For any $N \in \mathbb{N}$, we say that $x \in \ell_2(\mathbb{Z})$ is time-limited to $[N]$ if $x[n] = 0$ for $n \in \mathbb{Z} \setminus [N]$. Also, for any $W \in (0, \frac{1}{2})$, we say that $x \in \ell_2(\mathbb{Z})$ is bandlimited to $[-W, W]$ if $\widehat{x}(f) = 0$ for $W < |f| \leq \frac{1}{2}$.

We can now ask the question "what discrete-time signal bandlimited to $[-W, W]$ has a maximum concentration of energy over the time indices $[N]$?", i.e.,

$$\underset{x \in \ell_2(\mathbb{Z})}{\text{maximize}} \sum_{n=0}^{N-1} |x[n]|^2 \quad \text{subject to} \quad \|x\|_{\ell_2(\mathbb{Z})}^2 = 1 \quad \text{and} \quad \widehat{x}(f) = 0 \text{ for } W < |f| \leq \tfrac{1}{2}.$$

To help answer this question, we define two self-adjoint operators. For a given $N \in \mathbb{N}$ we define a timelimiting operator $\mathcal{T}_N : \ell_2(\mathbb{Z}) \to \ell_2(\mathbb{Z})$ by

$$(\mathcal{T}_N x)[n] = \begin{cases} x[n] & \text{if } n \in [N] \\ 0 & \text{if } n \in \mathbb{Z} \setminus [N] \end{cases},$$

and for a given bandwidth parameter $W \in (0, \frac{1}{2})$, we define a bandlimiting operator $\mathcal{B}_W$:

$\ell_2(\mathbb{Z}) \to \ell_2(\mathbb{Z})$ by

$$(\mathcal{B}_W x)[n] = \sum_{m=-\infty}^{\infty} \frac{\sin[2\pi W(m-n)]}{\pi(m-n)} x[m] \quad \text{for} \quad n \in \mathbb{Z}.$$

Note that for any $x \in \ell_2(\mathbb{Z})$, we have $\widehat{\mathcal{B}_W x}(f) = \widehat{x}(f)$ for $|f| \leq W$ and $\widehat{\mathcal{B}_W x}(f) = 0$ for $W < |f| \leq \frac{1}{2}$.

For discrete-time signals $x \in \ell_2(\mathbb{Z})$ which are bandlimited to $[-W, W]$, we can write

$$\sum_{n=0}^{N-1} |x[n]|^2 = \langle x, \mathcal{T}_N x \rangle_{\ell_2(\mathbb{Z})} = \langle \mathcal{B}_W x, \mathcal{T}_N \mathcal{B}_W x \rangle_{\ell_2(\mathbb{Z})} = \langle x, \mathcal{B}_W \mathcal{T}_N \mathcal{B}_W x \rangle_{\ell_2(\mathbb{Z})}.$$

Subject to the constraint $\|x\|^2_{\ell_2(\mathbb{Z})} = 1$, this is maximized by the eigensequence of $\mathcal{B}_W \mathcal{T}_N \mathcal{B}_W$ corresponding to the largest eigenvalue. Slepian defined the discrete prolate spheroidal sequences (DPSSs) $s_0, \ldots, s_{N-1} \in \ell_2(\mathbb{Z})$ as the N orthonormal eigensequences of $\mathcal{B}_W \mathcal{T}_N \mathcal{B}_W$ corresponding to non-zero eigenvalues. The corresponding eigenvalues $1 > \lambda_0 > \lambda_1 > \cdots > \lambda_{N-1} > 0$ are referred to as the DPSS eigenvalues and are sorted in descending order. Slepian [5] showed that these eigenvalues are all distinct and strictly between 0 and 1. Note that the notation s_k and λ_k hides the dependence on N and W. When it is necessary to make this dependence explicit, we will use the expanded notation $s_k(N, W)$ and $\lambda_k(N, W)$ respectively.

In addition to s_0 being the discrete-time signal bandlimited to $[-W, W]$ with a maximum concentration of energy in $[N]$, it is also true that for each $k = 1, \ldots, N-1$, s_k is the discrete-time signal bandlimited to $[-W, W]$ with a maximum concentration of energy in $[N]$ subject to the additional constraint of being orthogonal to $s_0, \ldots, s_{k-1}$. Furthermore λ_k is equal to the amount of energy s_k has in the time interval $[N]$.

We can also ask the question "what discrete-time signal timelimited to $[N]$ has a maxi-

mum concentration of energy in the frequency band $[-W, W]$?", i.e.

$$\underset{x \in \ell_2(\mathbb{Z})}{\text{maximize}} \int_{-W}^{W} |\widehat{x}(f)|^2 \, df \quad \text{subject to} \quad \|x\|_{\ell_2(\mathbb{Z})}^2 = 1 \quad \text{and} \quad x[n] = 0 \text{ for } n \in \mathbb{Z} \setminus [N].$$

For discrete-time signals $x \in \ell_2(\mathbb{Z})$ which are timelimited to $[N]$, we can write

$$\begin{aligned} \int_{-W}^{W} |\widehat{x}(f)|^2 \, df &= \left\langle \widehat{x}, \widehat{\mathcal{B}_W x} \right\rangle_{L_2([-1/2,1/2])} = \langle x, \mathcal{B}_W x \rangle_{\ell_2(\mathbb{Z})} \\ &= \langle \mathcal{T}_N x, \mathcal{B}_W \mathcal{T}_N x \rangle_{\ell_2(\mathbb{Z})} = \langle x, \mathcal{T}_N \mathcal{B}_W \mathcal{T}_N x \rangle_{\ell_2(\mathbb{Z})} . \end{aligned}$$

Subject to the constraint $\|x\|_{\ell_2(\mathbb{Z})}^2 = 1$, this is maximized by the eigensequence of $\mathcal{T}_N \mathcal{B}_W \mathcal{T}_N$ corresponding to the largest eigenvalue. Clearly, the range of $\mathcal{T}_N \mathcal{B}_W \mathcal{T}_N$ and the orthogonal complement of the kernel of $\mathcal{T}_N \mathcal{B}_W \mathcal{T}_N$ is the N-dimesional space of discrete-time signals which are timelimited to $[N]$. Hence, we can reduce this eigenproblem on $\ell_2(\mathbb{Z})$ to an eigenproblem on $\mathbb{C}^N$. With respect to the Euclidean basis for the space discrete-time signals which are timelimited to $[N]$, the matrix representation of $\mathcal{T}_N \mathcal{B}_W \mathcal{T}_N$ is given by

$$\boldsymbol{B}[m, n] = \frac{\sin[2\pi W(m-n)]}{\pi(m-n)} \quad \text{for} \quad m, n \in [N]. \tag{2.1}$$

This Toeplitz matrix $\boldsymbol{B} \in \mathbb{R}^{N \times N}$ is known in the literature as the prolate matrix [18, 19]. The Slepian basis vectors $\boldsymbol{s}_0, \ldots, \boldsymbol{s}_{N-1} \in \mathbb{R}^N$ are the orthonormal eigenvectors of $\boldsymbol{B}$, where again the eigenvalues $1 > \lambda_0 > \lambda_1 > \cdots > \lambda_{N-1} > 0$ are sorted in descending order. Note that the eigenvalues of $\boldsymbol{B}$ are the same as the eigenvalues of $\mathcal{T}_N \mathcal{B}_W \mathcal{T}_N$, which are the same as the eigenvalues of $\mathcal{B}_W \mathcal{T}_N \mathcal{B}_W$. Hence, we can reuse the notation λ_k for $k \in [N]$ to denote the eigenvalues of $\boldsymbol{B}$. The eigensequences $s'_0, \ldots, s'_{N-1} \in \ell_2(\mathbb{Z})$ of $\mathcal{T}_N \mathcal{B}_W \mathcal{T}_N$ are then given by $s'_k = \mathcal{T}_N s_k$ for $k \in [N]$, or more explicitly, $s'_k[n] = \boldsymbol{s}_k[n]$ for $n \in [N]$ and $s'_k[n] = 0$ for $n \in \mathbb{Z} \setminus [N]$. Note that in addition to s'_0 being the discrete-time signal that is timelimited to $[N]$ whose DTFT has a maximum concentration of energy in $[-W, W]$, it is also true that for each $k = 1, \ldots, N-1$, s'_k is the discrete-time signal that

is timelimited to $[N]$ whose DTFT has a maximum concentration of energy in $[-W, W]$ subject to the additional constraint of being orthogonal to $s'_0, \ldots, s'_{k-1}$. Furthermore, the eigenvalue λ_k is equal to the amount of energy that the DTFT of s'_k has in the frequency band $[-W, W]$.

Continuous-time case

These concentration problems for discrete-time signals have analogous formulations for continuous-time signals. For a continuous-time signal $y \in L_2(\mathbb{R})$, we define its continuous-time Fourier transform $\widehat{y} \in L_2(\mathbb{R})$ by

$$\widehat{y}(f) = \int_{-\infty}^{\infty} y(t) e^{-j2\pi ft}\, dt \quad \text{for} \quad f \in \mathbb{R}.$$

For any $\widehat{y} \in L_2(\mathbb{R})$, its inverse continuous-time Fourier transform is given by

$$y(t) = \int_{-\infty}^{\infty} \widehat{y}(f) e^{j2\pi ft}\, df \quad \text{for} \quad t \in \mathbb{R}.$$

With these definitions, any continuous-time signals $y, y' \in L_2(\mathbb{R})$ satisfy the Parseval-Plancherel identity $\langle y, y' \rangle_{L_2(\mathbb{R})} = \langle \widehat{y}, \widehat{y}' \rangle_{L_2(\mathbb{R})}$. For any $T > 0$, we say that $y \in L_2(\mathbb{R})$ is timelimited to $[-\frac{T}{2}, \frac{T}{2}]$ if $y(t) = 0$ for $|t| > \frac{T}{2}$. Also, for any $W > 0$, we say that $y \in L_2(\mathbb{R})$ is bandlimited to $[-W, W]$ if $\widehat{y}(f) = 0$ for $|f| > W$.

For a given bandlimit $W > 0$ and duration $T > 0$, we can ask "what continuous-time signal bandlimited to $[-W, W]$ has a maximum concentration of energy in the time interval $[-\frac{T}{2}, \frac{T}{2}]$?", i.e.

$$\underset{y \in L_2(\mathbb{R})}{\text{maximize}} \int_{-T/2}^{T/2} |y(t)|^2\, dt \quad \text{subject to} \quad \|y\|^2_{L_2(\mathbb{R})} = 1 \quad \text{and} \quad \widehat{y}(f) = 0 \text{ for } |f| > W.$$

Just as was done with the discrete-time case, we can define a self-adjoint timelimiting

operator $\mathcal{T}_T^{\mathrm{c}} : L_2(\mathbb{R}) \to L_2(\mathbb{R})$ by

$$(\mathcal{T}_T^{\mathrm{c}} y)(t) = \begin{cases} y(t) & \text{if } |t| \leq \frac{T}{2} \\ 0 & \text{if } |t| > \frac{T}{2} \end{cases},$$

and a self-adjoint bandlimiting operator $\mathcal{B}_W^{\mathrm{c}} : L_2(\mathbb{R}) \to L_2(\mathbb{R})$ by

$$(\mathcal{B}_W^{\mathrm{c}} y)(t) = \int_{-\infty}^{\infty} \frac{\sin[2\pi W(t-t')]}{\pi(t-t')} y(t')\, dt' \quad \text{for} \quad t \in \mathbb{R}.$$

For continuous-time signals $y \in L_2(\mathbb{R})$ which are bandlimited to $[-W, W]$, we can write

$$\int_{-T/2}^{T/2} |y(t)|^2 \, dt = \langle y, \mathcal{T}_T^{\mathrm{c}} y \rangle_{L_2(\mathbb{R})} = \langle \mathcal{B}_W^{\mathrm{c}} y, \mathcal{T}_T^{\mathrm{c}} \mathcal{B}_W^{\mathrm{c}} y \rangle_{L_2(\mathbb{R})} = \langle y, \mathcal{B}_W^{\mathrm{c}} \mathcal{T}_T^{\mathrm{c}} \mathcal{B}_W^{\mathrm{c}} y \rangle_{L_2(\mathbb{R})}.$$

Subject to the constraint $\|y\|_{L_2(\mathbb{R})}^2 = 1$, this is maximized by the eigenfunction of the operator $\mathcal{B}_W^{\mathrm{c}} \mathcal{T}_T^{\mathrm{c}} \mathcal{B}_W^{\mathrm{c}}$ corresponding to the largest eigenvalue. The orthonormal eigenfunctions $\psi_0, \psi_1, \ldots \in L_2(\mathbb{R})$ of the self-adjoint operator $\mathcal{B}_W^{\mathrm{c}} \mathcal{T}_T^{\mathrm{c}} \mathcal{B}_W^{\mathrm{c}}$ are known as the prolate spheroidal wave functions (PSWFs), and the corresponding eigenvalues $1 > \widetilde{\lambda}_0 > \widetilde{\lambda}_1 > \cdots > 0$ are known as the PSWF eigenvalues, and are sorted in decreasing order. Just like the DPSS eigenvalues, the PSWF eigenvalues are all distinct and strictly between 0 and 1. In addition to ψ_0 being the continuous-time signal bandlimited to $[-W, W]$ which has a maximum concentration of energy in $[-\frac{T}{2}, \frac{T}{2}]$, it is also true that for each positive integer k, ψ_k is the continuous-time signal bandlimited to $[-W, W]$ which has a maximum concentration of energy in $[-\frac{T}{2}, \frac{T}{2}]$ subject to the additional constraint of being orthogonal to $\psi_0, \ldots, \psi_{k-1}$. Furthermore $\widetilde{\lambda}_k$ is equal to the amount of energy ψ_k has in the time interval $[-\frac{T}{2}, \frac{T}{2}]$.

Again, we can also ask "what continuous-time signal timelimited to $[-\frac{T}{2}, \frac{T}{2}]$ has a max-

imum concentration of energy in the frequency band $[-W, W]$?", i.e.

$$\underset{y \in L_2(\mathbb{R})}{\text{maximize}} \int_{-W}^{W} |\widehat{y}(f)|^2 \, df \quad \text{subject to} \quad \|y\|_{L_2(\mathbb{R})}^2 = 1 \quad \text{and} \quad \widehat{y}(f) = 0 \text{ for } |f| > W.$$

For continuous-time signals $y \in L_2(\mathbb{R})$ which are timelimited to $t \in [-\frac{T}{2}, \frac{T}{2}]$, we can write

$$\begin{aligned} \int_{-W}^{W} |\widehat{y}(f)|^2 \, df &= \left\langle \widehat{y}, \widehat{\mathcal{B}_W^{\mathrm{c}} y} \right\rangle_{L_2(\mathbb{R})} = \langle y, \mathcal{B}_W^{\mathrm{c}} y \rangle_{L_2(\mathbb{R})} \\ &= \langle \mathcal{T}_T^{\mathrm{c}} y, \mathcal{B}_W^{\mathrm{c}} \mathcal{T}_T^{\mathrm{c}} y \rangle_{L_2(\mathbb{R})} = \langle y, \mathcal{T}_T^{\mathrm{c}} \mathcal{B}_W^{\mathrm{c}} \mathcal{T}_T^{\mathrm{c}} y \rangle_{L_2(\mathbb{R})} . \end{aligned}$$

Subject to the constraint $\|y\|_{L_2(\mathbb{R})}^2 = 1$, this is maximized by the eigenfunction of $\mathcal{T}_T^{\mathrm{c}} \mathcal{B}_W^{\mathrm{c}} \mathcal{T}_T^{\mathrm{c}}$ corresponding to the largest eigenvalue. It is easy to check that the eigenfunctions of the operator $\mathcal{T}_T^{\mathrm{c}} \mathcal{B}_\Omega^{\mathrm{c}} \mathcal{T}_T^{\mathrm{c}}$ are the timelimited PSWFs $\mathcal{T}_T^{\mathrm{c}} \psi_0, \mathcal{T}_T^{\mathrm{c}} \psi_1, \ldots$, and that these have the same corresponding eigenvalues $\widetilde{\lambda}_k$. The action of the operator $\mathcal{T}_T^{\mathrm{c}} \mathcal{B}_W^{\mathrm{c}} \mathcal{T}_T^{\mathrm{c}}$ on a signal $y \in L_2(\mathbb{R})$ is given by

$$(\mathcal{T}_T^{\mathrm{c}} \mathcal{B}_W^{\mathrm{c}} \mathcal{T}_T^{\mathrm{c}} y)(t) = \begin{cases} \displaystyle\int_{-T/2}^{T/2} \frac{\sin[2\pi W(t-t')]}{\pi(t-t')} y(t') \, dt' & \text{if } |t| \leq \frac{T}{2} \\ 0 & \text{if } |t| > \frac{T}{2} \end{cases} .$$

With a simple change of variable, it can be shown that the eigenvalues of the above kernel integral operator only depend on the product WT. When it is necessary to denote this dependence, we use the notation $\widetilde{\lambda}_k(c)$ to denote $\widetilde{\lambda}_k$ for values of $W, T > 0$ which satisfy $\pi WT = c$.

In addition to $\mathcal{T}_T^{\mathrm{c}} \psi_0$ being the continuous-time signal timelimited to $[-\frac{T}{2}, \frac{T}{2}]$ whose energy is maximally concentrated in the time interval $[-W, W]$, it is also true that for each integer $k \geq 1$, $\mathcal{T}_T^{\mathrm{c}} \psi_k$ is the continuous-time signal timelimited to $[-\frac{T}{2}, \frac{T}{2}]$ whose energy is maximally concentrated in the time interval $[-W, W]$ subject to the additional constraint of being orthogonal to $\mathcal{T}_T^{\mathrm{c}} \psi_0, \ldots, \mathcal{T}_T^{\mathrm{c}} \psi_{k-1}$. Furthermore, the eigenvalue $\widetilde{\lambda}_k$ is the equal to

the energy of $\mathcal{T}_T^{\mathrm{c}}\psi_k$ in the frequency band $[-W, W]$.

2.3 Clustering Behavior of the DPSS Eigenvalues and the PSWF Eigenvalues

Showing that the DPSS eigenvalues are strictly between 0 and 1 is a trivial consequence of the facts that $\lambda_k = \left(\int_{-W}^{W} |\widehat{s}_k'(f)|^2\, df\right) / \left(\int_{-1/2}^{1/2} |\widehat{s}_k'(f)|^2\, df\right)$ and that $\widehat{s}_k'(f)$ is a non-zero analytic function. It is also easy to check that the sum of all the DPSS eigenvalues is $\sum_{k=0}^{N-1} \lambda_k = \mathrm{trace}(\boldsymbol{B}) = 2NW$. What is perhaps more interesting is that the DPSS eigenvalues obey a particular clustering behavior. For any $\epsilon \in (0, \frac{1}{2})$, slightly fewer than $2NW$ eigenvalues lie in $[1-\epsilon, 1)$, slightly fewer than $N - 2NW$ eigenvalues lie in $(0, \epsilon]$, and very few eigenvalues lie in the transition region $(\epsilon, 1-\epsilon)$. In Figure 1, we demonstrate this phenomenon by plotting the DPSS eigenvalues for $N = 1000$ and $W = \frac{1}{8}$ (so $2NW = 250$). The first 244 eigenvalues lie in $[0.999, 1)$ and the last 744 eigenvalues lie in $(0, 0.001]$. Only 12 eigenvalues lie between 0.001 and 0.999. Experimentally, we can see that the width of this transition region behaves like $\#\{k : \epsilon < \lambda_k < 1-\epsilon\} = O(\log(NW) \log \frac{1}{\epsilon})$. This is demonstrated in Figures 3.1 and 3.2 in Section 3.4.

Since the eigenvalue λ_k represents the amount of energy s_k', or equivalently $\boldsymbol{s}_k$, has in the frequency band $[-W, W]$, the eigenvalue clustering behavior tells us that the first slightly fewer than $2NW$ Slepian basis vectors have a very high concentration of energy in the frequency band $[-W, W]$, and the last slightly fewer than $N - 2NW$ Slepian basis vectors have a very low concentration of energy in the frequency band $[-W, W]$.

The PSWF eigenvalues $\widetilde{\lambda}_k$ have a similar behavior as the DPSS eigenvalues. The PSWF eigenvalues are also all strictly between 0 and 1, and they have a sum of $\sum_{k=0}^{\infty} \widetilde{\lambda}_k = \frac{2c}{\pi}$, which is the analogous time-bandwidth product in the continuous case. Furthermore, for any $\epsilon \in (0, \frac{1}{2})$, slightly fewer than $\frac{2c}{\pi}$ eigenvalues lie in $[1-\epsilon, 1)$, very few eigenvalues lie in $(\epsilon, 1-\epsilon)$, and the rest lie in $(0, \epsilon]$. Experimentally, we can see that the width of this transition region behaves like $\#\{k : \epsilon < \widetilde{\lambda}_k < 1-\epsilon\} = O(\log(c) \log \frac{1}{\epsilon})$. This is demonstrated in Figure 3.3 in Section 3.4.

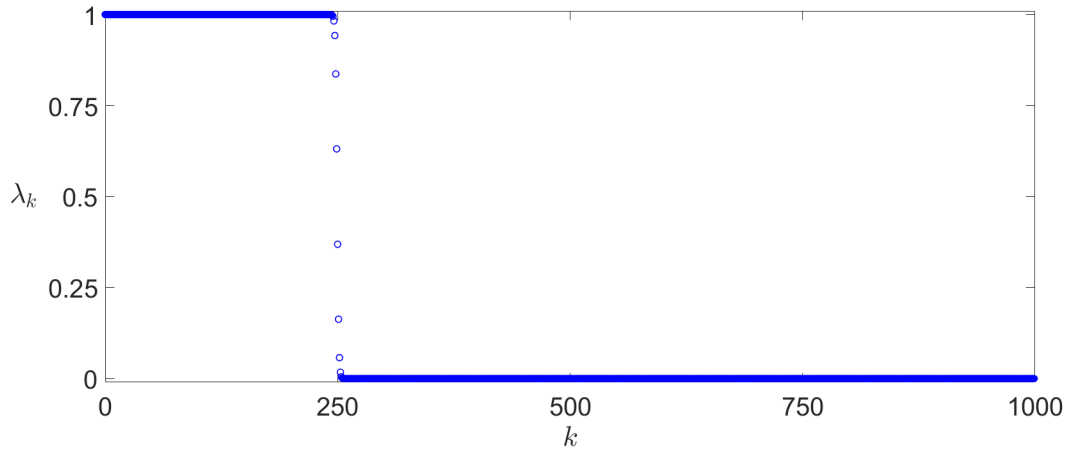

Figure 2.1: A plot of the DPSS Eigenvalues $\{\lambda_k\}_{k=0}^{N-1}$ for $N = 1000$ and $W = \frac{1}{8}$. These eigenvalues satisfy $\lambda_{243} \approx 0.9997$ and $\lambda_{256} \approx 0.0003$. Only 12 of the 1000 DPSS eigenvalues lie in $(0.001, 0.999)$.

2.4 Signal Representation with Slepian Basis Vectors

The Slepian basis provides an excellent low-dimensional representation for samples of a signal which is bandlimited to $f \in [-W, W]$. Unlike the DFT basis, the Slepian basis does not suffer from the problem of spectral leakage. As an illustrative example, in Figure 2.4, we plot the magnitudes of the DFT coefficients and the magnitudes of the Slepian basis coefficients (with $N = 100$ and $W = 0.1$) of the discrete signal $\boldsymbol{x}_1[n] = \boldsymbol{x}_1[n] = 3\cos(\frac{2\pi\cdot 2}{100}n) - 2\cos(\frac{2\pi\cdot 5}{100}n) + 4\cos(\frac{2\pi\cdot 9}{100}n)$ for $n = 0, 1, \ldots, 99$. In Figure 2.4, we plot the magnitudes of the DFT coefficients and the magnitudes of the Slepian basis coefficients (with $N = 100$ and $W = 0.1$) of the discrete signal $\boldsymbol{x}_2[n] = \boldsymbol{x}_1[n] = 3\cos(\frac{2\pi\cdot 1.6}{100}n) - 2\cos(\frac{2\pi\cdot 5.1}{100}n) + 4\cos(\frac{2\pi\cdot 8.5}{100}n)$ for $n = 0, 1, \ldots, 99$.

Since $\boldsymbol{x}_1$ is a sum of three real sinusoids at grid frequencies, only 6 DFT coefficients are non-zero. However, $\boldsymbol{x}_2$ is a sum of three real sinusoids at off-grid frequencies. As a result, all 100 DFT coefficients are non-zero. Furthermore, the largest 23 and 67 DFT coefficients capture 94.11% and 99.02% of the energy in $\boldsymbol{x}_2$ respectively. In contrast, the first 23 and 26 Slepian basis coefficients capture 99.996% and 99.99993% of the energy in $\boldsymbol{x}_1$ respectively. Also, the first 23 and 26 Slepian basis coefficients capture 99.993% and 99.99997% of the

$$\boldsymbol{x}_1[n] = 3\cos(\tfrac{2\pi\cdot 2}{100}n) - 2\cos(\tfrac{2\pi\cdot 5}{100}n) + 4\cos(\tfrac{2\pi\cdot 9}{100}n), \quad n = 0, 1, \ldots, 99$$

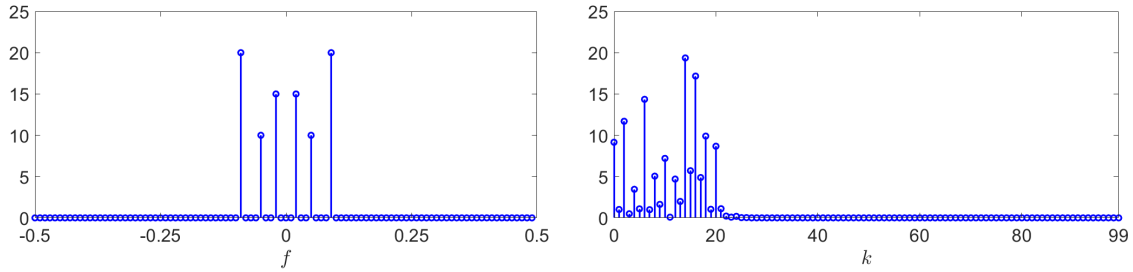

Figure 2.2: A plot of the magnitudes of the DFT coefficients (left) and the Slepian basis coefficients with $N = 100$ and $W = \frac{1}{10}$ (right) for the signal $\boldsymbol{x}_1[n]$, which is a sum of three sinusoids at grid frequencies.

$$\boldsymbol{x}_2[n] = 3\cos(\tfrac{2\pi\cdot 1.6}{100}n) - 2\cos(\tfrac{2\pi\cdot 5.1}{100}n) + 4\cos(\tfrac{2\pi\cdot 8.5}{100}n), \quad n = 0, 1, \ldots, 99$$

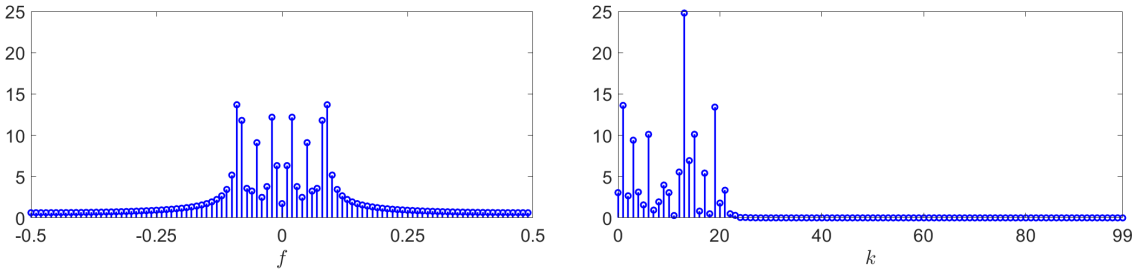

Figure 2.3: A plot of the magnitudes of the DFT coefficients (left) and the Slepian basis coefficients with $N = 100$ and $W = \frac{1}{10}$ (right) for the signal $\boldsymbol{x}_2[n]$, which is a sum of three sinusoids at off-grid frequencies.

energy in $\boldsymbol{x}_2$ respectively. The Slepian basis does a significantly better job than the DFT basis at representing a discrete signal bandlimited to $f \in [-W, W]$.

2.5 Thomson's Multitaper Method

Perhaps one of the most fundamental problems in digital signal processing is spectral estimation, i.e., estimating the power spectrum of a signal from a window of N evenly spaced samples. The simplest solution is the periodogram, which simply takes the squared-magnitude of the discrete time Fourier transform (DTFT) of the samples. Obtaining only a finite number of samples is equivalent to multiplying the signal by a rectangular function before sampling. As a result, the DTFT of the samples is the DTFT of the signal

convolved with the DTFT of the rectangular function, which is a slowly-decaying sinc function. Hence, narrow frequency components in the true signal appear more spread out in the periodogram. This phenomenon is known as "spectral leakage".

The most common approach to mitigating the spectral leakage phenomenon is to multiply the samples by a taper before computing the periodogram. Since multiplying the signal by the taper is equivalent to convolving the DTFT of the signal with the DTFT of the taper, using a taper whose DTFT is highly concentrated around $f = 0$ will help mitigate the spectral leakage phenomenon. Numerous kinds of tapers have been proposed [20] which all have DTFTs which are highly concentrated around $f = 0$. As mentioned in Section 2.2, the Slepian basis vectors, are designed such that their DTFTs have a maximal concentration of energy in the frequency band $[-W, W]$ subject to being orthonormal [5]. The first $\approx 2NW$ of these Slepian basis vectors have DTFTs which are highly concentrated in the frequency band $[-W, W]$. Thus, any of the first $\approx 2NW$ Slepian basis vectors provides a good choice to use as a taper.

In 1982, David Thomson [9] proposed a multitaper method which computes a tapered periodogram for each of the first $K \approx 2NW$ Slepian basis vectors, and then averages these periodograms. Due to the spectral concentration properties of the Slepian basis vectors, Thomson's multitaper method also does an excellent job mitigating spectral leakage. Furthermore, by averaging K tapered periodograms, Thomson's multitaper method is more robust than a single tapered periodogram. As such, Thomson's multitaper method has been used in a wide variety of applications, such as cognitive radio [21–25], digital audio coding [26, 27], as well as to analyze EEG [28, 29] and other neurological signals [30–34], climate data [35–41], breeding calls of Adélie penguins [42] and songs of other birds [43–46], topography of terrestrial planets [47], solar waves[48], and gravitational waves [49].

Traditional view

Let $x(n), n \in \mathbb{Z}$ be a stationary, ergodic, zero-mean, Gaussian process. The autocorrelation and power spectral density of $x(n)$ are defined by

$$R_n = \mathbb{E}\left[x(m)\overline{x(m+n)}\right] \quad \text{for} \quad m, n \in \mathbb{Z},$$

and

$$S(f) = \sum_{n=-\infty}^{\infty} R_n e^{-j2\pi fn} \quad \text{for} \quad f \in \mathbb{R}$$

respectively. The goal of spectral estimation is to estimate $S(f)$ from the vector $\boldsymbol{x} \in \mathbb{C}^N$ of equispaced samples $\boldsymbol{x}[n] = x(n)$ for $n \in [N]$.

One of the earliest, and perhaps the simplest estimator of $S(f)$ is the periodogram [50, 51]

$$\widehat{S}(f) = \frac{1}{N}\left|\sum_{n=0}^{N-1} \boldsymbol{x}[n]e^{-j2\pi fn}\right|^2.$$

This estimator can be efficiently evaluated at a grid of evenly spaced frequencies via the FFT. However, the periodogram has high variance and suffers from the spectral leakage phenomenon [52].

A modification to the periodogram is to pick a data taper $\boldsymbol{w} \in \mathbb{R}^N$ with $\|\boldsymbol{w}\|_2 = 1$, and then weight the samples by the taper as follows

$$\widehat{S}_{\boldsymbol{w}}(f) = \left|\sum_{n=0}^{N-1} \boldsymbol{w}[n]\boldsymbol{x}[n]e^{-j2\pi fn}\right|^2.$$

If $\boldsymbol{w}[n]$ is small near $n = 0$ and $n = N-1$, then this "smoothes" the "edges" of the sample window. Note that the expectation of the tapered periodogram is given by a convolution of the true spectrum and the spectral window of the taper,

$$\mathbb{E}[\widehat{S}_{\boldsymbol{w}}(f)] = S(f) \circledast |\widetilde{\boldsymbol{w}}(f)|^2$$

where

$$\widetilde{\boldsymbol{w}}(f) = \sum_{n=0}^{N-1} \boldsymbol{w}[n] e^{-j2\pi fn}.$$

Hence, a good taper will have its spectral window $|\widetilde{\boldsymbol{w}}(f)|^2$ concentrated around $f = 0$ so that $\mathbb{E}\left[\widehat{S}_{\boldsymbol{w}}(f)\right] = S(f) \circledast |\widetilde{\boldsymbol{w}}(f)|^2 \approx S(f)$, i.e., the tapered periodogram will be approximately unbiased.

As mentioned in the previous section, the first slightly less than $2NW$ Slepian basis vectors are highly concentrated in the frequency band $[-W, W]$. Hence, any of these will be a good choice of taper. Thomson [9] proposed a multitaper spectral estimate by using each of the first $K \approx 2NW$ Slepian basis vectors as tapers, and taking an average of the resulting tapered periodograms, i.e.,

$$\widehat{S}_K^{\text{mt}}(f) = \frac{1}{K} \sum_{k=0}^{K-1} \widehat{S}_k(f) \quad \text{where} \quad \widehat{S}_k(f) = \left| \sum_{n=0}^{N-1} \boldsymbol{s}_k[n] \boldsymbol{x}[n] e^{-j2\pi fn} \right|^2.$$

The expectation of the multitaper spectral estimate satisfies

$$\mathbb{E}\left[\widehat{S}_K^{\text{mt}}(f)\right] = S(f) \circledast \psi(f)$$

where

$$\psi(f) = \frac{1}{K} \sum_{k=0}^{K-1} \left| \sum_{n=0}^{N-1} \boldsymbol{s}_k[n] e^{-j2\pi fn} \right|^2$$

is known as the spectral window of the multitaper spectral estimate. It can be shown that when $K \approx 2NW$, the spectral window $\psi(f)$ approximates $\frac{1}{2W} \mathbb{1}_{[-W,W]}(f)$ on $f \in [-\frac{1}{2}, \frac{1}{2}]$. Thus, the multitaper spectral estimate behaves in expectation like a smoothed version of the true spectrum $S(f)$.

It can be shown that if the spectrum $S(f)$ is slowly varying around a frequency f, then the tapered spectral estimates $\widehat{S}_k(f)$ are approximately uncorrelated, and $\text{Var}[\widehat{S}_k(f)] \approx S(f)^2$. Hence, $\text{Var}[\widehat{S}_K^{\text{mt}}(f)] \approx \frac{1}{K} S(f)^2$. Thus, Thomson's multitaper method produces a spectral estimate whose variance is a factor of $K \approx 2NW$ smaller than the variance of a

single tapered periodogram.

As we increase W, the width of the spectral window $\psi(f)$ increases, which causes the expectation of the multitaper spectral estimate to be further smoothed. However, increasing W also allows us to increase the number of tapers $K \approx 2NW$, which reduces the variance of the multitaper spectral estimate. Intuitively, Thomson's multitaper method introduces a tradeoff between resolution and robustness.

Linear Algebra View

Here we provide an alternate perspective on Thomson's multitaper method which is based on linear algebra and subspace projections. Suppose that for each frequency $f \in \mathbb{R}$, we choose a low-dimensional subspace $\mathcal{S}_f \subset \mathbb{C}^N$, and form a spectral estimate by computing $\|\text{proj}_{\mathcal{S}_f}(\boldsymbol{x})\|_2^2$, i.e., the energy in the projection of $\boldsymbol{x}$ onto the subspace $\mathcal{S}_f$. One simple choice is the one-dimensional subspace $\mathcal{S}_f = \text{span}\{\boldsymbol{e}_f\}$ where

$$\boldsymbol{e}_f = \begin{bmatrix} 1 & e^{j2\pi f \cdot 1} & e^{j2\pi f \cdot 2} & \dots & e^{j2\pi f \cdot (N-1)} \end{bmatrix}^T$$

is a vector of equispaced samples from a complex sinusoid with frequency f. For this choice of $\mathcal{S}_f$, we have

$$\left\| \text{proj}_{\mathcal{S}_f}(\boldsymbol{x}) \right\|_2^2 = \frac{|\langle \boldsymbol{e}_f, \boldsymbol{x} \rangle|^2}{\|\boldsymbol{e}_f\|_2^2} = \frac{1}{N} \left| \sum_{n=0}^{N-1} \boldsymbol{x}[n] e^{-j2\pi f n} \right|^2,$$

which is exactly the classic periodogram.

We can also choose a low-dimensional subspace $\mathcal{S}_f$ which minimizes the average representation error of sinusoids $\boldsymbol{e}_{f'}$ with frequency $f' \in [f - W, f + W]$ for some small $W > 0$, i.e.,

$$\underset{\substack{\mathcal{S}_f \subset \mathbb{C}^N \\ \dim(\mathcal{S}_f) = K}}{\text{minimize}} \int_{f-W}^{f+W} \left\| \boldsymbol{e}_{f'} - \text{proj}_{\mathcal{S}_f}(\boldsymbol{e}_{f'}) \right\|_2^2 df',$$

where the dimension of the subspace K is fixed. Using ideas from the Karhunen-Loeve

(KL) transform [53], it can be shown that the optimal K-dimensional subspace is the span of the top K eigenvectors of the covariance matrix

$$\boldsymbol{C}_f := \frac{1}{2W} \int_{f-W}^{f+W} \boldsymbol{e}_{f'} \boldsymbol{e}_{f'}^* \, df'.$$

The entries of this covariance matrix are

$$\begin{aligned}
\boldsymbol{C}_f[m,n] &= \frac{1}{2W} \int_{f-W}^{f+W} \boldsymbol{e}_{f'}[m] \overline{\boldsymbol{e}_{f'}[n]} \, df' \\
&= \frac{1}{2W} \int_{f-W}^{f+W} e^{j2\pi f'(m-n)} \, df' \\
&= \frac{\sin[2\pi W(m-n)]}{2\pi W(m-n)} e^{j2\pi f(m-n)} \\
&= \frac{1}{2W} \boldsymbol{e}_f[m] \boldsymbol{B}[m,n] \overline{\boldsymbol{e}_f[n]},
\end{aligned}$$

where again $\boldsymbol{B}$ is the $N \times N$ prolate matrix. Hence, we can write

$$\boldsymbol{C}_f = \frac{1}{2W} \boldsymbol{E}_f \boldsymbol{B} \boldsymbol{E}_f^*,$$

where $\boldsymbol{E}_f = \operatorname{diag}(\boldsymbol{e}_f) \in \mathbb{C}^{N \times N}$ is a unitary matrix which modulates vectors by pointwise multiplying them by the sinusoid $\boldsymbol{e}_f$. Therefore, the eigenvectors of $\boldsymbol{C}_f$ are the modulated Slepian basis vectors $\boldsymbol{E}_f \boldsymbol{s}_k$ for $k \in [N]$, and the corresponding eigenvalues are $\frac{\lambda_k}{2W}$. Hence, we can choose $\mathcal{S}_f = \operatorname{span}\{\boldsymbol{E}_f \boldsymbol{s}_0, \ldots, \boldsymbol{E}_f \boldsymbol{s}_{K-1}\}$, i.e., the span of the first K Slepian basis vectors modulated to the frequency f. Since $\boldsymbol{s}_0, \ldots, \boldsymbol{s}_{K-1}$ are orthonormal vectors, and $\boldsymbol{E}_f$ is a unitary matrix, $\boldsymbol{E}_f \boldsymbol{s}_0, \ldots, \boldsymbol{E}_f \boldsymbol{s}_{K-1}$ are orthonormal vectors. Hence, $\operatorname{proj}_{\mathcal{S}_f}(\boldsymbol{x}) =$

$\boldsymbol{E}_f \boldsymbol{S}_K \boldsymbol{S}_K^* \boldsymbol{E}_f^* \boldsymbol{x}$ where $\boldsymbol{S}_K = \begin{bmatrix} \boldsymbol{s}_0 & \dots & \boldsymbol{s}_{K-1} \end{bmatrix}$, and thus,

$$\begin{aligned}
\left\| \text{proj}_{\mathcal{S}_f}(\boldsymbol{x}) \right\|_2^2 &= \left\| \boldsymbol{E}_f \boldsymbol{S}_K \boldsymbol{S}_K^* \boldsymbol{E}_f^* \boldsymbol{x} \right\|_2^2 \\
&= \left\| \boldsymbol{S}_K^* \boldsymbol{E}_f^* \boldsymbol{x} \right\|_2^2 \\
&= \sum_{k=0}^{K-1} \left| (\boldsymbol{S}_K^* \boldsymbol{E}_f^* \boldsymbol{x})[k] \right|^2 \\
&= \sum_{k=0}^{K-1} \left| \boldsymbol{s}_k^* \boldsymbol{E}_f \boldsymbol{x} \right|^2 \\
&= \sum_{k=0}^{K-1} \left| \sum_{n=0}^{N-1} \boldsymbol{s}_k[n] \boldsymbol{x}[n] e^{-j2\pi f n} \right|^2 .
\end{aligned}$$

Up to a constant scale factor, this is precisely the multitaper spectral estimate. Hence, we can view the the multitaper spectral estimate $\widehat{S}_K^{\text{mt}}(f) = \frac{1}{K} \| \boldsymbol{S}_K^* \boldsymbol{E}_f^* \boldsymbol{x} \|_2^2$ as the energy in $\boldsymbol{x}$ after it is projected onto the K-dimensional subspace which best represents the collection of sinusoids $\{ \boldsymbol{e}_{f'} : f' \in [f - W, f + W] \}$.

2.6 Structured Linear Algebra

For a generic matrix $\boldsymbol{A} \in \mathbb{C}^{N \times N}$, it takes $O(N^2)$ operations to compute a matrix-vector product $\boldsymbol{A}\boldsymbol{x}$ and $O(N^{2.3728639})$ operations to solve the system of equations $\boldsymbol{A}\boldsymbol{y} = \boldsymbol{x}$ [54]. For large-scale applications, this may be unfeasible. However, in many signal processing applications, the linear operations or systems of equations will be highly structured, i.e. the matrices will depend on far fewer parameters than the number of entries. Some basic examples of structured matrices are circulant matrices and Topelitz matrices. Both circulant matrices and Toeplitz matrices can be applied to a vector in $O(N \log N)$ operations via the FFT. Circulant systems can also be solved in $O(N \log N)$ operations via the FFT. In recent years, many superfast Toeplitz solvers have been developed, which have runtimes ranging from $O(N \log^3 N)$ to $O(N \log N)$ [55–57]

We present four more sophisticated types of structured matrices. A matrix $\boldsymbol{C} \in \mathbb{R}^{M \times N}$

is called a *Cauchy matrix* if its entries are of the form

$$\boldsymbol{C}[m,n] = \frac{1}{\sigma'_m - \sigma_n} \quad \text{for} \quad m \in [M] \text{ and } n \in [N]$$

where $\sigma'_0, \ldots, \sigma'_{M-1} \in \mathbb{R}$ and $\sigma_0, \ldots, \sigma_{N-1} \in \mathbb{R}$ are such that $\sigma'_m \neq \sigma_n$ for all indices $m \in [M]$ and $n \in [N]$. Using the fast multipole method [58–61], it is possible to apply an $M \times N$ Cauchy matrix to an $N \times 1$ vector in $O((M+N)\log\frac{1}{\alpha})$ operations, where α is the desired level of precision. See [60] for details on using the fast multipole method for Cauchy matrices.

A matrix $\boldsymbol{K} \in \mathbb{C}^{N\times N}$ is called a *Cauchy-like matrix* if its entries are of the form

$$\boldsymbol{K}[n,n'] = \begin{cases} \dfrac{1}{\sigma_n - \sigma_{n'}} & \text{if } n \neq n' \\ 0 & \text{if } n = n' \end{cases}$$

where $\sigma_0, \ldots, \sigma_{N-1} \in \mathbb{R}$ are such that $\sigma_n \neq \sigma_{n'}$ if $n \neq n'$. Again, we can use the fast multipole method to apply an $N \times N$ Cauchy-like matrix to an $N \times 1$ vector in $O(N \log\frac{1}{\alpha})$ operations, where α is the desired level of precision.

A matrix $\widetilde{\boldsymbol{C}} \in \mathbb{C}^{M\times N}$ is called a *generalized Cauchy matrix* if its entries are of the form

$$\widetilde{\boldsymbol{C}}[m,n] = \sum_{\ell=0}^{r-1} \frac{\boldsymbol{p}_\ell[m]\overline{\boldsymbol{q}_\ell[n]}}{\sigma'_m - \sigma_n} \quad \text{for} \quad m \in [M] \text{ and } n \in [N]$$

where $\boldsymbol{p}_0, \ldots, \boldsymbol{p}_{r-1} \in \mathbb{C}^M$, $\boldsymbol{q}_0, \ldots, \boldsymbol{q}_{r-1} \in \mathbb{C}^N$, and $\sigma'_0, \ldots, \sigma'_{M-1} \in \mathbb{R}$ and $\sigma_0, \ldots, \sigma_{N-1} \in \mathbb{R}$ are such that $\sigma'_m \neq \sigma_n$ for all indices $m \in [M]$ and $n \in [N]$. Note that we can write[2]

$$\widetilde{\boldsymbol{C}} = \sum_{\ell=0}^{r-1} \boldsymbol{D}_{\boldsymbol{p}_\ell} \boldsymbol{C} \boldsymbol{D}^*_{\boldsymbol{q}_\ell}$$

where $\boldsymbol{C}$ is a Cauchy matrix. Applying each term $\boldsymbol{D}_{\boldsymbol{p}_\ell} \boldsymbol{C} \boldsymbol{D}^*_{\boldsymbol{q}_\ell}$ to an $N \times 1$ vector takes

[2]For a vector $\boldsymbol{v}$, we use $\boldsymbol{D}_{\boldsymbol{v}}$ to denote a diagonal matrix whose diagonal entries match the entries of the vector $\boldsymbol{v}$, i.e. $\boldsymbol{D}_{\boldsymbol{v}}[n,n] = \boldsymbol{v}[n]$.

$O((M+N)\log\frac{1}{\alpha})$ operations via two diagonal matrix multiplies and a Cauchy matrix multiply. Hence, applying the sum of r matrices of that form takes $O(r(M+N)\log\frac{1}{\alpha})$ operations.

A matrix $\widetilde{\boldsymbol{K}} \in \mathbb{C}^{N\times N}$ is called a *symmetric generalized Cauchy-like matrix* if its entries are of the form

$$\widetilde{\boldsymbol{K}}[n,n'] = \begin{cases} \displaystyle\sum_{\ell=0}^{r-1} \frac{\boldsymbol{p}_\ell[n]\overline{\boldsymbol{q}_\ell[n']} - \boldsymbol{q}_\ell[n]\overline{\boldsymbol{p}_\ell[n']}}{\sigma_n - \sigma_{n'}} & \text{if } n \neq n' \\ d_n & \text{if } n = n' \end{cases}$$

where $\boldsymbol{p}_0,\ldots,\boldsymbol{p}_{r-1} \in \mathbb{C}^N$, $\boldsymbol{q}_0,\ldots,\boldsymbol{q}_{r-1} \in \mathbb{C}^N$, and $\sigma_0,\ldots,\sigma_{N-1} \in \mathbb{R}$ are such that $\sigma_n \neq \sigma_{n'}$ if $n \neq n'$. Note that we can write

$$\widetilde{\boldsymbol{K}} = \boldsymbol{D}_{\boldsymbol{d}} + \sum_{\ell=0}^{r-1} \boldsymbol{D}_{\boldsymbol{p}_\ell}\boldsymbol{K}\boldsymbol{D}_{\boldsymbol{q}_\ell}^* - \boldsymbol{D}_{\boldsymbol{q}_\ell}\boldsymbol{K}\boldsymbol{D}_{\boldsymbol{p}_\ell}^*$$

where $\boldsymbol{K}$ is a Cauchy-like matrix. Applying each term $\boldsymbol{D}_{\boldsymbol{p}_\ell}\boldsymbol{K}\boldsymbol{D}_{\boldsymbol{q}_\ell}$ or $\boldsymbol{D}_{\boldsymbol{q}_\ell}\boldsymbol{K}\boldsymbol{D}_{\boldsymbol{p}_\ell}^*$ to an $N\times 1$ vector takes $O(N\log\frac{1}{\alpha})$ operations via two diagonal matrix multiplies and a Cauchy matrix multiply. Applying $\boldsymbol{D}_{\boldsymbol{d}}$ to a vector takes $O(N)$ operations via a diagonal matrix multiply. Hence, applying the above sum to an $N\times 1$ vector takes $O(rN\log\frac{1}{\alpha})$ operations.

Solving an $N\times N$ symmetric generalized Cauchy-like system of equations can be done in $O(rN\log N\log\frac{1}{\alpha})$ operations via a Schur recursion method [61, 62]. However, this requires the matrix to be well-conditioned. In Chapter 6, we will study the problem of reconstructing a multiband signal from nonuniform samples. This problem requires solving a symmetric generalized Cauchy-like system of equations which is ill-conditioned. Hence, the Schur recursion method is unsuitable for that problem.

2.7 Compressed Sensing

Compressed sensing is a framework for recovering signals which are sparse or approximately sparse in some dictionary from relatively few linear measurements [63, 64]. In the standard setting, we have a signal $\boldsymbol{x} \in \mathbb{C}^N$ which we wish to recover from $M \ll N$ linear measurements $\boldsymbol{y} \in \mathbb{C}^M$ of the form $\boldsymbol{y} = \boldsymbol{A}\boldsymbol{x} + \boldsymbol{\eta}$, where $\boldsymbol{A} \in \mathbb{C}^{M \times N}$ represents the linear measurement operator, and $\boldsymbol{\eta} \in \mathbb{C}^M$ represents noise. With no assumptions on $\boldsymbol{x}$ and $\boldsymbol{A}$, this task is impossible, as $\boldsymbol{A}$ has a nullspace of dimension at least $N - M$, and thus, there is at least an $N - M$ dimensional affine space of signals $\boldsymbol{x}$ which yield the same measurements $\boldsymbol{y}$. However, if the signal is assumed to come from a low dimensional model and the sensing matrix $\boldsymbol{A}$ is chosen appropriately, recovery is a possibility. The most basic assumptions are that

- $\boldsymbol{x}$ is sparse, i.e. $\|\boldsymbol{x}\|_0 = \#\{n : \boldsymbol{x}[n] \neq 0\} \leq S$ where $S \ll N$ is known a priori,
- $\boldsymbol{A}$ satisfies the restricted isometry property (RIP), i.e. there exists $\delta \in (0, 1)$ such that $(1 - \delta)\|\boldsymbol{x}\|_2^2 \leq \|\boldsymbol{A}\boldsymbol{x}\|_2^2 \leq (1 + \delta)\|\boldsymbol{x}\|_2^2$ for all $\boldsymbol{x} \in \mathbb{C}^N$ with $\|\boldsymbol{x}\|_0 \leq 2S$.

Conceptually, the sparsity assumption means that $\boldsymbol{x}$ has significantly less than N degrees of freedom, and thus, suggests the potential to be recovered with fewer than N linear measurements. Furthermore, the RIP guarantees that for S-sparse vectors $\boldsymbol{x}_1, \boldsymbol{x}_2$, $\|A\boldsymbol{x}_1 - A\boldsymbol{x}_2\|_2$ is small iff $\|\boldsymbol{x}_1 - \boldsymbol{x}_2\|_2$ is small. In other words, the only way for two sparse signals to yield similar measurements is if the two signals themselves are close. This ensures that any S-sparse signal $\widehat{\boldsymbol{x}}$ for which $\|\boldsymbol{y} - \boldsymbol{A}\widehat{\boldsymbol{x}}\|_2$ is small will be a good approximation to the true signal $\boldsymbol{x}$. It should be noted that while verifying that a specified matrix $\boldsymbol{A}$ satisfies the RIP condition is NP-hard [65], there are random constructions of matrices $\boldsymbol{A}$ with $M = O(\delta^{-2} S \log^{\cdot} N)$ rows which satisfy the RIP with high probability [66, 67].

With the two assumptions above, there are several methods for recovering the signal $\boldsymbol{x}$. One class of methods involves solving an optimization problem using the convex ℓ_1-norm

to promote sparsity instead of the ℓ_0 pseudonorm which is nonconvex. Examples include Basis Pursuit Denoising (BPDN) [68, 69], Least Absolute Shrinkage Selection Operator (LASSO) [70], and the Dantzig Selector [71]. Another class of methods involve so-called "greedy" approaches, which generally involve alternating between identifying the support of $\boldsymbol{x}$ and solving a least squares problem conditioned on the identified support. Examples include Orthogonal Matching Pursuit (OMP) [72, 73], Compressive Sampling Matching Pursuit (CoSaMP) [67], and Iterative Hard Thresholding (IHT) [74].

These methods have been generalized to handle situations where the signal $\boldsymbol{x}$ has a sparse representation in some known dictionary [75], or has a block-sparse representation in a known dictionary [76–78]. There are also theoretical recovery guarantees if the signal $\boldsymbol{x}$ is compressible, i.e. approximately sparse [79]. In the above methods, the signal of interest is discrete and finite-dimensional. Recent works have studied acquiring continuous time signals which fit some low dimensional model. Many works deal with a multitone signal model [80–85], i.e. the signal of interest is a sum of a small number of pure sinusoids. However, this model is unrealistic in many radar scenarios where each source is transmitting a signal with bandwidth as opposed to a pure sinusoid. Some recent works have considered a multiband signal model. Mishali and Eldar [86] proposed a method called Xampling to recover a multiband signal with a small number of low rate analog-to-digital converters. Davenport and Wakin [6] proposed acquiring multiband signals from compressed measurements using block-based CoSaMP along with a dictionary consisting of Slepian basis vectors modulated to different frequency intervals.

CHAPTER 3

ON THE EIGENVALUES OF DISCRETE PROLATE SPHEROIDAL SEQUENCES AND PROLATE SPHEROIDAL WAVE FUNCTIONS

As mentioned in Section 2.3, both the DPSS eigenvalues and the PSWF eigenvalues are all strictly between 0 and 1, and all but a few of these eigenvalues are very close to 0 or 1. In this chapter, we establish novel non-asymptotic bounds on the DPSS eigenvalues and the PSWF eigenvalues. The results in this chapter may seem esoteric to most practitioners. However, these non-asymptotic bounds are of significant interest to harmonic analysts and will play a critical role in many of the other results in this thesis. Hence, an entire chapter is devoted to these results. The material in this chapter has appeared in [87].

3.1 Prior results on DPSS eigenvalues

We start by reviewing some of the prior results on the clustering behavior of the DPSS eigenvalues. We begin with the original results from Slepian [5]. For any fixed $W \in (0, \frac{1}{2})$ and $b \in \mathbb{R}$,

$$\lambda_{\lfloor 2NW+(b/\pi)\log N \rfloor} \sim \frac{1}{1+e^{b\pi}} \quad \text{as} \quad N \to \infty.$$

From this result, it is easy to show that for any fixed $W \in (0, \frac{1}{2})$ and $\epsilon \in (0, \frac{1}{2})$,

$$\#\{k : \epsilon < \lambda_k < 1-\epsilon\} \sim \frac{2}{\pi^2} \log N \log\left(\frac{1}{\epsilon} - 1\right) \quad \text{as} \quad N \to \infty.$$

This asymptotic bound on the width of the transition region correctly captures the logarithmic dependence on both N and ϵ, but not the dependence on W. Slepian also stated that if

$0.2 < \lambda_k < 0.8$, then

$$\lambda_k \approx \left[1 + \exp\left(-\frac{\pi^2(2NW - k - \frac{1}{2})}{\log[8N\sin(2\pi W)] + \gamma}\right)\right]^{-1}$$

is a good approximation to λ_k where $\gamma \approx 0.5772$ is the Euler-Mascheroni constant. This would suggest that

$$\#\{k : \epsilon < \lambda_k < 1 - \epsilon\} \approx \frac{2}{\pi^2}\log\left[8e^{\gamma}N\sin(2\pi W)\right]\log\left(\frac{1}{\epsilon} - 1\right)$$

for $\epsilon \in (0.2, 0.5)$. This correctly captures the logarithmic dependence on N, W, and ϵ, but only holds for large values of ϵ.

Very few papers provide non-asymptotic bounds regarding the width of the transition region $\#\{k : \epsilon < \lambda_k < 1 - \epsilon\}$. Zhu and Wakin [14] showed that

$$\#\{k : \epsilon \leq \lambda_k \leq 1 - \epsilon\} \leq \frac{\frac{2}{\pi^2}\log(N-1) + \frac{2}{\pi^2}\frac{2N-1}{N-1}}{\epsilon(1-\epsilon)} \tag{3.1}$$

for all integers $N \geq 2$, $W \in (0, \frac{1}{2})$, and $\epsilon \in (0, \frac{1}{2})$. This non-asymptotic bound correctly highlights the logarithmic dependence on N, but fails to capture the dependence on W. Also, the dependence on ϵ is $O(\frac{1}{\epsilon})$ as opposed to $O(\log\frac{1}{\epsilon})$. When ϵ is small, this bound is considerably worse than a $O(\log\frac{1}{\epsilon})$ bound. For example, when $N = 1000$, $W = \frac{1}{8}$, and $\epsilon = 10^{-3}$, this result becomes $\#\{k : \epsilon < \lambda_k < 1 - \epsilon\} \leq 1806$. More generally, when $\epsilon < \frac{2\log(N-1)}{\pi^2 N}$, this bound is worse than the trivial bound of $\#\{k : \epsilon < \lambda_k < 1 - \epsilon\} \leq N$.

Recently, Boulsane, Bourguiba, and Karoui [88] improved this bound to

$$\#\{k : \epsilon \leq \lambda_k \leq 1 - \epsilon\} \leq \frac{\frac{1}{\pi^2}\log(2NW) + 0.45 - \frac{2}{3}W^2 + \frac{\sin^2(2\pi NW)}{6\pi^2N^2}}{\epsilon(1-\epsilon)} \tag{3.2}$$

for all integers $N \geq 1$, $W \in (0, \frac{1}{2})$, and $\epsilon \in (0, \frac{1}{2})$. For a fixed $W \in (0, \frac{1}{2})$ and large N, this bound is roughly half of (3.1). Also, this bound correctly captures the logarithmic

dependence on $2NW$ as opposed to just N. However, this bound still has a dependence on ϵ that is $O(\frac{1}{\epsilon})$. Again, when $N = 1000$, $W = \frac{1}{8}$, and $\epsilon = 10^{-3}$, this result becomes $\#\{k : \epsilon < \lambda_k < 1 - \epsilon\} \leq 1000$. More generally, when $\epsilon < \frac{\log(2NW)}{\pi^2 N}$, this bound is worse than the trivial bound of $\#\{k : \epsilon < \lambda_k < 1 - \epsilon\} \leq N$. Boulsane et. al. also used a result on PSWF eigenvalues by Bonami, Jamming, and Karoui [89] to prove that the DPSS eigenvalues satisfy

$$\lambda_k \leq 2 \exp\left[-\eta \frac{k - 2NW}{\log(\pi NW) + 5}\right] \quad \text{for} \quad 2NW + \log(\pi NW) + 6 \leq k \leq \pi NW, \quad (3.3)$$

where $\eta = 0.069$, and

$$\lambda_k \leq 2 \exp\left[-(2k+1) \log\left(\frac{2k+2}{e\pi NW}\right)\right] \quad \text{for} \quad 2 \leq \frac{e\pi}{2} NW \leq k \leq N - 1. \quad (3.4)$$

However, with no similar lower bounds on the DPSS eigenvalues λ_k for $k < 2NW$, they were unable to obtain a bound on $\#\{k : \epsilon < \lambda_k < 1 - \epsilon\}$ which has a logarithmic dependence on ϵ.

In [8], we proved that

$$\#\{k : \epsilon < \lambda_k < 1 - \epsilon\} \leq \left(\frac{8}{\pi^2} \log(8N) + 12\right) \log\left(\frac{15}{\epsilon}\right) \quad (3.5)$$

for all $N \in \mathbb{N}$, $W \in (0, \frac{1}{2})$, and $\epsilon \in (0, \frac{1}{2})$. This bound correctly captures the logarithmic dependence on both N and ϵ, but not the dependence on W. Also, the leading constant $\frac{8}{\pi^2}$ is four times larger than that of the asymptotic results by Slepian. For comparison with the previous two non-asymptotic bounds, when $N = 1000$, $W = \frac{1}{8}$, and $\epsilon = 10^{-3}$, then this result becomes $\#\{k : \epsilon < \lambda_k < 1 - \epsilon\} \leq 185$, which is still much larger than the actual value of $\#\{k : \epsilon < \lambda_k < 1 - \epsilon\} = 12$.

3.2 Prior results on PSWF eigenvalues

We now review similar results regarding the PSWF eigenvalues. Landau and Widom [90] showed that for any fixed $\epsilon \in (0, \frac{1}{2})$,

$$\#\left\{k : \epsilon < \widetilde{\lambda}_k < 1 - \epsilon\right\} = \frac{2}{\pi^2}\log(c)\log\left(\frac{1}{\epsilon} - 1\right) + o(\log(c)) \quad \text{as} \quad c \to \infty.$$

This asymptotic result is similar in form to Slepian's result from [5], except the first logarithm contains the time-bandwidth product instead of the time duration. Also, this result specifies that the error term scales like $o(\log(c))$.

Osipov [91] showed that for any numbers $c > 22$ and $3 < \delta < \frac{\pi c}{16}$, the PSWF eigenvalues satisfy

$$\widetilde{\lambda}_k < \frac{7056^2 c^3}{2\pi}\exp\left[-2\delta\left(1 - \frac{\delta}{2\pi c}\right)\right] \quad \text{for all} \quad k \geq \frac{2c}{\pi} + \frac{2}{\pi^2}\delta\log\left(\frac{4\pi e c}{\delta}\right).$$

With an appropriate choice of δ, this result implies that

$$\#\left\{k : \widetilde{\lambda}_k > \epsilon\right\} \leq \frac{2c}{\pi} + \frac{32}{31\pi^2}\log\left(\frac{7056^2 c^3}{2\pi\epsilon}\right)\log\left(\frac{31\pi e c}{4\log\left(\frac{7056^2 c^3}{2\pi\epsilon}\right)}\right)$$

for

$$\frac{7056^2 c^3}{2\pi}\exp\left(-\frac{31\pi c}{256}\right) < \epsilon < \frac{1}{2}.$$

Since Landau [92] showed that $\widetilde{\lambda}_{\lfloor 2c/\pi \rfloor - 1} \geq \frac{1}{2}$, the above result by Osipov shows that $\#\left\{k : \epsilon < \widetilde{\lambda}_k \leq \frac{1}{2}\right\} \leq O(\log^2(c) + \log(c)\log(\frac{1}{\epsilon}))$. This only bounds roughly half of the transition region. Also, the bound has a suboptimal dependence on c, and the constants are rather large.

Israel [93] showed that for any $\alpha \in (0, \frac{1}{2}]$, there exists a constant $C_\alpha \geq 1$ such that

$$\# \left\{ k : \epsilon < \widetilde{\lambda}_k < 1 - \epsilon \right\} \leq C_\alpha \log^{1+\alpha} \left(\frac{\log\left(\frac{2c}{\pi}\right)}{\epsilon} \right) \log\left(\frac{2c}{\pi\epsilon}\right)$$

for all $c \geq \pi$ and $\epsilon \in (0, \frac{1}{2})$. When compared to the bound by Osipov, this bound has an improved dependence on c, but a worse dependence on ϵ. Also, the constant C_α is not explicitly given.

Bonami, Jamming, and Karoui [89] established the following bounds on PSWF eigenvalues

$$\widetilde{\lambda}_k \geq 1 - \frac{7}{\sqrt{c}} \frac{(2c)^k}{k!} e^{-c} \quad \text{for} \quad c > 0 \text{ and } 0 \leq k < \frac{2c}{2.7}$$

$$\widetilde{\lambda}_k \leq \frac{1}{2} \exp\left[-\eta \frac{k - \frac{2c}{\pi}}{\log(c) + 5} \right] \quad \text{for} \quad c \geq 22 \text{ and } \frac{2c}{\pi} + \log(c) + 6 \leq k \leq c$$

$$\widetilde{\lambda}_k \leq \exp\left[-(2k+1) \log\left(\frac{2k+2}{ec} \right) \right] \quad \text{for} \quad c > 0 \text{ and } k \geq \max\left(\frac{ec}{2}, 2 \right),$$

where $\eta = 0.069$. The first bound shows that $\widetilde{\lambda}_k$ approaches 1 as k decreases at a faster than exponential rate. The second bound shows that $\widetilde{\lambda}_k$ decreases exponentially over a bounded range of values of k that are slightly greater than the time-bandwidth product $\frac{2c}{\pi}$. The third bound shows that $\widetilde{\lambda}_k$ approaches 0 a faster than exponential rate once $k > \max(\frac{ec}{2}, 2)$. Unfortunately, one can check that for any $c > 0$ and any integer $0.43c \leq k < \frac{2c}{2.7}$, the first bound is negative, and thus, uninformative. Thus, these bounds give no information about $\widetilde{\lambda}_k$ for $k \in [0.43c, \frac{2c}{\pi} + \log(c) + 6) \cup (c, \frac{ec}{2})$, which is a total of $O(c)$ values of k.

3.3 New results on DPSS eigenvalues and PSWF eigenvalues

In Section A.1, we prove the following two non-asymptotic bounds on the number of DPSS eigenvalues in the transition region $(\epsilon, 1-\epsilon)$.

Theorem 1. *For any $N \in \mathbb{N}$, $W \in (0, \frac{1}{2})$, and $\epsilon \in (0, \frac{1}{2})$,*

$$\#\{k : \epsilon < \lambda_k < 1-\epsilon\} \leq 2 \left\lceil \frac{1}{\pi^2} \log(4N) \log\left(\frac{4}{\epsilon(1-\epsilon)}\right) \right\rceil.$$

Theorem 2. *For any $N \in \mathbb{N}$, $W \in (0, \frac{1}{2})$, and $\epsilon \in (0, \frac{1}{2})$,*

$$\#\{k : \epsilon < \lambda_k < 1-\epsilon\} \leq \frac{2}{\pi^2} \log(100NW + 25) \log\left(\frac{5}{\epsilon(1-\epsilon)}\right) + 7.$$

Both Theorem 1 and Theorem 2 capture the logarithmic dependence of the width of the transition region on N and ϵ. Also, both bounds have a leading constant of $\frac{2}{\pi^2}$, which is consistent with the asymptotic result by Slepian. Furthermore, Theorem 2 also captures the logarithmic dependence on W. We choose to include Theorem 1 since the proof is much simpler and since the bound in Theorem 1 is better than the bound in Theorem 2 when $W \geq \frac{1}{25}$. Again for comparison with the existing non-asymptotic bounds, when $N = 1000$, $W = \frac{1}{8}$, and $\epsilon = 10^{-3}$, the bound in Theorem 1 becomes $\#\{k : \epsilon < \lambda_k < 1-\epsilon\} \leq 14$ and the bound in Theorem 2 becomes $\#\{k : \epsilon < \lambda_k < 1-\epsilon\} \leq 23$. Both of these bounds are much closer to the actual value $\#\{k : \epsilon < \lambda_k < 1-\epsilon\} = 12$ than any of the existing non-asymptotic bounds.

With the non-asymptotic bounds in Theorem 1 and Theorem 2, the following bounds on the eigenvalues themselves are almost immediate.

Corollary 1. *For any $N \in \mathbb{N}$, $W \in (0, \frac{1}{2})$, we have*

$$\lambda_k \geq 1 - \min\left\{ 8\exp\left[-\frac{\lfloor 2NW \rfloor - k - 2}{\frac{2}{\pi^2}\log(4N)} \right], 10\exp\left[-\frac{\lfloor 2NW \rfloor - k - 7}{\frac{2}{\pi^2}\log(100NW+25)} \right] \right\}$$

for $0 \leq k \leq \lfloor 2NW \rfloor - 1$, *and*

$$\lambda_k \leq \min\left\{8\exp\left[-\frac{k-\lceil 2NW\rceil - 1}{\frac{2}{\pi^2}\log(4N)}\right], 10\exp\left[-\frac{k-\lceil 2NW\rceil - 6}{\frac{2}{\pi^2}\log(100NW+25)}\right]\right\}$$

for $\lceil 2NW \rceil \leq k \leq N-1$.

The first bound in Corollary 1 represents the first non-asymptotic lower bound on the DPSS eigenvalues λ_k for $k \leq \lfloor 2NW \rfloor - 1$.

The second bound in Corollary 1 is similar in form to (3.3), except this result has an exponential decay rate of $\frac{\pi^2}{2\log(100NW+25)}$ instead of $\frac{0.069}{\log(\pi NW)+5}$. It is not hard to check that when $NW \geq 0.07$, the exponential decay rate from the second bound is at least 71 times larger than the exponential decay rate in (3.3).

The second bound in Corollary 1 does not capture the faster than exponential decay rate of λ_k for $k \geq \frac{e\pi}{2}NW$ that is demonstrated by (3.4). However, we note that for $NW \geq 15$, the second bound in Corollary 1 will yield an upper bound for $\lambda_{\lceil e\pi NW/2\rceil}$ that is less than the single precision machine epsilon of $2^{-23} \approx 1.2 \times 10^{-7}$. Also, for $NW \geq 31$, the second bound in Corollary 1 will yield an upper bound for $\lambda_{\lceil e\pi NW/2\rceil}$ that is below the double precision machine epsilon of $2^{-52} \approx 2.2 \times 10^{-16}$. So these bounds are still useful.

From the eigenvalue bounds in Corollary 1, we can obtain the following bounds on the sums of the leading and trailing DPSS eigenvalues.

Corollary 2. *For any* $N \in \mathbb{N}$, $W \in (0, \frac{1}{2})$, *we have*

$$\sum_{k=0}^{K-1}(1-\lambda_k) \leq \min\left\{\frac{16}{\pi^2}\log(4N)\exp\left[-\frac{\lfloor 2NW\rfloor - K - 2}{\frac{2}{\pi^2}\log(4N)}\right], \frac{20}{\pi^2}\log(100NW+25)\exp\left[-\frac{\lfloor 2NW\rfloor - K - 7}{\frac{2}{\pi^2}\log(100NW+25)}\right]\right\}$$

for $1 \leq K \leq \lfloor 2NW \rfloor$, *and*

$$\sum_{k=K}^{N-1} \lambda_k \leq \min \left\{ \frac{16}{\pi^2} \log(4N) \exp\left[-\frac{K - \lceil 2NW \rceil - 2}{\frac{2}{\pi^2}\log(4N)} \right], \right.$$
$$\left. \frac{20}{\pi^2} \log(100NW + 25) \exp\left[-\frac{K - \lceil 2NW \rceil - 7}{\frac{2}{\pi^2}\log(100NW + 25)} \right] \right\}$$

for $\lceil 2NW \rceil \leq K \leq N - 1$.

Note that all of the above bounds which depend on W can be easily refined if W is close to $\frac{1}{2}$. Let $\boldsymbol{B}' \in \mathbb{R}^{N \times N}$ be the prolate matrix with bandwidth parameter $\frac{1}{2} - W$, i.e. $\boldsymbol{B}'[m,n] = \frac{\sin[2\pi(1/2-W)(m-n)]}{\pi(m-n)}$. One can check that $\boldsymbol{B} = \boldsymbol{D}(\mathbf{I} - \boldsymbol{B}')\boldsymbol{D}^*$ where $\boldsymbol{D} \in \mathbb{R}^{N \times N}$ is a unitary diagonal matrix with entries $\boldsymbol{D}[n,n] = (-1)^n$. Hence, the eigenvalues of $\boldsymbol{B}$ and $\boldsymbol{B}'$ are related by $\lambda_k(N,W) = 1 - \lambda_{N-1-k}(N, \frac{1}{2} - W)$ for $k = 0, \ldots, N-1$. So when W is close to $\frac{1}{2}$, we can obtain stronger bounds on $\lambda_k(N,W)$ by applying the bounds in Corollary 1 for $\lambda_{N-1-k}(N, \frac{1}{2} - W)$. Also, due to that relation, we have $\epsilon < \lambda_k(N,W) < 1 - \epsilon$ if and only if $\epsilon < \lambda_{N-1-k}(N, \frac{1}{2} - W) < 1 - \epsilon$, and thus, $\#\{k : \epsilon < \lambda_k(N,W) < 1 - \epsilon\} = \#\{k : \epsilon < \lambda_k(N, \frac{1}{2} - W) < 1 - \epsilon\}$, i.e., the widths of the transition regions for the bandwidth parameters W and $\frac{1}{2} - W$ are the same. So for W close to $\frac{1}{2}$, we can obtain a stronger bound on $\#\{k : \epsilon < \lambda_k(N,W) < 1 - \epsilon\}$ by applying the bound in Theorem 2 for $\#\{k : \epsilon < \lambda_k(N, \frac{1}{2} - W) < 1 - \epsilon\}$.

Finally, we note that a result by Boulsane, Bourguiba, and Karoui [88] shows that the DPSS eigenvalues and the PSWF eigenvalues satisfy $\lambda_k(N,W) \to \widetilde{\lambda}_k(\pi NW)$ as $N \to \infty$ and $W \to 0^+$ with NW held constant. Intuitively, this means that the continuous energy concentration problem is the limit of the discrete energy concentration problem as the discritization gets arbitrarily fine. With this result, the above non-asymptotic results on the DPSS eigenvalues which depend on NW (and not just N) can be used to obtain the following non-asymptotic results on the PSWF eigenvalues.

Theorem 3. *For any $c > 0$ and $\epsilon \in (0, \frac{1}{2})$,*

$$\#\left\{k : \epsilon < \widetilde{\lambda}_k < 1 - \epsilon\right\} \leq \frac{2}{\pi^2} \log\left(\frac{100c}{\pi} + 25\right) \log\left(\frac{5}{\epsilon(1-\epsilon)}\right) + 7.$$

Corollary 3. *For any $c > 0$ and $\epsilon \in (0, \frac{1}{2})$,*

$$\widetilde{\lambda}_k \geq 1 - 10 \exp\left[-\frac{\left\lfloor \frac{2c}{\pi} \right\rfloor - k - 7}{\frac{2}{\pi^2} \log\left(\frac{100c}{\pi} + 25\right)}\right] \quad \textit{for} \quad 0 \leq k \leq \left\lfloor \frac{2c}{\pi} \right\rfloor - 1,$$

and

$$\widetilde{\lambda}_k \leq 10 \exp\left[-\frac{k - \left\lceil \frac{2c}{\pi} \right\rceil - 6}{\frac{2}{\pi^2} \log\left(\frac{100c}{\pi} + 25\right)}\right] \quad \textit{for} \quad k \geq \left\lceil \frac{2c}{\pi} \right\rceil.$$

Corollary 4. *For any $c > 0$, we have*

$$\sum_{k=0}^{K-1} \left(1 - \widetilde{\lambda}_k\right) \leq \frac{20}{\pi^2} \log\left(\frac{100c}{\pi} + 25\right) \exp\left[-\frac{\left\lfloor \frac{2c}{\pi} \right\rfloor - K - 7}{\frac{2}{\pi^2} \log(\frac{100c}{\pi} + 25)}\right] \quad \textit{for} \quad 1 \leq K \leq \left\lfloor \frac{2c}{\pi} \right\rfloor,$$

and

$$\sum_{k=K}^{\infty} \widetilde{\lambda}_k \leq \frac{20}{\pi^2} \log\left(\frac{100c}{\pi} + 25\right) \exp\left[-\frac{K - \left\lceil \frac{2c}{\pi} \right\rceil - 7}{\frac{2}{\pi^2} \log(\frac{100c}{\pi} + 25)}\right] \quad \textit{for} \quad K \geq \left\lceil \frac{2c}{\pi} \right\rceil.$$

We note that the non-asymptotic bound in Theorem 3 is similar in form to the asymptotic bound by Landau and Widom [90] in that it scales like $O(\log(c)\log(\frac{1}{\epsilon}))$ and has the correct leading constant $\frac{2}{\pi^2}$. Furthermore, the constants in this bound are all specified and are mild. As such, this is a substantial improvement over the existing non-asymptotic bounds.

The bounds in Corollary 3 show that the PSWF eigenvalues $\widetilde{\lambda}_k$ approach 1 and 0 exponentially as k moves away from the time-bandwidth product $\frac{2c}{\pi}$. Also, these bounds are useful (i.e. something stronger than $0 < \widetilde{\lambda}_k < 1$) for all but $O(\log(c))$ values of k.

3.4 Numerical Results

We demonstrate the quality of our bounds in Theorems 1, 2, and 3 with some numerical computations.

First, we fix $W = \frac{1}{4}$ (a large value of W), and for each integer $2^4 \leq N \leq 2^{16}$ we use the method described in [94] to compute the DPSS eigenvalues, λ_k, for a range $k_{\min} \leq k \leq k_{\max}$ such that $\lambda_{k_{\min}} > 1 - 10^{-13}$ and $\lambda_{k_{\max}} < 10^{-13}$. From this, we can determine $\#\{k : \epsilon < \lambda_k < 1 - \epsilon\}$ for $\epsilon = 10^{-3}, 10^{-8}, 10^{-13}$. We plot $\#\{k : \epsilon < \lambda_k < 1 - \epsilon\}$ as well as the upper bound on $\#\{k : \epsilon < \lambda_k < 1 - \epsilon\}$ from Theorem 1 in Figure 3.1. We note that over this range of parameters, the difference between the bound in Theorem 1 and the true width of the transition region $\#\{k : \epsilon < \lambda_k < 1 - \epsilon\}$ is between 1 and 14.

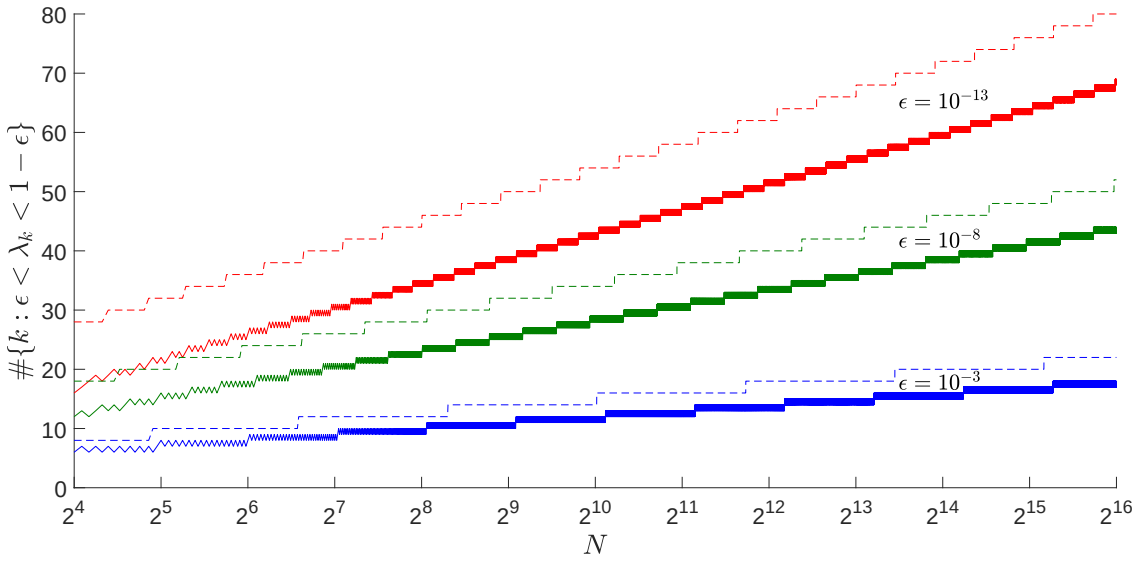

Figure 3.1: Plots of the width of the transition region of DPSS eigenvalues $\#\{k : \epsilon < \lambda_k < 1 - \epsilon\}$ vs. N where $W = \frac{1}{4}$ and $\epsilon = 10^{-3}$(blue), $\epsilon = 10^{-8}$(green), and 10^{-13}(red) are fixed. The dashed lines indicate the upper bound from Theorem 1.

Next, we fix $N = 2^{16}$ and for 10001 logarithmically spaced values of W between 2^{-14} and 2^{-2}, we use the method described in [94] to compute the DPSS eigenvalues, λ_k, for a

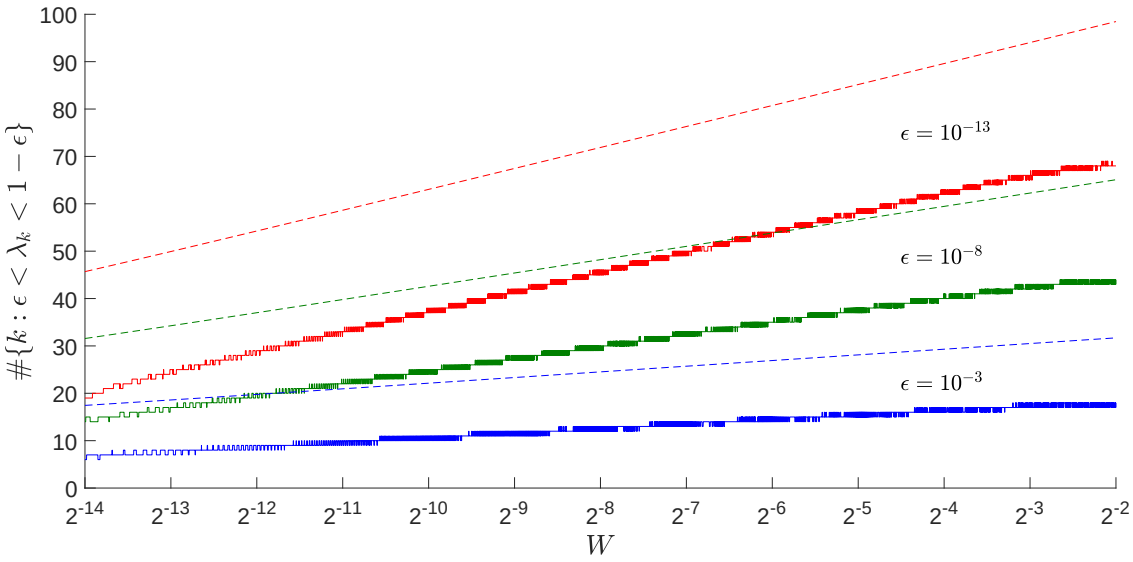

Figure 3.2: Plots of the width of the transition region of DPSS eigenvalues $\#\{k : \epsilon < \lambda_k < 1-\epsilon\}$ vs. W where $N = 2^{16}$ and $\epsilon = 10^{-3}$(blue), $\epsilon = 10^{-8}$(green), and 10^{-13}(red) are fixed. The dashed lines indicate the upper bound from Theorem 2.

range $k_{\min} \leq k \leq k_{\max}$ such that $\lambda_{k_{\min}} > 1 - 10^{-13}$ and $\lambda_{k_{\max}} < 10^{-13}$. From this, we can determine $\#\{k : \epsilon < \lambda_k < 1-\epsilon\}$ for $\epsilon = 10^{-3}, 10^{-8}, 10^{-13}$. We plot $\#\{k : \epsilon < \lambda_k < 1-\epsilon\}$ as well as the upper bound on $\#\{k : \epsilon < \lambda_k < 1-\epsilon\}$ from Theorem 2 in Figure 3.2. We note that over this range of parameters, the difference between the bound in Theorem 2 and the true width of the transition region $\#\{k : \epsilon < \lambda_k < 1-\epsilon\}$ is between ≈ 9.8 and ≈ 30.7.

In Figure 3.1, we see that the plots of both $2\left\lceil \frac{1}{\pi^2}\log(4N)\log(\frac{4}{\epsilon(1-\epsilon)})\right\rceil$ (the bound in Theorem 1) and the actual width of the transition region increase roughly linearly with $\log N$ and at roughly the same rate. However, the difference between the bound in Theorem 1 and the actual width of the transition region is noticeably larger for smaller values of ϵ than for larger values of ϵ. This provides numerical evidence that for a large bandwidth W, the bound's dependence on N is close to correct, but the dependence on ϵ has some room for improvement.

In Figure 3.2, we see that the plots of both $\frac{2}{\pi^2}\log(100NW+25)\log\left(\frac{5}{\epsilon(1-\epsilon)}\right)+7$ and the actual width of the transition region increase roughly linearly with $\log(NW)$ and at

roughly the same rate. However, the difference between the bound in Theorem 2 and the actual width of the transition region is quite noticeable. This provides numerical evidence that the leading constant of $\frac{2}{\pi^2}$ is indeed correct, but that the other constants leave significant room for improvement.

We note that for the range of parameters in both plots, the non-asymptotic bounds on the width of the transition region given by (3.1), (3.2), and (3.5) (in Section 3.1) would all be well above the range of the plots in Figures 3.1 and 3.2. The bounds in (3.1) and (3.2) are proportional to $\frac{1}{\epsilon(1-\epsilon)}$. Thus, they are only useful when ϵ is not too small. Also, the bound in (3.5) is rather large since the leading constant $\frac{8}{\pi^2}$ being 4 times larger than that in Theorems 1 and 2, and the trailing constant 12 dominates $\frac{8}{\pi^2}\log(8N)$ when N isn't too large. In particular, for $\epsilon = 10^{-3}$ and any $N \in \mathbb{N}$, if we impose the mild constraint that $NW \geq \frac{1}{2}$, then the bound in (3.1) is at least $\frac{4/\pi^2}{\epsilon(1-\epsilon)} \approx 405$, the bound in (3.2) is at least $\frac{0.45-1/6}{\epsilon(1-\epsilon)} \approx 283$, and the bound in (3.5) is at least $(\frac{8}{\pi^2}\log(8)+12)\log(\frac{15}{\epsilon}) \approx 131$.

Finally, for 10001 logarithmically spaced values of c between 10 and 10^4, we use the method described in [95] to compute the PSWF eigenvalues, $\widetilde{\lambda}_k$, for a range $k_{\text{min}} \leq k \leq k_{\text{max}}$ such that $\widetilde{\lambda}_{k_{\text{min}}} > 1 - 10^{-13}$ and $\widetilde{\lambda}_{k_{\text{max}}} < 10^{-13}$. From this, we can determine $\#\{k : \epsilon < \widetilde{\lambda}_k < 1-\epsilon\}$ for $\epsilon = 10^{-3}, 10^{-8}, 10^{-13}$. We plot $\#\{k : \epsilon < \widetilde{\lambda}_k < 1-\epsilon\}$ as well as the upper bound on $\#\{k : \epsilon < \widetilde{\lambda}_k < 1-\epsilon\}$ from Theorem 3 in Figure 3.3. We note that over this range of parameters, the difference between the bound in Theorem 3 and the true width of the transition region $\#\{k : \epsilon < \widetilde{\lambda}_k < 1-\epsilon\}$ is between ≈ 9.9 and ≈ 29.6.

In Figure 3.3, we see that the plots of both $\frac{2}{\pi^2}\log\left(\frac{100c}{\pi}+25\right)\log\left(\frac{5}{\epsilon(1-\epsilon)}\right)+7$ and the actual width of the transition region increase roughly linearly with $\log(c)$ and at roughly the same rate. However, the difference between the bound in Theorem 3 and the actual width of the transition region is quite noticeable. This provides numerical evidence that the leading constant of $\frac{2}{\pi^2}$ is indeed correct, but that the other constants leave significant room for improvement.

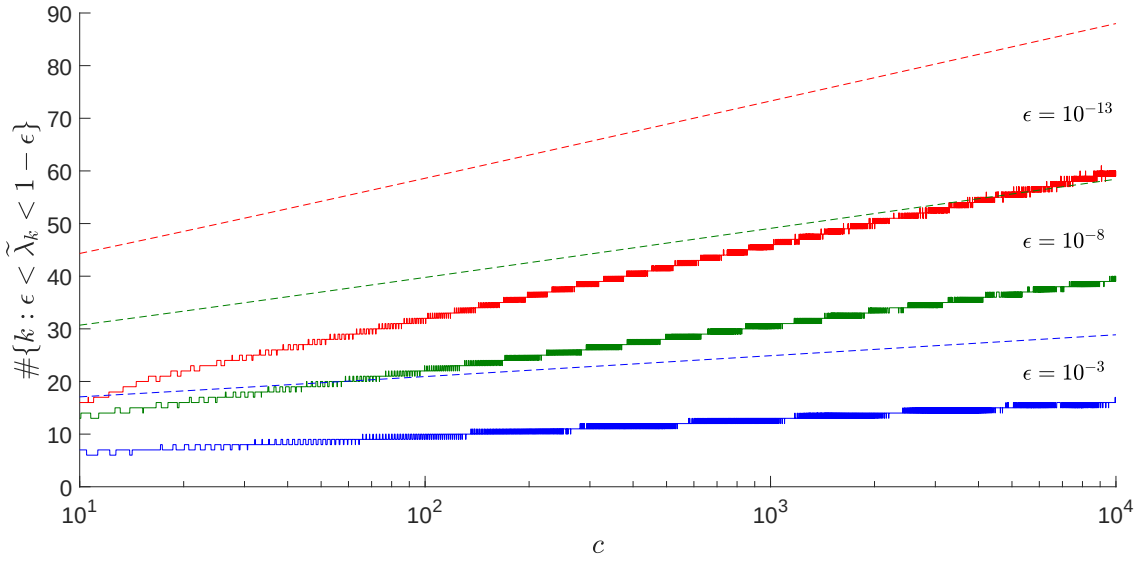

Figure 3.3: Plots of the width of the transition region of PSWF eigenvalues $\#\{k : \epsilon < \widetilde{\lambda}_k < 1-\epsilon\}$ vs. c where $\epsilon = 10^{-3}$(blue), $\epsilon = 10^{-8}$(green), and 10^{-13}(red) are fixed. The dashed lines indicate the upper bound from Theorem 3.

CHAPTER 4

FAST COMPUTATIONS WITH SLEPIAN BASIS VECTORS

In this chapter, we present fast algorithms for projecting a vector onto the span of the leading Slepian basis vectors, for performing dimensionality reduction with Slepian basis vectors, and for solving systems of equations involving the prolate matrix. First, we state theorems which show that certain matrices involving either the Slepian basis vectors or the prolate matrix can be well-approximated by the sum of a Toeplitz matrix and a factored low-rank matrix. Since Toeplitz matrices and factored low-rank matrices can both be applied to a vector efficiently, these theorems give us fast algorithms to approximate certain operations involving the Slepian basis vectors or the prolate matrix. The key to these theorems is exploiting the fact that very few of the DPSS eigenvalues are not near 0 or 1, as demonstrated by Theorems 1 and 2 in Section 3.3. Material in this section has appeared in [8, 96].

4.1 Toeplitz Plus Low Rank Approximations

We start by presenting a theorem showing that the orthogonal projection matrix onto the span of the first $K \approx 2NW$ Slepian basis vectors, the rank-$K \approx 2NW$ truncated pseudoinverse of the prolate matrix $\boldsymbol{B}$, and the Tikhonov regularization matrix $(\boldsymbol{B}^2 + \alpha \mathbf{I})^{-1}\boldsymbol{B}$ can each be well-approximated by the prolate matrix plus a rank-$O(\log(NW)\log\frac{1}{\epsilon})$ correction.

Theorem 4. *Let $N \in \mathbb{N}$, $W \in (0, \frac{1}{2})$, and $\epsilon \in (0, \frac{1}{2})$ be given. Let $\boldsymbol{B} \in \mathbb{R}^{N\times N}$ be the prolate matrix, whose entries are*

$$\boldsymbol{B}[m,n] = \frac{\sin[2\pi W(m-n)]}{\pi(m-n)} \quad \textit{for} \quad m,n \in [N].$$

Define the Slepian basis vectors $\boldsymbol{s}_0, \ldots, \boldsymbol{s}_{N-1} \in \mathbb{R}^N$ *to be the orthonormal eigenvectors of* $\boldsymbol{B}$ *where the corresponding eigenvalues* $1 > \lambda_0 > \cdots > \lambda_{N-1} > 0$ *are sorted in descending order. Let* $r = \#\{k : \epsilon < \lambda_k < 1 - \epsilon\}$*, and define* $\boldsymbol{S}_\epsilon \in \mathbb{R}^{N \times r}$ *to be the matrix whose* r *columns are the Slepian basis vectors* $\boldsymbol{s}_k$ *for* k *such that* $\epsilon < \lambda_k < 1 - \epsilon$*.*

a. Suppose $K \in [N]$ *is such that* $\lambda_{K-1} > \epsilon$ *and* $\lambda_K < 1-\epsilon$*. Let* $\boldsymbol{S}_K = \begin{bmatrix} \boldsymbol{s}_0 & \boldsymbol{s}_1 & \cdots & \boldsymbol{s}_{K-1} \end{bmatrix} \in \mathbb{R}^{N \times K}$*. Then, there exists a diagonal matrix* $\boldsymbol{D}_1 \in \mathbb{R}^{r \times r}$ *such that*

$$\|\boldsymbol{S}_K \boldsymbol{S}_K^* - (\boldsymbol{B} + \boldsymbol{S}_\epsilon \boldsymbol{D}_1 \boldsymbol{S}_\epsilon^*)\| \leq \epsilon.$$

b. Suppose $K \in [N]$ *is such that* $\lambda_{K-1} > \epsilon$ *and* $\lambda_K < 1-\epsilon$*. Let* $\boldsymbol{S}_K = \begin{bmatrix} \boldsymbol{s}_0 & \boldsymbol{s}_1 & \cdots & \boldsymbol{s}_{K-1} \end{bmatrix} \in \mathbb{R}^{N \times K}$ *and* $\boldsymbol{\Lambda}_K = \operatorname{diag}(\lambda_0, \lambda_1, \ldots, \lambda_{K-1}) \in \mathbb{R}^{K \times K}$*. Then, there exists a diagonal matrix* $\boldsymbol{D}_2 \in \mathbb{R}^{r \times r}$ *such that*

$$\left\|\boldsymbol{S}_K \boldsymbol{\Lambda}_K^{-1} \boldsymbol{S}_K^* - (\boldsymbol{B} + \boldsymbol{S}_\epsilon \boldsymbol{D}_2 \boldsymbol{S}_\epsilon^*)\right\| \leq 3\epsilon.$$

c. Suppose $\alpha \in (0, 1)$*. Then, there exists a diagonal matrix* $\boldsymbol{D}_3 \in \mathbb{R}^{r \times r}$ *such that*

$$\left\|(\boldsymbol{B}^2 + \alpha \mathbf{I})^{-1} \boldsymbol{B} - \left(\frac{1}{1+\alpha} \boldsymbol{B} + \boldsymbol{S}_\epsilon \boldsymbol{D}_3 \boldsymbol{S}_\epsilon^*\right)\right\| \leq \frac{\epsilon}{\alpha}.$$

We note that the conditions $\lambda_{K-1} > \epsilon$ and $\lambda_K < 1 - \epsilon$ only require that $K \approx 2NW$. Before moving on, we provide an intuitive explanation of Theorem 4. Note that the Slepian basis vectors are the eigenvectors of each of the matrices $\boldsymbol{B}$, $\boldsymbol{S}_K \boldsymbol{S}_K^*$, $\boldsymbol{S}_K \boldsymbol{\Lambda}_K^{-1} \boldsymbol{S}_K^*$, $\frac{1}{1+\alpha}\boldsymbol{B}$, and $(\boldsymbol{B}^2 + \alpha \mathbf{I})^{-1}\boldsymbol{B}$. For indices k such that $\lambda_k \in [1 - \epsilon, 1)$, the eigenvalues of $\boldsymbol{B}$, $\boldsymbol{S}_K \boldsymbol{S}_K^*$, and $\boldsymbol{S}_K \boldsymbol{\Lambda}_K^{-1} \boldsymbol{S}_K^*$ corresponding to $\boldsymbol{s}_k$ are very close to 1, and the eigenvalues of $\frac{1}{1+\alpha}\boldsymbol{B}$ and $(\boldsymbol{B}^2 + \alpha \mathbf{I})^{-1}\boldsymbol{B}$ corresponding to $\boldsymbol{s}_k$ are very close to $\frac{1}{1+\alpha}$. Also, for indices k such that $\lambda_k \in (0, \epsilon]$, the eigenvalues of $\boldsymbol{B}$, $\boldsymbol{S}_K \boldsymbol{S}_K^*$, $\boldsymbol{S}_K \boldsymbol{\Lambda}_K^{-1} \boldsymbol{S}_K^*$, $\frac{1}{1+\alpha}\boldsymbol{B}$, and $(\boldsymbol{B}^2 + \alpha \mathbf{I})^{-1}\boldsymbol{B}$ corresponding to $\boldsymbol{s}_k$ are very close to 0. This comparison is shown in more detail in Table 4.1 below. From

Table 4.1: Comparison of the eigenvalues of $\boldsymbol{B}$, $\boldsymbol{S}_K\boldsymbol{S}_K^*$, $\boldsymbol{S}_K\boldsymbol{\Lambda}_K^{-1}\boldsymbol{S}_K^*$, $\frac{1}{1+\alpha}\boldsymbol{B}$, and $(\boldsymbol{B}^2+\alpha\mathbf{I})^{-1}\boldsymbol{B}$ corresponding to the eigenvectors $\boldsymbol{s}_k$ for which $\lambda_k \notin (\epsilon, 1-\epsilon)$.

Matrix	$\boldsymbol{B}$	$\boldsymbol{S}_K\boldsymbol{S}_K^*$	$\boldsymbol{S}_K\boldsymbol{\Lambda}_K^{-1}\boldsymbol{S}_K^*$	$\frac{1}{1+\alpha}\boldsymbol{B}$	$(\boldsymbol{B}^2+\alpha\mathbf{I})^{-1}\boldsymbol{B}$
Eigenvalue corresponding to $\boldsymbol{s}_k$ if $\lambda_k \geq 1-\epsilon$	$\lambda_k \approx 1$	1	$\frac{1}{\lambda_k} \approx 1$	$\frac{\lambda_k}{1+\alpha} \approx \frac{1}{1+\alpha}$	$\frac{\lambda_k}{\lambda_k^2+\alpha} \approx \frac{1}{1+\alpha}$
Eigenvalue corresponding to $\boldsymbol{s}_k$ if $\lambda_k \leq \epsilon$	$\lambda_k \approx 0$	0	0	$\frac{\lambda_k}{1+\alpha} \approx 0$	$\frac{\lambda_k}{\lambda_k^2+\alpha} \approx 0$

this, it is easy to see that both $\boldsymbol{S}_K\boldsymbol{S}_K^*$ and $\boldsymbol{S}_K\boldsymbol{\Lambda}_K^{-1}\boldsymbol{S}_K^*$ can be well-approximated by adding a low-rank correction to $\boldsymbol{B}$ which adjusts the eigenvalues corresponding to the eigenvectors $\boldsymbol{s}_k$ for which $\lambda_k \in (\epsilon, 1-\epsilon)$. Similarly, $(\boldsymbol{B}^2+\alpha\mathbf{I})^{-1}\boldsymbol{B}$ can be well-approximated by adding a low-rank correction to $\frac{1}{1+\alpha}\boldsymbol{B}$ which adjusts the eigenvalues corresponding to the eigenvectors $\boldsymbol{s}_k$ for which $\lambda_k \in (\epsilon, 1-\epsilon)$.

Next, we present a theorem which shows that the prolate matrix $\boldsymbol{B}$ can be well-approximated by the orthogonal projection matrix onto the $2\lfloor NW \rfloor + 1$ lowest frequency discrete Fourier transform (DFT) vectors plus a rank-$O(\log N \log \frac{1}{\epsilon})$ correction.

Theorem 5. *Let $N \in \mathbb{N}$, $W \in (0, \frac{1}{2})$, and $\epsilon \in (0, \frac{1}{2})$ be given. Let $\boldsymbol{B} \in \mathbb{R}^{N\times N}$ be the prolate matrix, whose entries are*

$$\boldsymbol{B}[m,n] = \frac{\sin[2\pi W(m-n)]}{\pi(m-n)} \quad \textit{for} \quad m,n \in [N],$$

and let $\boldsymbol{F}_W \in \mathbb{C}^{N\times(2\lfloor NW\rfloor+1)}$ be a matrix whose columns are the $2\lfloor NW \rfloor + 1$ lowest frequency DFT vectors, i.e.

$$\boldsymbol{F}_W[n,\ell] = \frac{1}{\sqrt{N}} \exp\left(j2\pi n \frac{\ell - \lfloor NW \rfloor}{N}\right) \quad \textit{for} \quad n \in [N] \textit{ and } \ell \in [2\lfloor NW \rfloor + 1].$$

Then, there exist matrices $\boldsymbol{L}_1, \boldsymbol{L}_2 \in \mathbb{C}^{N \times r'}$ such that

$$\|\boldsymbol{B} - (\boldsymbol{F}_W \boldsymbol{F}_W^* + \boldsymbol{L}_1 \boldsymbol{L}_2^*)\| \leq \epsilon,$$

where

$$r' \leq \left(\frac{4}{\pi^2} \log(8N) + 6 \right) \log\left(\frac{15}{\epsilon} \right).$$

The intuition behind this theorem is that the prolate matrix $\boldsymbol{B}$ is a Toeplitz matrix whose entries $\boldsymbol{B}[m,n] = \frac{\sin[2\pi W(m-n)]}{\pi(m-n)}$ are samples of a sinc function, and the orthogonal projection matrix $\boldsymbol{F}_W \boldsymbol{F}_W^*$ is a circulant matrix whose entries

$$\begin{aligned}
(\boldsymbol{F}_W \boldsymbol{F}_W^*)[m,n] &= \sum_{\ell=0}^{2\lfloor NW \rfloor} \boldsymbol{F}_W[m,\ell] \overline{\boldsymbol{F}_W[n,\ell]} \\
&= \sum_{\ell=0}^{2\lfloor NW \rfloor} \frac{1}{N} \exp\left(j2\pi(m-n) \frac{\ell - \lfloor NW \rfloor}{N} \right) \\
&= \frac{\sin\left(\frac{2\lfloor NW \rfloor + 1}{N} \pi(m-n) \right)}{N \sin\left(\pi \frac{m-n}{N} \right)}
\end{aligned}$$

are samples of a digital sinc or Dirichlet function. The difference $\boldsymbol{B} - \boldsymbol{F}_W \boldsymbol{F}_W^*$ has entries which are a smooth function of m, n. Hence, it is reasonable to expect that $\boldsymbol{B} - \boldsymbol{F}_W \boldsymbol{F}_W^*$ is approximately low-rank.

In [8], we use Theorem 5 to prove that the number of Slepian basis eigenvalues in $(\epsilon, 1-\epsilon)$ satisfies $\#\{k : \epsilon < \lambda_k < 1-\epsilon\} \leq 2r' \leq \left(\frac{8}{\pi^2} \log(8N) + 12 \right) \log\left(\frac{15}{\epsilon} \right)$. However, compared to the results in Section 3.3, this result is strictly weaker than Theorem 1 and does not capture the dependence on W that Theorem 2 captures.

Finally, we note that the proof of Theorem 4 provides explicit constructions of the matrices $\boldsymbol{D}_1$, $\boldsymbol{D}_2$, $\boldsymbol{D}_3$. Precomputing the matrices $\boldsymbol{D}_1$, $\boldsymbol{D}_2$, $\boldsymbol{D}_3$, and $\boldsymbol{S}_\epsilon$ requires computing $O(\log(NW) \log \frac{1}{\epsilon})$ Slepian basis eigenvectors and corresponding eigenvalues, which can be done in $O(N \log N \log(NW) \log \frac{1}{\epsilon})$ operations using the method in [94]. Also, the proof of Theorem 5 provides explicit constructions of the matrices $\boldsymbol{L}_1$ and $\boldsymbol{L}_2$ which require

$O(N \log N \log \frac{1}{\epsilon})$ operations to precompute. The fact that these matrices can be efficiently precomputed is essential for using our fast algorithms in practice.

4.2 Fast Computations

In this section, we use the approximations from the previous section to demonstrate fast algorithms for certain operations with the Slepian basis vectors or the prolate matrix.

A fast factorization of $\boldsymbol{S}_K \boldsymbol{S}_K^*$

Suppose we wish to compress a vector $\boldsymbol{x} \in \mathbb{C}^N$ of N uniformly spaced samples of a signal down to a vector of $K \approx 2NW$ elements in such a way that best preserves the DTFT of the signal over $[-W, W]$. We can do this by storing $\boldsymbol{S}_K^* \boldsymbol{x}$, which is a vector of $K \approx 2NW < N$ elements, and then later recovering $\boldsymbol{S}_K \boldsymbol{S}_K^* \boldsymbol{x}$, which contains nearly all of the energy of the signal in the frequency band $[-W, W]$. However, naïve multiplication of $\boldsymbol{S}_K$ or $\boldsymbol{S}_K^*$ takes $O(NK) = O(2WN^2)$ operations. For certain applications, this may be intractable.

If we define

$$\boldsymbol{T}_1 = \begin{bmatrix} \boldsymbol{F}_W & \boldsymbol{L}_1 & \boldsymbol{S}_\epsilon \boldsymbol{D}_1 \end{bmatrix} \quad \text{and} \quad \boldsymbol{T}_2 = \begin{bmatrix} \boldsymbol{F}_W & \boldsymbol{L}_2 & \boldsymbol{S}_\epsilon \end{bmatrix}$$

where $\boldsymbol{F}_W$, $\boldsymbol{L}_1$, $\boldsymbol{L}_2$ are as defined in Theorem 5 and $\boldsymbol{D}_1$ is as defined in Theorem 4a, then we have

$$\begin{aligned} \|\boldsymbol{S}_K \boldsymbol{S}_K^* - \boldsymbol{T}_1 \boldsymbol{T}_2^*\| &= \|\boldsymbol{S}_K \boldsymbol{S}_K^* - (\boldsymbol{F}_W \boldsymbol{F}_W^* + \boldsymbol{L}_1 \boldsymbol{L}_2^* + \boldsymbol{S}_\epsilon \boldsymbol{D}_1 \boldsymbol{S}_\epsilon^*)\| \\ &= \|\boldsymbol{S}_K \boldsymbol{S}_K^* - \boldsymbol{B} - \boldsymbol{S}_\epsilon \boldsymbol{D}_1 \boldsymbol{S}_\epsilon^* + \boldsymbol{B} - \boldsymbol{F}_W \boldsymbol{F}_W^* - \boldsymbol{L}_1 \boldsymbol{L}_2^*\| \\ &\leq \|\boldsymbol{S}_K \boldsymbol{S}_K^* - (\boldsymbol{B} + \boldsymbol{S}_\epsilon \boldsymbol{D}_1 \boldsymbol{S}_\epsilon^*)\| + \|\boldsymbol{B} - (\boldsymbol{F}_W \boldsymbol{F}_W^* + \boldsymbol{L}_1 \boldsymbol{L}_2^*)\| \\ &\leq \epsilon + \epsilon \\ &= 2\epsilon. \end{aligned}$$

Both $\boldsymbol{T}_1$ and $\boldsymbol{T}_2$ are $N \times K'$ matrices where $K' = 2\lfloor NW \rfloor + 1 + r + r' = 2NW + O(\log N \log \frac{1}{\epsilon})$. So we can compress $\boldsymbol{x}$ by computing $\boldsymbol{T}_2^* \boldsymbol{x}$, which is a vector of $K' \approx 2NW$ elements, and then later recover $\boldsymbol{T}_1 \boldsymbol{T}_2^* \boldsymbol{x}$. Since $\|\boldsymbol{S}_K \boldsymbol{S}_K^* - \boldsymbol{T}_1 \boldsymbol{T}_2^*\| \leq 2\epsilon$, we have that $\|\boldsymbol{S}_K \boldsymbol{S}_K^* \boldsymbol{x} - \boldsymbol{T}_1 \boldsymbol{T}_2^* \boldsymbol{x}\|_2 \leq 2\epsilon \|\boldsymbol{x}\|_2$ for any vector $\boldsymbol{x} \in \mathbb{C}^N$. Both $\boldsymbol{F}_W$ and $\boldsymbol{F}_W^*$ can be applied to a vector in $O(N \log N)$ operations via the FFT. Since $\boldsymbol{L}_1$, $\boldsymbol{L}_2$, $\boldsymbol{S}_\epsilon \boldsymbol{D}_1$, and $\boldsymbol{S}_\epsilon$ are $N \times O(\log N \log \frac{1}{\epsilon})$ matrices, $\boldsymbol{L}_1$, $\boldsymbol{L}_2^*$, $\boldsymbol{S}_\epsilon \boldsymbol{D}_1$, and $\boldsymbol{S}_\epsilon^*$ can each be applied to a vector in $O(N \log N \log \frac{1}{\epsilon})$ operations. Therefore, computing $\boldsymbol{T}_2^* \boldsymbol{x}$ and later recovering $\boldsymbol{T}_1 \boldsymbol{T}_2^* \boldsymbol{x}$ (as an approximation for $\boldsymbol{S}_K \boldsymbol{S}_K^* \boldsymbol{x}$) takes $O(N \log N \log \frac{1}{\epsilon})$ operations.

Fast projections onto the range of $\boldsymbol{S}_K$

Alternatively, if we only require computing the projected vector $\boldsymbol{S}_K \boldsymbol{S}_K^* \boldsymbol{x}$, and compression is not required, then there is a simpler solution. Theorem 4a tells us that $\|\boldsymbol{S}_K \boldsymbol{S}_K^* - (\boldsymbol{B} + \boldsymbol{S}_\epsilon \boldsymbol{D}_1 \boldsymbol{S}_\epsilon^*)\| \leq \epsilon$, and thus, $\|\boldsymbol{S}_K \boldsymbol{S}_K^* \boldsymbol{x} - (\boldsymbol{B}\boldsymbol{x} + \boldsymbol{S}_\epsilon \boldsymbol{D}_1 \boldsymbol{S}_\epsilon^* \boldsymbol{x})\|_2 \leq \epsilon \|\boldsymbol{x}\|_2$ for any vector $\boldsymbol{x} \in \mathbb{C}^N$. Since $\boldsymbol{B}$ is a Toeplitz matrix, computing $\boldsymbol{B}\boldsymbol{x}$ can be done in $O(N \log N)$ operations via the FFT. Since $\boldsymbol{S}_\epsilon$ is a $N \times O(\log(NW) \log \frac{1}{\epsilon})$ matrix, computing $\boldsymbol{S}_\epsilon \boldsymbol{D}_1 \boldsymbol{S}_\epsilon^* \boldsymbol{x}$ can be done in $O(N \log(NW) \log \frac{1}{\epsilon})$ operations. Therefore, we can compute $\boldsymbol{B}\boldsymbol{x} + \boldsymbol{S}_\epsilon \boldsymbol{D}_1 \boldsymbol{S}_\epsilon^* \boldsymbol{x}$ as an approximation to $\boldsymbol{S}_K \boldsymbol{S}_K^* \boldsymbol{x}$ using only $O(N \log N + N \log(NW) \log \frac{1}{\epsilon})$ operations.

Fast rank-K truncated pseudoinverse of $\boldsymbol{B}$

A closely related problem to working with the matrix $\boldsymbol{S}_K \boldsymbol{S}_K^*$ concerns the task of solving a linear system of the form $\boldsymbol{y} = \boldsymbol{B}\boldsymbol{x}$. Since the prolate matrix has several eigenvalues that are close to 0, the system is often solved by using the rank-K truncated pseudoinverse of $\boldsymbol{B}$ where $K \approx 2NW$. Even if the pseudoinverse is precomputed and factored ahead of time, it still takes $O(NK) = O(2WN^2)$ operations to apply to a vector $\boldsymbol{y} \in \mathbb{C}^N$. Theorem 4b tells us that $\|\boldsymbol{B}_K^\dagger - (\boldsymbol{B} + \boldsymbol{S}_\epsilon \boldsymbol{D}_2 \boldsymbol{S}_\epsilon^*)\| \leq 3\epsilon$, and thus, $\|\boldsymbol{B}_K^\dagger \boldsymbol{y} - (\boldsymbol{B}\boldsymbol{y} + \boldsymbol{S}_\epsilon \boldsymbol{D}_2 \boldsymbol{S}_\epsilon^* \boldsymbol{y})\|_2 \leq 3\epsilon \|\boldsymbol{y}\|_2$ for any vector $\boldsymbol{y} \in \mathbb{C}^N$. Again, computing $\boldsymbol{B}\boldsymbol{y}$ can be done in $O(N \log N)$ operations using the FFT, and computing $\boldsymbol{S}_\epsilon \boldsymbol{D}_2 \boldsymbol{S}_\epsilon^* \boldsymbol{y}$ can be done in $O(N \log(NW) \log \frac{1}{\epsilon})$ operations.

Therefore, we can compute $\boldsymbol{B}\boldsymbol{y} + \boldsymbol{S}_\epsilon \boldsymbol{D}_2 \boldsymbol{S}_\epsilon^* \boldsymbol{y}$ as an approximation to $\boldsymbol{B}_K^\dagger \boldsymbol{y}$ using only $O(N \log N + N \log(NW) \log \frac{1}{\epsilon})$ operations.

Fast Tikhonov regularization involving $\boldsymbol{B}$

Another approach to solving the ill-conditioned system $\boldsymbol{y} = \boldsymbol{B}\boldsymbol{x}$ is to use Tikhonov regularization, i.e., minimize $\|\boldsymbol{y} - \boldsymbol{B}\boldsymbol{x}\|_2^2 + \alpha \|\boldsymbol{x}\|_2^2$ where $\alpha \in (0, 1)$ is a regularization parameter. The solution to this minimization problem is $\boldsymbol{x} = (\boldsymbol{B}^2 + \alpha \mathbf{I})^{-1} \boldsymbol{B}\boldsymbol{y}$. Even if the matrix $(\boldsymbol{B}^2 + \alpha \mathbf{I})^{-1} \boldsymbol{B}$ is precomputed ahead of time, it still takes $O(N^2)$ operations to apply to a vector $\boldsymbol{y} \in \mathbb{C}^N$. Theorem 4c (with $\alpha\epsilon$ instead of ϵ) tells us that $\|(\boldsymbol{B}^2 + \alpha \mathbf{I})^{-1} \boldsymbol{B} - (\boldsymbol{B} + \boldsymbol{S}_{\alpha\epsilon} \boldsymbol{D}_3 \boldsymbol{S}_{\alpha\epsilon}^*)\| \leq \epsilon$, and thus, $\|(\boldsymbol{B}^2 + \alpha \mathbf{I})^{-1} \boldsymbol{B}\boldsymbol{y} - (\boldsymbol{B}\boldsymbol{y} + \boldsymbol{S}_{\alpha\epsilon} \boldsymbol{D}_3 \boldsymbol{S}_{\alpha\epsilon}^* \boldsymbol{y})\|_2 \leq \epsilon \|\boldsymbol{y}\|_2$ for any vector $\boldsymbol{y} \in \mathbb{C}^N$. Again, computing $\boldsymbol{B}\boldsymbol{y}$ can be done in $O(N \log N)$ operations via the FFT. Since $\boldsymbol{S}_{\alpha\epsilon}$ is a $N \times O(\log(NW) \log \frac{1}{\alpha\epsilon})$ matrix, computing $\boldsymbol{S}_{\alpha\epsilon} \boldsymbol{D}_3 \boldsymbol{S}_{\alpha\epsilon}^* \boldsymbol{y}$ can be done in $O(N \log(NW) \log \frac{1}{\alpha\epsilon})$ operations. Therefore, we can compute $\boldsymbol{B}\boldsymbol{y} + \boldsymbol{S}_{\alpha\epsilon} \boldsymbol{D}_3 \boldsymbol{S}_{\alpha\epsilon}^* \boldsymbol{y}$ as an approximation to $(\boldsymbol{B}^2 + \alpha \mathbf{I})^{-1} \boldsymbol{B}\boldsymbol{y}$ using only $O\left(N \log N + N \log(NW) \log \frac{1}{\alpha\epsilon}\right)$ operations.

4.3 Applications

Owing to the concentration in the time and frequency domains, the Slepian basis vectors have proved to be useful in numerous signal processing problems [5, 6, 10, 12, 97]. Linear systems of equations involving the prolate matrix $\boldsymbol{B}$ also arise in several problems, such as band-limited extrapolation [5]. In this section, we describe some specific applications that stand to benefit from the fast algorithms described in the previous section.

Representation and compression of sampled bandlimited and multiband signals.

Consider a length-N vector $\boldsymbol{x}$ obtained by uniformly sampling a baseband analog signal $x(t)$ over the time interval $[0, NT_s)$ with sampling period $T_s \leq \frac{1}{B_{\text{band}}}$ chosen to satisfy the Nyquist sampling rate. Here, $x(t)$ is assumed to be bandlimited with frequency range

$[-B_{\text{band}}/2, B_{\text{band}}/2]$. Under this assumption, the sample vector $\boldsymbol{x}$ can be expressed as

$$\boldsymbol{x}[n] = \int_{-W}^{W} X(f) e^{j2\pi fn}\, df,\ n = 0, 1, \ldots, N-1, \tag{4.1}$$

or equivalently,

$$\boldsymbol{x} = \int_{-W}^{W} X(f) \boldsymbol{e}_f\, df \tag{4.2}$$

where $W = T_s B_{\text{band}}/2 \leq \frac{1}{2}$ and $X(f)$ is the DTFT of the infinite sample sequence $x[n] = x(nT_s), n \in \mathbb{Z}$. Such finite-length vectors of samples from bandlimited signals arise in problems such as time-variant channel estimation [10] and mitigation of narrowband interference [98]. Solutions to these and many other problems benefit from representations that efficiently capture the structure inherent in vectors $\boldsymbol{x}$ of the form (4.2).

In [6], the authors showed that such a vector $\boldsymbol{x}$ has a low-dimensional structure by building a dictionary in which $\boldsymbol{x}$ can be approximated with a small number of atoms. The $N \times N$ DFT basis is insufficient to capture the low dimensional structure in $\boldsymbol{x}$ due to the "DFT leakage" phenomenon. In particular, the DFT basis is comprised of vectors $\boldsymbol{e}_f$ with f sampled uniformly between $-1/2$ and $1/2$. From (4.2), one can interpret $\boldsymbol{x}$ as being comprised of a linear combination of vectors $\boldsymbol{e}_f$ with f ranging continuously between $-W$ and W. It is natural to ask whether $\boldsymbol{x}$ could be efficiently represented using only the DFT vectors $\boldsymbol{e}_f$ with f between $-W$ and W; in particular, these are the columns of the matrix $\boldsymbol{F}_W$ defined in Theorem 5. Unfortunately, this is not the case—while a majority of the energy of $\boldsymbol{x}$ can be captured using the columns of $\boldsymbol{F}_W$, a nontrivial amount will be missed and this is contained in the familiar sidelobes in the DFT outside the band of interest.

An efficient alternative to the partial DFT $\boldsymbol{F}_W$ is given by the partial Slepian basis $\boldsymbol{S}_K$ when $K \approx 2NW$. In [6], for example, it is established that when $\boldsymbol{x}$ is generated by sampling a bandlimited analog random process with flat power spectrum over $[-B_{\text{band}}/2, B_{\text{band}}/2]$, and when one chooses $K = 2NW(1+\rho)$, then on average $\boldsymbol{S}_K \boldsymbol{S}_K^* \boldsymbol{x}$ will capture all but an exponentially small amount of the energy from $\boldsymbol{x}$. Zemen and Meck-

lenbräuke [10] showed that expressing the time-varying subcarrier coefficients in a Slepian basis yields better performance than that obtained with a DFT basis, which suffers from frequency leakage.

By modulating the (baseband) Slepian basis vectors to different frequency bands and then merging these dictionaries, one can also obtain a new dictionary that offers an efficient representation of sampled *multiband* signals. Zemen et al. [11] proposed one such dictionary for estimating a time-variant flat-fading channel whose spectral support is a union of several intervals. In the context of compressive sensing, Davenport and Wakin [6] investigated multiband modulated DPSS dictionaries for sparse recovery of sampled multiband signals, and Sejdić et al. [99] applied such dictionaries for recovery of physiological signals from compressive measurements. Zhu and Wakin [14] employed such dictionaries for detecting targets behind the wall in through-the-wall radar imaging, and modulated DPSS's can also be useful for mitigating wall clutter [97].

In summary, many of the above mentioned problems are facilitated by projecting a length-N vector onto the subspace spanned by the first $K \approx 2NW$ Slepian basis vectors (i.e., computing $\boldsymbol{S}_K \boldsymbol{S}_K^* \boldsymbol{x}$). One version of the Block-Based CoSaMP algorithm in [6] involves computing the projection of a vector onto the column space of a modulated DPSS dictionary. The channel estimates proposed in [100] are based on the projection of the subcarrier coefficients onto the column space of the modulated multiband DPSS dictionary. Of course, one can also compress $\boldsymbol{x}$ by keeping the $K \approx 2NW$ Slepian basis coefficients $\boldsymbol{S}_K^* \boldsymbol{x}$ instead of the N entries of $\boldsymbol{x}$. Computationally, all of these problems benefit from having a fast Slepian transform: whereas direct matrix-vector multiplication would require $O(NK) = O(2WN^2)$ operations, the fast Slepian constructions allow these computations to be approximated in only $O\left(N \log N \log \frac{1}{\epsilon}\right)$ operations.

Prolate matrix linear systems.

Linear equations of the form $\boldsymbol{B}_{N,W}\boldsymbol{y} = \boldsymbol{b}$ arise naturally in signal processing. For example, suppose we obtain the length-N sampled bandlimited vector $\boldsymbol{x}$ as defined in (4.1) and we are interested in estimating the infinite-length sequence $x[n] = x(nT_s)$ for $n \in \mathbb{Z}$. The discrete-time signal $x[n]$ is assumed to be bandlimited to $[-W, W]$ for $W < \frac{1}{2}$. Let $\mathcal{I}_N : \ell_2(\mathbb{Z}) \to \mathbb{C}^N$ denote the index-limiting operator that restricts a sequence to its entries on $[N]$ (and produces a vector of length N); that is $\mathcal{I}_N(y)[m] := y[m]$ for $m \in [N]$. Also, recall that $\mathcal{B}_W : \ell_2(\mathbb{Z}) \to \ell_2(\mathbb{Z})$ denotes the band-limiting operator that bandlimits the DTFT of a discrete-time signal to the frequency range $[-W, W]$. Given $\boldsymbol{x}$, the least-squares estimate $\widehat{x}[n] \in \ell_2(\mathbb{Z})$ for the infinite-length bandlimited sequence takes the form

$$\widehat{x}[n] = [(\mathcal{I}_N\mathcal{B}_W)^\dagger \boldsymbol{x}][n] = \sum_{m=0}^{N-1} \boldsymbol{v}[m] \frac{\sin[2\pi W(n-m)]}{\pi(n-m)},$$

where $\boldsymbol{v} = \boldsymbol{B}_K^\dagger \boldsymbol{x}$.

Another problem involves linear prediction of bandlimited signals based on past samples. Suppose $x(t)$ is a continuous, zero-mean, wide sense stationary random process with power spectrum

$$P_x(F) = \begin{cases} \frac{1}{B_{\text{band}}}, & -\frac{B_{\text{band}}}{2} \le F \le \frac{B_{\text{band}}}{2}, \\ 0, & \text{otherwise.} \end{cases}$$

Let $x[n] = x(nT_s)$ denote the samples acquired from $x(t)$ with a sampling interval of $T_s \le \frac{1}{B_{\text{band}}}$. A linear prediction of $x[N]$ based on the previous N samples $x[0], x[1], \ldots, x[N-1]$ takes the form [5]

$$\widehat{x}[N] = \sum_{n=0}^{N-1} a_n x[n].$$

Choosing a_n such that $\widehat{x}[N]$ has the minimum mean-squared error is equivalent to solving

$$\min_{a_n} \varrho := \mathbb{E}\left[\left(\sum_{n=0}^{N-1} a_n x[n] - x[N]\right)^2\right].$$

Let $W = \frac{T_s}{2B_{\text{band}}}$. Taking the derivative of ϱ and setting it to zero yields

$$\boldsymbol{B}\boldsymbol{a} = \boldsymbol{b}$$

with $\boldsymbol{a} = [a_0\ a_1\ \cdots\ a_{N-1}]^T$ and $\boldsymbol{b} = \left[\frac{\sin(2\pi WN)}{\pi N}\ \frac{\sin(2\pi W(N-1))}{\pi(N-1)}\ \cdots\ \frac{\sin(2\pi W1)}{\pi 1}\right]^T$. Thus the optimal $\widehat{\boldsymbol{a}}$ is simply given by $\widehat{\boldsymbol{a}} = \boldsymbol{B}_K^\dagger \boldsymbol{b}$.

We present one more example: the Fourier extension [16]. The partial Fourier series sum

$$y_{N'}(t) = \frac{1}{\sqrt{2}} \sum_{|n|\leq N'} \widehat{y}_n e^{jn\pi t},\ \ \widehat{y}_n = \frac{1}{\sqrt{2}} \int_{-1}^{1} y(t) e^{-jn\pi t} dt$$

of a non-periodic function $y \in L_2([-1,1])$ (such as $y(t) = t$) suffers from the Gibbs phenomenon. One approach to overcome the Gibbs phenomenon is to extend the function y to a function g that is periodic on a larger interval $[-T,T]$ with $T > 1$ and compute the partial Fourier series of g [16]. Let $G_{N''}$ be the space of bandlimited $2T$-periodic functions

$$G_{N''} := \left\{ g : g(t) = \sum_{n=-N''}^{N''} \widehat{g}_n e^{\frac{jn\pi t}{T}},\ \widehat{g}_n \in \mathbb{C} \right\}.$$

The Fourier extension problem involves finding

$$g_{N''} := \arg\min_{g \in G_{N''}} \|y - g\|_{L_2([-1,1])}. \tag{4.3}$$

The solution $g_{N''}$ is called the Fourier extension of y to the interval $[-T,T]$. Let $\widehat{\boldsymbol{g}} = [\widehat{g}_{-N''}\ \cdots\ \widehat{g}_0\ \cdots\ \widehat{g}_{N''}]^T$ and define $\mathcal{F}_{N''} : L_2([-1,1]) \to \mathbb{C}^{2N''+1}$ as

$$(\mathcal{F}_{N''}(u))[n] = \frac{1}{\sqrt{2T}} \int_{-1}^{1} u(t) e^{-\frac{jn\pi t}{T}} dt,\ \ |n| \leq N''.$$

For convenience, here we index all vectors and matrices beginning at $-N''$. Any minimizer

$\widehat{\boldsymbol{g}}$ of the least-squares problem (4.3) must satisfy the normal equations

$$\mathcal{F}_{N''}\mathcal{F}_{N''}^{*}\widehat{\boldsymbol{g}} = \mathcal{F}_{N''}y, \tag{4.4}$$

where $\mathcal{F}_{N''}y$ can be efficiently approximately computed via the FFT. One can show that $\mathcal{F}_{N''}\mathcal{F}_{N''}^{*} = \boldsymbol{B}$, for $N = 2N'' + 1$ and $W = \frac{1}{2T} \leq \frac{1}{2}$.

Each of the above least-squares problems could be solved by computing a rank-K truncated pseudo-inverse of $\boldsymbol{B}$ with $K \approx 2NW$. Direct multiplication of this matrix with a vector, however, would require $O(NK) = O(2WN^2)$ operations. The fast methods we have developed allow a fast approximation to the truncated pseudo-inverse to be applied in only $O\left(N \log N + N \log(NW) \log \frac{1}{\epsilon}\right)$ operations.

4.4 Numerical Experiments

In this section, we perform numerical experiments to demonstrate the usefulness and computational efficiency of our fast Slepian methods.

Fast projection onto the span of $\boldsymbol{S}_K$

To test our fast factorization of $\boldsymbol{S}_K\boldsymbol{S}_K^{*}$ and our fast projection method, we fix the half-bandwidth $W = \frac{1}{4}$ and vary the signal length N over several values between 2^8 and 2^{20}. For each value of N we randomly generate several length-N vectors and project each one onto the span of the first $K = \text{round}(2NW)$ elements of the Slepian basis using the fast factorization $\boldsymbol{T}_1\boldsymbol{T}_2^{*}$ and the fast projection matrix $\boldsymbol{B} + \boldsymbol{S}_\epsilon\boldsymbol{D}_1\boldsymbol{S}_\epsilon^{*}$ for tolerances of $\epsilon = 10^{-3}$, 10^{-6}, 10^{-9}, and 10^{-12}. The prolate matrix, $\boldsymbol{B}$, is applied to the length N vectors via an FFT whose length is the smallest power of 2 that is at least $2N$. For values of $N \leq 12288$, we also projected each vector onto the span of the first K elements of the Slepian basis using the exact projection matrix $\boldsymbol{S}_K\boldsymbol{S}_K^{*}$. The exact projection could not be tested for values of $N > 12288$ due to computational limitations. A plot of the average time needed to project

a vector onto the span of the first $K = \text{round}(2NW)$ elements of the Slepian basis using the exact projection matrix $\boldsymbol{S}_K \boldsymbol{S}_K^*$ and the fast factorization $\boldsymbol{T}_1 \boldsymbol{T}_2^*$ is shown in the top left in Figure 4.1. A similar plot comparing the exact projection $\boldsymbol{S}_K \boldsymbol{S}_K^*$ and the fast projection $\boldsymbol{B} + \boldsymbol{S}_\epsilon \boldsymbol{D}_1 \boldsymbol{S}_\epsilon^*$ is shown in the top right in Figure 4.1. As can be seen in the figures the time required by the exact projection grows quadratically with N, while the time required by the fast factorization as well as the fast projection grows roughly linearly in N.

For the exact projection, all of the first $K = \text{round}(2NW)$ elements of the Slepian basis must be precomputed. For the fast factorization, the low rank matrices $\boldsymbol{L}_1, \boldsymbol{L}_2$ (from Theorem 5) and the Slepian basis elements $\boldsymbol{s}_k$ for k such that $\epsilon < \lambda_k < 1 - \epsilon$ are precomputed. For the fast projection, the FFT of the sinc kernel, as well as the Slepian basis elements $\boldsymbol{s}_k$ for k such that $\epsilon < \lambda_k < 1 - \epsilon$ are precomputed. A plot of the average precomputation time needed for both the exact projection $\boldsymbol{S}_K \boldsymbol{S}_K^*$ as well as the fast factorization $\boldsymbol{T}_1 \boldsymbol{T}_2^*$ is shown in the top left in Figure 4.2. A similar plot comparing the exact projection $\boldsymbol{S}_K \boldsymbol{S}_K^*$ and the fast projection $\boldsymbol{B} + \boldsymbol{S}_\epsilon \boldsymbol{D}_1 \boldsymbol{S}_\epsilon^*$ is shown in the top right in Figure 4.2. As can be seen in the figures the precomputation time required by the exact projection grows roughly quadratically with N, while the precomputation time required by the fast factorization as well as the fast projection grows just faster than linearly in N.

This experiment was repeated with $W = \frac{1}{16}$ and $W = \frac{1}{64}$ (instead of $W = \frac{1}{4}$). The results for $W = \frac{1}{16}$ and $W = \frac{1}{64}$ are shown in the middle and bottom, respectively, of Figures 4.1 and 4.2. The exact projection onto the first $K \approx 2NW$ elements of the Slepian basis takes $O(NK) = O(2WN^2)$ operations, whereas our fast factorization algorithm takes $O(N \log N \log \frac{1}{\epsilon})$ operations and our fast projection algorithm takes $O(N \log N + N \log(NW) \log \frac{1}{\epsilon})$ operations. The smaller W gets, the larger N needs to be for our fast methods to be faster than the exact projection via matrix multiplication. Our fast factorization and our fast projection lose their advantage over the exact factoriation and exact projection when $W \lesssim \frac{1}{N} \log N \log \frac{1}{\epsilon}$ and $W \lesssim \frac{1}{N} \log N + \frac{1}{N} \log(NW) \log \frac{1}{\epsilon}$ respectively. However, in this case the exact projection is fast enough to not require a fast

approximate algorithm.

Solving least-squares systems involving $\boldsymbol{B}$

We demonstrate the effectiveness of our fast prolate pseudoinverse method and our fast prolate Tikhonov regularization method on an instance of the Fourier extension problem, as described in Section 4.3.

To choose an appropriate function f, we note that if f is continuous and $f(-1) = f(1)$, then the Fourier sum approximations will not suffer from Gibbs phenomenon, and so, there is no need to compute a Fourier extension sum approximation for f. Also, if f is smooth on $[-1, 1]$ but $f(-1) \neq f(1)$, then the Fourier sum approximations will suffer from Gibbs phenomenon, but the Fourier extension series coefficients will decay exponentially fast. Hence, relatively few Fourier extension series coefficients will be needed to accurately approximate f, which makes the least squares problem of solving for these coefficients small enough for our fast methods to not be useful. However, in the case where f is continuous but not smooth on $[-1, 1]$ and $f(-1) \neq f(1)$, the Fourier series will suffer from Gibbs phenomenon, and the Fourier extension series coefficients will decay faster than the Fourier series coefficients, but not exponentially fast. So in this case, the number of Fourier extension series coefficients required to accurately approximate f is not trivially small, but still less than the number of Fourier series coefficients required to accurately approximate f. Hence, computing a Fourier extension sum approximation to f is useful and requires our fast methods.

We construct such a function $f : [-1, 1] \to \mathbb{R}$ in the form

$$f(t) = a_0 t + \sum_{\ell=1}^{L} a_\ell \exp\left(-\frac{|t - \mu_\ell|}{\sigma_\ell}\right)$$

where $a_0 = 5$, $L = 500$, and a_ℓ, μ_ℓ, and σ_ℓ are chosen in a random manner. A plot of $f(t)$ over $t \in [-1, 1]$ is shown on the left in Figure 4.3. Also on the right in Figure 4.3, we show

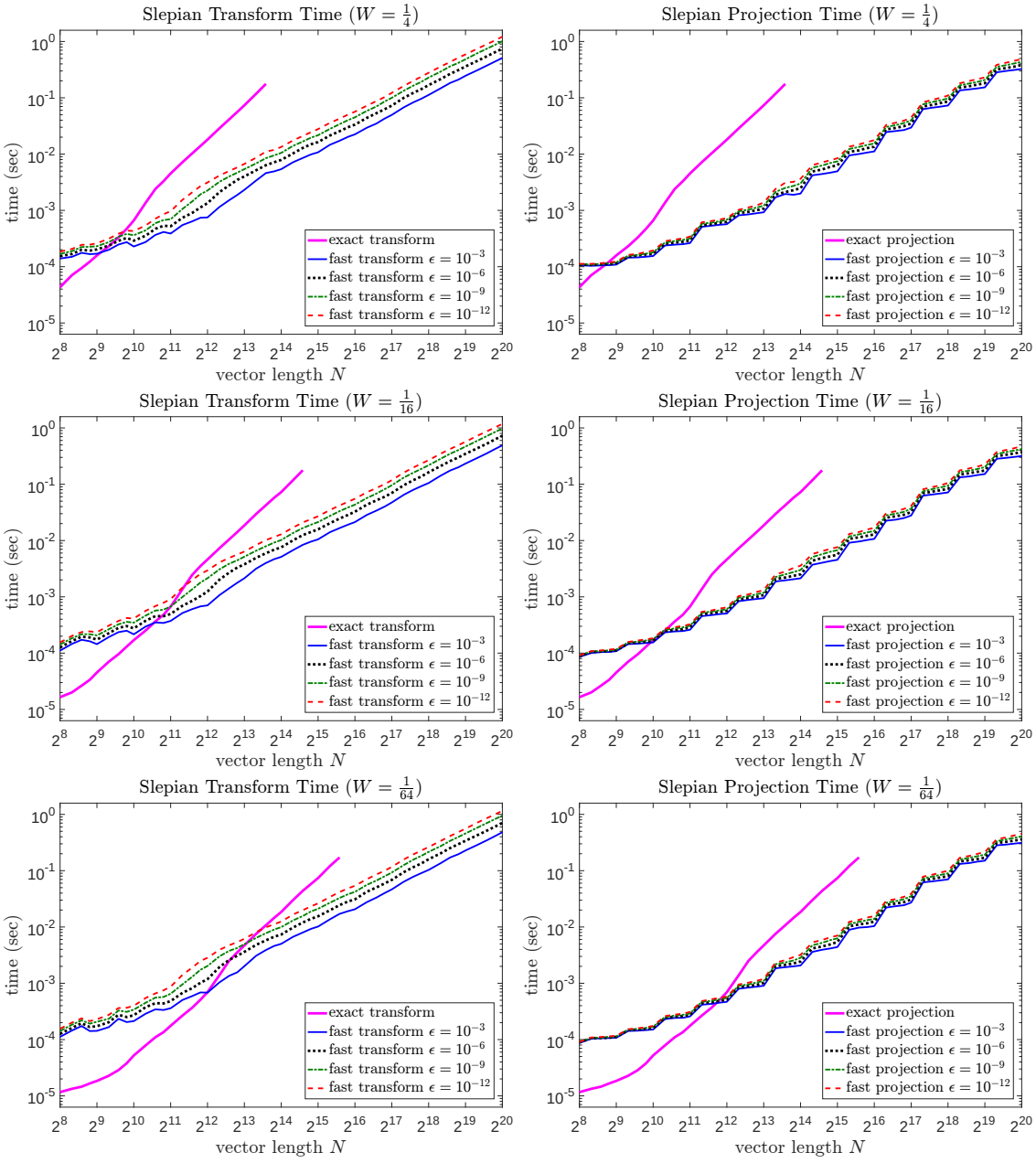

Figure 4.1: *(Left) Plots of the average time needed to project a vector onto the first* $\mathrm{round}(2NW)$ *Slepian basis elements using the exact projection* $\boldsymbol{S}_K\boldsymbol{S}_K^*$ *and using the fast factorization* $\boldsymbol{T}_1\boldsymbol{T}_2^*$. *(Right) Plots of the average time needed to project a vector onto the first* $\mathrm{round}(2NW)$ *Slepian basis elements using the exact projection* $\boldsymbol{S}_K\boldsymbol{S}_K^*$ *and using the fast projection* $\boldsymbol{B} + \boldsymbol{S}_\epsilon\boldsymbol{D}_1\boldsymbol{S}_\epsilon^*$.

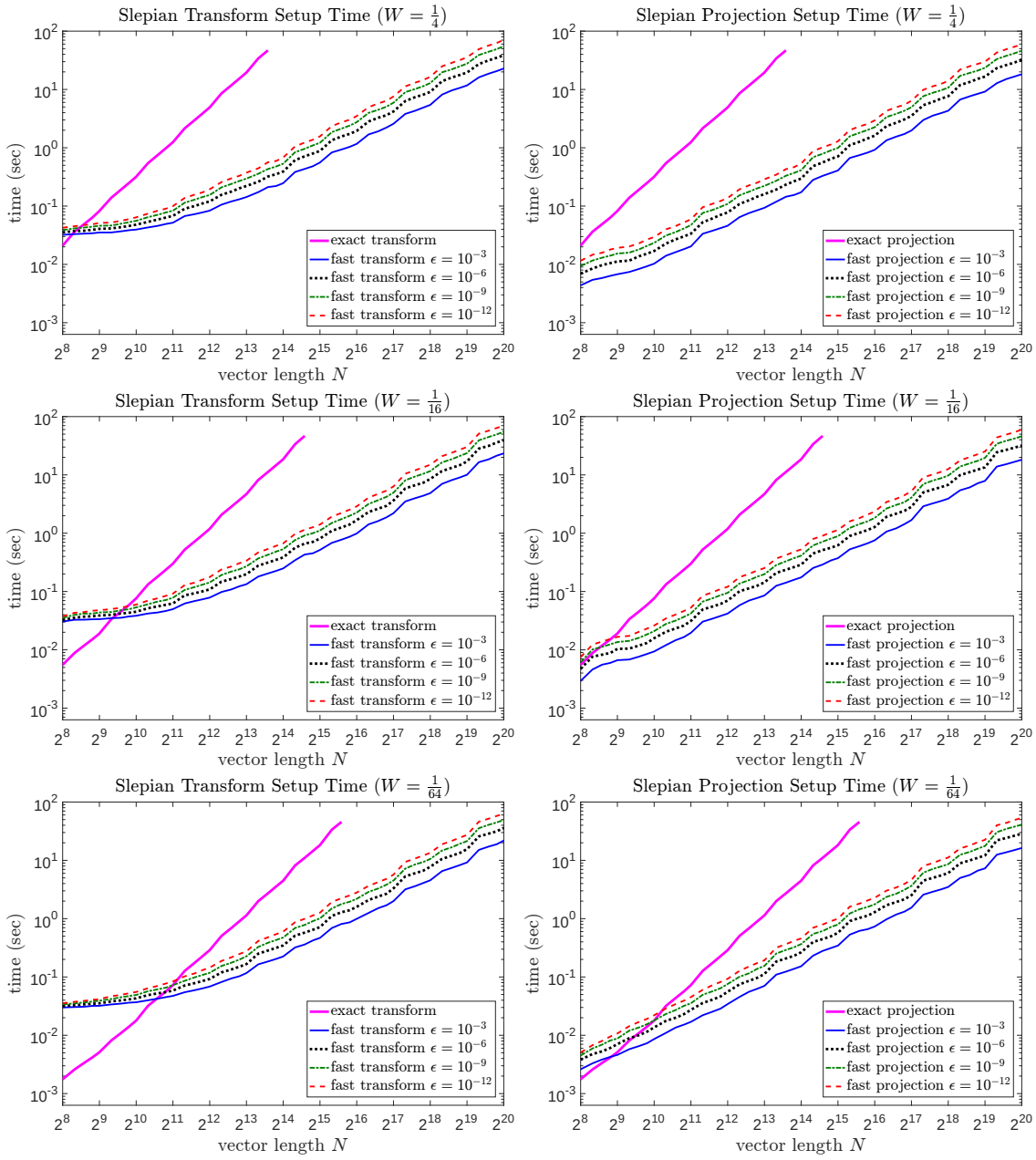

Figure 4.2: *(Left) Plots of the average precomputation time for the exact projection* $\boldsymbol{S}_K \boldsymbol{S}_K^*$ *and the fast factorization* $\boldsymbol{T}_1 \boldsymbol{T}_2^*$. *(Right) Plots of the average precomputation time for the exact projection* $\boldsymbol{S}_K \boldsymbol{S}_K^*$ *and the fast projection* $\boldsymbol{B} + \boldsymbol{S}_\epsilon \boldsymbol{D}_1 \boldsymbol{S}_\epsilon^*$.

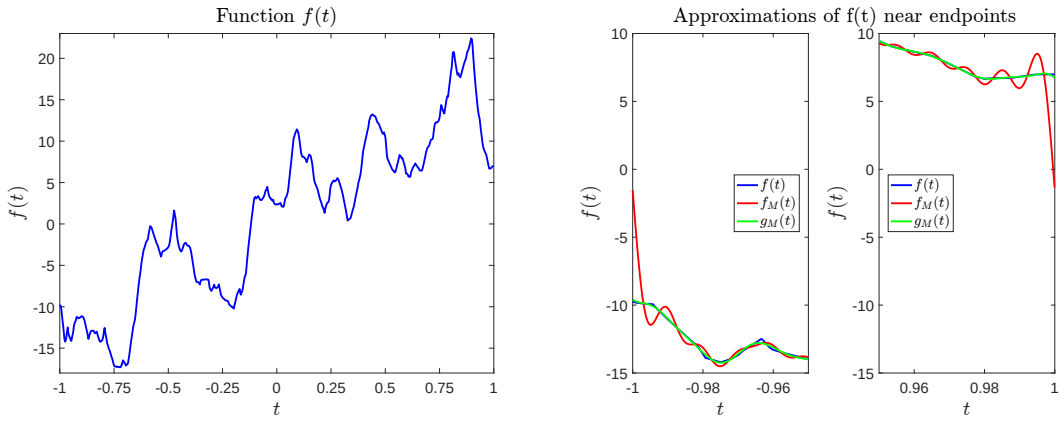

Figure 4.3: *(Left) A plot of the function used in the experiments described in Section 4.4. (Right) Plots of the function, the Fourier sum approximation to $f(t)$ using 401 terms, and the Fourier extension approximation to $f(t)$ using 401 terms. Note that the Fourier sum approximation suffers from Gibbs phenomenon oscillations while the Fourier extension sum does not.*

an example of a Fourier sum approximation and a Fourier extension approximation, both with 401 terms. Notice that the Fourier sum approximation suffers from Gibbs phenomenon near the endpoints of the interval $[-1, 1]$, while the Fourier extension approximation does not exhibit such oscillations near the endpoints of $[-1, 1]$.

For several positive integers M between 1 and 2560, we compute three approximations to $f(t)$:

1. The $2M + 1$ term truncated Fourier series of $f(t)$, i.e.,

$$f_M(t) = \frac{1}{\sqrt{2}} \sum_{m=-M}^{M} \widehat{f}_m e^{j\pi mt},$$

where

$$\widehat{f}_m = \frac{1}{\sqrt{2}} \int_{-1}^{1} f(t) e^{j\pi mt}\, dt.$$

2. The $2M + 1$ term Fourier extension of $f(t)$ to the interval $[-T, T]$, i.e.,

$$g_M(t) = \frac{1}{\sqrt{2T}} \sum_{m=-M}^{M} \widehat{g}_m e^{j\pi mt/T}$$

where

$$\widehat{y}_m = \frac{1}{\sqrt{2T}} \int_{-1}^{1} f(t) e^{j\pi m t/T}\, dt,$$

and

$$\widehat{g} = \boldsymbol{B}_K^{\dagger} \widehat{y}.$$

Here, we set $T = 1.5$, and we let $\boldsymbol{B}$ be the prolate matrix with $N = 2M + 1$ and $W = \frac{1}{2T}$, and we let $\boldsymbol{B}_K^{\dagger}$ be the truncated pseudoinverse of $\boldsymbol{B}$ which zeros out eigenvalues λ_k smaller than 10^{-4}.

3. The $2M + 1$ term Fourier extension of $f(t)$ to the interval $[-T, T]$ (as described above), except we use the fast prolate pseudoinverse method (Theorem 4b) with tolerance $\epsilon = 10^{-5}$ instead of the exact truncated pseudoinverse.

The integrals used in computing the coefficients are approximated using an FFT of length 2^{13+q} where $q = \lfloor \log_2 M \rfloor$. By increasing the FFT length with M, we ensure that the coefficients are sufficiently approximated, while also ensuring that the time needed to compute the FFT does not dominate the time needed to solve the system $\boldsymbol{B}\widehat{g} = \widehat{y}$. Given an approximation $\hat{f}(t)$ to $f(t)$, we quantify the performance via the relative root-mean-square (RMS) error:

$$\frac{\|f - \hat{f}\|_{L_2([-1,1])}}{\|f\|_{L_2([-1,1])}}$$

A plot of the relative RMS error versus M for each of the three approximations to $f(t)$ is shown on the left in Figure 4.4. For values of M at least 448, the Fourier extension $g_M(t)$ (computed with either the exact or the fast pseudoinverse) yielded a relative RMS error at least 10 times lower than that for the truncated Fourier series $f_M(t)$. Using the exact pseudoinverse instead of the fast pseudoinverse does not yield a noticable improvement in the approximation error. A plot of the average time needed to compute the approximation coefficients versus M is shown on the right in Figure 4.4. For large

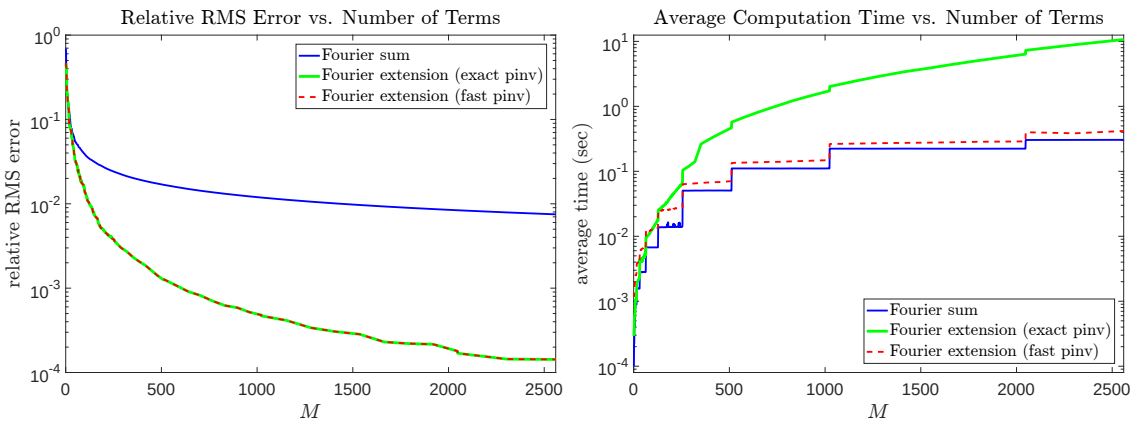

Figure 4.4: *A comparison of the relative RMS error (left) and the computation time required (right) for the* $2M+1$ *term truncated Fourier series as well as the* $2M+1$ *term Fourier extension using both the exact and fast pseudoinverse methods. Note that the exact and fast methods are virtually indistinguishable in terms of relative RMS error.*

M, computing the Fourier extension coefficients using the fast prolate pseudoinverse is significantly faster than computing the Fourier extension coefficients using the fast prolate pseudoinverse. Also, computing the Fourier extension coefficients using the fast prolate pseudoinverse takes only around twice the time required for computing the Fourier series coefficients.

We repeated this experiment, except using Tikhonov regularization to solve the system $\boldsymbol{B}\widehat{g} = \widehat{y}$ instead of the truncated pseudoinverse. We tested both the exact Tikhonov regularization procedure $\widehat{g} = (\boldsymbol{B}^2 + \alpha \mathbf{I})^{-1}\boldsymbol{B}\widehat{y}$ (for $\alpha = 10^{-8}$) as well as the fast Tikhonov regularization method (Theorem 4c) with a tolerance of $\epsilon = 10^{-5}$. The results, which are similar to those for the pseudoinverse case, are shown in Figure 4.5.

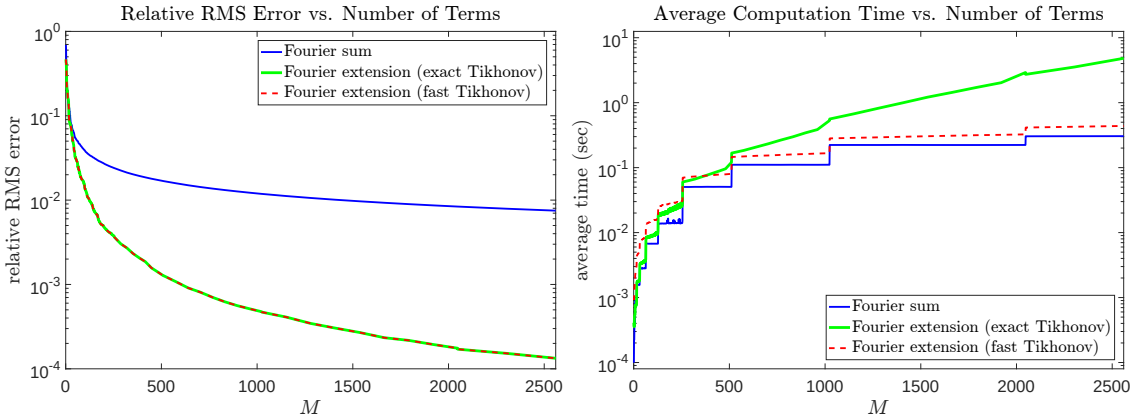

Figure 4.5: *A comparison of the relative RMS error (left) and the computation time required (right) for the* $2M + 1$ *term truncated Fourier series as well as the* $2M + 1$ *term Fourier extension using both the exact and fast Tikhonov regularization methods. Note that the exact and fast methods are virtually indistinguishable in terms of relative RMS error.*

CHAPTER 5

THOMSON'S MULTITAPER METHOD FOR SPECTRAL ESTIMATION

In this chapter, we present non-asymptotic results regarding some of the statistical properties of Thomson's multitaper spectral estimator. In particular, we show that by using $K = 2NW - O(\log(NW))$ tapers instead of the traditional choice of $K = 2NW - O(1)$ tapers can significantly reduce the effects of spectral leakage, which is especially important when the underlying power spectrum has a high dynamic range. We also present a fast algorithm to approximate Thomson's multitaper method on a grid of evenly spaced frequencies which requires only $O(\log(NW)\log\frac{1}{\epsilon})$ FFTs instead of $K \approx 2NW$ FFTs. This is useful in problems where many samples are taken, and thus, using many tapers is desirable. Material in this section has appeared in [101, 102]

5.1 Statistical Properties and Spectral Leakage

For a given vector of signal samples $\boldsymbol{x} \in \mathbb{C}^N$, using Thomson's multitaper method for spectral estimation requires selecting two parameters: the half-bandwidth W of the Slepian basis tapers and the number of tapers K which are used in the multitaper spectral estimate. The selection of these parameters can greatly impact the accuracy of the multitaper spectral estimate.

In some applications, a relatively small number of samples N are taken, and the desired frequency resolution for the spectral estimate is $O(\frac{1}{N})$, i.e., a small multiple of the fundamental Rayleigh resolution limit. In such cases, many practitioners [30, 33, 35, 36, 38, 41, 44, 45] choose the half-bandwidth parameter W such that $2NW$ is between 3 and 10, and then choose the number of Slepian basis tapers to be between $K = \lfloor 2NW \rfloor$ and $K = \lfloor 2NW \rfloor - 2$. However, in applications where a large number of samples N are taken, and some loss of resolution is acceptable, choosing a larger half-bandwidth parameter W

can result in a more accurate spectral estimate. Furthermore, if the power spectral density $S(f)$ has a high dynamic range (that is $\max_f S(f) \gg \min_f S(f)$), we aim to show that choosing $K = 2NW - O(\log(NW)\log\frac{1}{\delta})$ tapers for some small $\delta > 0$ (instead of $K = 2NW - O(1)$ tapers) can provide significantly better protection against spectral leakage.

For all the theorems in this section, we assume that $\boldsymbol{x} \in \mathbb{C}^N$ is a vector of samples from a complex Gaussian process whose power spectral density $S(f)$ is bounded and integrable. Note that the analogous results for a real Gaussian process would be similar, but slightly more complicated to state. To state our results, define

$$M = \max_{f \in \mathbb{R}} S(f),$$

i.e., the global maximum of the power spectral density, and for each frequency $f \in \mathbb{R}$ we define:

$$m_f = \min_{f' \in [f-W, f+W]} S(f'),$$

$$M_f = \max_{f' \in [f-W, f+W]} S(f'),$$

$$A_f = \frac{1}{2W} \int_{f-W}^{f+W} S(f')\, df',$$

$$R_f = \sqrt{\frac{1}{2W} \int_{f-W}^{f+W} S(f')^2\, df'},$$

i.e. the minimum, maximum, average, and root-mean-squared values of the power spectral density over the interval $[f - W, f + W]$. We also define the quantities

$$\Sigma_K^{(1)} = \frac{1}{K} \sum_{k=0}^{K-1} (1 - \lambda_k)$$

$$\Sigma_K^{(2)} = \sqrt{\frac{1}{K} \sum_{k=0}^{K-1} (1 - \lambda_k)^2}.$$

Before we proceed to our results, we make note of the fact that m_f, M_f, A_f, and R_f are all "local" properties of the power spectral density, i.e., they depend only on values of $S(f')$ for $f' \in [f - W, f + W]$, whereas M is a "global" property. Note that if the power spectral density is "slowly varying" over the interval $[f - W, f + W]$, then $m_f \approx M_f \approx A_f \approx R_f \approx S(f)$. However, M could be several orders of magnitude larger than m_f, M_f, A_f, and R_f if the power spectral density has a high dynamic range.

By using the bound on the Slepian basis eigenvalues in Corollary 1, we can obtain $\lambda_{K-1} \geq 1 - \delta$ for some suitably small $\delta > 0$ by choosing the number of tapers to be $K = 2NW - O(\log(NW) \log \frac{1}{\delta})$. This choice of K guarantees that $0 \leq \Sigma_K^{(1)} \leq \Sigma_K^{(2)} \leq 1 - \lambda_{K-1} \leq \delta$, i.e., $\Sigma_K^{(1)}$, $\Sigma_K^{(2)}$, and $1 - \lambda_{K-1}$ are all small, and thus, the global property $M = \max_f S(f)$ of the power spectral density will have a minimal impact on the non-asymptotic results below. In other words, using $K = 2NW - O(\log(NW) \log \frac{1}{\delta})$ tapers mitigates the ability for values of the power spectral density $S(f')$ at frequencies $f' \notin [f - W, f + W]$ to impact the estimate $\widehat{S}_K^{\text{mt}}(f)$. However, if $K = 2NW - O(1)$ tapers are used, then the quantities $\Sigma_K^{(1)}$, $\Sigma_K^{(2)}$, and $1 - \lambda_{K-1}$ could be large enough for the global property $M = \max_f S(f)$ of the power spectral density to significantly weaken the non-asymptotic results below. In other words, energy in the power spectral density $S(f')$ at frequencies $f' \notin [f - W, f + W]$ can "leak" into the estimate $\widehat{S}_K^{\text{mt}}(f)$.

We begin with a bound on the bias of the multitaper spectral estimate under the additional assumption that the power spectral density is twice differentiable. Note this assumption is only used in Theorem 6.

Theorem 6. *For any frequency $f \in \mathbb{R}$, if $S(f')$ is twice continuously differentiable in $[f - W, f + W]$, then the bias of the multitaper spectral estimate is bounded by*

$$\text{Bias}\left[\widehat{S}_K^{mt}(f)\right] = \left|\mathbb{E}\widehat{S}_K^{mt}(f) - S(f)\right| \leq \frac{M_f'' NW^3}{3K} + (M + M_f)\Sigma_K^{(1)},$$

where

$$M_f'' = \max_{f' \in [f-W, f+W]} |S''(f')|.$$

If $K = 2NW - O(\log(NW) \log \frac{1}{\delta})$ tapers are used for some small $\delta > 0$, then this upper bound is slightly larger than $\frac{1}{6} M_f'' W^2$, which is similar to the asymptotic results in [9, 103–106] which state that the bias is roughly $\frac{1}{6} S''(f) W^2$. However, if $K = 2NW - O(1)$ tapers are used, the term $(M + M_f)\Sigma_K^{(1)}$ could dominate this bound, and the bias could be much larger than the asymptotic result.

If the power spectral density is not twice-differentiable, we can still obtain the following bound on the bias of the multitaper spectral estimate.

Theorem 7. *For any frequency $f \in \mathbb{R}$, the bias of the multitaper spectral estimate is bounded by*

$$\text{Bias}\left[\widehat{S}_K^{mt}(f)\right] = \left|\mathbb{E}\widehat{S}_K^{mt}(f) - S(f)\right| \leq (M_f - m_f)(1 - \Sigma_K^{(1)}) + M\Sigma_K^{(1)}.$$

If $K = 2NW - O(\log(NW) \log \frac{1}{\delta})$ tapers are used for some small $\delta > 0$, then this upper bound is slightly larger than $M_f - m_f$. This guarantees the bias is small when the power spectral density is "slowly varying" over $[f - W, f + W]$. However, if $K = 2NW - O(1)$ tapers are used, the term $M\Sigma_K^{(1)}$ could dominate this bound, and the bias could be much larger than the asymptotic result.

Next, we state our bound on the variance of the multitaper spectral estimate.

Theorem 8. *For any frequency $f \in \mathbb{R}$, the variance of the multitaper spectral estimate is bounded by*

$$\text{Var}\left[\widehat{S}_K^{mt}(f)\right] \leq \frac{1}{K}\left(R_f\sqrt{\frac{2NW}{K}} + M\Sigma_K^{(2)}\right)^2.$$

If $K = 2NW - O(\log(NW) \log \frac{1}{\delta})$ tapers are used for some small $\delta > 0$, then this upper bound is slightly larger than $\frac{1}{K} R_f^2$, which is similar to the asymptotic results in [9, 103–106] which state that the variance is roughly $\frac{1}{K} S(f)^2$. However, if $K = 2NW - O(1)$

tapers are used, the term $M\Sigma_K^{(2)}$ could dominate this bound, and the variance could be much larger than the asymptotic result.

We also note that if the frequencies f_1, f_2 are more than $2W$ apart, then the multitaper spectral estimates at those frequencies have a very low covariance.

Theorem 9. *For any frequencies $f_1, f_2 \in \mathbb{R}$ such that $2W < |f_1 - f_2| < 1 - 2W$, the covariance of the multitaper spectral estimates at those frequencies is bounded by*

$$0 \leq \mathrm{Cov}\left[\widehat{S}_K^{mt}(f_1), \widehat{S}_K^{mt}(f_2)\right] \leq \left((R_{f_1} + R_{f_2})\sqrt{\frac{2NW}{K}\Sigma_K^{(1)}} + M\Sigma_K^{(1)}\right)^2.$$

If $K = 2NW - O(\log(NW)\log\frac{1}{\delta})$ tapers are used for some small $\delta > 0$, then the covariance is guaranteed to be small. However, if $K = 2NW - O(1)$ tapers are used, the upper bound is no longer guaranteed to be small, and the covariance could be large.

Finally, we also provide a concentration result for the multitaper spectral estimate.

Theorem 10. *For any frequency $f \in \mathbb{R}$, the multitaper spectral estimate satisfies the concentration inequalities*

$$\mathbb{P}\left\{\widehat{S}_K^{mt}(f) \geq \beta\mathbb{E}\widehat{S}_K^{mt}(f)\right\} \leq \beta^{-1}\mathrm{e}^{-\kappa_f(\beta-1-\ln\beta)} \quad \textit{for} \quad \beta > 1,$$

and

$$\mathbb{P}\left\{\widehat{S}_K^{mt}(f) \leq \beta\mathbb{E}\widehat{S}_K^{mt}(f)\right\} \leq \mathrm{e}^{-\kappa_f(\beta-1-\ln\beta)} \quad \textit{for} \quad 0 < \beta < 1,$$

where the frequency dependent constant κ_f satisfies

$$\kappa_f \geq \frac{K\left(1 - \Sigma_K^{(1)}\right)M_f - 2NW(M_f - A_f)}{M_f + (M - M_f)(1 - \lambda_{K-1})}.$$

We note that these are identical to the concentration bounds for a chi-squared random variable with $2\kappa_f$ degrees of freedom. If $K = 2NW - O(\log(NW)\log\frac{1}{\delta})$ tapers are used for some small $\delta > 0$ and the power spectral density is "slowly varying" over $[f - W, f +$

$W]$, then this lower bound on κ_f is slightly less than K. Hence, $\widehat{S}_K^{\text{mt}}(f)$ has a concentration behavior that is similar to a chi-squared random variable with $2K$ degrees of freedom, as the asymptotic results in [9, 107] suggest. However, if $K = 2NW - O(1)$ tapers are used, then κ_f could be much smaller, and thus, the multitaper spectral estimate would have significantly worse concentration about its mean.

The proofs of Theorems 6-10 are given in Appendix C.1. In Section 5.3, we perform simulations demonstrating that using $K = 2NW - O(1)$ tapers results in a multitaper spectral estimate that is vulnerable to spectral leakage, whereas using $K = 2NW - O(\log(NW) \log \frac{1}{\delta})$ tapers for a suitably small $\delta > 0$ significantly reduces the impact of spectral leakage on the multitaper spectral estimate.

5.2 Fast Algorithms

Given a vector of N samples $\boldsymbol{x} \in \mathbb{C}^N$, evaluating the multitaper spectral estimate $\widehat{S}_K^{\text{mt}}(f)$ at a grid of L evenly spaced frequencies $f \in [L]/L$ (where we assume $L \geq N$) can be done in $O(KL \log L)$ operations and using $O(KL)$ memory via K length-L fast Fourier transforms (FFTs). In applications where the number of samples N is small, the number of tapers K used is usually a small constant, and so, the computational requirements are a small constant factor more than that of an FFT. However in many applications, using a large number of tapers is desirable, but the computational requirements make this impractical. As mentioned in Section 2.5, if the power spectrum $S(f)$ is twice-differentiable, then the MSE of the multitaper spectral estimate is minimized when the bandwidth parameter is $W = O(N^{-1/5})$ and $K = O(N^{4/5})$ tapers are used [105]. For medium to large scale problems, precomputing and storing $O(N^{4/5})$ tapers and/or performing $O(N^{4/5})$ FFTs may be impractical.

In this section, we present an ϵ-approximation $\widetilde{S}_K^{\text{mt}}(f)$ to the multitaper spectral estimate $\widehat{S}_K^{\text{mt}}(f)$ which requires $O(L \log L \log(NW) \log \frac{1}{\epsilon})$ operations and $O(L \log(NW) \log \frac{1}{\epsilon})$ memory. This is faster than the exact multitaper spectral estimation provided the number of

tapers satisfies $K \gtrsim \log(NW) \log \frac{1}{\epsilon}$.

To construct this approximation, we first fix a tolerance parameter $\epsilon \in (0, \frac{1}{2})$, and suppose that the number of tapers, K, is chosen such that $\lambda_{K-1} \geq \frac{1}{2}$ and $\lambda_K \leq 1 - \epsilon$. Note that this is a very mild assumption as it only forces K to be slightly less than $2NW$. Next, we partition the indices $[N]$ into four sets:

$$\begin{aligned}
\mathcal{I}_1 &= \{k \in [K] : \lambda_k \geq 1 - \epsilon\} \\
\mathcal{I}_2 &= \{k \in [K] : \epsilon < \lambda_k < 1 - \epsilon\} \\
\mathcal{I}_3 &= \{k \in [N] \setminus [K] : \epsilon < \lambda_k < 1 - \epsilon\} \\
\mathcal{I}_4 &= \{k \in [N] \setminus [K] : \lambda_k \leq \epsilon\}
\end{aligned}$$

and define the approximate estimator

$$\widetilde{S}_K^{\text{mt}}(f) := \frac{1}{K}\Psi(f) + \frac{1}{K}\sum_{k \in \mathcal{I}_2}(1 - \lambda_k)\widehat{S}_k(f) - \frac{1}{K}\sum_{k \in \mathcal{I}_3}\lambda_k \widehat{S}_k(f),$$

where

$$\Psi(f) := \sum_{k=0}^{N-1} \lambda_k \widehat{S}_k(f).$$

Both $\widehat{S}_K^{\text{mt}}(f)$ and $\widetilde{S}_K^{\text{mt}}(f)$ are weighted sums of the single taper estimates $\widehat{S}_k(f)$ for $k \in [N]$. Additionally, it can be shown that the weights are similar, i.e., the first K weights are exactly or approximately $\frac{1}{K}$, and the last $N - K$ weights are exactly or approximately 0. Hence, it is reasonable to expect that $\widetilde{S}_K^{\text{mt}}(f) \approx \widehat{S}_K^{\text{mt}}(f)$. The following theorem shows that is indeed the case.

Theorem 11. *The approximate multitaper spectral estimate $\widetilde{S}_K^{mt}(f)$ defined above satisfies*

$$\left|\widetilde{S}_K^{mt}(f) - \widehat{S}_K^{mt}(f)\right| \leq \frac{\epsilon}{K}\|\boldsymbol{x}\|_2^2 \quad \textit{for all} \quad f \in \mathbb{R}.$$

Furthermore, we show in Lemma 13 that $\Psi(f) = \boldsymbol{x}^* \boldsymbol{E}_f \boldsymbol{B} \boldsymbol{E}_f^* \boldsymbol{x}$. This formula doesn't

involve any of the Slepian tapers. By exploiting the fact that the prolate matrix $\boldsymbol{B}$ is Toeplitz, we also show in Lemma 13 that if $L \geq 2N$, then

$$\left[\Psi(\tfrac{0}{L}) \quad \Psi(\tfrac{1}{L}) \quad \cdots \quad \Psi(\tfrac{L-2}{L}) \quad \Psi(\tfrac{L-1}{L})\right]^T = \boldsymbol{F}^{-1}\left(\boldsymbol{b} \circ \boldsymbol{F}\left|\boldsymbol{F}\boldsymbol{Z}\boldsymbol{x}\right|^2\right),$$

where $\boldsymbol{Z} \in \mathbb{R}^{L\times N}$ is a matrix which zero-pads length-N vectors to length-L, $\boldsymbol{F} \in \mathbb{C}^{L\times L}$ is a length-L FFT matrix, $\boldsymbol{b} \in \mathbb{R}^L$ is the first column of the matrix formed by extending the prolate matrix $\boldsymbol{B}$ to an $L \times L$ circulant matrix, $|\cdot|^2$ denotes the pointwise magnitude-squared, and $\circ$ denotes a pointwise multiplication. Hence, $\Psi(f)$ can be evaluated at a grid of L evenly spaced frequencies $f \in [L]/L$ in $O(L\log L)$ operations via three length-L FFTs/inverse FFTs. Evaluating the other $\#(\mathcal{I}_2 \cup \mathcal{I}_3) = O(\log(NW)\log\frac{1}{\epsilon})$ terms in the expression for $\widetilde{S}_K^{\text{mt}}(f)$ at the L grid frequencies can be done in $O(L\log L\log(NW)\log\frac{1}{\epsilon})$ operations via $\#(\mathcal{I}_2 \cup \mathcal{I}_3)$ length-L FFTs. Using these results, we establish the following theorem which states how quickly $\widetilde{S}_K^{\text{mt}}(f)$ can be evaluated at the grid frequencies.

Theorem 12. *For any vector of samples $\boldsymbol{x} \in \mathbb{C}^N$ and any number of grid frequencies $L \geq N$, the approximate multitaper spectral estimate $\widetilde{S}_K^{mt}(f)$ can be evaluated at the L grid frequencies $f \in [L]/L$ in $O(L\log L\log(NW)\log\frac{1}{\epsilon})$ operations and using $O(L\log(NW)\log\frac{1}{\epsilon})$ memory.*

Note if $N \leq L < 2N$, we can apply the method briefly described above to evaluate $\Psi(f)$ at $f \in [2L]/2L$, and then downsample the result. The proofs of Theorems 11 and 12 are given in Appendix C.2. In Section 5.3, we perform simulations comparing the time needed to evaluate $\widehat{S}_K^{\text{mt}}(f)$ and $\widetilde{S}_K^{\text{mt}}(f)$ at a grid of frequencies.

5.3 Numerical Experiments

In this section, we show simulations to demonstrate three observations. (1) Using $K = 2NW - O(\log(NW))$ tapers instead of the traditional choice of $K = \lfloor 2NW\rfloor - 1$ tapers significantly reduce the effects of spectral leakage. (2) Using a larger bandwidth W, and

thus, more tapers can produce a more robust spectral estimate. (3) As the number of samples N and the number of tapers K grows, our approximation $\widetilde{S}_K^{\text{mt}}(f)$ becomes significantly faster to use than the exact multitaper spectral estimate $\widehat{S}_K^{\text{mt}}(f)$.

First, we demonstrate that choosing $K = 2NW - O(\log(NW))$ tapers instead of the traditional choice of $K = \lfloor 2NW \rfloor - 1$ tapers significantly reduces the effects of spectral leakage. We fix a signal length of $N = 2000$, a bandwidth parameter of $W = \frac{1}{100}$ (so $2NW = 40$) and consider four choices for the number of tapers: $K = 39$, 36, 32, and 29. Note that $K = 39 = \lfloor 2NW \rfloor - 1$ is the traditional choice as to how many tapers to use, while 36, 32, and 29 are the largest values of K such that λ_{K-1} is at least $1 - 10^{-3}$, $1 - 10^{-6}$, and $1 - 10^{-9}$ respectively.

In Figure 5.1, we show three plots of the spectral window

$$\psi(f) = \frac{1}{K} \sum_{k=0}^{K-1} \left| \sum_{n=0}^{N-1} \boldsymbol{s}_k[n] e^{-j2\pi fn} \right|^2$$

of the multitaper spectral estimate for each of those values of K. At the top of Figure 5.1, we plot $\psi(f)$ over the entire range $[-\frac{1}{2}, \frac{1}{2}]$ using a logarithmic scale. The lines outside appear thick due to the highly oscillatory behavior of $\psi(f)$. This can be better seen in the middle of Figure 5.1, where we plot $\psi(f)$ over $[-2W, 2W]$ using a logarithmic scale. The behavior of $\psi(f)$ inside $[-W, W]$ can be better seen at the bottom of Figure 5.1, where we plot $\psi(f)$ over $[-2W, 2W]$ using a linear scale.

All four spectral windows have similar behavior in that $\psi(f)$ is small outside $[-W, W]$ and large near 0. However, outside of $[-W, W]$ the spectral windows using $K = \lfloor 2NW \rfloor - O(\log(NW))$ tapers are multiple orders of magnitude smaller than the spectral window using $K = \lfloor 2NW \rfloor - 1$ tapers. Hence, the amount of spectral leakage can be reduced by multiple orders of magnitude by trimming the number of tapers used from $K = \lfloor 2NW \rfloor - 1$ to $K = 2NW - O(\log(NW))$.

We further demonstrate the importance of using $K = 2NW - O(\log(NW))$ tapers

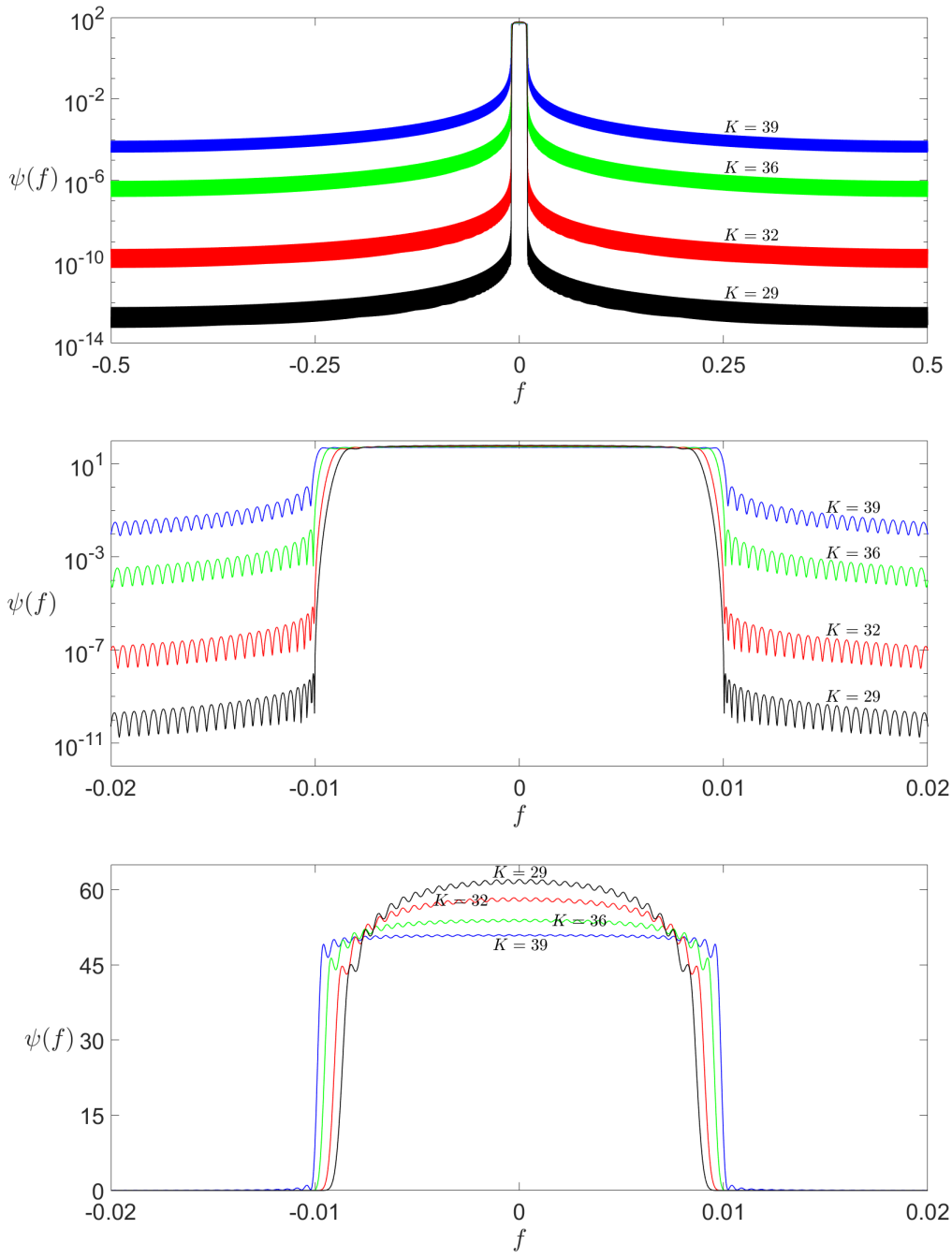

Figure 5.1: Plots of the spectral windows $\psi(f)$ for $N = 2000$, $W = \frac{1}{100}$, and $K = 39$, 36, 32, and 29 tapers. (Top) A logarithmic scale plot over $f \in [-\frac{1}{2}, \frac{1}{2}]$. (Middle) A logarithmic scale plot over $f \in [-2W, 2W]$. (Bottom) A linear scale plot over $f \in [-2W, 2W]$.

to reduce spectral leakage by showing a signal detection example. We generate a vector $\boldsymbol{x} \in \mathbb{C}^N$ of $N = 2000$ samples of a Gaussian random process with a power spectral density function of

$$S(f) = \begin{cases} 10^3 & \text{if } f \in [0.18, 0.22] \\ 10^9 & \text{if } f \in [0.28, 0.32] \\ 10^2 & \text{if } f \in [0.38, 0.42] \\ 10^1 & \text{if } f \in [0.78, 0.82] \\ 10^0 & \text{else} \end{cases}.$$

This simulates an antenna receiving signals from four narrowband sources with some background noise. Note that one source is significantly stronger than the other three sources. In Figure 5.2, we plot:

- the periodogram of $\boldsymbol{x}$,
- the multitaper spectral estimate of $\boldsymbol{x}$ with $W = \frac{1}{100}$ and $K = \lfloor 2NW \rfloor - 1 = 39$ tapers,
- the multitaper spectral estimate of $\boldsymbol{x}$ with $W = \frac{1}{100}$ and $K = 29$ tapers (chosen so $\lambda_{K-1} \geq 1 - 10^{-9}$).

We note that all three spectral estimates yield large values in the frequency band $[0.28, 0.32]$. However, in the periodogram and the multitaper spectral estimate with $K = 39$ tapers, the energy in the frequency band $[0.28, 0.32]$ "leaks" into the frequency bands occupied by the smaller three sources. As a result, the smaller three sources are hard to detect using the periodogram or the multitaper spectral estimate with $K = 39$ tapers. However, all four sources are clearly visible when looking at the multitaper spectral estimate with $K = 29$ tapers. For frequencies f not within W of the edges of the frequency band, the multitaper spectral estimate is within a small constant factor of the true power spectral density.

Next, we demonstrate a few key points about selecting the bandwidth parameter W and

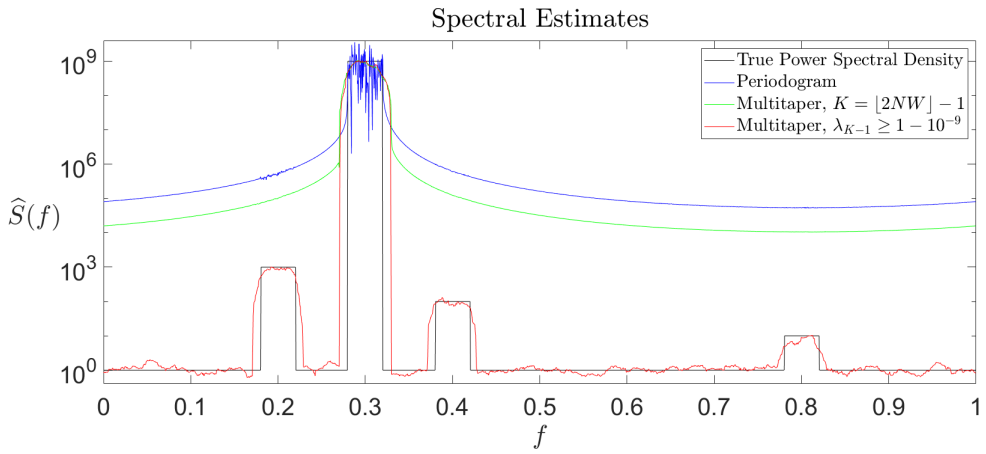

Figure 5.2: Plots of the true power spectral density, the periodogram, the multitaper spectral estimate with $W = \frac{1}{100}$ and $K = \lfloor 2NW \rfloor - 1 = 39$, and the multitaper spectral estimate with $W = \frac{1}{100}$ and $K = 29$ tapers (chosen so $\lambda_{K-1} \geq 1 - 10^{-9}$).

the number of tapers K used in the multitaper spectral estimate. We compare the following eight methods to estimate the power spectrum of a Gaussian random process from a vector $\boldsymbol{x} \in \mathbb{C}^N$ of $N = 2^{18} = 262144$ samples:

1. The classic periodogram

2. A tapered periodogram using a single DPSS taper $\boldsymbol{s}_0$ with $2NW = 8$ (chosen such that $\lambda_0 \geq 1 - 10^{-9}$)

3. The exact multitaper spectral estimate $\widehat{S}_K^{\text{mt}}(f)$ with a small bandwidth parameter of $W = 1.25 \times 10^{-4}$ and $K = \lfloor 2NW \rfloor - 1 = 64$ tapers

4. The exact multitaper spectral estimate $\widehat{S}_K^{\text{mt}}(f)$ with a small bandwidth parameter of $W = 1.25 \times 10^{-4}$ and $K = 53$ tapers (chosen such that $\lambda_{K-1} \geq 1 - 10^{-9} > \lambda_K$)

5. The approximate multitaper spectral estimate $\widetilde{S}_K^{\text{mt}}(f)$ with a larger bandwidth parameter of $W = 2.0 \times 10^{-3}$, $K = \lfloor 2NW \rfloor - 1 = 1047$ tapers, and a tolerance parameter of $\epsilon = 10^{-9}$

6. The approximate multitaper spectral estimate $\widetilde{S}_K^{\text{mt}}(f)$ with a larger bandwidth parameter of $W = 2.0 \times 10^{-3}$, $K = 1031$ tapers (chosen such that $\lambda_{K-1} \geq 1 - 10^{-9} > \lambda_K$),

and a tolerance parameter of $\epsilon = 10^{-9}$

7. The exact multitaper spectral estimate with the adaptive weighting scheme suggested by Thomson[9] with a small bandwidth parameter of $W = 1.25 \times 10^{-4}$ and $K = \lfloor 2NW \rfloor - 1 = 64$ tapers

8. The exact multitaper spectral estimate with the adaptive weighting scheme suggested by Thomson[9] with a larger bandwidth parameter of $W = 2.0 \times 10^{-3}$ and $K = \lfloor 2NW \rfloor - 1 = 1047$ tapers

The adaptive weighting scheme computes the single taper periodograms $\widehat{S}_k(f)$ for $k \in [K]$, and then forms a weighted estimate

$$\widehat{S}_K^{\text{ad}}(f) = \frac{\sum_{k=0}^{K-1} \alpha_k(f) \widehat{S}_k(f)}{\sum_{k=0}^{K-1} \alpha_k(f)}$$

where the frequency dependent weights $\alpha_k(f)$ satisfy

$$\alpha_k(f) = \frac{\lambda_k \widehat{S}_K^{\text{ad}}(f)^2}{\left(\lambda_k \widehat{S}_K^{\text{ad}}(f) + (1 - \lambda_k)\sigma^2\right)^2}$$

where $\sigma^2 = \frac{1}{N}\|\boldsymbol{x}\|_2^2$. Of course, solving for the weights directly is difficult, so this method requires initializing the weights and alternating between updating the estimate $\widehat{S}_K^{\text{ad}}(f)$ and updating the weights $\alpha_k(f)$. This weighting procedure is designed to keep all the weights large at frequencies where $S(f)$ is large and reduce the weights of the last few tapers at frequencies where $S(f)$ is small. Effectively, this allows the spectrum to be estimated with more tapers at frequencies where $S(f)$ is large while simultaneously reducing the spectral leakage from the last few tapers at frequencies where $S(f)$ is small. The cost is the increased computation time due to setting the weights iteratively. For more details regarding this adaptive scheme, see [24].

In Figure 5.3, we plot the power spectrum and the eight estimates for a single realization $\boldsymbol{x} \in \mathbb{C}^N$ of the Gaussian random process. Additionally, for 1000 realizations $\boldsymbol{x}_i \in \mathbb{C}^N$,

$i = 1, \ldots, 1000$ of the Gaussian random process, we compute a spectral estimate using each of the above eight methods. In Figure 5.4, we plot the empirical mean logarithmic deviation in dB, i.e.,

$$\frac{1}{1000} \sum_{i=1}^{1000} \left| 10 \log_{10} \frac{\widehat{S}[\boldsymbol{x}_i](f)}{S(f)} \right|$$

for each of the eight methods. In Table 5.1, we list the average time needed to precompute the DPSS tapers, the average time to compute the spectral estimate after the tapers are computed, and the average of the empirical mean logarithmic deviation in dB across the frequency spectrum.

We make the following observations:

- The periodogram and the single taper periodogram (methods 1 and 2) are too noisy to be useful spectral estimates.

- Methods 3, 4, and 7 yield a noticeably noisier spectral estimate than methods 5, 6, and 8. This is due to the fact that methods 5, 6, and 8 use a larger bandwidth parameter and more tapers.

- The spectral estimates obtained with methods 1, 3 and 5 suffer from spectral leakage, i.e., the error is large at frequencies f where $S(f)$ is small, as can be seen in Figure 5.4. This is due to the fact that they use $K = \lfloor 2NW \rfloor - 1$ tapers, and thus, include tapered periodograms $\widehat{S}_k(f)$ for which λ_k is not very close to 1.

- Methods 4 and 6 avoid using tapered periodograms $\widehat{S}_k(f)$ for which $\lambda_k < 1 - 10^{-9}$ and methods 7 and 8 use these tapered periodograms but assign a low weight to them at frequencies where $S(f)$ is small. Hence, methods 4, 6, 7, and 8 are able to mitigate the spectral leakage phenomenon.

- Methods 5 and 6 are slightly faster than methods 3 and 4 due to the fact that our approximate multitaper spectral estimate only needs to compute $\#\{k : \epsilon < \lambda_k < 1 - \epsilon\} = 36$ tapers and 36 tapered periodograms.

Table 5.1: Table of mean logarithmic deviations (averaged across entire frequency spectrum), precomputation times, and computation times for each of the eight spectral estimation methods.

Method	Avg MLD (dB)	Avg Precomputation Time (sec)	Avg Run Time (sec)
1	5.83030	N/A	0.0111
2	4.41177	0.1144	0.0111
3	1.48562	4.3893	0.3771
4	0.47836	3.6274	0.3093
5	1.56164	3.3303	0.2561
6	0.12534	3.3594	0.2533
7	0.45080	4.3721	1.4566
8	0.12532	78.9168	17.2709

- Method 7 takes noticeably longer than methods 3 and 4, and method 8 takes considerably longer than methods 5 and 6. This is because the iterative method for computing the adaptive weights requires many iterations to converge when the underlying power spectral density has a high dynamic range.

- Methods 6 and 8 exhibit very similar performance. This is to be expected, as using a weighted average of 1047 tapered periodograms is similar to using the unweighted average of the first 1031 tapered periodograms. The empirical mean logarithmic deviation is larger at frequencies where $S(f)$ is rapidly varying and smaller at frequencies where $S(f)$ is slowly varying. This is to be expected as the local bias (caused due to the smoothing effect of the tapers) dominates the variance at these frequencies.

From this, we can draw several conclusions. First, by slightly trimming the number of tapers from $K = \lfloor 2NW \rfloor - 1$ to $2NW - O(\log(NW))$, one can significantly mitigate the amount of spectral leakage in the spectral estimate. Second, using a larger bandwidth parameter and averaging over more tapered periodograms will result in a less noisy spectral estimate. Third, our fast approximate multitaper spectral estimate can yield a more accurate estimate in the same amount of time as an exact multitaper spectral estimate because our fast approximation needs to compute significantly fewer tapers and tapered periodograms.

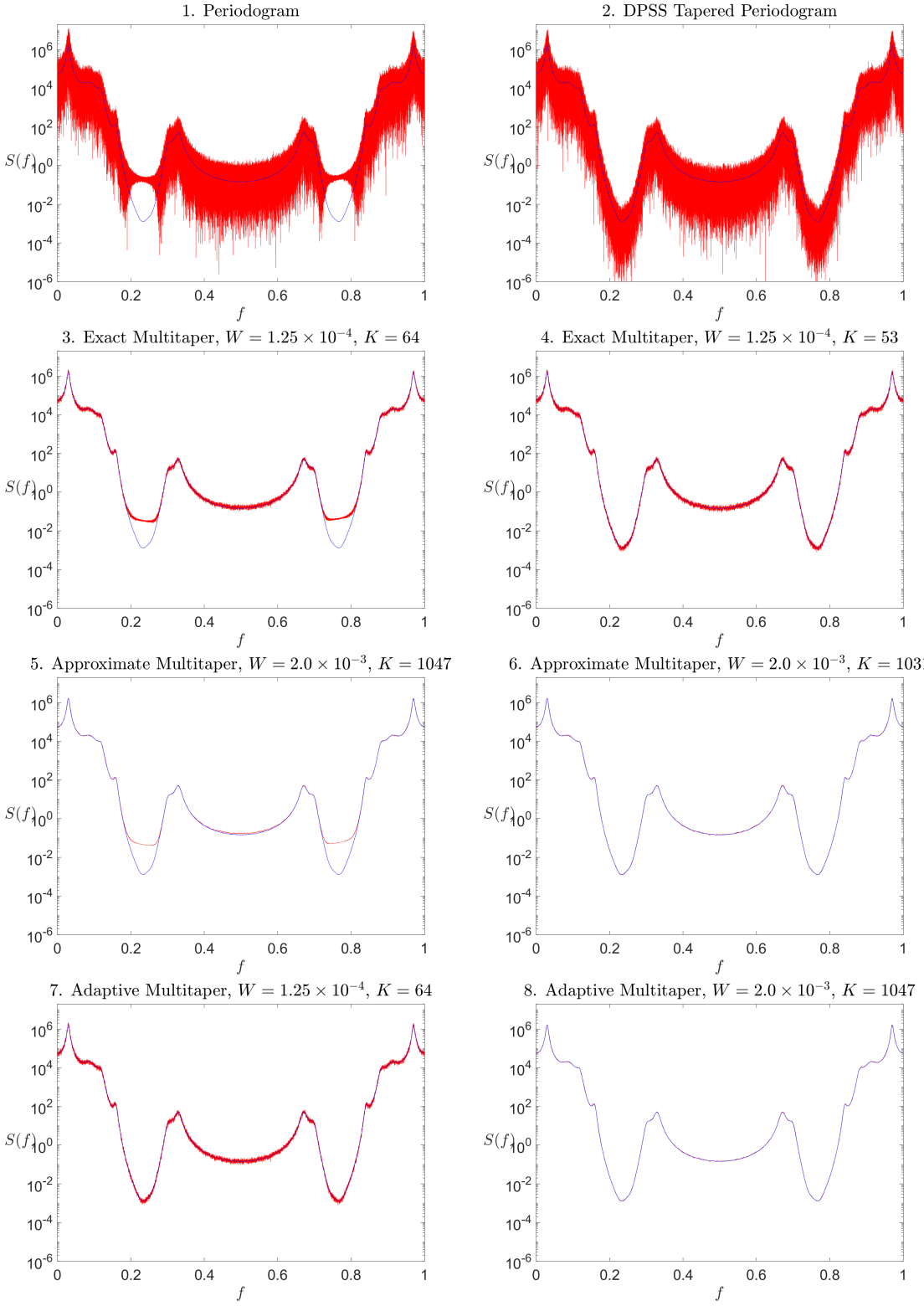

Figure 5.3: Plots of the true spectrum (blue) and the spectral estimates (red) using each of the eight methods.

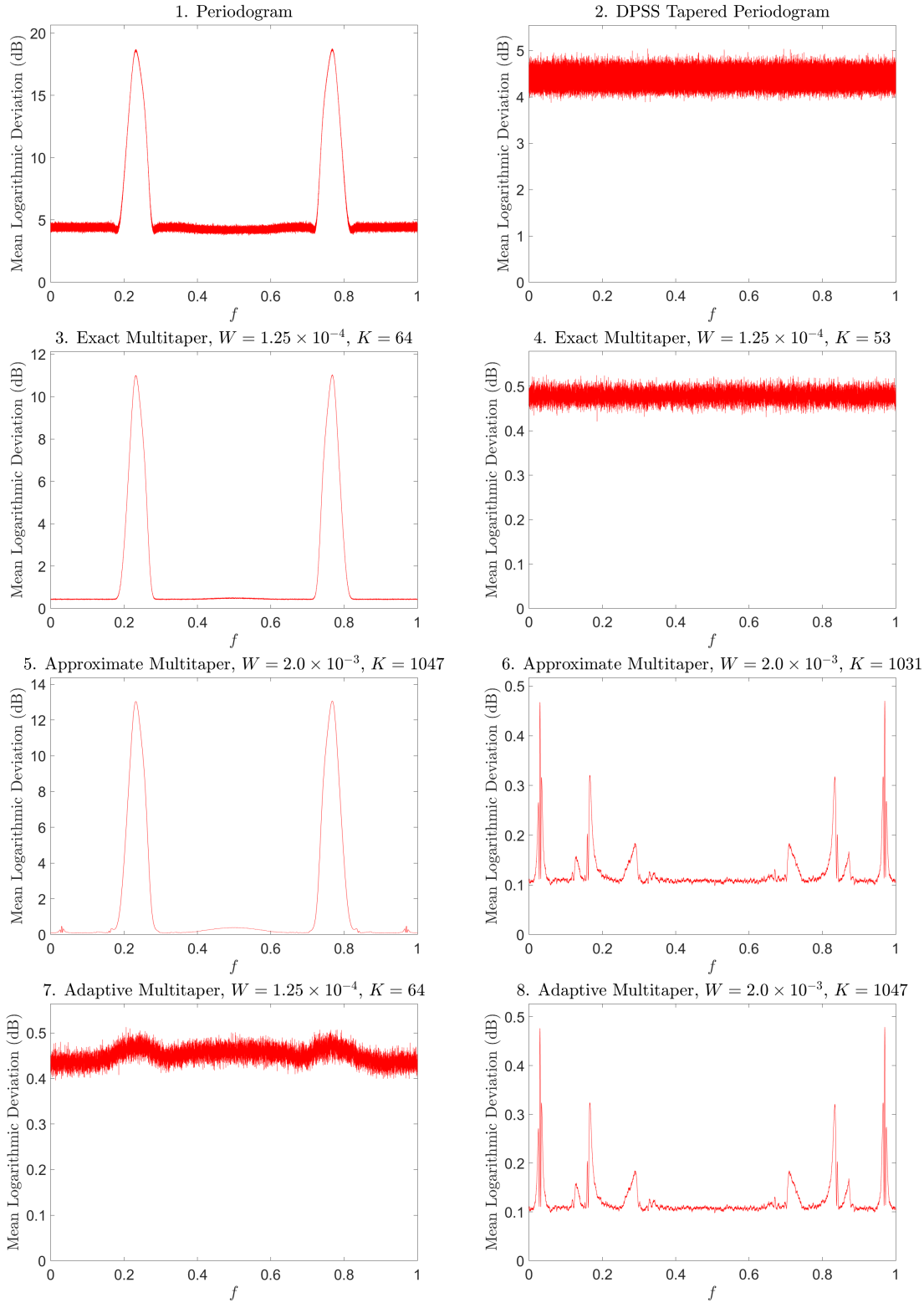

Figure 5.4: Plots of the empirical mean logarithmic deviation using each of the eight methods.

Fourth, a multitaper spectral estimate with $\lfloor 2NW \rfloor - 1$ tapers and adaptive weights can yield a slightly lower error than a multitaper spectral estimate with $2NW - O(\log(NW))$ tapers and fixed weights, but as $2NW$ increases, this effect becomes minimal and not worth the increased computational cost.

Finally, we demonstrate that the runtime for computing the approximate multitaper spectral estimate $\widetilde{S}_K^{\text{mt}}(f)$ scales roughly linearly with the number of samples. We vary the signal length N over several values between 2^{10} and 2^{20}. For each value of N, we set the bandwidth parameter to be $W = 0.08 \cdot N^{-1/5}$ as this is similar to what is asymptotically optimal for a twice differentiable spectrum [105]. We then choose a number of tapers K such that $\lambda_{K-1} \geq 1 - 10^{-3} > \lambda_K$, and then compute the approximate multitaper spectral estimate $\widetilde{S}_K^{\text{mt}}(f)$ at $f \in [N]/N$ for each of the tolerances $\epsilon = 10^{-4}$, 10^{-8}, and 10^{-12}. If $N \leq 2^{17}$, we also compute the exact multitaper spectral estimate $\widehat{S}_K^{\text{mt}}(f)$ at $f \in [N]/N$. For $N > 2^{17}$, we did not evaluate the exact multitaper spectral estimate due to the excessive computational requirements.

We split the work needed to produce the spectral estimate into a precomputation stage and a computation stage. The precomputation stage involves computing the Slepian tapers which are required for the spectral estimate. In applications where a multitaper spectral estimate needs to be computed for several signals (using the same parameters N, W, K), computing the tapers only needs to be done once. The exact multitaper spectral estimate $\widehat{S}_K^{\text{mt}}(f)$ requires computing $\boldsymbol{s}_k$ for $k \in [K]$, while the approximate multitaper spectral estimate $\widetilde{S}_K^{\text{mt}}(f)$ requires computing $\boldsymbol{s}_k$ for $k \in \mathcal{I}_2 \cup \mathcal{I}_3 = \{k : \epsilon < \lambda_k < 1 - \epsilon\}$. The computation stage involves evaluating $\widehat{S}_K^{\text{mt}}(f)$ or $\widetilde{S}_K^{\text{mt}}(f)$ at $f \in [N]/N$ with the required tapers $\boldsymbol{s}_k$ already computed.

In Figures 5.5 and 5.6, we plot the precomputation and computation time respectively versus the signal length N for the exact multitaper spectral estimate $\widehat{S}_K^{\text{mt}}(f)$ as well as the approximate multitaper spectral estimate $\widetilde{S}_K^{\text{mt}}(f)$ for $\epsilon = 10^{-4}$, 10^{-8}, and 10^{-12}. The times were averaged over 100 trials of the procedure described above. The plots are on a log-

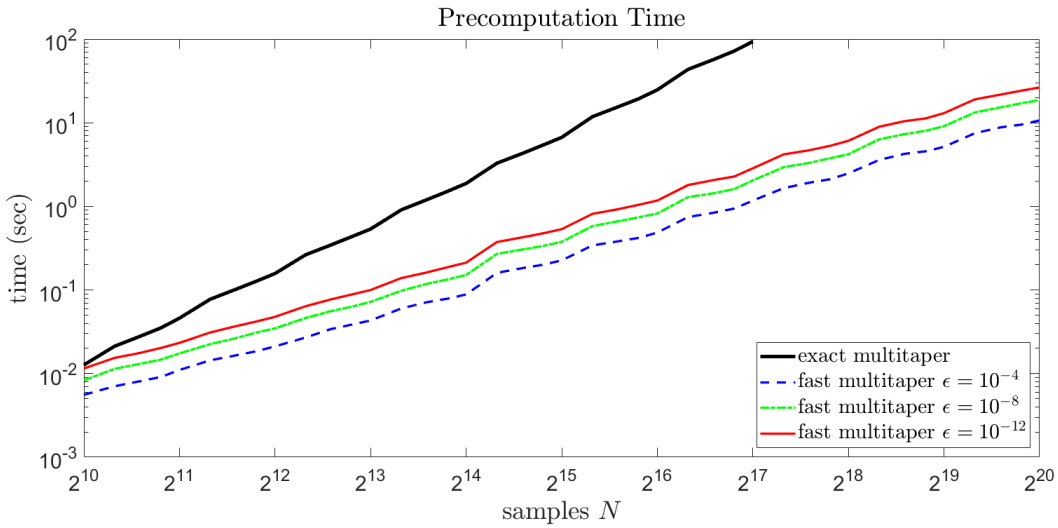

Figure 5.5: Plot of the average precomputation time vs. signal length N for the exact multitaper spectral estimate and our fast approximation for $\epsilon = 10^{-4}$, 10^{-8}, and 10^{-12}.

log scale. We note that the precomputation and computation times for the approximate multitaper spectral estimate grow roughly linearly with N while the precomputation and computation times for the exact multitaper spectral estimate grow significantly faster. Also, the precomputation and computation times for the approximate multitaper spectral estimate with the very small tolerance $\epsilon = 10^{-12}$ are only two to three times more than those for the larger tolerance $\epsilon = 10^{-4}$.

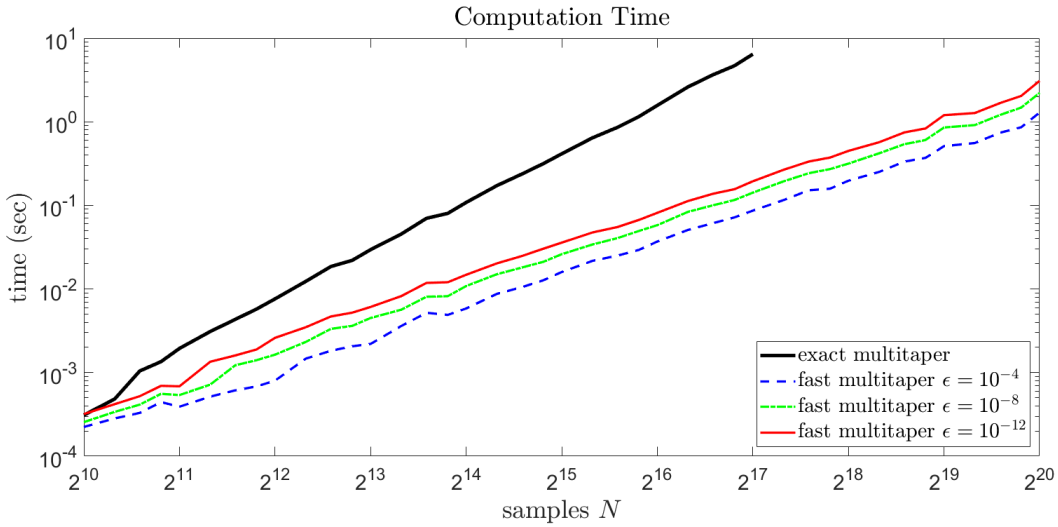

Figure 5.6: Plot of the average computation time vs. signal length N for the exact multitaper spectral estimate and our fast approximation for $\epsilon = 10^{-4}$, 10^{-8}, and 10^{-12}.

CHAPTER 6

NONUNIFORM SAMPLING OF MULTIBAND SIGNALS

In this chapter, we demonstrate a fast method to reconstruct a multiband signal from nonuniform samples, provided we know the active frequency bands (i.e. the support of the signal's Fourier transform) a priori. We first formulate the signal reconstruction as a linear inverse problem involving and show that the solution is a linear combination of shifted sinc functions. We then observe that the resulting system of equations has a generalized Cauchy-like structure, which allows the corresponding matrix to be applied to a vector in linear time with respect to the number of samples. Fast solvers for generalized Cauchy-like matrices exist, but unfortunately, our particular matrix is ill-conditioned, which makes these fast solvers unstable. However, we show that the method of conjugate gradient descent can be used to solve the system, and only a polylogarithmic number of iterations are required for convergence. This along with the fast generalized Cauchy-like matrix multiply gives us a fast algorithm for reconstructing a multiband signal from nonuniform samples. Material in this section has appeared in [108].

6.1 Problem Formulation

Let

$$\Omega = \bigcup_{\ell=0}^{L-1} [f_\ell - W_\ell, f_\ell + W_\ell] \subset \mathbb{R}$$

be a union of L non-overlapping frequency bands, and define the Paley–Wiener space

$$\mathrm{PW}_\Omega(\mathbb{R}) = \left\{ x \in L_2(\mathbb{R}) \ : \ \widehat{x}(f) = \int_{-\infty}^{\infty} x(t) e^{-j2\pi ft}\, dt = 0 \ \forall f \in \mathbb{R} \setminus \Omega \right\},$$

i.e. the subspace of signals in $L_2(\mathbb{R})$ whose Fourier transform is supported only on the L frequency bands in Ω. Our goal is to reconstruct a multiband signal $x \in \mathrm{PW}_\Omega(\mathbb{R})$ from a

vector $\boldsymbol{y} \in \mathbb{C}^N$ containing N (possibly noisy) samples of x at times $t_0, \ldots, t_{N-1} \in [-\frac{T}{2}, \frac{T}{2}]$, i.e.

$$\boldsymbol{y}[n] = x(t_n) + \boldsymbol{\eta}[n] \quad \text{for} \quad n \in [N],$$

where $\boldsymbol{\eta} \in \mathbb{C}^N$ is a noise vector.

We can treat recovering x as a linear inverse problem. To formulate this problem, we start by defining a kernel function $\phi \in \mathrm{PW}_\Omega(\mathbb{R})$ by

$$\phi(t) = \int_\Omega e^{j2\pi ft}\, df = \sum_{\ell=0}^{L-1} \int_{f_\ell - W_\ell}^{f_\ell + W_\ell} e^{j2\pi ft}\, df = \sum_{\ell=0}^{L-1} \frac{\sin(2\pi W_\ell t)}{\pi t} e^{j2\pi f_\ell t} \quad \text{for} \quad t \in \mathbb{R},$$

and for any time-shift $\tau \in \mathbb{R}$, we define a shifted kernel function $a_\tau \in \mathrm{PW}_\Omega(\mathbb{R})$ by

$$a_\tau(t) = \phi(t - \tau) \quad \text{for} \quad t \in \mathbb{R}.$$

Since the Fourier transform of the kernel function is $\widehat{\phi}(f) = 1_\Omega(f)$, the Fourier transform of the shifted kernel function is $\widehat{a}_\tau(f) = 1_\Omega(f) e^{-j2\pi f\tau}$. Therefore, any multiband signal $x \in \mathrm{PW}_\Omega(\mathbb{R})$ satisfies

$$x(\tau) = \int_\Omega \widehat{x}(f) e^{j2\pi f\tau}\, df = \int_\Omega \widehat{x}(f)\overline{\widehat{a}_\tau(f)}\, df = \langle \widehat{a}_\tau, \widehat{x} \rangle_{L_2(\Omega)} = \langle a_\tau, x \rangle_{\mathrm{PW}_\Omega(\mathbb{R})},$$

where the last equality holds by the Parseval-Plancherel identity. Hence, if we define a sampling operator $\mathcal{A} : \mathrm{PW}_\Omega(\mathbb{R}) \to \mathbb{C}^N$ by

$$(\mathcal{A}x)[n] = \langle a_{t_n}, x \rangle_{\mathrm{PW}_\Omega(\mathbb{R})} \quad \text{for} \quad n \in [N],$$

then our vector of samples can be written as

$$\boldsymbol{y} = \mathcal{A}x + \boldsymbol{\eta}.$$

We can then attempt to reconstruct x by solving a Tikhonov regularization problem

$$\widetilde{x} = \underset{x \in \mathrm{PW}_\Omega(\mathbb{R})}{\arg\min} \|\boldsymbol{y} - \mathcal{A}x\|_2^2 + \delta \|x\|_{\mathrm{PW}_\Omega(\mathbb{R})}^2.$$

The solution to this Tikhonov regularization problem can be written as

$$\widetilde{x} = \mathcal{A}^*(\mathcal{A}\mathcal{A}^* + \delta \mathbf{I})^{-1}\boldsymbol{y} = \mathcal{A}^*[(\boldsymbol{G} + \delta \mathbf{I})^{-1}\boldsymbol{y}],$$

where the adjoint $\mathcal{A}^* : \mathbb{C}^N \to \mathrm{PW}_\Omega(\mathbb{R})$ is given by

$$\mathcal{A}^*\boldsymbol{z} = \sum_{n=0}^{N-1} \boldsymbol{z}[n] a_{t_n} \quad \text{for} \quad \boldsymbol{z} \in \mathbb{C}^N,$$

and the Gram matrix $\boldsymbol{G} \in \mathbb{C}^{N \times N}$ has entries

$$\boldsymbol{G}[n, n'] = \left\langle a_{t_n}, a_{t_{n'}} \right\rangle = \phi(t_n - t_{n'}) \quad \text{for} \quad n, n' \in [N].$$

In other words, the reconstruction of the multiband signal x is given by

$$\widetilde{x}(t) = \sum_{n=0}^{N-1} \boldsymbol{z}[n] \phi(t - t_n) \quad \text{for} \quad t \in \mathbb{R},$$

i.e. a linear combination of kernel functions shifted by the sample times. The coefficients $\boldsymbol{z}[n]$ are found by solving the system of equations $(\boldsymbol{G} + \delta \mathbf{I})\boldsymbol{z} = \boldsymbol{y}$.

After solving the system $(\boldsymbol{G} + \delta \mathbf{I})\boldsymbol{z} = \boldsymbol{y}$, we can evaluate $\widetilde{x}(t)$ at M sample times $t'_0, t'_1, \ldots, t'_{M-1} \in \mathbb{R}$ via a matrix-vector multiply

$$\begin{bmatrix} \widetilde{x}(t'_0) & \widetilde{x}(t'_1) & \cdots & \widetilde{x}_c(t'_{M-1}) \end{bmatrix}^T = \boldsymbol{H}\boldsymbol{z}$$

where the matrix $\boldsymbol{H} \in \mathbb{R}^{M \times N}$ has entries

$$\boldsymbol{H}[m,n] = \phi(t'_m - t_n).$$

For large N, explicitly forming $\boldsymbol{G} + \delta\mathbf{I}$ and solving $(\boldsymbol{G} + \delta\mathbf{I})\boldsymbol{z} = \boldsymbol{y}$ takes $O(N^{2.3728596})$ operations [54] via an improvement over the Coppersmith–Winograd algorithm [109][1]. Also, for large M and N, explicitly forming $\boldsymbol{H}$ and computing $\boldsymbol{H}\boldsymbol{z}$ takes $O(MN)$ operations.

6.2 Structured Matrices

The matrix $\boldsymbol{H}$ defined in the previous section is a generalized Cauchy matrix (defined in Section 2.6). To see this, note that the entries of $\boldsymbol{H}$ can be written as

$$\begin{aligned}
\boldsymbol{H}[m,n] &= \phi(t'_m - t_n) \\
&= \sum_{\ell=0}^{L-1} \frac{\sin[2\pi W_\ell (t'_m - t_n)]}{\pi(t'_m - t_n)} e^{j2\pi f_\ell (t'_m - t_n)} \\
&= \sum_{\ell=0}^{L-1} \frac{\sin(2\pi W_\ell t'_m)\cos(2\pi W_\ell t_n) - \cos(2\pi W_\ell t'_m)\sin(2\pi W_\ell t_n)}{\pi(t'_m - t_n)} e^{j2\pi f_\ell (t'_m - t_n)} \\
&= \sum_{\ell=0}^{L-1} \left[\frac{e^{j2\pi f_\ell t'_m} \sin(2\pi W_\ell t'_m) e^{-j2\pi f_\ell t_n} \cos(2\pi W_\ell t_n)}{\pi(t'_m - t_n)} \right. \\
&\qquad \left. - \frac{e^{j2\pi f_\ell t'_m} \cos(2\pi W_\ell t'_m) e^{-j2\pi f_\ell t_n} \sin(2\pi W_\ell t_n)}{\pi(t'_m - t_n)} \right].
\end{aligned}$$

[1] It should be noted that Strassen's algorithm, which has a runtime of $O(N^{2.807})$ is often used in practice over the Coppersmith–Winograd algorithm as it is faster for practical values of N [110].

Hence, $\boldsymbol{H}$ fits the form of a generalized Cauchy matrix with the parameters

$$
\begin{aligned}
r &= 2L \\
\sigma'_m &= \pi t'_m && \text{for} \quad m \in [M] \\
\sigma_n &= \pi t_n && \text{for} \quad n \in [N] \\
\boldsymbol{p}_{2\ell}[m] &= e^{j2\pi f_\ell t'_m} \sin(2\pi W_\ell t'_m) && \text{for} \quad m \in [M] \text{ and } \ell \in [L] \\
\boldsymbol{p}_{2\ell+1}[m] &= e^{j2\pi f_\ell t'_m} \cos(2\pi W_\ell t'_m) && \text{for} \quad m \in [M] \text{ and } \ell \in [L] \\
\boldsymbol{q}_{2\ell}[n] &= e^{j2\pi f_\ell t_n} \cos(2\pi W_\ell t_n) && \text{for} \quad n \in [N] \text{ and } \ell \in [L] \\
\boldsymbol{q}_{2\ell+1}[n] &= e^{j2\pi f_\ell t_n} \sin(2\pi W_\ell t_n) && \text{for} \quad n \in [N] \text{ and } \ell \in [L]
\end{aligned}
$$

Therefore, $\boldsymbol{H}$ can be applied to an $N \times 1$ vector in $O(L(M+N)\log\frac{1}{\alpha})$ operations.

Also, the matrix $\boldsymbol{G} + \delta\mathbf{I}$ defined in the previous section is a symmetric generalized Cauchy-like matrix (defined in Section 2.6). The diagonal entries are all

$$
(\boldsymbol{G} + \delta\mathbf{I})[n,n] = \phi(t_n - t_n) + \delta = \phi(0) + \delta = \delta + \sum_{\ell=0}^{L-1} 2W_\ell,
$$

and the off-diagonal entries are

$$
\begin{aligned}
\boldsymbol{G}[n,n'] &= \phi(t_n - t_{n'}) \\
&= \sum_{\ell=0}^{L-1} \frac{\sin[2\pi W_\ell(t_n - t_{n'})]}{\pi(t_n - t_{n'})} e^{j2\pi f_\ell(t_n - t_{n'})} \\
&= \sum_{\ell=0}^{L-1} \frac{\sin(2\pi W_\ell t_n)\cos(2\pi W_\ell t_{n'}) - \cos(2\pi W_\ell t_n)\sin(2\pi W_\ell t_{n'})}{\pi(t_n - t_{n'})} e^{j2\pi f_\ell(t_n - t_{n'})} \\
&= \sum_{\ell=0}^{L-1} \left[\frac{e^{j2\pi f_\ell t_n}\sin(2\pi W_\ell t_n) e^{-j2\pi f_\ell t_{n'}}\cos(2\pi W_\ell t_{n'})}{\pi(t_n - t_{n'})} \right. \\
&\qquad \left. - \frac{e^{j2\pi f_\ell t_n}\cos(2\pi W_\ell t_n) e^{-j2\pi f_\ell t_{n'}}\sin(2\pi W_\ell t_{n'})}{\pi(t_n - t_{n'})} \right].
\end{aligned}
$$

Hence, $\boldsymbol{G} + \delta\mathbf{I}$ fits the form of a generalized Cauchy-like matrix with the parameters

$$
\begin{aligned}
r &= L \\
d_n &= \delta + \sum_{\ell=0}^{L-1} 2W_\ell && \text{for} \quad n \in [N] \\
\sigma_n &= \pi t_n && \text{for} \quad n \in [N] \\
\boldsymbol{p}_\ell[n] &= e^{j2\pi f_\ell t_n} \sin(2\pi W_\ell t_n) && \text{for} \quad n \in [N] \text{ and } \ell \in [L] \\
\boldsymbol{q}_\ell[n] &= e^{j2\pi f_\ell t_n} \cos(2\pi W_\ell t_n) && \text{for} \quad n \in [N] \text{ and } \ell \in [L]
\end{aligned}
$$

Therefore, $\boldsymbol{G} + \delta\mathbf{I}$ can be applied to an $N \times 1$ vector in $O(LN \log \frac{1}{\alpha})$ operations.

6.3 Spectral Properties

A symmetric generalized Cauchy-like matrix $\widetilde{\boldsymbol{K}}$ satisfies a low-rank displacement equation

$$\boldsymbol{D}_{\boldsymbol{\sigma}}\widetilde{\boldsymbol{K}} - \widetilde{\boldsymbol{K}}\boldsymbol{D}_{\boldsymbol{\sigma}} = \boldsymbol{P}\boldsymbol{Q}^* - \boldsymbol{Q}\boldsymbol{P}^*,$$

where $\boldsymbol{P} = \begin{bmatrix} \boldsymbol{p}_0 & \cdots & \boldsymbol{p}_{r-1} \end{bmatrix} \in \mathbb{C}^{N\times r}$ and $\boldsymbol{Q} = \begin{bmatrix} \boldsymbol{q}_0 & \cdots & \boldsymbol{q}_{r-1} \end{bmatrix} \in \mathbb{C}^{N\times r}$. Also, the entries of $\widetilde{\boldsymbol{K}}$ can be recovered from the parameters $\sigma_0, \ldots, \sigma_{N-1}$, $d_0, \ldots, d_{N-1}$, and the "generators" $\boldsymbol{P}$ and $\boldsymbol{Q}$.

Furthermore, if $\widetilde{\boldsymbol{K}}$ is invertible, then $\widetilde{\boldsymbol{K}}^{-1}$ also satisfies a low-rank displacement equation

$$\boldsymbol{D}_{\boldsymbol{\sigma}}\widetilde{\boldsymbol{K}}^{-1} - \widetilde{\boldsymbol{K}}^{-1}\boldsymbol{D}_{\boldsymbol{\sigma}} = \widetilde{\boldsymbol{K}}^{-1}\boldsymbol{Q}\boldsymbol{P}^*\widetilde{\boldsymbol{K}}^{-1} - \widetilde{\boldsymbol{K}}^{-1}\boldsymbol{P}\boldsymbol{Q}^*\widetilde{\boldsymbol{K}}^{-1},$$

and thus, $\widetilde{\boldsymbol{K}}^{-1}$ is also a symmetric generalized Cauchy-like matrix.

This fact has been exploited to yield recursive methods for inverting symmetric generalized Cauchy-like matrices[61, 111]. These methods partition the generalized Cauchy-like matrix $\widetilde{\boldsymbol{K}}$ into a 2×2 block matrix, compute the generators of the $(1,1)$-block and its Schur complement via recursion, and then determine the "generators" of $\widetilde{\boldsymbol{K}}$. This Schur recursion

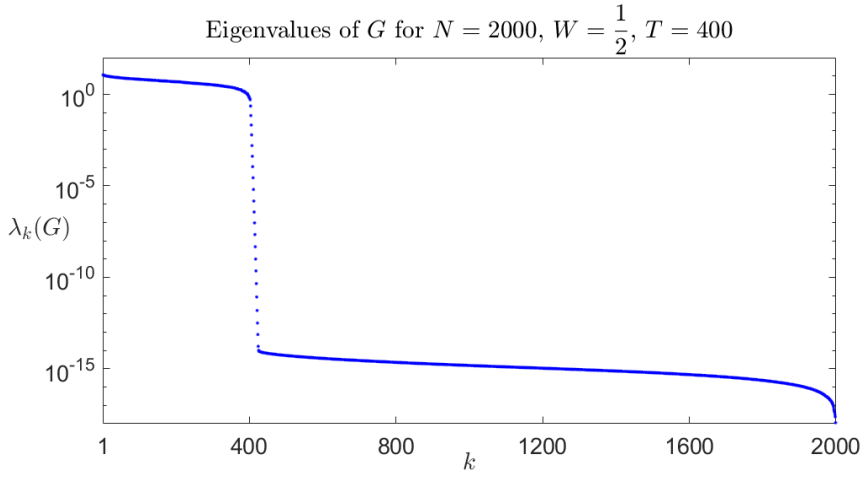

Figure 6.1: A plot of the eigenvalues of $\boldsymbol{G}$. The largest $2WT = 400$ eigenvalues are all between $\lambda_1(\boldsymbol{G}) \approx 11.43$ and $\lambda_{400}(\boldsymbol{G}) \approx 0.6597$. The smallest 1577 eigenvalues are all between $\lambda_{424}(\boldsymbol{G}) \approx 1.68 \times 10^{-14}$ and 0. Only 24 eigenvalues fail to fit in one of those ranges.

takes $O(rN \log N \log \frac{1}{\alpha})$ operations to compute the generators of $\widetilde{\boldsymbol{K}}^{-1}$. Unfortunately, for our problem, when the number of samples exceeds $\sum_{\ell=0}^{L-1} (2W_\ell T + O(\log(2W_\ell T))$, the matrix $\boldsymbol{G}$ becomes numerically rank deficient. As such, these recursive methods for inverting $\boldsymbol{G}$ are unstable if more than a few recursive stages are used.

Figure 6.1 shows a plot of the eigenvalues of $\boldsymbol{G}$ in descending order where we have chosen $N = 2000$, $L = 1$, $f_0 = 0$, $W_0 = \frac{1}{2}$, $T = 400$, and $t_0, \ldots, t_{N-1}$ are i.i.d. Uniform$[-\frac{T}{2}, \frac{T}{2}]$, i.e. our signal's Fourier transform is supported on the single interval $\Omega = [-\frac{1}{2}, \frac{1}{2}]$. It can be seen that the first $\approx |\Omega|T = 400$ eigenvalues are all roughly the same order of magnitude, and for $k > |\Omega|T$, the eigenvalues $\lambda_k(\boldsymbol{G})$ decay exponentially towards zero as k increases.

We remark that this behavior is very similar to that of the eigenvalues of the prolate spheroidal wave functions (PSWF) [1–4]. The first $\approx 2WT$ PSWF eigenvalues are ≈ 1, and the rest exponentially decay towards zero. Also, if our sample times were chosen to be uniformly spaced, then the above matrix $\boldsymbol{G}$ becomes the prolate matrix (up to a constant scale factor), and then, the first $\approx |\Omega|T$ eigenvalues would tightly cluster around $\frac{N}{T}$.

6.4 Conjugate Gradient Descent

Conjugate gradient descent (CGD) is an iterative algorithm which aims to solve the system of equations $\boldsymbol{A}\boldsymbol{z} = \boldsymbol{y}$ for a positive definite matrix $\boldsymbol{A} \in \mathbb{C}^{N\times N}$ and a vector $\boldsymbol{y} \in \mathbb{C}^N$. If we initialize CGD to start at $\boldsymbol{z}^{(0)} = \mathbf{0}$, then the output of CGD at the k-th iteration is

$$\boldsymbol{z}^{(k)} = \underset{\boldsymbol{z}\in\mathcal{K}_k(\boldsymbol{A},\boldsymbol{y})}{\arg\min} \left\|\boldsymbol{z} - \boldsymbol{A}^{-1}\boldsymbol{y}\right\|_{\boldsymbol{A}}^2,$$

where the $\boldsymbol{A}$-norm is defined as $\|\boldsymbol{v}\|_{\boldsymbol{A}}^2 := \boldsymbol{v}^*\boldsymbol{A}\boldsymbol{v}$, and

$$\mathcal{K}_k(\boldsymbol{A},\boldsymbol{y}) = \text{span}\{\boldsymbol{y}, \boldsymbol{A}\boldsymbol{y}, \boldsymbol{A}^2\boldsymbol{y}, \ldots, \boldsymbol{A}^{k-1}\boldsymbol{y}\}$$

is the order-k Krylov subspace generated by $\boldsymbol{A}$ and $\boldsymbol{y}$.

As a result, it can be shown that the error after k iterations satisfies the bound

$$\left\|\boldsymbol{z}^{(k)} - \boldsymbol{A}^{-1}\boldsymbol{y}\right\|_{\boldsymbol{A}}^2 \le \left\|\boldsymbol{A}^{-1}\boldsymbol{y}\right\|_{\boldsymbol{A}}^2 \cdot \min_{\substack{\text{polynomials } P \\ \deg P = k \\ P(0)=1}} \left[\max_{\lambda\in\text{Spec}(\boldsymbol{A})} |P(\lambda)|^2\right].$$

For a general matrix $\boldsymbol{A}$, this bound is often simplified by first relaxing the maximum over $\lambda \in \text{Spec}(\boldsymbol{A})$ to the maximum over $\lambda \in [\lambda_{\min}(\boldsymbol{A}), \lambda_{\max}(\boldsymbol{A})]$, and then using properties of Chebyshev polynomials to get

$$\left\|\boldsymbol{z}^{(k)} - \boldsymbol{A}^{-1}\boldsymbol{y}\right\|_{\boldsymbol{A}} \le \left\|\boldsymbol{A}^{-1}\boldsymbol{y}\right\|_{\boldsymbol{A}} \cdot 2\left(\frac{\sqrt{\kappa}-1}{\sqrt{\kappa}+1}\right)^k,$$

where $\kappa = \lambda_{\max}(\boldsymbol{A})/\lambda_{\min}(\boldsymbol{A})$ is the condition number of $\boldsymbol{A}$. Hence, CGD returns a vector $\boldsymbol{z}^{(k)}$ which satisfies $\left\|\boldsymbol{z}^{(k)} - \boldsymbol{A}^{-1}\boldsymbol{y}\right\|_{\boldsymbol{A}} \le \epsilon \left\|\boldsymbol{A}^{-1}\boldsymbol{y}\right\|_{\boldsymbol{A}}$ in at most $\lceil \frac{1}{2}\sqrt{\kappa}\log\frac{2}{\epsilon}\rceil$ iterations. A more detailed discussion regarding CGD can be found in [112].

For our matrix $\boldsymbol{G}+\delta\mathbf{I}$, the largest eigenvalue is $\sim \frac{N}{T}$ and the smallest eigenvalue is $\approx \delta$. Hence, the condition number is roughly $\kappa \sim \frac{N}{T\delta}$. Typically, the regularization parameter δ

will be chosen to be small (values of 10^{-2} to 10^{-5} are typical), and thus, κ will be rather large. Hence, the bound of $\left\lceil \frac{1}{2}\sqrt{\kappa}\log\frac{2}{\epsilon}\right\rceil$ iterations is worrisome. It is possible to get a better bound if we exploit the clustering behavior of the eigenvalues of $\boldsymbol{G}+\delta\mathbf{I}$.

By using the fact that $\boldsymbol{G} = \mathcal{A}\mathcal{A}^*$ has the same non-zero eigenvalues as $\mathcal{A}^*\mathcal{A} = \sum_{n=0}^{N-1} a_{t_n}a_{t_n}^*$, matrix concentration inequalities from [113], and our bounds on the number of prolate spheroidal wave function eigenvalues in the transition region (Theorem 3 in Section 3.3), we can get the following result.

Lemma 1. *Suppose* $N \geq |\Omega|T$, $2W_\ell T \geq 1$ *for all* $\ell \in [L]$, $\delta > 0$, $\epsilon \in (0,1)$, *and that the sample times* $t_0,\ldots,t_{N-1}$ *are i.i.d. Uniform*$[-\frac{T}{2},\frac{T}{2}]$. *Then there exist constants* $C_0, C_1, C_2 > 0$ *and indices* K_1 *and* K_2 *such that*

$$K_2 - K_1 \leq C_0 L \log\left(\frac{\pi}{2}|\Omega|T\right)\log\left(\frac{N^2|\Omega|^2}{\delta^2\epsilon^{1/4}}\right)$$

and with probability at least $1-(3|\Omega|T+2)e^{-\frac{2N}{3|\Omega|T}}$ *the following bound hold simultaneously:*

$$\begin{aligned}\lambda_1(\boldsymbol{G}) &\leq C_1\frac{N}{|\Omega|T},\\ \lambda_{K_1}(\boldsymbol{G}) &\geq C_2\frac{N}{|\Omega|T},\\ \lambda_{K_2+1}(\boldsymbol{G}) &\leq 2\delta\epsilon^{1/8}.\end{aligned}$$

Furthermore, the following lemma gives a bound of the number of CGD iterations required when working with a matrix with similar eigenvalue clustering behavior.

Lemma 2. *Let* $\boldsymbol{A}\in\mathbb{C}^{N\times N}$ *be a positive-definite matrix, and let* $\boldsymbol{y}\in\mathbb{C}^N$. *Let* $\boldsymbol{z}^{(k)}\in\mathbb{C}^N$ *be the CGD iterates produced when solving the system of equations* $\boldsymbol{A}\boldsymbol{z}=\boldsymbol{y}$ *using CGD with the initial point* $\boldsymbol{z}^{(0)}=\mathbf{0}$, *and let* $\epsilon\in(0,1)$ *be the desired CGD tolerance. Suppose*

there exist real numbers $\delta, a, b, c_0, c_1, \ldots, c_{p-1}$ *with*

$$\delta(1 + 2\epsilon^{1/8}) < c_0 < c_1 < \cdots < c_{p-1} < a < b$$

such that

$$\textit{Spec}(\boldsymbol{A}) \subseteq \left[\delta, \delta(1 + 2\epsilon^{1/8})\right] \bigcup \{c_i\}_{i=0}^{p-1} \bigcup [a, b].$$

Then, for some non-negative integer

$$k \leq \left\lceil \frac{1}{2}\sqrt{\frac{b}{a}} \left((p+8) \log \frac{b}{\delta} + \log \frac{2}{\epsilon} \right) \right\rceil + p + 8,$$

we have

$$\|\boldsymbol{z}^{(k)} - \boldsymbol{A}^{-1}\boldsymbol{y}\|_{\boldsymbol{A}} \leq \epsilon \|\boldsymbol{A}^{-1}\boldsymbol{y}\|_{\boldsymbol{A}}.$$

The proof of this lemma invokes properties of Chebyshev polynomials to explicitly construct a polynomial $P(\lambda)$ such that $P(0) = 1$, $P(c_i) = 0$ for $i = 1, \ldots, p$, and $|P(\lambda)| \leq \epsilon$ for $\lambda \in [\delta, \delta(1 + 2\epsilon^{1/8})]$ and $\lambda \in [a, b]$. Then, the degree of the polynomial is a bound on the number of CGD iterations needed for convergence.

By applying Lemma 2 to the matrix $\boldsymbol{G} + \delta\mathbf{I}$ along with the eigenvalue bounds from Lemma 1, we obtain the following theorem.

Theorem 13. *Suppose* $N \geq |\Omega|T$, $2W_\ell T \geq 1$ *for all* $\ell \in [L]$, $\delta > 0$, $\epsilon \in (0, 1)$, *and that the sample times* $t_0, \ldots, t_{N-1}$ *are i.i.d. Uniform*$[-\frac{T}{2}, \frac{T}{2}]$. *Suppose we run CGD with the initial starting point* $\boldsymbol{z}^{(0)} = \mathbf{0}$ *to solve the system of equations* $(\boldsymbol{G} + \delta\mathbf{I})\boldsymbol{z} = \boldsymbol{y}$. *Then, with probability at least* $1 - (3|\Omega|T + 2)e^{-\frac{2N}{3|\Omega|T}}$, *CGD will need at most*

$$k \leq O\left(L \cdot \textit{polylog}\left(|\Omega|T, \frac{N}{|\Omega|T}, \frac{1}{\delta}, \frac{1}{\epsilon} \right) \right)$$

iterations to return a solution $\boldsymbol{z}^{(k)} \in \mathbb{C}^N$ *such that*

$$\left\|\boldsymbol{z}^{(k)} - (\boldsymbol{G} + \delta\mathbf{I})^{-1}\boldsymbol{y}\right\|_{\boldsymbol{G}+\delta\mathbf{I}} \leq \epsilon \left\|(\boldsymbol{G} + \delta\mathbf{I})^{-1}\boldsymbol{y}\right\|_{\boldsymbol{G}+\delta\mathbf{I}}.$$

6.5 Experiments

We run a synthetic experiment to test the efficiency of our proposed method for multiband signal reconstruction as the number of samples M gets large. We first generate a multiband signal $x(t)$ whose Fourier transform is supported on $\Omega = [-0.9, -0.6] \cup [0.1, 0.2] \cup [0.9, 1.0]$ by summing several sinusoids at random frequencies in those bands. For several values of N between 2^{10} and 2^{18}, we pick T such that $N \approx |\Omega| T \log\left(\frac{|\Omega|T}{0.01}\right)$ where $|\Omega| = 0.5$ is the total occupied bandwidth, and then draw N random sample times $t_0, \ldots, t_{N-1}$ i.i.d. Uniform$[-\frac{T}{2}, \frac{T}{2}]$. This choice of T ensures that the spectrum of $\boldsymbol{G}$ is very likely to have the clustering behavior described in section 6.3. We then set $\delta = 10^{-4}$ and attempt reconstruct the signal on a grid of $M = N$ uniformly spaced sample times in $[-\frac{T}{2}, \frac{T}{2}]$ using three methods:

- Use CGD along with the fast method for applying $\boldsymbol{G} + \delta\mathbf{I}$ to solve $(\boldsymbol{G} + \delta\mathbf{I})\boldsymbol{z} = \boldsymbol{y}$. Then, use the fast method for computing $\boldsymbol{H}\boldsymbol{z}$ to evaluate $\widetilde{x}(t)$ at the uniformly spaced times.

- Use CGD to solve $(\boldsymbol{G} + \delta\mathbf{I})\boldsymbol{z} = \boldsymbol{y}$, but explicitly form $\boldsymbol{G} + \delta\mathbf{I}$. Then, explicitly form $\boldsymbol{H}$ to evaluate $\widetilde{x}(t)$ at the uniformly spaced times.

- Solve the system $(\boldsymbol{G} + \delta\mathbf{I})\boldsymbol{z} = \boldsymbol{y}$ using MATLAB's backslash operator. Then, explicitly form $\boldsymbol{H}$ to evaluate $\widetilde{x}(t)$ at the uniformly spaced times.

Note that due to memory constraints, we were only able to test the 2nd and 3rd methods for $N < 2^{15}$. For each value of N, we repeat this experiment 10 times, to get an accurate average result. The average time to compute the reconstructed signal at the uniform grid of sample times versus the number of samples is shown in figure 6.2 and the average relative

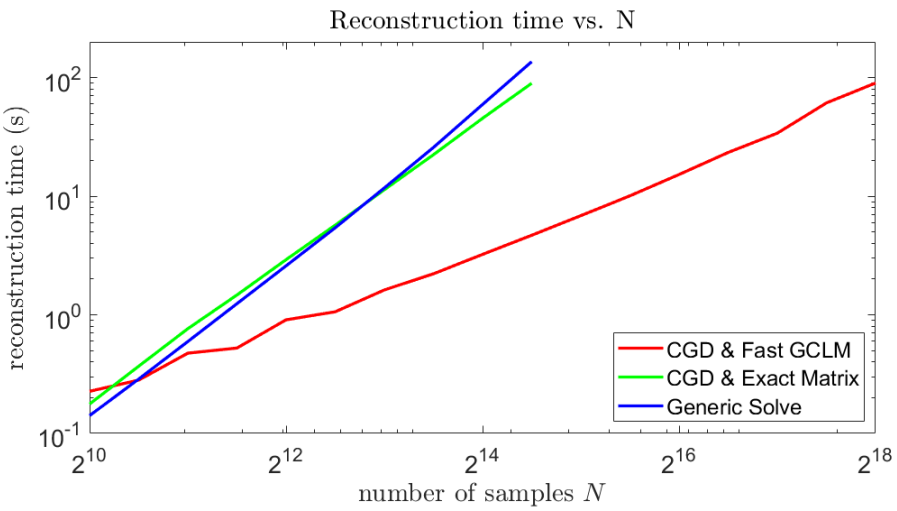

Figure 6.2: Plot of the time needed for each of the three methods to compute the reconstructed signal on a uniformly spaced grid of M points from the N nonuniformly spaced samples.

RMS error of the reconstructed uniform samples versus the number of samples is shown in figure 6.3. All three methods achieve nearly identical reconstruction errors. For $N > 2^{11}$, our proposed method is noticeably faster than the methods which don't take advantage of the structure of $\boldsymbol{G} + \delta\mathbf{I}$ and $\boldsymbol{H}$. Also, the total computation time needed for our method scales roughly linearly with the number of samples. The average number of CGD iterations vs. the number of samples N is shown in figure 6.4. By using the fast and approximate method for applying $\boldsymbol{G} + \delta\mathbf{I}$, CGD takes slightly more iterations to converge.

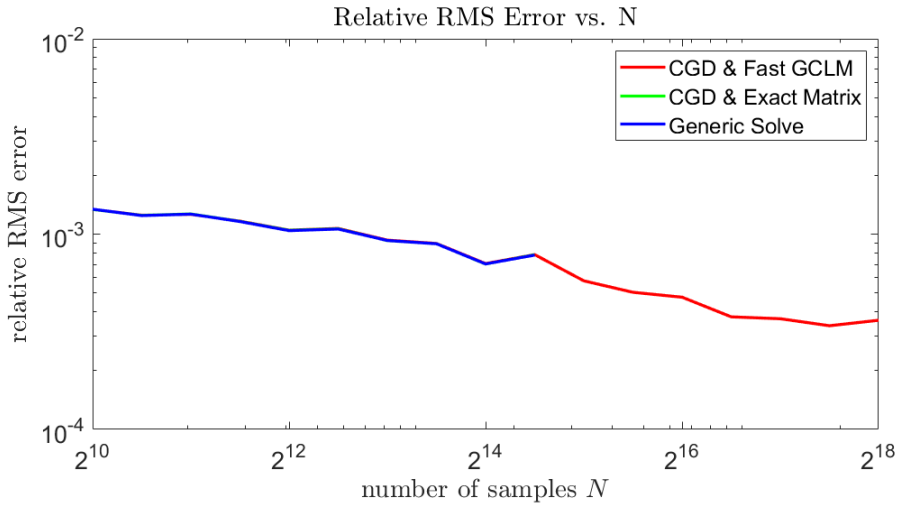

Figure 6.3: Plot of the relative RMS error of the reconstructed signal for each of the three methods. All three methods yield a nearly identical reconstruction error for the values of N for which all of them could be tested.

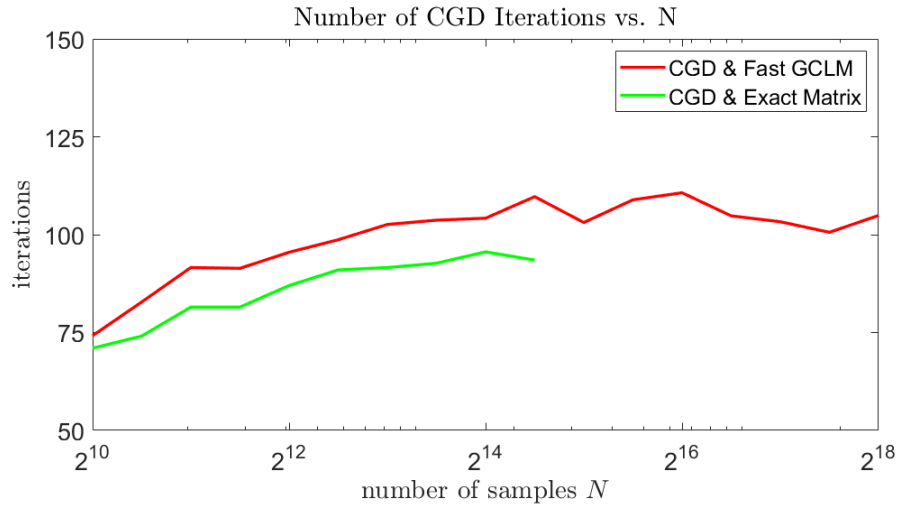

Figure 6.4: Plot of the number of CGD iterations needed for the first two methods versus the number of samples N.

CHAPTER 7

COMPRESSED SENSING OF MULTIBAND SIGNALS

In this chapter, we demonstrate a fast method to recover a multiband signal from compressed measurements without knowing the active frequency bands a priori. In [6], the authors use Slepian basis vectors to form a dictionary in which multiband signals have a block-sparse representation. Then, they recover the multiband signal from compressed measurements by using block-based CoSaMP, which works by alternating between estimating the locations of the active frequency bands and solving a least squares problem to obtain the optimal signal given the estimated frequency bands. We will make two novel and significant improvements to their method. First, [6] assumed that the active frequency bands are a subset of a fixed, finite set of non-overlapping frequency bands of constant bandwidth. We will allow the frequency bands to have center frequencies from a continuum of possibilities, and we will allow the bandwidths to vary. Second, we will replace some of the steps involved with the method in [6] with some of our fast algorithms developed in earlier chapters of this thesis. This will allow us to efficiently solve large scale instances of this problem.

7.1 Signal Model

Let $\boldsymbol{x} \in \mathbb{C}^N$ be a vector containing N samples from a multiband signal, i.e.

$$\boldsymbol{x}[n] = \sum_{\ell=0}^{L-1} \int_{f_\ell - W_\ell}^{f_\ell + W_\ell} X(f) e^{j2\pi f n} \, df$$

where the intervals $[f_\ell - W_\ell, f_\ell + W_\ell]$ for $\ell \in [L]$ are disjoint, and contained in $[-\frac{1}{2}, \frac{1}{2}]$. Note that for ease of notation, we use digital frequency, i.e. we assume the sampling frequency is 1, and that none of the frequency bands are above the Nyquist rate.

Now suppose we observe $M \ll N$ compressed measurements of $\boldsymbol{x}$, i.e. $\boldsymbol{y} = \boldsymbol{A}\boldsymbol{x}$ for some matrix $\boldsymbol{A} \in \mathbb{C}^{M \times N}$. Our goal is to recover the vector of uncompressed samples $\boldsymbol{x}$ from the compressed measurements $\boldsymbol{y}$.

7.2 Modulated Slepian Dictionary

In [6], they construct a dictionary for representing multiband signals as follows. First, they divide the interval $[-\frac{1}{2}, \frac{1}{2}]$ into J frequency bands $[-\frac{1}{2} + \frac{i}{J}, -\frac{1}{2} + \frac{i+1}{J}]$ for $i \in [J]$ which have half-bandwidth $W = \frac{1}{2J}$. For each of these J frequency bands, they take the first K Slepian basis vectors (where K is slightly larger than $2NW$) and modulate them to the center frequency of the i-th frequency band, i.e.

$$\boldsymbol{\Psi}_i = \boldsymbol{E}_{f_c^{(i)}} \boldsymbol{S}_K \in \mathbb{C}^{N \times K}$$

where we again use the notation $\boldsymbol{E}_f \in \mathbb{C}^{N \times N}$ for $f \in \mathbb{R}$ to denote the diagonal modulation matrix $\boldsymbol{E}_f[n, n] = e^{j2\pi f n}$, and $f_c^{(i)} = -\frac{1}{2} + \frac{2i+1}{2J}$ for $i \in [J]$. Finally, they concatenate the $\boldsymbol{\Psi}_i$'s to form the multiband modulated Slepian dictionary

$$\boldsymbol{\Psi} = \begin{bmatrix} \boldsymbol{\Psi}_0 & \boldsymbol{\Psi}_1 & \cdots & \boldsymbol{\Psi}_{J-1} \end{bmatrix} \in \mathbb{C}^{N \times JK}.$$

Since samples of signals bandlimited to $[-W, W]$ are typically well-approximated by the span of the first K Slepian basis vectors, samples of signals bandlimited to $[f_c - W, f_c + W]$ will typically be well-approximated by the span of the first K Slepian basis vectors modulated to the center frequency f_c, i.e. the span of the columns of $\boldsymbol{E}_{f_c} \boldsymbol{S}_K$. Hence, if our multiband signal had L active frequency bands of the form $\{[-\frac{1}{2} + \frac{i}{J}, -\frac{1}{2} + \frac{i+1}{J}]\}_{i \in \mathcal{I}}$ for some subset $\mathcal{I} \subset [J]$ with $\#(\mathcal{I}) = L$, then $\boldsymbol{x}$ will be well-approximated by the span of the columns of $\boldsymbol{\Psi}_{\mathcal{I}}$, i.e. the submatrix of $\boldsymbol{\Psi}$ formed by the blocks $\boldsymbol{\Psi}_i$ for $i \in \mathcal{I}$. This means

that

$$\boldsymbol{x} \approx \boldsymbol{\Psi}\boldsymbol{\alpha} = \sum_{i=0}^{J} \boldsymbol{\Psi}_i \boldsymbol{\alpha}_i$$

where $\boldsymbol{\alpha} \in \mathbb{C}^{JK}$ is a vector with J blocks $\boldsymbol{\alpha}_i \in \mathbb{C}^K$ for $i \in [J]$, and $\boldsymbol{\alpha}_i = \mathbf{0}$ for $i \notin \mathcal{I}$. In other words, $\boldsymbol{x} \approx \boldsymbol{\Psi}\boldsymbol{\alpha}$ for a group-sparse vector $\boldsymbol{\alpha}$.

7.3 Block-based CoSaMP

In [6], the authors propose using block-based CoSaMP to reconstruct the multiband signal $\boldsymbol{x}$ from the compressed measurements $\boldsymbol{y}$. They perform simulations demonstrating the effectiveness of block-based CoSaMP for recovering multiband signals. We briefly outline the main steps of block-based CoSaMP here.

First, initialize $\boldsymbol{r}^{(0)} = \boldsymbol{y}$ (residual), $\boldsymbol{x}^{(0)} = \mathbf{0}$, $\mathcal{I}^{(0)} = \emptyset$ (support set), $m = 0$ (iteration number). Then, for each iteration m, perform the following steps:

1. Form the "proxy" of the residual $\boldsymbol{h}^{(m)} = \boldsymbol{A}^* \boldsymbol{r}^{(m)} = \boldsymbol{A}^*(\boldsymbol{y} - \boldsymbol{A}\boldsymbol{x}^{(m)})$.

2. Identify a set $\Omega^{(m)} \subset [J] \setminus \mathcal{I}^{(m)}$ of the $\#(\Omega^{(m)}) = 2L$ new frequency bands with the largest values of $\|\boldsymbol{\Psi}_i^* \boldsymbol{h}^{(m)}\|_2$

3. Merge the new bands with the current bands $\Lambda^{(m)} = \Omega^{(m)} \cup \mathcal{I}^{(m)}$.

4. Solve the least-squares problem

$$\widetilde{\boldsymbol{\alpha}} = \underset{\boldsymbol{\alpha} \in \mathbb{C}^{JK}}{\arg\min} \|\boldsymbol{y} - \boldsymbol{A}\boldsymbol{\Psi}\boldsymbol{\alpha}\|_2 \quad \text{subject to} \quad \boldsymbol{\alpha}_i = \mathbf{0} \text{ for } i \notin \Lambda^{(m)}.$$

5. Prune $\Lambda^{(m)}$ from $3L$ indices (or $2L$ if this is the 0-th iteration) down to the subset $\mathcal{I}^{(m+1)} \subset \Lambda^{(m)}$ with $\#(\mathcal{I}^{(m+1)}) = L$ indices which have the largest values of $\|\widetilde{\boldsymbol{\alpha}}_i\|_2$.

6. Update $\boldsymbol{x}^{(m+1)} = \sum_{i \in \mathcal{I}^{(m+1)}} \boldsymbol{\Psi}_i \widetilde{\boldsymbol{\alpha}}_i$ and $\boldsymbol{r}^{(m+1)} = \boldsymbol{y} - \boldsymbol{A}\boldsymbol{x}^{(m+1)}$. Also, increment m.

7.4 Fast Block-based CoSaMP for Multiband Signals

We make two significant improvements to the approach in [6]. First, [6] assumes that the active frequency bands are each of the form $[-\frac{1}{2} + \frac{i}{J}, -\frac{1}{2} + \frac{i+1}{J}]$ for $i \in [J]$. This effectively restricts the L center frequencies of the active bands to lie on a coarse grid of J possible center frequencies, and the bandwidth of each frequency band are the same $\frac{1}{J}$. We allow the center frequencies to lie on the continuum subject to mild separation conditions, and we allow the bandwidths of each source to be different. Second, we speed up the computationally intensive steps using some of the fast algorithms presented earlier in this thesis. We outline our approach here.

Again, initialize $\boldsymbol{r}^{(0)} = \boldsymbol{y}$ (residual), $\boldsymbol{x}^{(0)} = \boldsymbol{0}$, $\mathcal{I}^{(0)} = \emptyset$ (support set), $m = 0$ (iteration number). Then, for each iteration m, perform the following steps:

1. Form the "proxy" of the residual $\boldsymbol{h}^{(m)} = \boldsymbol{A}^* \boldsymbol{r}^{(m)} = \boldsymbol{A}^*(\boldsymbol{y} - \boldsymbol{A}\boldsymbol{x}^{(m)})$.

2. Identify a set $\Omega^{(m)}$ of $2L$ new frequency bands by computing our fast approximation of the multitaper spectral estimate of $\boldsymbol{h}^{(m)}$.

3. Merge the new bands with the current bands $\Lambda^{(m)} = \Omega^{(m)} \cup \mathcal{I}^{(m)}$. Note that because the active bands lie on the continuum, some of the newly identified frequency bands in $\Omega^{(m)}$ may overlap with the previous support set $\mathcal{I}^{(m)}$.

4. Form a "fast" dictionary as follows: For each of the L' frequency bands in $\Omega^{(m)} = \{[f'_\ell - W'_\ell, f'_\ell + W'_\ell]\}_{\ell=0}^{L'-1}$, let $\boldsymbol{F}_\ell$ be an $N \times \approx 2NW'_\ell$ matrix whose columns are the $\approx 2NW'_\ell$ DFT vectors with frequencies in $[f'_\ell - W'_\ell, f'_\ell + W'_\ell]$, and let $\boldsymbol{S}_\ell$ be an $N \times O(\log(NW'_\ell) \log \frac{1}{\epsilon})$ matrix whose columns are the modulated Slepian basis vectors $\boldsymbol{E}_{f'_\ell} \boldsymbol{s}_k$ for k such that $\epsilon < \lambda_k < 1 - \epsilon$. Then, set $\boldsymbol{\Psi}_\ell^{(m)} = \begin{bmatrix} \boldsymbol{F}_\ell & \boldsymbol{S}_\ell \end{bmatrix}$. Finally, concatenate the $\boldsymbol{\Psi}_\ell^{(m)}$'s to form the fast dictionary $\boldsymbol{\Psi}^{(m)} = \begin{bmatrix} \boldsymbol{\Psi}_0^{(m)} & \boldsymbol{\Psi}_1^{(m)} & \cdots & \boldsymbol{\Psi}_{L'-1}^{(m)} \end{bmatrix}$.

5. Use conjugate gradient descent to solve the regularized least squares problem

$$\begin{aligned}\widetilde{\boldsymbol{\alpha}}^{(m)} &= \arg\min_{\boldsymbol{\alpha}} \|\boldsymbol{y} - \boldsymbol{A}\boldsymbol{\Psi}^{(m)}\boldsymbol{\alpha}\|_2^2 + \gamma\|\boldsymbol{\alpha}\|_2^2 \\ &= \left(\boldsymbol{\Psi}^{(m)*}\boldsymbol{A}^*\boldsymbol{A}\boldsymbol{\Psi}^{(m)} + \gamma\mathbf{I}\right)^{-1}\boldsymbol{\Psi}^{(m)*}\boldsymbol{A}^*\boldsymbol{y}\end{aligned}$$

6. Prune $\Lambda^{(m)}$ from L' indices down to the subset $\mathcal{I}^{(m+1)} \subset \Lambda^{(m)}$ with $\#(\mathcal{I}^{(m+1)}) = L$ indices which have the largest values of $\|\widetilde{\boldsymbol{\alpha}}_\ell^{(m)}\|_2$.

7. Update $\boldsymbol{x}^{(m+1)} = \sum_{\ell \in \mathcal{I}^{(m+1)}} \boldsymbol{\Psi}_\ell^{(m)}\widetilde{\boldsymbol{\alpha}}_\ell$ and $\boldsymbol{r}^{(m+1)} = \boldsymbol{y} - \boldsymbol{A}\boldsymbol{x}^{(m+1)}$. Also, increment m.

We now compare the computational complexities of the steps in our method to the steps of the method in [6]. Instead of computing the norms of J modulated Slepian projections $\|\boldsymbol{\Psi}_i^*\boldsymbol{h}^{(m)}\|_2 = \|\boldsymbol{S}_K^*\boldsymbol{E}_{f_c^{(i)}}^*\boldsymbol{h}^{(m)}\|_2$ which takes $O(J \cdot NK) = O(N^2)$ operations, our identification step takes $O(N \log N \log(NW_{\text{multi}}) \log \frac{1}{\epsilon_{\text{multi}}})$ operations to compute the multitaper spectral estimate of $\boldsymbol{h}^{(m)}$, which is equivalent to computing the norms of N modulated Slepian projections $\|\boldsymbol{S}_K^*\boldsymbol{E}_{n/N}^*\boldsymbol{h}^{(m)}\|_2$ for $n \in [N]$.

To solve the least squares problem in [6], one must first compute the vector $\boldsymbol{\Psi}_{\Lambda^{(m)}}^*\boldsymbol{A}^*\boldsymbol{y}$ and the matrix $\boldsymbol{\Psi}_{\Lambda^{(m)}}^*\boldsymbol{A}^*\boldsymbol{A}\boldsymbol{\Psi}_{\Lambda^{(m)}}$, and then compute $\widetilde{\boldsymbol{\alpha}} = (\boldsymbol{\Psi}_{\Lambda^{(m)}}^*\boldsymbol{A}^*\boldsymbol{A}\boldsymbol{\Psi}_{\Lambda^{(m)}})^{-1}\boldsymbol{\Psi}_{\Lambda^{(m)}}^*\boldsymbol{A}^*\boldsymbol{y}$. Even if $\boldsymbol{A}$ is a fast compressed sensing matrix (such as a fast Johnson-Lindenstrauss matrix), solving the system of equations $\boldsymbol{\Psi}_{\Lambda^{(m)}}^*\boldsymbol{A}^*\boldsymbol{A}\boldsymbol{\Psi}_{\Lambda^{(m)}}\widetilde{\boldsymbol{\alpha}} = \boldsymbol{\Psi}_{\Lambda^{(m)}}^*\boldsymbol{A}^*\boldsymbol{y}$ takes $O((3LK)^\omega) = O((LN/J)^\omega)$ operations where ω is the exponent in the runtime for solving linear systems. In our method, the matrix $\boldsymbol{\Psi}^{(m)}$ contains several DFT vectors and $\sum_{\ell=0}^{L'-1} O(\log(NW_\ell') \log \frac{1}{\epsilon}) \leq O(L \log N \log \frac{1}{\epsilon})$ modulated Slepian basis vectors. Hence, applying the matrices $\boldsymbol{\Psi}^{(m)}$ or $\boldsymbol{\Psi}^{(m)*}$ to a vector takes $O(LN \log N \log \frac{1}{\epsilon})$ operations. If $\boldsymbol{A}$ is a fast compressed sensing matrix, applying $\boldsymbol{A}$ or $\boldsymbol{A}^*$ to a vector can be done in $O(N \log N)$ operations. Thus, each iteration of conjugate gradient descent takes $O(LN \log N \log \frac{1}{\epsilon})$ operations. Although we have no mathematical justification, our experiments suggest the number of conjugate gradient iterations required is not too large.

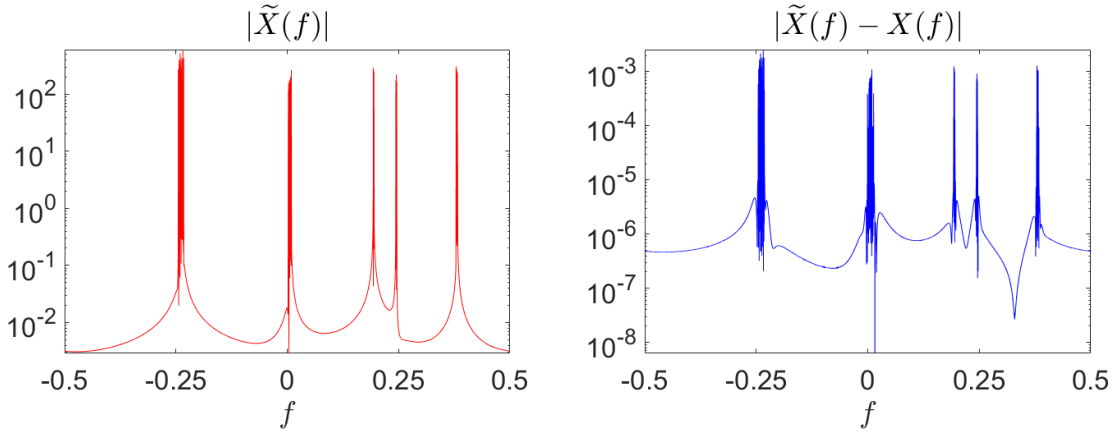

Figure 7.1: Plots of the magnitude of the DTFT of the recovered signal (left) and the difference between the recovered signal and the original signal (right).

7.5 Numerical Experiments

We test our fast version of block-based CoSaMP for multiband signals on a large scale problem. We generate a vector $\boldsymbol{x} \in \mathbb{C}^N$ with $N = 2^{20}$ samples of a multiband signal with $L = 5$ active frequency bands of widths W_ℓ between 1.0×10^{-4} and 6.0×10^{-3}. We then take $M = 281589$ compressed measurements using a simple subsampling matrix. Our method recovers a vector $\widetilde{\boldsymbol{x}}$ with a residual error of $\|\widetilde{\boldsymbol{x}} - \boldsymbol{x}\|_2 / \|\boldsymbol{x}\|_2 = 2.71 \times 10^{-6}$. Roughly 150 seconds of precomputation time was needed to precompute the Slepian tapers for the multitaper spectral estimate as well as the baseband Slepians for the fast dictionary. Roughly 40 seconds of computation time were needed to recover the signal using our fast version of block-based CoSaMP for multiband signals. We show a plot of the DTFT of the original signal and the residual in Figure 7.5 above. Although our experiment involved a signal that was 4096 times longer than that in [6], our algorithm was able to recover the multiband signal to a high degree of accuracy in a reasonable amount of time.

CHAPTER 8
CONCLUSIONS

This thesis presented several fast algorithms for working with a finite window of samples from a multiband signal. These algorithms all revolve around the Slepian basis vectors whose time-frequency localization properties make them useful in a wide variety of signal processing applications. The computational complexity and memory requirements of all of these algorithms scale linearly (times a few log factors) with respect to the number of samples, which make them a feasible option in large scale problems. We conclude this thesis with a brief summary of our results.

DPSS and PSWF Eigenvalues

We established novel non-asymptotic results (Theorems 1 and 2) which show that the number of DPSS eigenvalues between ϵ and $1 - \epsilon$ scales logarithmically with ϵ and logarithmically with the time-bandwidth product. Our non-asymptotic results are similar to the known asymptotic results, and they are substantively better than previous non-asymptotic results. We were also able to use Theorems 1 and 2 to obtain non-asymptotic bounds on the DPSS eigenvalues (Corollary 1) and sums involving the DPSS eigenvalues (Corollary 2), and we extended our results to the PSWF eigenvalues (Theorem 3 and Corollaries 3 and 4). These results enabled the fast algorithms in this thesis, and have important implications in other works.

Fast computations with Slepian basis vectors

We presented fast algorithms for projecting a vector onto the span of the leading Slepian basis vectors (Theorem 4a), for performing dimensionality reduction with Slepian basis vec-

tors (Theorem 4a combined with Theorem 5), and for solving systems of linear equations involving the prolate matrix (Theorems 4b and 4c). These algorithms work by approximating the matrix of interest as the sum of a Toeplitz (or circulant) matrix plus a factored low-rank matrix, both of which can be applied to a vector efficiently.

Thomson's multitaper method for spectral estimation

We derived novel non-asymptotic bounds on the bias, variance, covariance, and probability tails of Thomson's multitaper spectral estimate (Theorems 6-10. These bounds are similar to the existing asymptotic results when the multitaper spectral estimate uses $K = 2NW - O(\log(NW))$ tapers. However, when the traditional choice of $K = 2NW - O(1)$ tapers are used, the multitaper spectral estimate is prone to the effects of spectral leakage, and the non-asymptotic bounds can be significantly worse, especially when the power spectrum of interest has a high dynamic range. We also performed simulations to demonstrate these principles.

We also presented a fast algorithm for approximating Thomson's multitaper spectral estimate on a grid of uniformly spaced frequencies (Theorems 11 and 12). Just like the other fast algorithms involving the Slepian basis or the prolate matrix, the key to this fast algorithm is that only logarithmically many of the Slepian basis eigenvalues are not very close to 0 or 1.

Fast reconstruction from nonuniform samples

We presented a fast algorithm for reconstructing a multiband signal from nonuniform samples, provided we know the active frequency bands a priori. We first formulated reconstructing the signal as a Tikhonov regularization problem, whose solution involves solving a particular system of equations. The matrix corresponding to this system of equations has a generalized Cauchy-like structure, which enables this matrix to be applied to a vector efficiently. Furthermore, although this matrix is ill-conditioned, we were able to prove

in the single band case that the eigenvalues have a clustering behavior similar to that of the PSWFs. We then used this to show that conjugate gradient descent could solve this system of equations in a polylogarithmic number of iterations (Theorem 13). These observations show that using conjugate gradient descent along with a fast generalized Cauchy-like matrix-vector multiply yields a fast algorithm for reconstructing a bandlimited signal from nonuniform samples. We also showed simulations showing that this method works in the multiband case as well, although we do not yet have theoretical results to justify this rigorously.

Fast compressed sensing for multiband signals

We presented a fast version of the block-based CoSaMP algorithm for recovering a multiband signal from compressed measurements. Although we do not have rigorous guarantees on the runtime or the accuracy, we performed a large scale simulation to demonstrate that our algorithm runs in a reasonable amount of time, even when the signal of interest has over a million samples.

REFERENCES

[1] D. Slepian and H. Pollak, "Prolate spheroidal wave functions, Fourier analysis, and uncertainty. I," *Bell Systems Tech. J.*, vol. 40, no. 1, pp. 43–64, 1961.

[2] H. Landau and H. Pollak, "Prolate spheroidal wave functions, Fourier analysis, and uncertainty. II," *Bell Systems Tech. J.*, vol. 40, no. 1, pp. 65–84, 1961.

[3] ——, "Prolate spheroidal wave functions, Fourier analysis, and uncertainty. III," *Bell Systems Tech. J.*, vol. 41, no. 4, pp. 1295–1336, 1962.

[4] D. Slepian, "Prolate spheroidal wave functions, Fourier analysis, and uncertainty. IV," *Bell Systems Tech. J.*, vol. 43, no. 6, pp. 3009–3058, 1964.

[5] ——, "Prolate spheroidal wave functions, Fourier analysis, and uncertainty. V – The discrete case," *Bell Systems Tech. J.*, vol. 57, no. 5, pp. 1371–1430, 1978.

[6] M. Davenport and M. Wakin, "Compressive sensing of analog signals using discrete prolate spheroidal sequences," *Applied and computational harmonic analysis*, vol. 33, no. 3, pp. 438–472, 2012.

[7] Z. Zhu and M. B. Wakin, "Approximating sampled sinusoids and multiband signals using multiband modulated dpss dictionaries," *Journal of Fourier Analysis and Applications*, vol. 23, no. 6, pp. 1263–1310, 2017.

[8] S. Karnik, Z. Zhu, M. B. Wakin, J. Romberg, and M. A. Davenport, "The fast Slepian transform," *Applied and Computational Harmonic Analysis*, 2019.

[9] D. Thomson, "Spectrum estimation and harmonic analysis," *Proc. IEEE*, vol. 70, no. 9, pp. 1055–1095, 1982.

[10] T. Zemen and C. Mecklenbräuker, "Time-variant channel estimation using Discrete Prolate Spheroidal Sequences," *IEEE Transactions on Signal Processing*, vol. 53, no. 9, pp. 3597–3607, 2005.

[11] T. Zemen, C. F. Mecklenbrauker, F. Kaltenberger, and B. H. Fleury, "Minimum-energy band-limited predictor with dynamic subspace selection for time-variant flat-fading channels," *IEEE Transactions on Signal Processing*, vol. 55, no. 9, pp. 4534–4548, 2007.

[12] M. A. Davenport, S. R. Schnelle, J. P. Slavinsky, R. G. Baraniuk, M. B. Wakin, and P. T. Boufounos, "A wideband compressive radio receiver," in *2010-MILCOM 2010 Military Communications Conference*, IEEE, 2010, pp. 1193–1198.

[13] F. Yin, C. Debes, and A. M. Zoubir, "Parametric waveform design using discrete prolate spheroidal sequences for enhanced detection of extended targets," *IEEE Transactions on Signal Processing*, vol. 60, no. 9, pp. 4525–4536, 2012.

[14] Z. Zhu and M. B. Wakin, "Wall clutter mitigation and target detection using Discrete Prolate Spheroidal Sequences," in *Proc. Int. Work. on Compressed Sensing Theory Appl. Radar, Sonar and Remote Sens. (CoSeRa)*, Pisa, Italy, Jun. 2015.

[15] R. Matthysen and D. Huybrechs, "Fast algorithms for the computation of fourier extensions of arbitrary length," *SIAM Journal on Scientific Computing*, vol. 38, no. 2, A899–A922, 2016.

[16] D. Huybrechs, "On the Fourier extension of nonperiodic functions," *SIAM J. Numer. Anal.*, vol. 47, no. 6, pp. 4326–4355, 2010.

[17] B. Adcock, D. Huybrechs, and J. Martín-Vaquero, "On the numerical stability of fourier extensions," *Foundations of Computational Mathematics*, vol. 14, no. 4, pp. 635–687, 2014.

[18] J. Varah, "The prolate matrix," *Linear Algebra and its Applications*, vol. 187, pp. 269 –278, 1993.

[19] A. W. Bojanczyk, R. P. Brent, F. R. De Hoog, and D. R. Sweet, "On the stability of the bareiss and related toeplitz factorization algorithms," *SIAM J. Matrix Analysis and Applications*, vol. 16, pp. 40–57, 1995.

[20] J. H. McClellan, R. W. Schafer, and M. A. Yoder, *Signal Processing First*. Upper Saddle River, NJ: Pearson, 2003, ISBN: 9780130909992 9780130655622.

[21] S. Haykin, "Cognitive radio: Brain-empowered wireless communications," *IEEE journal on selected areas in communications*, vol. 23, no. 2, pp. 201–220, 2005.

[22] B. Farhang-Boroujeny, "Filter Bank Spectrum Sensing for Cognitive Radios," *IEEE Trans. Signal Process.*, vol. 56, no. 5, pp. 1801–1811, May 2008.

[23] B. Farhang-Boroujeny and R. Kempter, "Multicarrier communication techniques for spectrum sensing and communication in cognitive radios," *IEEE Communications Magazine*, vol. 46, no. 4, pp. 80–85, Apr. 2008.

[24] S. Haykin, D. J. Thomson, and J. H. Reed, "Spectrum sensing for cognitive radio," *Proceedings of the IEEE*, vol. 97, no. 5, pp. 849–877, 2009.

[25] E. Axell, G. Leus, E. Larsson, and H. Poor, "Spectrum sensing for cognitive radio : State-of-the-art and recent advances," *IEEE Signal Processing Magazine*, vol. 29, no. 3, pp. 101–116, May 2012.

[26] K. N. Hamdy, M. Ali, and A. H. Tewfik, "Low bit rate high quality audio coding with combined harmonic and wavelet representations," in *1996 IEEE International Conference on Acoustics, Speech, and Signal Processing (ICASSP) Conference Proceedings*, vol. 2, Atlanta, GA, USA: IEEE, 1996, pp. 1045–1048, ISBN: 9780780331921.

[27] T. Painter and A. Spanias, "Perceptual coding of digital audio," *Proc. IEEE*, vol. 88, no. 4, pp. 451–515, Apr. 2000.

[28] A. Delorme and S. Makeig, "EEGLAB: An open source toolbox for analysis of single-trial EEG dynamics including independent component analysis," *J. Neuroscience Methods*, vol. 134, no. 1, pp. 9–21, Mar. 2004.

[29] A. Delorme, T. Sejnowski, and S. Makeig, "Enhanced detection of artifacts in EEG data using higher-order statistics and independent component analysis," *NeuroImage*, vol. 34, no. 4, pp. 1443–1449, Feb. 2007.

[30] R. R. Llinas, U. Ribary, D. Jeanmonod, E. Kronberg, and P. P. Mitra, "Thalamocortical dysrhythmia: A neurological and neuropsychiatric syndrome characterized by magnetoencephalography," *Proc. Nat. Acad. Sci.*, vol. 96, no. 26, pp. 15 222–15 227, Dec. 1999.

[31] B. Pesaran, J. S. Pezaris, M. Sahani, P. P. Mitra, and R. A. Andersen, "Temporal structure in neuronal activity during working memory in macaque parietal cortex," *Nature Neuroscience*, vol. 5, no. 8, pp. 805–811, Aug. 2002.

[32] J. Csicsvari, B. Jamieson, K. D. Wise, and G. Buzsáki, "Mechanisms of gamma oscillations in the hippocampus of the behaving rat," *Neuron*, vol. 37, no. 2, pp. 311–322, Jan. 2003.

[33] P. P. Mitra and B. Pesaran, "Analysis of dynamic brain imaging data," *Biophysical Journal*, vol. 76, no. 2, pp. 691–708, Feb. 1999.

[34] M. W. Jones and M. A. Wilson, "Theta rhythms coordinate hippocampal–prefrontal interactions in a spatial memory task," *PLoS Biology*, vol. 3, no. 12, R. Morris, Ed., e402, Nov. 2005.

[35] G. Bond *et al.*, "A pervasive millennial-scale cycle in north atlantic holocene and glacial climates," *science*, vol. 278, no. 5341, pp. 1257–1266, 1997.

[36] M. Ghil *et al.*, "Advanced spectral methods for climatic time series," *Reviews of geophysics*, vol. 40, no. 1, pp. 3–1, 2002.

[37] R. Vautard and M. Ghil, "Singular spectrum analysis in nonlinear dynamics, with applications to paleoclimatic time series," *Physica D: Nonlinear Phenomena*, vol. 35, no. 3, pp. 395–424, May 1989.

[38] M. E. Mann and J. M. Lees, "Robust estimation of background noise and signal detection in climatic time series," *Climatic Change*, vol. 33, no. 3, pp. 409–445, Jul. 1996.

[39] S. Minobe, "A 50-70 year climatic oscillation over the north pacific and north america," *Geophys. Res. Lett.*, vol. 24, no. 6, pp. 683–686, Mar. 1997.

[40] J. Jouzel *et al.*, "Extending the Vostok ice-core record of palaeoclimate to the penultimate glacial period," *Nature*, vol. 364, no. 6436, pp. 407–412, Jul. 1993.

[41] D. J. Thomson, "Time series analysis of holocene climate data," *Philos. Trans. Roy. Soc. London. Ser. A, Math. and Physical Sci.*, vol. 330, no. 1615, pp. 601–616, 1990.

[42] D. Brunton, A. Rodrigo, and E. Marks, "Ecstatic display calls of the Adélie penguin honestly predict male condition and breeding success," *Behaviour*, vol. 147, no. 2, pp. 165–184, 2010.

[43] S. Saar and P. P. Mitra, "A technique for characterizing the development of rhythms in bird song," *PLoS ONE*, vol. 3, no. 1, B. McCabe, Ed., e1461, Jan. 2008.

[44] M. Hansson-Sandsten, M. Tarka, J. Caissy-Martineau, B. Hansson, and D. Hasselquist, "SVD-based classification of bird singing in different time-frequency domains using multitapers," in *2011 19th European Signal Processing Conference*, ISSN: 2076-1465, Aug. 2011, pp. 966–970.

[45] A. Leonardo and M. Konishi, "Decrystallization of adult birdsong by perturbation of auditory feedback," *Nature*, vol. 399, no. 6735, pp. 466–470, Jun. 1999.

[46] O. Tchernichovski, F. Nottebohm, C. E. Ho, B. Pesaran, and P. P. Mitra, "A procedure for an automated measurement of song similarity," *Animal Behaviour*, vol. 59, no. 6, pp. 1167–1176, Jun. 2000.

[47] M. A. Wieczorek, "Gravity and topography of the terrestrial planets," in *Treatise on Geophysics*, G. Schubert, Ed., 2nd, Amsterdam: Elsevier, Jan. 2007, pp. 165–206, ISBN: 9780444527486.

[48] S. G. Claudepierre, S. R. Elkington, and M. Wiltberger, "Solar wind driving of magnetospheric ULF waves: Pulsations driven by velocity shear at the magnetopause: ULF waves driven by velocity shear at the magnetopause," *J. Geophys. Res.: Space Phys.*, vol. 113, no. A5, May 2008.

[49] B. Allen and J. D. Romano, "Detecting a stochastic background of gravitational radiation: Signal processing strategies and sensitivities," *Phys. Rev. D*, vol. 59, no. 10, p. 102 001, Mar. 1999.

[50] G. G. Stokes, "On a method of detecting inequalities of unknown periods in a series of observations," *Proc. R. Soc. London*, vol. 29, pp. 122–123, 1879.

[51] A. Schuster, "On the investigation of hidden periodicities with application to a supposed 26 day period of meteorological phenomena," *Terrestrial Magnetism*, vol. 3, no. 1, pp. 13–41, 1898.

[52] F. Harris, "On the use of windows for harmonic analysis with the discrete fourier transform," *Proc. IEEE*, vol. 66, no. 1, pp. 51–83, 1978.

[53] H. Stark and J. W. Woods, *Probability, random processes, and estimation theory for engineers*. Englewood Cliffs, N.J: Prentice-Hall, 1986, ISBN: 9780137117062.

[54] J. Alman and V. V. Williams, "A refined laser method and faster matrix multiplication," in *Proceedings of the 2021 ACM-SIAM Symposium on Discrete Algorithms (SODA)*, SIAM, 2021, pp. 522–539.

[55] M. Morf, "Doubling algorithms for toeplitz and related equations," in *ICASSP'80. IEEE International Conference on Acoustics, Speech, and Signal Processing*, IEEE, vol. 5, 1980, pp. 954–959.

[56] M. Stewart, "A superfast toeplitz solver with improved numerical stability," *SIAM journal on matrix analysis and applications*, vol. 25, no. 3, pp. 669–693, 2003.

[57] S. Chandrasekaran, M. Gu, X Sun, J. Xia, and J. Zhu, "A superfast algorithm for toeplitz systems of linear equations," *SIAM Journal on Matrix Analysis and Applications*, vol. 29, no. 4, pp. 1247–1266, 2007.

[58] L Greengard and V Rokhlin, "A fast algorithm for particle simulations," *Journal of Computational Physics*, vol. 73, no. 2, pp. 325 –348, 1987.

[59] J. Carrier, L. Greengard, and V. Rokhlin, "A fast adaptive multipole algorithm for particle simulations," *SIAM Journal on Scientific and Statistical Computing*, vol. 9, no. 4, pp. 669–686, 1988.

[60] A. Dutt, M. Gu, and V. Rokhlin, "Fast algorithms for polynomial interpolation, integration, and differentiation," *SIAM Journal on Numerical Analysis*, vol. 33, no. 5, pp. 1689–1711, 1996.

[61] V. Y. Pan and A. Zheng, "Superfast algorithms for Cauchy-like matrix computations and extensions," *Linear Algebra and its Applications*, vol. 310, no. 1, pp. 83 –108, 2000.

[62] S. Chandrasekaran, N. Govindarajan, and A. Rajagopal, "Fast algorithms for displacement and low-rank structured matrices," *arXiv preprint arXiv:1807.03437*, 2018.

[63] E. J. Candes, J. K. Romberg, and T. Tao, "Stable signal recovery from incomplete and inaccurate measurements," *Communications on Pure and Applied Mathematics*, vol. 59, no. 8, pp. 1207–1223, 2006.

[64] Y. C. Eldar and G. Kutyniok, *Compressed sensing: theory and applications*. Cambridge University Press, 2013.

[65] A. S. Bandeira, E. Dobriban, D. G. Mixon, and W. F. Sawin, "Certifying the restricted isometry property is hard," *IEEE Trans. Inform. Theory*, vol. 59, no. 9, pp. 3448–3450, 2013.

[66] R. Baraniuk, M. Davenport, R. DeVore, and M. Wakin, "A simple proof of the restricted isometry property for random matrices," *Const. Approx.*, vol. 28, no. 3, pp. 253–263, 2008.

[67] D. Needell and J. A. Tropp, "Cosamp: Iterative signal recovery from incomplete and inaccurate samples," *Applied and computational harmonic analysis*, vol. 26, no. 3, pp. 301–321, 2009.

[68] S. Chen, D. Donoho, and M. Saunders, "Atomic decomposition by basis pursuit," *SIAM Rev.*, vol. 43, no. 1, pp. 129–159, 2001.

[69] S. Becker, J. Bobin, and E. J. Candès, "Nesta: A fast and accurate first-order method for sparse recovery," *SIAM Journal on Imaging Sciences*, vol. 4, no. 1, pp. 1–39, 2011.

[70] R. Tibshirani, "Regression shrinkage and selection via the lasso," *Journal of the Royal Statistical Society: Series B (Methodological)*, vol. 58, no. 1, pp. 267–288, 1996.

[71] E. Candes, T. Tao, *et al.*, "The dantzig selector: Statistical estimation when p is much larger than n," *The annals of Statistics*, vol. 35, no. 6, pp. 2313–2351, 2007.

[72] S. G. Mallat and Z. Zhang, "Matching pursuits with time-frequency dictionaries," *IEEE Transactions on signal processing*, vol. 41, no. 12, pp. 3397–3415, 1993.

[73] Y. C. Pati, R. Rezaiifar, and P. S. Krishnaprasad, "Orthogonal matching pursuit: Recursive function approximation with applications to wavelet decomposition," in *Proceedings of 27th Asilomar conference on signals, systems and computers*, IEEE, 1993, pp. 40–44.

[74] T. Blumensath and M. E. Davies, "Iterative hard thresholding for compressed sensing," *Applied and computational harmonic analysis*, vol. 27, no. 3, pp. 265–274, 2009.

[75] E. J. Candes, Y. C. Eldar, D. Needell, and P. Randall, "Compressed sensing with coherent and redundant dictionaries," *Applied and Computational Harmonic Analysis*, vol. 31, no. 1, pp. 59–73, 2011.

[76] M. Stojnic, F. Parvaresh, and B. Hassibi, "On the reconstruction of block-sparse signals with an optimal number of measurements," *IEEE Transactions on Signal Processing*, vol. 57, no. 8, pp. 3075–3085, 2009.

[77] Y. C. Eldar and M. Mishali, "Robust recovery of signals from a structured union of subspaces," *IEEE Transactions on Information Theory*, vol. 55, no. 11, pp. 5302–5316, 2009.

[78] Y. C. Eldar, P. Kuppinger, and H. Bolcskei, "Block-sparse signals: Uncertainty relations and efficient recovery," *IEEE Transactions on Signal Processing*, vol. 58, no. 6, pp. 3042–3054, 2010.

[79] M. F. Duarte, C. Hegde, V. Cevher, and R. G. Baraniuk, "Recovery of compressible signals in unions of subspaces," in *2009 43rd Annual Conference on Information Sciences and Systems*, IEEE, 2009, pp. 175–180.

[80] L. Hu, Z. Shi, J. Zhou, and Q. Fu, "Compressed sensing of complex sinusoids: An approach based on dictionary refinement," *IEEE Transactions on Signal Processing*, vol. 60, no. 7, pp. 3809–3822, 2012.

[81] M. F. Duarte and R. G. Baraniuk, "Spectral compressive sensing," *Applied and Computational Harmonic Analysis*, vol. 35, no. 1, pp. 111–129, 2013.

[82] L. Hu, J. Zhou, Z. Shi, and Q. Fu, "A fast and accurate reconstruction algorithm for compressed sensing of complex sinusoids," *IEEE Transactions on Signal Processing*, vol. 61, no. 22, pp. 5744–5754, 2013.

[83] G. Tang, B. N. Bhaskar, P. Shah, and B. Recht, "Compressed sensing off the grid," *IEEE transactions on information theory*, vol. 59, no. 11, pp. 7465–7490, 2013.

[84] Z. Yang and L. Xie, "Continuous compressed sensing with a single or multiple measurement vectors," in *2014 IEEE Workshop on Statistical Signal Processing (SSP)*, IEEE, 2014, pp. 288–291.

[85] J. Fang, F. Wang, Y. Shen, H. Li, and R. S. Blum, "Super-resolution compressed sensing for line spectral estimation: An iterative reweighted approach," *IEEE Transactions on Signal Processing*, vol. 64, no. 18, pp. 4649–4662, 2016.

[86] M. Mishali, Y. C. Eldar, O. Dounaevsky, and E. Shoshan, "Xampling: Analog to digital at sub-nyquist rates," *IET circuits, devices & systems*, vol. 5, no. 1, pp. 8–20, 2011.

[87] S. Karnik, J. Romberg, and M. A. Davenport, "Improved bounds for the eigenvalues of prolate spheroidal wave functions and discrete prolate spheroidal sequences," *Applied and Computational Harmonic Analysis*, vol. 55, pp. 97–128, 2021.

[88] M. Boulsane, N. Bourguiba, and A. Karoui, "Discrete prolate spheroidal wave functions: Further spectral analysis and some related applications," *Journal of Scientific Computing*, vol. 82, no. 3, pp. 1–19, 2020.

[89] A. Bonami, P. Jaming, and A. Karoui, "Non-asymptotic behaviour of the spectrum of the sinc kernel operator and related applications," *arXiv preprint arXiv:1804.01257*, 2018.

[90] H. Landau and H. Widom, "Eigenvalue distribution of time and frequency limiting," *Journal of Mathematical Analysis and Applications*, vol. 77, no. 2, pp. 469–481, 1980.

[91] A. Osipov, "Certain upper bounds on the eigenvalues associated with prolate spheroidal wave functions," *Applied and Computational Harmonic Analysis*, vol. 35, no. 2, pp. 309–340, 2013.

[92] H. Landau, "On the density of phase-space expansions," *IEEE transactions on information theory*, vol. 39, no. 4, pp. 1152–1156, 1993.

[93] A. Israel, "The eigenvalue distribution of time-frequency localization operators," *arXiv preprint arXiv:1502.04404*, 2015.

[94] D. M. Gruenbacher and D. R. Hummels, "A simple algorithm for generating discrete prolate spheroidal sequences," *IEEE Transactions on Signal Processing*, vol. 42, no. 11, pp. 3276–3278, 1994.

[95] A. Osipov and V. Rokhlin, "On the evaluation of prolate spheroidal wave functions and associated quadrature rules," *Applied and Computational Harmonic Analysis*, vol. 36, no. 1, pp. 108–142, 2014.

[96] S. Karnik, Z. Zhu, M. B. Wakin, J. K. Romberg, and M. A. Davenport, "Fast computations for approximation and compression in slepian spaces," in *2016 IEEE Global Conference on Signal and Information Processing (GlobalSIP)*, IEEE, 2016, pp. 1359–1363.

[97] F. Ahmad, Q. Jiang, and M. Amin, "Wall clutter mitigation using Discrete Prolate Spheroidal Sequences for sparse reconstruction of indoor stationary scenes," *IEEE Trans. Geosci. Remote Sens.*, vol. 53, no. 3, pp. 1549–1557, 2015.

[98] M. A. Davenport, P. T. Boufounos, M. B. Wakin, and R. G. Baraniuk, "Signal processing with compressive measurements," *IEEE Journal of Selected topics in Signal processing*, vol. 4, no. 2, pp. 445–460, 2010.

[99] E. Sejdić, A. Can, L. Chaparro, C. Steele, and T. Chau, "Compressive sampling of swallowing accelerometry signals using time-frequency dictionaries based on modulated Discrete Prolate Spheroidal Sequences," *EURASIP J. Adv. Signal Processing*, vol. 2012, no. 1, pp. 1–14, 2012.

[100] E. Sejdic, M. Luccini, S. Primak, K. Baddour, and T. Willink, "Channel estimation using dpss based frames," in *2008 IEEE International Conference on Acoustics, Speech and Signal Processing*, IEEE, 2008, pp. 2849–2852.

[101] S. Karnik, J. Romberg, and M. A. Davenport, "Fast multitaper spectral estimation," in *2019 International Conference on Sampling Theory and Applications (SampTA)*, IEEE, 2019.

[102] S. Karnik, J. Romberg, and M. A. Davenport, "Thomson's multitaper method revisited," *arXiv preprint arXiv:2103.11586*, 2021.

[103] A. T. Walden, "A unified view of multitaper multivariate spectral estimation," *Biometrika*, vol. 87, no. 4, pp. 767–788, 2000.

[104] K. S. Lii and M. Rosenblatt, "Prolate spheroidal spectral estimates," *Statist. & Probability. Lett.*, vol. 78, no. 11, pp. 1339–1348, Aug. 2008.

[105] L. Abreu and J. Romero, "MSE estimates for multitaper spectral estimation and off-grid compressive sensing," *IEEE Trans. Inform. Theory*, vol. 63, no. 12, 7770–7776, 2017.

[106] C. L. Haley and M. Anitescu, "Optimal bandwidth for multitaper spectrum estimation," *IEEE Sig. Proc. Lett.*, vol. 24, no. 11, pp. 1696–1700, Nov. 2017.

[107] D. B. Percival, A. T. Walden, *et al.*, *Spectral analysis for physical applications*. cambridge university press, 1993.

[108] S. Karnik, J. Romberg, and M. A. Davenport, "Bandlimited signal reconstruction from nonuniform samples," in *2019 Proc. Work. on Signal Processing with Adaptive Sparse Structured Representations (SPARS)*, IEEE, 2019.

[109] D. Coppersmith and S. Winograd, "Matrix multiplication via arithmetic progressions," *Journal of Symbolic Computation*, vol. 9, no. 3, pp. 251 –280, 1990, Computational algebraic complexity editorial.

[110] F. Le Gall, "Faster algorithms for rectangular matrix multiplication," in *2012 IEEE 53rd Annual Symposium on Foundations of Computer Science*, 2012, pp. 514–523.

[111] J.-P. Cardinal, "On a property of cauchy-like matrices," *Comptes Rendus de l'Académie des Sciences - Series I - Mathematics*, vol. 328, no. 11, pp. 1089 –1093, 1999.

[112] J. R. Shewchuk, "An introduction to the conjugate gradient method without the agonizing pain," 1994.

[113] J. A. Tropp *et al.*, "An introduction to matrix concentration inequalities," *Foundations and Trends in Machine Learning*, vol. 8, no. 1-2, pp. 1–230, 2015.

[114] B. Beckermann and A. Townsend, "Bounds on the singular values of matrices with displacement structure," *SIAM Review*, vol. 61, no. 2, pp. 319–344, 2019.

[115] E. I. Zolotarev, "Application of elliptic functions to questions of functions deviating least and most from zero," *Zap. Imp. Akad. Nauk. St. Petersburg*, vol. 30, no. 5, pp. 1–59, 1877.

[116] I. Schur, "Bemerkungen zur theorie der beschränkten bilinearformen mit unendlich vielen veränderlichen," *J. Reine Angew. Math.*, vol. 140, pp. 1–28, 1911.

[117] P. H. M. Janssen and P. Stoica, "On the expectation of the product of four matrix-valued Gaussian random variables," *IEEE Trans. Autom. Control*, vol. 33, no. 9, pp. 867–870, Sep. 1988.

[118] S. Janson, "Tail bounds for sums of geometric and exponential variables," *Statist. & Probability. Lett.*, vol. 135, pp. 1–6, Apr. 2018.

[119] D. L. Hanson and F. T. Wright, "A bound on tail probabilities for quadratic forms in independent random variables," *Ann. Math. Statist.*, vol. 42, no. 3, pp. 1079–1083, Jun. 1971.

[120] F. T. Wright, "A bound on tail probabilities for quadratic forms in independent random variables whose distributions are not necessarily symmetric," *Ann. Probability*, vol. 1, no. 6, pp. 1068–1070, Dec. 1973.

[121] S. Minsker, "On some extensions of bernstein's inequality for self-adjoint operators," *Statistics & Probability Letters*, vol. 127, pp. 111–119, 2017.

[122] N. I. Akhiezer, "Elements of the theory of elliptic functions. transl. of mathematical monographs, vol. 79," *American Mathematical Soc.*, 1990.

[123] E. Süli and D. Mayers, *An Introduction to Numerical Analysis*. Cambridge University Press, 2003, p. 244.

[124] A. Lu and E. Wachspress, "Solution of Lyapunov equations by alternating direction implicit iteration," *Computers & Mathematics with Applications*, vol. 21, no. 9, pp. 43–58, 1991.

[125] E. Wachspress, *The ADI Model Problem*. Springer-Verlag, 2013.

[126] J.-R. Li and J. White, "Low rank solution of Lyapunov equations," *SIAM J. Matrix Anal. Appl.*, vol. 24, no. 1, pp. 260–280, 2002.

[127] D. Lawden, *Elliptic Functions and Applications*. Springer-Verlag, 1989.

Appendices

APPENDIX A

PROOFS FOR CHAPTER 3

A.1 Proof of Bounds on the Number of DPSS Eigenvalues in the Transition Region (Theorems 1 and 2)

A.1.1 Proof overview

For any rectangular matrix $\boldsymbol{X} \in \mathbb{C}^{M\times N}$. we use the notation $\sigma_k(\boldsymbol{X})$ to denote the k^{th} largest singular value of $\boldsymbol{X}$. If $k > \min\{M, N\}$, we define $\sigma_k(\boldsymbol{X}) = 0$. Also, for a Hermitian matrix $\boldsymbol{A} \in \mathbb{C}^{N\times N}$, we use the notation $\mu_k(\boldsymbol{A})$ to denote k^{th} largest eigenvalue of a symmetric matrix. Again, if $k > N$, we define $\mu_k(\boldsymbol{A}) = 0$. To be consistent with standard notation, we define $\lambda_k = \mu_{k+1}(\boldsymbol{B})$ for $k \in [N]$, i.e. λ_k is the $(k+1)^{\text{th}}$ largest eigenvalue of the $N\times N$ prolate matrix $\boldsymbol{B}$ with bandwidth parameter W, which is defined in (2.1). Although both $\boldsymbol{B}$ and λ_k depend on N and W, our notation will omit this dependence for convenience.

We first sketch a non-rigorous outline of our proof. We aim to show that $\boldsymbol{B} - \boldsymbol{B}^2$ has a low numerical rank. Therefore, very few of the eigenvalues of $\boldsymbol{B} - \boldsymbol{B}^2$ are not near 0, and thus, very few of the eigenvalues of $\boldsymbol{B}$ are not near 1 or 0. To show $\boldsymbol{B} - \boldsymbol{B}^2$ has a low numerical rank, recall that $\boldsymbol{B}$ is a matrix representation of the self-adjoint operator $\mathcal{T}_N\mathcal{B}_W\mathcal{T}_N$. Hence, $\boldsymbol{B} - \boldsymbol{B}^2$ is a matrix representation of the operator

$$\begin{aligned}\mathcal{T}_N\mathcal{B}_W\mathcal{T}_N - (\mathcal{T}_N\mathcal{B}_W\mathcal{T}_N)^2 &= \mathcal{T}_N\mathcal{B}_W\mathcal{B}_W\mathcal{T}_N - \mathcal{T}_N\mathcal{B}_W\mathcal{T}_N\mathcal{B}_W\mathcal{T}_N \\ &= \mathcal{T}_N\mathcal{B}_W(\mathcal{I} - \mathcal{T}_N)\mathcal{B}_W\mathcal{T}_N \\ &= \mathcal{T}_N\mathcal{B}_W(\mathcal{I} - \mathcal{T}_N)(\mathcal{I} - \mathcal{T}_N)\mathcal{B}_W\mathcal{T}_N\end{aligned}$$

Thus showing that the matrix $\boldsymbol{B} - \boldsymbol{B}^2$ has a low numerical rank is equivalent to showing

that the operator $(\mathcal{I} - \mathcal{T}_N)\mathcal{B}_W\mathcal{T}_N$ has a low numerical rank. This operator satisfies

$$\langle \delta_\ell, (\mathcal{I} - \mathcal{T}_N)\mathcal{B}_W\mathcal{T}_N\delta_n\rangle = \frac{\sin[2\pi W(\ell - n)]}{\pi(\ell - n)} \quad \text{for} \quad \ell \in \mathbb{Z} \setminus [N], n \in [N],$$

where $\{\delta_n\}_{n\in\mathbb{Z}}$ are the Euclidean basis sequences for $\ell_2(\mathbb{Z})$. If we let $\boldsymbol{X}$ be the "matrix" representation of this operator with respect to the Euclidean basis, then the entries of $\boldsymbol{X}$ are a smooth function of the row and column indices, and $\boldsymbol{X}$ has what is known as a low displacement-rank structure. These facts can be exploited to show that $\boldsymbol{X}$, and thus also $(\mathcal{I}-\mathcal{T}_N)\mathcal{B}_W\mathcal{T}_N$, has a low numerical rank. Proving this rigorously requires that we truncate $(\mathcal{I} - \mathcal{T}_N)\mathcal{B}_W\mathcal{T}_N$ to a finite dimensional subspace, and take the limit as the dimension goes to infinity. The following lemma allows us to start a formal and rigorous version of the above argument.

Lemma 3. *Suppose for some $r \in [N]$ and $L_0 \in \mathbb{N}$, there exists a sequence of matrices $\boldsymbol{X}_L \in \mathbb{R}^{2L\times N}$ for $L = L_0, L_0 + 1, \ldots,$ such that:*

- $\lim_{L\to\infty} \left\|(\boldsymbol{B} - \boldsymbol{B}^2) - \boldsymbol{X}_L^*\boldsymbol{X}_L\right\|_F^2 = 0$,
- $\sigma_{r+1}(\boldsymbol{X}_L) \le \sqrt{\epsilon(1-\epsilon)}$ *for all* $L \ge L_0$.

Then, $\#\{k : \epsilon < \lambda_k < 1 - \epsilon\} \le r$.

Proof. By the first property, $\lim_{L\to\infty} \mu_{r+1}(\boldsymbol{X}_L^*\boldsymbol{X}_L)$ exists and is equal to $\mu_{r+1}(\boldsymbol{B}-\boldsymbol{B}^2)$. Then by using the fact that $\mu_{r+1}(\boldsymbol{X}_L^*\boldsymbol{X}_L) = \sigma_{r+1}(\boldsymbol{X}_L)^2$ for all $L \ge L_0$ along with the second property, we have

$$\mu_{r+1}(\boldsymbol{B} - \boldsymbol{B}^2) = \lim_{L\to\infty} \mu_{r+1}(\boldsymbol{X}_L^*\boldsymbol{X}_L) = \lim_{L\to\infty} \sigma_{r+1}(\boldsymbol{X}_L)^2 \le \epsilon(1-\epsilon).$$

The eigenvalues of $\boldsymbol{B} - \boldsymbol{B}^2$ are $\{\lambda_k(1 - \lambda_k)\}_{k=0}^{N-1}$. Also, the function $\lambda \mapsto \lambda(1 - \lambda)$ is increasing for $\lambda < \frac{1}{2}$ and decreasing for $\lambda > \frac{1}{2}$ and symmetric about $\lambda = \frac{1}{2}$. As a result,

$\epsilon < \lambda < 1-\epsilon$ if and only if $\lambda(1-\lambda) > \epsilon(1-\epsilon)$. Therefore,

$$\#\{k : \epsilon < \lambda_k < 1-\epsilon\} = \#\{k : \lambda_k(1-\lambda_k) > \epsilon(1-\epsilon)\} = \#\{k : \mu_k(\boldsymbol{B}-\boldsymbol{B}^2) > \epsilon(1-\epsilon)\} \leq r.$$

□

We will prove both Theorem 1 and Theorem 2 by using Lemma 3. In Section A.1.2, we construct a sequence of matrices $\boldsymbol{X}_L \in \mathbb{R}^{2L\times N}$ which satisfies the first property above. In Section A.1.3, we show that the singular values of each matrix $\boldsymbol{X}_L$ decays exponentially, which allows us to obtain the bound in Theorem 1. In Section A.1.4, we refine the rate at which the singular values of each $\boldsymbol{X}_L$ decay, which allows us to obtain the bound in Theorem 2.

A.1.2 Constructing the sequence of matrices $\boldsymbol{X}_L$

First, we state a sinc function identity. For any $W \in (0, \frac{1}{2})$ and any $m, n \in \mathbb{Z}$,

$$\sum_{\ell=-\infty}^{\infty} \frac{\sin[2\pi W(\ell-m)]}{\pi(\ell-m)} \frac{\sin[2\pi W(\ell-n)]}{\pi(\ell-n)} = \frac{\sin[2\pi W(m-n)]}{\pi(m-n)}.$$

By using this identity, we can write the entries of $\boldsymbol{B}-\boldsymbol{B}^2$ as:

$$\begin{aligned}
&(\boldsymbol{B}-\boldsymbol{B}^2)[m,n] \\
&= \boldsymbol{B}[m,n] - \sum_{\ell=0}^{N-1} \boldsymbol{B}[m,\ell]\boldsymbol{B}[\ell,n] \\
&= \frac{\sin[2\pi W(m-n)]}{\pi(m-n)} - \sum_{\ell=0}^{N-1} \frac{\sin[2\pi W(m-\ell)]}{\pi(m-\ell)} \frac{\sin[2\pi W(\ell-n)]}{\pi(\ell-n)} \\
&= \sum_{\ell=-\infty}^{\infty} \frac{\sin[2\pi W(\ell-m)]}{\pi(\ell-m)} \frac{\sin[2\pi W(\ell-n)]}{\pi(\ell-n)} - \sum_{\ell=0}^{N-1} \frac{\sin[2\pi W(\ell-m)]}{\pi(\ell-m)} \frac{\sin[2\pi W(\ell-n)]}{\pi(\ell-n)} \\
&= \sum_{\ell=-\infty}^{-1} \frac{\sin[2\pi W(\ell-m)]}{\pi(\ell-m)} \frac{\sin[2\pi W(\ell-n)]}{\pi(\ell-n)} + \sum_{\ell=N}^{\infty} \frac{\sin[2\pi W(\ell-m)]}{\pi(\ell-m)} \frac{\sin[2\pi W(\ell-n)]}{\pi(\ell-n)}
\end{aligned}$$

where the rearranging of terms is valid since the summands decay like $O(|\ell|^{-2})$ as $\ell \to \pm\infty$, and thus, all the sums are absolutely convergent.

For each integer $L \geq 1$, we define an index set

$$\mathcal{I}_L = \{-L, -L+1 \ldots, -2, -1\} \cup \{N, N+1, \ldots, N+L-2, N+L-1\}$$

and we define $\boldsymbol{X}_L \in \mathbb{R}^{2L \times N}$ by

$$\boldsymbol{X}_L[\ell, n] = \frac{\sin[2\pi W(\ell - n)]}{\pi(\ell - n)} \quad \text{for} \quad \ell \in \mathcal{I}_L \text{ and } n \in [N].$$

Note that we index the rows of $\boldsymbol{X}_L$ by $\mathcal{I}_L$ instead of the usual $[2L]$ for convenience. We will also index the rows and/or columns of other matrices with dimension $2L$ by $\mathcal{I}_L$. With this definition, the entries of $\boldsymbol{X}_L^* \boldsymbol{X}_L$ are

$$\begin{aligned}
&(\boldsymbol{X}_L^* \boldsymbol{X}_L)[m, n] \\
&= \sum_{\ell \in \mathcal{I}_L} \boldsymbol{X}_L[\ell, m] \boldsymbol{X}_L[\ell, n] \\
&= \sum_{\ell=-L}^{-1} \frac{\sin[2\pi W(\ell - m)]}{\pi(\ell - m)} \frac{\sin[2\pi W(\ell - n)]}{\pi(\ell - n)} + \sum_{\ell=N}^{N+L-1} \frac{\sin[2\pi W(\ell - m)]}{\pi(\ell - m)} \frac{\sin[2\pi W(\ell - n)]}{\pi(\ell - n)}
\end{aligned}$$

From the equations for $(\boldsymbol{B} - \boldsymbol{B}^2)[m, n]$ and $(\boldsymbol{X}_L^* \boldsymbol{X}_L)[m, n]$ above, we have that

$$\lim_{L \to \infty} (\boldsymbol{X}_L^* \boldsymbol{X}_L)[m, n] = (\boldsymbol{B} - \boldsymbol{B}^2)[m, n]$$

for each of the N^2 entries. Therefore,

$$\lim_{L \to \infty} \left\| (\boldsymbol{B} - \boldsymbol{B}^2) - \boldsymbol{X}_L^* \boldsymbol{X}_L \right\|_F^2 = \lim_{L \to \infty} \sum_{m=0}^{N-1} \sum_{n=0}^{N-1} \left| (\boldsymbol{B} - \boldsymbol{B}^2)[m, n] - (\boldsymbol{X}_L^* \boldsymbol{X}_L)[m, n] \right|^2 = 0.$$

This shows that the sequence of matrices $\boldsymbol{X}_L \in \mathbb{R}^{2L \times N}$ satisfies the first property of Lemma 3. We will now focus on bounding the singular values of each $\boldsymbol{X}_L$ in order to

prove that these matrices $\boldsymbol{X}_L$ satisfy the second property of Lemma 3.

A.1.3 Proof of Theorem 1

In [114], Beckermann and Townsend showed that matrices with a low-rank displacement have rapidly decaying singular values provided the spectra of the left and right displacement matrices are well separated. More specifically, suppose a matrix $\boldsymbol{X} \in \mathbb{C}^{M\times N}$ satisfies the displacement equation

$$\boldsymbol{C}\boldsymbol{X} - \boldsymbol{X}\boldsymbol{D} = \boldsymbol{U}\boldsymbol{V}^*$$

where $\boldsymbol{C} \in \mathbb{C}^{M\times M}$ and $\boldsymbol{D} \in \mathbb{C}^{N\times N}$ are normal matrices and $\boldsymbol{U} \in \mathbb{C}^{M\times \nu}$ and $\boldsymbol{D} \in \mathbb{C}^{N\times \nu}$. If there are closed, disjoint subsets E, F of $\mathbb{C}$ such that $\mathrm{Spec}(\boldsymbol{C}) \subset E$ and $\mathrm{Spec}(\boldsymbol{D}) \subset F$ then the singular values of $\boldsymbol{X}$ satisfy

$$\sigma_{\nu k+1}(\boldsymbol{X}) \leq \sigma_1(\boldsymbol{X}) Z_k(E, F)$$

for all integers $k \geq 0$, where $Z_k(E, F)$ are the Zolotarev numbers [115] for the sets E and F. As a rule of thumb, when E and F are "well-separated", $Z_k(E, F)$ decays exponentially with k. For more details about Zolotarev numbers, see Appendix E.1.

In Appendix E.2, we build on the work of Beckermann and Townsend to prove the following theorem.

Theorem 14. *Suppose $\boldsymbol{X} \in \mathbb{C}^{M\times N}$ satisfies the displacement equation*

$$\boldsymbol{C}\boldsymbol{X} - \boldsymbol{X}\boldsymbol{D} = \boldsymbol{U}\boldsymbol{V}^*$$

where $\boldsymbol{C} \in \mathbb{C}^{M\times M}$ and $\boldsymbol{D} \in \mathbb{C}^{N\times N}$ are normal matrices with real eigenvalues and $\boldsymbol{U} \in \mathbb{C}^{M\times \nu}$ and $\boldsymbol{V} \in \mathbb{C}^{N\times \nu}$. If Spec$(\boldsymbol{C}) \subset (-\infty, c_1] \cup [c_2, \infty)$ and Spec$(\boldsymbol{D}) \subset [d_1, d_2]$ where

$c_1 < d_1 < d_2 < c_2$, *then for any integer* $k \geq 0$,

$$\sigma_{\nu k+1}(\boldsymbol{X}) \leq 4\|\boldsymbol{X}\| \exp\left[-\frac{\pi^2 k}{\log(16\gamma)}\right] \quad \textit{where} \quad \gamma = \frac{(c_2-d_1)(d_2-c_1)}{(c_2-d_2)(d_1-c_1)}.$$

We now show that the matrices $\boldsymbol{X}_L$ defined in Section A.1.2 satisfy a low-rank displacement equation, and use Theorem 14 to bound their singular values. Define a diagonal matrix $\boldsymbol{D} \in \mathbb{R}^{N\times N}$ by $\boldsymbol{D}[n,n] = n$ for $n \in [N]$. For each integer $L \geq 1$, define a diagonal matrix $\boldsymbol{C}_L \in \mathbb{R}^{2L\times 2L}$ by $\boldsymbol{C}_L[\ell,\ell] = \ell$ for $\ell \in \mathcal{I}_L$ (again, we index $\boldsymbol{C}_L$ by $\ell \in \mathcal{I}_L$ for convenience). With this definition, we have

$$\begin{aligned}
(\boldsymbol{C}_L\boldsymbol{X}_L - \boldsymbol{X}_L\boldsymbol{D})[\ell,n] &= \boldsymbol{C}_L[\ell,\ell]\boldsymbol{X}_L[\ell,n] - \boldsymbol{X}_L[\ell,n]\boldsymbol{D}[n,n] \\
&= \ell \cdot \frac{\sin[2\pi W(\ell-n)]}{\pi(\ell-n)} - \frac{\sin[2\pi W(\ell-n)]}{\pi(\ell-n)} \cdot n \\
&= \frac{1}{\pi}\sin[2\pi W(\ell-n)] \\
&= \frac{1}{\pi}\left[\sin(2\pi W\ell)\cos(2\pi Wn) - \cos(2\pi W\ell)\sin(2\pi Wn)\right].
\end{aligned}$$

From this, it is clear that we can factor

$$\boldsymbol{C}_L\boldsymbol{X}_L - \boldsymbol{X}_L\boldsymbol{D} = \boldsymbol{U}_L\boldsymbol{V}^*$$

where $\boldsymbol{U}_L \in \mathbb{R}^{2L\times 2}$ is defined by

$$\boldsymbol{U}_L[\ell,0] = \frac{1}{\sqrt{\pi}}\sin(2\pi W\ell) \quad \text{and} \quad \boldsymbol{U}_L[\ell,1] = \frac{1}{\sqrt{\pi}}\cos(2\pi W\ell) \quad \text{for} \quad \ell \in \mathcal{I}_L,$$

and $\boldsymbol{V} \in \mathbb{R}^{N\times 2}$ is defined by

$$\boldsymbol{V}[n,0] = \frac{1}{\sqrt{\pi}}\cos(2\pi Wn) \quad \text{and} \quad \boldsymbol{V}[n,1] = -\frac{1}{\sqrt{\pi}}\sin(2\pi Wn) \quad \text{for} \quad n \in [N].$$

In other words, $\boldsymbol{X}_L$ has a rank-2 displacement with respect to the matrices $\boldsymbol{C}_L$ and $\boldsymbol{D}$.

Since $\mathrm{Spec}(\boldsymbol{C}_L) = \mathcal{I}_L \subset (-\infty, -1] \cup [N, \infty)$ and $\mathrm{Spec}(\boldsymbol{D}) = [N] \subset [0, N-1]$, we can apply Theorem 14 with parameters $c_1 = -1$, $d_1 = 0$, $d_2 = N-1$, $c_2 = N$, and $\nu = 2$. The theorem tells us that for every integer $k \geq 0$,

$$\sigma_{2k+1}(\boldsymbol{X}_L) \leq 4\|\boldsymbol{X}_L\| \exp\left[-\frac{\pi^2 k}{\log(16\gamma)}\right] \quad \text{where} \quad \gamma = \frac{(c_2 - d_1)(d_2 - c_1)}{(c_2 - d_2)(d_1 - c_1)} = N^2.$$

For any $L \geq 1$, $\boldsymbol{X}_L$ is a submatrix of $\boldsymbol{X}_{L+1}$, and so, $\boldsymbol{X}_L^* \boldsymbol{X}_L \preceq \boldsymbol{X}_{L+1}^* \boldsymbol{X}_{L+1}$. Hence, $\boldsymbol{X}_L^* \boldsymbol{X}_L \preceq \lim_{L\to\infty} \boldsymbol{X}_L^* \boldsymbol{X}_L = \boldsymbol{B} - \boldsymbol{B}^2$. Therefore,

$$\|\boldsymbol{X}_L\|^2 = \|\boldsymbol{X}_L^* \boldsymbol{X}_L\| \leq \|\boldsymbol{B} - \boldsymbol{B}^2\| = \max_k \left[\lambda_k - \lambda_k^2\right] \leq \max_{0\leq\lambda\leq 1} [\lambda - \lambda^2] = \frac{1}{4},$$

and thus, $\|\boldsymbol{X}_L\| \leq \frac{1}{2}$ for all $L \geq 1$. Substituting $\gamma = N^2$ and $\|\boldsymbol{X}_L\| \leq \frac{1}{2}$ into the above bound yields

$$\sigma_{2k+1}(\boldsymbol{X}_L) \leq 2\exp\left[-\frac{\pi^2 k}{\log(16N^2)}\right]$$

for all integers $k \geq 0$. So, if we set

$$k = \left\lceil \frac{1}{\pi^2} \log(16N^2) \log\left(\frac{2}{\sqrt{\epsilon(1-\epsilon)}}\right)\right\rceil = \left\lceil \frac{1}{\pi^2} \log(4N) \log\left(\frac{4}{\epsilon(1-\epsilon)}\right)\right\rceil,$$

we obtain $\sigma_{2k+1}(\boldsymbol{X}_L) \leq \sqrt{\epsilon(1-\epsilon)}$ for all $L \geq 1$.

This proves the second property in Lemma 3 for $r = 2k$ and $L_0 = 1$. Therefore, we have proved that

$$\#\{k : \epsilon < \lambda_k < 1 - \epsilon\} \leq 2k = 2\left\lceil \frac{1}{\pi^2} \log(4N) \log\left(\frac{4}{\epsilon(1-\epsilon)}\right)\right\rceil,$$

which is exactly the content of Theorem 1.

A.1.4 Proof of Theorem 2

First, note that if $W \in [\frac{1}{4}, \frac{1}{2})$, the bound in Theorem 2 is greater than the bound in Theorem 1, which has already been established. So we will henceforth assume that $W \in (0, \frac{1}{4})$.

Now, set $L_1 = \left\lfloor \frac{1}{4W} \right\rfloor$ (clearly, $L_1 \geq 1$). For each integer $L \geq L_1 + 1$, we partition the index set

$$\mathcal{I}_L = \{-L, -L+1 \ldots, -2, -1\} \cup \{N, N+1, \ldots, N+L-2, N+L-1\}$$

into three sets

$$\begin{aligned}
\mathcal{I}_L^{(0)} &= \{-L, -L+1 \ldots, -L_1-2, -L_1-1\} \\
&\qquad \cup \{N+L_1, N+L_1+1, \ldots, N+L-2, N+L-1\} \\
\mathcal{I}_L^{(1)} &= \{-L_1, -L_1+1, \ldots, -2, -1\} \\
\mathcal{I}_L^{(2)} &= \{N, N+1, \ldots, N+L_1-2, N+L_1-1\}
\end{aligned}$$

and then accordingly partition $\boldsymbol{X}_L$ into three submatrices $\boldsymbol{X}_L^{(0)} \in \mathbb{R}^{2(L-L_1)\times N}$, $\boldsymbol{X}_L^{(1)} \in \mathbb{R}^{L_1 \times N}$, and $\boldsymbol{X}_L^{(2)} \in \mathbb{R}^{L_1 \times N}$ defined by

$$\boldsymbol{X}_L^{(i)}[\ell, n] = \boldsymbol{X}_L[\ell, n] \quad \text{for} \quad \ell \in \mathcal{I}_L^{(i)} \text{ and } n \in [N].$$

Once again, we index the rows of each $\boldsymbol{X}_L^{(i)}$ by $\ell \in \mathcal{I}_L^{(i)}$ for convenience. We proceed to bound the singular values of $\boldsymbol{X}_L^{(0)}, \boldsymbol{X}_L^{(1)}, \boldsymbol{X}_L^{(2)}$, and then use these bounds to bound the singular values of $\boldsymbol{X}_L$.

Singular values of $\boldsymbol{X}_L^{(0)}$

The submatrix $\boldsymbol{X}_L^{(0)}$, has the same low-rank displacement structure as $\boldsymbol{X}_L$. Specifically, we can write

$$\boldsymbol{C}_L^{(0)}\boldsymbol{X}_L^{(0)} - \boldsymbol{X}_L^{(0)}\boldsymbol{D} = \boldsymbol{U}_L^{(0)}\boldsymbol{V}^*$$

where $\boldsymbol{C}_L^{(0)} \in \mathbb{R}^{2(L-L_1)\times 2(L-L_1)}$ is the diagonal submatrix of $\boldsymbol{C}_L$ defined by $\boldsymbol{C}_L^{(0)}[\ell,\ell] = \ell$ for $\ell \in \mathcal{I}_L^{(0)}$, $\boldsymbol{U}_L^{(0)} \in \mathbb{R}^{2(L-L_1)\times 2}$ is the submatrix of $\boldsymbol{U}_L$ defined in by $\boldsymbol{U}_L^{(0)}[\ell,q] = \boldsymbol{U}_L[\ell,q]$ for $\ell \in \mathcal{I}_L^{(0)}$ and $q \in \{0,1\}$, and $\boldsymbol{D}$ and $\boldsymbol{V}$ are the same as defined in Section A.1.3.

Since $\mathrm{Spec}(\boldsymbol{C}_L^{(0)}) = \mathcal{I}_L^{(0)} \subset (-\infty, -L_1 - 1] \cup [N + L_1, \infty)$ and $\mathrm{Spec}(\boldsymbol{D}) = [N] \subset [0, N-1]$, we can once again apply Theorem 14, but with the parameters $c_1 = -L_1 - 1$, $d_1 = 0$, $d_2 = N - 1$, $c_2 = N + L_1$, and $\nu = 2$. Then, the theorem tells us that for any integer $k_0 \geq 0$,

$$\sigma_{2k_0+1}(\boldsymbol{X}^{(0)}) \leq 4\|\boldsymbol{X}_L^{(0)}\| \exp\left[-\frac{\pi^2 k_0}{\log(16\gamma)}\right] \text{ where } \gamma = \frac{(c_2-d_1)(d_2-c_1)}{(c_2-d_2)(d_1-c_1)} = \left(\frac{N+L_1}{L_1+1}\right)^2.$$

Since $\boldsymbol{X}_L^{(0)}$ is a submatrix of $\boldsymbol{X}_L$, we have $\|\boldsymbol{X}_L^{(0)}\| \leq \|\boldsymbol{X}_L\| \leq \frac{1}{2}$. Also, since $L_1 = \left\lfloor \frac{1}{4W} \right\rfloor \geq \frac{1}{4W} - 1 > 0$ and $\frac{N+x}{x+1}$ is a non-increasing function of $x > 0$, we can bound

$$\gamma = \left(\frac{N+L_1}{L_1+1}\right)^2 \leq \left(\frac{N+(\frac{1}{4W}-1)}{(\frac{1}{4W}-1)+1}\right)^2 = (4NW+1-4W)^2 \leq (4NW+1)^2.$$

Substituting $\gamma \leq (4NW+1)^2$ and $\|\boldsymbol{X}_L^{(0)}\| \leq \frac{1}{2}$ into the above bound yields

$$\sigma_{2k_0+1}(\boldsymbol{X}_L^{(0)}) \leq 2\exp\left[-\frac{\pi^2 k_0}{\log[16(4NW+1)^2]}\right] = 2\exp\left[-\frac{\pi^2 k_0}{2\log(16NW+4)}\right]$$

for all integers $k_0 \geq 0$.

Singular values of $\boldsymbol{X}_L^{(1)}$

To bound the singular values of $\boldsymbol{X}_L^{(1)}$, we exploit the fact that its entries $\boldsymbol{X}_L^{(1)}[\ell, n] = \dfrac{\sin[2\pi W(\ell - n)]}{\pi(\ell - n)}$ are a smooth function of ℓ and n to construct a tunable low-rank approximation of $\boldsymbol{X}_L^{(1)}$.

Define the sinc function $g(t) = \dfrac{\sin(2\pi W t)}{\pi t}$. For each $n \in [N]$, define

$$g_n(t) = g(t - n) = \frac{\sin[2\pi W(t - n)]}{\pi(t - n)},$$

and let

$$P_{k,n}(t) = \sum_{m=0}^{k-1} p_{m,n} t^m$$

be the degree $k-1$ Chebyshev interpolating polynomial for $g_n(t)$ on the interval $[-L_1, -1]$.

We now define the low rank approximation $\widetilde{\boldsymbol{X}}_L^{(1)} \in \mathbb{R}^{L_1 \times N}$ by

$$\widetilde{\boldsymbol{X}}_L^{(1)}[\ell, n] = P_{k,n}(\ell) = \sum_{m=0}^{k-1} p_{m,n} \ell^m \quad \text{for} \quad \ell \in \mathcal{I}_L^{(1)} \text{ and } n \in [N].$$

We can factor $\widetilde{\boldsymbol{X}}_L^{(1)} = \boldsymbol{W}\boldsymbol{P}$ where $\boldsymbol{W} \in \mathbb{R}^{L_1 \times k}$ and $\boldsymbol{P} \in \mathbb{R}^{k \times N}$ are defined by $\boldsymbol{W}[\ell, m] = \ell^m$ and $\boldsymbol{P}[m, n] = p_{m,n}$. Hence, $\operatorname{rank}(\widetilde{\boldsymbol{X}}_L^{(1)}) \le k$.

By Theorem 20 (in Appendix E.3), the Chebyshev interpolating polynomial satisfies

$$|g_n(t) - P_{k,n}(t)| \le \frac{(L_1 - 1)^k}{2^{2k-1} k!} \max_{\xi \in [-L_1, -1]} \left| g_n^{(k)}(\xi) \right| \quad \text{for all} \quad t \in [-L_1, -1].$$

Also, by Lemma 19 (in Appendix E.3), the derivatives of the unshifted sinc-function $g(t)$ can be bounded by

$$\left| g^{(k)}(t) \right| \le (2\pi W)^k \min\left\{ \frac{2W}{k+1}, \frac{2}{\pi |t|} \right\} \quad \text{for all} \quad t \in \mathbb{R}.$$

Hence, for any $\ell \in \mathcal{I}_L^{(1)}$ and $n \in [N]$, we have

$$\begin{aligned}
\left|\boldsymbol{X}_L^{(1)}[\ell,n] - \widetilde{\boldsymbol{X}}_L^{(1)}[\ell,n]\right| &= |g_n(\ell) - P_{k,n}(\ell)| \\
&\le \frac{(L_1-1)^k}{2^{2k-1}k!} \max_{\xi\in[-L_1,-1]} \left|g_n^{(k)}(\xi)\right| \\
&= \frac{(L_1-1)^k}{2^{2k-1}k!} \max_{\xi\in[-L_1,-1]} \left|g^{(k)}(\xi-n)\right| \\
&= \frac{(L_1-1)^k}{2^{2k-1}k!} \max_{t\in[-L_1-n,-n-1]} \left|g^{(k)}(t)\right| \\
&\le \frac{(L_1-1)^k}{2^{2k-1}k!} \max_{t\in[-L_1-n,-n-1]} (2\pi W)^k \min\left\{\frac{2W}{k+1}, \frac{2}{\pi|t|}\right\} \\
&= \frac{(L_1-1)^k}{2^{2k-1}k!} (2\pi W)^k \min\left\{\frac{2W}{k+1}, \frac{2}{\pi(n+1)}\right\} \\
&= \frac{4(\frac{\pi}{2}W(L_1-1))^k}{k!} \min\left\{\frac{W}{k+1}, \frac{1}{\pi(n+1)}\right\}.
\end{aligned}$$

We proceed to bound the Frobenius norm of $\boldsymbol{X}_L^{(1)} - \widetilde{\boldsymbol{X}}_L^{(1)}$. Set $N_1 = \lfloor \frac{k+1}{\pi W} \rfloor$. Then,

$$\begin{aligned}
\left\|\boldsymbol{X}_L^{(1)} - \widetilde{\boldsymbol{X}}_L^{(1)}\right\|_F^2 &= \sum_{n=0}^{N-1} \sum_{\ell=-L_1}^{-1} \left|\boldsymbol{X}_L^{(1)}[\ell,n] - \widetilde{\boldsymbol{X}}_L^{(1)}[\ell,n]\right|^2 \\
&\le \sum_{n=0}^{N-1} \sum_{\ell=-L_1}^{-1} \frac{16(\frac{\pi}{2}W(L_1-1))^{2k}}{(k!)^2} \min\left\{\frac{W^2}{(k+1)^2}, \frac{1}{\pi^2(n+1)^2}\right\} \\
&= \sum_{n=0}^{N-1} \frac{16L_1(\frac{\pi}{2}W(L_1-1))^{2k}}{(k!)^2} \min\left\{\frac{W^2}{(k+1)^2}, \frac{1}{\pi^2(n+1)^2}\right\} \\
&\le \sum_{n=0}^{\infty} \frac{16L_1(\frac{\pi}{2}W(L_1-1))^{2k}}{(k!)^2} \min\left\{\frac{W^2}{(k+1)^2}, \frac{1}{\pi^2(n+1)^2}\right\} \\
&\le \frac{16L_1(\frac{\pi}{2}W(L_1-1))^{2k}}{(k!)^2} \left[\sum_{n=0}^{N_1-1} \frac{W^2}{(k+1)^2} + \sum_{n=N_1}^{\infty} \frac{1}{\pi^2(n+1)^2}\right] \\
&\le \frac{16L_1(\frac{\pi}{2}W(L_1-1))^{2k}}{(k!)^2} \left[\frac{W^2N_1}{(k+1)^2} + \frac{1}{\pi^2 N_1}\right],
\end{aligned}$$

where the last line follows from the bound $\sum_{n=N_1}^{\infty} \frac{1}{(n+1)^2} \le \frac{1}{N_1}$.

We proceed to weaken this result to obtain a more usable upper bound as follows:

$$\begin{aligned}
\left\|\boldsymbol{X}_L^{(1)} - \widetilde{\boldsymbol{X}}_L^{(1)}\right\|_F^2 &\leq \frac{16L_1(\frac{\pi}{2}W(L_1-1))^{2k}}{(k!)^2}\left[\frac{W^2N_1}{(k+1)^2} + \frac{1}{\pi^2 N_1}\right] \\
&\leq \frac{16(L_1-1)(\frac{\pi}{2}WL_1)^{2k}}{(k!)^2}\left[\frac{W^2N_1}{(k+1)^2} + \frac{1}{\pi^2 N_1}\right] \\
&= \frac{16(\frac{\pi}{2}WL_1)^{2k}}{(k!)^2}\left[\frac{W^2(L_1-1)N_1}{(k+1)^2} + \frac{L_1-1}{\pi^2 N_1}\right] \\
&\leq \frac{16(\frac{\pi}{2}WL_1)^{2k}}{(k!)^2}\left[\frac{W^2N_1L_1}{(k+1)^2} + \frac{L_1}{\pi^2(N_1+1)}\right] \\
&\leq \frac{16(\frac{\pi}{2}W\cdot\frac{1}{4W})^{2k}}{(k!)^2}\left[\frac{W^2\cdot\frac{k+1}{\pi W}\cdot\frac{1}{4W}}{(k+1)^2} + \frac{\frac{1}{4W}}{\pi^2\cdot\frac{k+1}{\pi W}}\right] \\
&= \frac{8}{\pi(k+1)(k!)^2}\left(\frac{\pi}{8}\right)^{2k} \\
&\leq \frac{5600}{\pi}\left(\frac{\pi}{48}\right)^{2k}.
\end{aligned}$$

The 2nd line follows from the inequalities $(L_1-1)^{2k} \leq L_1^{2k}$ and $L_1(L_1-1)^{2k} \leq (L_1-1)L_1^{2k}$. The 4th line holds since $\frac{L_1-1}{N_1} \leq \frac{L_1}{N_1+1}$ is equivalent to $L_1 \leq N_1+1$, which is true since $L_1 \leq \left\lfloor\frac{1}{4W}\right\rfloor \leq \frac{1}{4W} < \frac{k+1}{\pi W} \leq \left\lfloor\frac{k+1}{\pi W}\right\rfloor + 1 = N_1 + 1$. The last line holds due to the fact that $(k+1)(k!)^2 \geq \frac{1}{700}6^{2k}$ for all integers $k \geq 0$.

Since $\operatorname{rank}(\widetilde{\boldsymbol{X}}_L^{(1)}) \leq k$, we have $\sigma_{k+1}(\widetilde{\boldsymbol{X}}_L^{(1)}) = 0$. Hence, we can bound

$$\begin{aligned}
\sigma_{k+1}(\boldsymbol{X}_L^{(1)}) &= \left|\sigma_{k+1}(\boldsymbol{X}_L^{(1)}) - \sigma_{k+1}(\widetilde{\boldsymbol{X}}_L^{(1)})\right| \\
&\leq \left\|\boldsymbol{X}_L^{(1)} - \widetilde{\boldsymbol{X}}_L^{(1)}\right\| \\
&\leq \left\|\boldsymbol{X}_L^{(1)} - \widetilde{\boldsymbol{X}}_L^{(1)}\right\|_F \\
&\leq \sqrt{\frac{5600}{\pi}}\left(\frac{\pi}{48}\right)^{k}.
\end{aligned}$$

Singular values of $\boldsymbol{X}_L^{(2)}$

We can exploit the symmetry between $\boldsymbol{X}_L^{(2)}$ and $\boldsymbol{X}_L^{(1)}$ to show that the singular values of $\widetilde{\boldsymbol{X}}_L^{(2)}$ are the same as those of $\widetilde{\boldsymbol{X}}_L^{(1)}$. Specifically, for any indices $\ell \in \mathcal{I}_L^{(2)}$ and $n \in [N]$, we

have that $N-1-\ell \in \mathcal{I}_L^{(1)}$ and $N-1-n \in [N]$, and that

$$\begin{aligned}\boldsymbol{X}_L^{(2)}[\ell,n] &= \frac{\sin[2\pi W(\ell-n)]}{\pi(\ell-n)} \\ &= \frac{\sin[2\pi W((N-1-\ell)-(N-1-n))]}{\pi((N-1-\ell)-(N-1-n))} \\ &= \boldsymbol{X}_L^{(1)}[N-1-\ell, N-1-n].\end{aligned}$$

Since the singular values of a matrix are invariant under permutations of rows/columns,

$$\sigma_{k+1}(\boldsymbol{X}_L^{(2)}) = \sigma_{k+1}(\boldsymbol{X}_L^{(1)}) \leq \sqrt{\frac{5600}{\pi}} \left(\frac{\pi}{48}\right)^k$$

for all integers $k \geq 0$.

Singular values of $\boldsymbol{X}_L$

Due to the way we partitioned $\boldsymbol{X}_L$ into three submatrices, we have

$$\boldsymbol{X}_L^* \boldsymbol{X}_L = \boldsymbol{X}_L^{(0)*} \boldsymbol{X}_L^{(0)} + \boldsymbol{X}_L^{(1)*} \boldsymbol{X}_L^{(1)} + \boldsymbol{X}_L^{(2)*} \boldsymbol{X}_L^{(2)}.$$

Then, by using the Weyl eigenvalue inequalities along with the bounds on the singular values of $\boldsymbol{X}_L^{(0)}$, $\boldsymbol{X}_L^{(1)}$, and $\boldsymbol{X}_L^{(2)}$, we have

$$\begin{aligned}\sigma_{2k_0+2k+1}(\boldsymbol{X}_L)^2 &= \mu_{2k_0+2k+1}(\boldsymbol{X}_L^* \boldsymbol{X}_L) \\ &\leq \mu_{2k_0+1}(\boldsymbol{X}_L^{(0)*} \boldsymbol{X}_L^{(0)}) + \mu_{k+1}(\boldsymbol{X}_L^{(1)*} \boldsymbol{X}_L^{(1)}) + \mu_{k+1}(\boldsymbol{X}_L^{(2)*} \boldsymbol{X}_L^{(2)}) \\ &= \sigma_{2k_0+1}(\boldsymbol{X}_L^{(0)})^2 + \sigma_{k+1}(\boldsymbol{X}_L^{(1)})^2 + \sigma_{k+1}(\boldsymbol{X}_L^{(2)})^2 \\ &\leq 4\exp\left[-\frac{\pi^2 k_0}{\log(16NW+4)}\right] + \frac{5600}{\pi}\left(\frac{\pi}{48}\right)^{2k} + \frac{5600}{\pi}\left(\frac{\pi}{48}\right)^{2k} \\ &= 4\exp\left[-\frac{\pi^2 k_0}{\log(16NW+4)}\right] + \frac{11200}{\pi}\left(\frac{\pi}{48}\right)^{2k}\end{aligned}$$

for any integers $k_0 \geq 0$ and $k \geq 1$.

If we set

$$k_0 = \left\lceil \frac{1}{\pi^2} \log(16NW+4) \log\left(\frac{5}{\epsilon(1-\epsilon)}\right) \right\rceil$$

and

$$k = \left\lceil \frac{1}{2\log(\frac{48}{\pi})} \log\left(\frac{\frac{56000}{\pi}}{\epsilon(1-\epsilon)}\right) \right\rceil$$

then we obtain

$$\begin{aligned}
\sigma_{2k_0+2k+1}(\boldsymbol{X}_L)^2 &\leq 4\exp\left[-\frac{\pi^2 k_0}{\log(16NW+4)}\right] + \frac{11200}{\pi}\left(\frac{\pi}{48}\right)^{2k} \\
&\leq \frac{4\epsilon(1-\epsilon)}{5} + \frac{\epsilon(1-\epsilon)}{5} \\
&= \epsilon(1-\epsilon),
\end{aligned}$$

i.e., $\sigma_{2k_0+2k+1}(\boldsymbol{X}_L) \leq \sqrt{\epsilon(1-\epsilon)}$. Our steps hold for all $L \geq L_1 + 1$.

This proves the second property of Lemma 3 for $r = 2k_0 + 2k$ and $L_0 = L_1 + 1$. Therefore, $\#\{k : \epsilon < \lambda_k < 1-\epsilon\} \leq 2k_0 + 2k$. We can loosen this bound to make it more "user friendly" as follows:

$$\begin{aligned}
&\#\{k : \epsilon < \lambda_k < 1-\epsilon\} \\
&\leq 2\left\lceil \frac{1}{\pi^2} \log(16NW+4) \log\left(\frac{5}{\epsilon(1-\epsilon)}\right) \right\rceil + 2\left\lceil \frac{1}{2\log(\frac{48}{\pi})} \log\left(\frac{\frac{56000}{\pi}}{\epsilon(1-\epsilon)}\right) \right\rceil \\
&\leq \frac{2}{\pi^2} \log(16NW+4) \log\left(\frac{5}{\epsilon(1-\epsilon)}\right) + \frac{1}{\log(\frac{48}{\pi})} \log\left(\frac{\frac{56000}{\pi}}{\epsilon(1-\epsilon)}\right) + 4 \\
&= \frac{2}{\pi^2} \log(16NW+4) \log\left(\frac{5}{\epsilon(1-\epsilon)}\right) + \frac{1}{\log(\frac{48}{\pi})} \log\left(\frac{5}{\epsilon(1-\epsilon)}\right) + \frac{\log\left(\frac{11200}{\pi}\right)}{\log(\frac{48}{\pi})} + 4 \\
&= \left(\frac{2}{\pi^2} \log(16NW+4) + \frac{1}{\log(\frac{48}{\pi})}\right) \log\left(\frac{5}{\epsilon(1-\epsilon)}\right) + \frac{\log\left(\frac{11200}{\pi}\right)}{\log(\frac{48}{\pi})} + 4 \\
&= \frac{2}{\pi^2} \log\left(\exp\left(\frac{\pi^2}{2\log(\frac{48}{\pi})}\right)(16NW+4)\right) \log\left(\frac{5}{\epsilon(1-\epsilon)}\right) + \frac{\log\left(\frac{11200}{\pi}\right)}{\log(\frac{48}{\pi})} + 4 \\
&\leq \frac{2}{\pi^2} \log(100NW+25) \log\left(\frac{5}{\epsilon(1-\epsilon)}\right) + 7,
\end{aligned}$$

which establishes Theorem 2.

A.2 Proof of DPSS Eigenvalue Bounds (Corollaries 1 and 2)

First, we state a result from [7] which bounds λ_k for two values of k near $2NW$.

Lemma 4. *For any $N \in \mathbb{N}$ and $W \in (0, \frac{1}{2})$,*

$$\lambda_{\lfloor 2NW \rfloor - 1} \geq \frac{1}{2} \geq \lambda_{\lceil 2NW \rceil}.$$

To derive bounds on λ_k, we will set ϵ such that the transition region is too narrow to contain k, and thus conclude either $\lambda_k \geq 1 - \epsilon$ (if $k \leq \lfloor 2NW \rfloor - 1$) or $\lambda_k \leq \epsilon$ (if $k \geq \lceil 2NW \rceil$). To derive bounds on $\sum_{k=0}^{K-1}(1 - \lambda_k)$ and $\sum_{k=K}^{N-1} \lambda_k$, we will simply apply the bounds on λ_k and the formula for the sum of a geometric series.

A.2.1 Lower bounds on λ_k for $k \leq \lfloor 2NW \rfloor - 1$

For any integer k such that $0 \leq k \leq \lfloor 2NW \rfloor - 1$, set

$$\epsilon = 8 \exp\left[-\frac{\lfloor 2NW \rfloor - k - 2}{\frac{2}{\pi^2} \log(4N)} \right],$$

and suppose for sake of contradiction that $\lambda_k < 1 - \epsilon$.

By using the assumption $k \leq \lfloor 2NW \rfloor - 1$ and Lemma 4, we have $\frac{1}{2} \leq \lambda_{\lfloor 2NW \rfloor - 1} \leq \lambda_k < 1 - \epsilon$, i.e., $\epsilon < \frac{1}{2}$. Therefore, $\epsilon < \frac{1}{2} \leq \lambda_{\lfloor 2NW \rfloor - 1} \leq \lambda_k < 1 - \epsilon$, i.e. both k and $\lfloor 2NW \rfloor - 1$ are in the transition region $\{k' : \epsilon < \lambda_{k'} < 1 - \epsilon\}$, and thus, so are all the indices k' between k and $\lfloor 2NW \rfloor - 1$. Hence,

$$\#\{k' : \epsilon < \lambda_{k'} < 1 - \epsilon\} \geq \#\{k' : k \leq k' \leq \lfloor 2NW \rfloor - 1\} = \lfloor 2NW \rfloor - k.$$

However, since $\epsilon < \frac{1}{2}$, by Theorem 1 we have

$$\begin{aligned}\#\{k' : \epsilon < \lambda_{k'} < 1-\epsilon\} &\leq 2\left\lceil \frac{1}{\pi^2}\log(4N)\log\left(\frac{4}{\epsilon(1-\epsilon)}\right)\right\rceil \\ &< \frac{2}{\pi^2}\log(4N)\log\left(\frac{8}{\epsilon}\right) + 2 \\ &= \lfloor 2NW \rfloor - k.\end{aligned}$$

This is a contradiction. Therefore,

$$\lambda_k \geq 1-\epsilon = 1 - 8\exp\left[-\frac{\lfloor 2NW\rfloor - k - 2}{\frac{2}{\pi^2}\log(4N)}\right] \quad \text{for} \quad 0 \leq k \leq \lfloor 2NW \rfloor - 1.$$

In a similar manner, we can assume $\lambda_k < 1-\epsilon$, where

$$\epsilon = 10\exp\left[-\frac{\lfloor 2NW\rfloor - k - 7}{\frac{2}{\pi^2}\log(100NW+25)}\right],$$

and then invoke Theorem 2 to obtain a contradiction. Therefore,

$$\lambda_k \geq 1-\epsilon = 1 - 10\exp\left[-\frac{\lfloor 2NW\rfloor - k - 7}{\frac{2}{\pi^2}\log(100NW+25)}\right] \quad \text{for} \quad 0 \leq k \leq \lfloor 2NW \rfloor - 1.$$

Combining these two bounds establishes the first part of Corollary 1.

A.2.2 Upper bounds on λ_k for $k \geq \lceil 2NW \rceil$

For any integer k such that $\lceil 2NW \rceil \leq k \leq N-1$, set

$$\epsilon = 8\exp\left[-\frac{k - \lceil 2NW\rceil - 1}{\frac{2}{\pi^2}\log(4N)}\right],$$

and suppose for sake of contradiction that $\lambda_k > \epsilon$.

By using the assumption $k \geq \lceil 2NW \rceil$ and Lemma 4, we have $\epsilon < \lambda_k \leq \lambda_{\lceil 2NW\rceil} \leq \frac{1}{2}$, i.e., $\epsilon < \frac{1}{2}$. Therefore, $\epsilon < \lambda_k \leq \lambda_{\lceil 2NW\rceil} \leq \frac{1}{2} < 1-\epsilon$, i.e., both k and $\lceil 2NW \rceil$ are in the

transition region $\{k' : \epsilon < \lambda_{k'} < 1 - \epsilon\}$, and thus, so are all the indices k' between k and $\lceil 2NW \rceil$. Hence,

$$\#\{k' : \epsilon < \lambda_{k'} < 1 - \epsilon\} \geq \#\{k' : \lceil 2NW \rceil \leq k' \leq k\} = k - \lceil 2NW \rceil + 1.$$

However, since $\epsilon < \frac{1}{2}$, by Theorem 1 we have

$$\begin{aligned}
\#\{k' : \epsilon < \lambda_{k'} < 1 - \epsilon\} &\leq 2 \left\lceil \frac{1}{\pi^2} \log(4N) \log\left(\frac{4}{\epsilon(1-\epsilon)}\right) \right\rceil \\
&< \frac{2}{\pi^2} \log(4N) \log\left(\frac{8}{\epsilon}\right) + 2 \\
&= k - \lceil 2NW \rceil + 1.
\end{aligned}$$

This is a contradiction. Therefore,

$$\lambda_k \leq \epsilon = 8 \exp\left[-\frac{k - \lceil 2NW \rceil - 1}{\frac{2}{\pi^2} \log(4N)} \right] \quad \text{for} \quad \lceil 2NW \rceil \leq k \leq N - 1.$$

In a similar manner, we can assume $\lambda_k > \epsilon$, where

$$\epsilon = 10 \exp\left[-\frac{k - \lceil 2NW \rceil - 6}{\frac{2}{\pi^2} \log(100NW + 25)} \right],$$

and then invoke Theorem 2 to obtain a contradiction. Therefore,

$$\lambda_k \leq \epsilon = 10 \exp\left[-\frac{k - \lceil 2NW \rceil - 6}{\frac{2}{\pi^2} \log(100NW + 25)} \right] \quad \text{for} \quad \lceil 2NW \rceil \leq k \leq N - 1.$$

Combining these two bounds establishes the second part of Corollary 1.

A.2.3 Bounds on $\sum_{k=0}^{K-1}(1-\lambda_k)$ for $K \leq \lfloor 2NW \rfloor$

For any integer K such that $1 \leq K \leq \lfloor 2NW \rfloor$, we can apply the first part of the lower bound for λ_k in Corollary 1 along with the inequality $\frac{e^{-x}}{1-e^{-x}} \leq \frac{1}{x}$ for $x > 0$ to obtain

$$\begin{aligned}
\sum_{k=0}^{K-1}(1-\lambda_k) &\leq \sum_{k=0}^{K-1} 8\exp\left[-\frac{\lfloor 2NW \rfloor - k - 2}{\frac{2}{\pi^2}\log(4N)}\right] \\
&\leq \sum_{k=-\infty}^{K-1} 8\exp\left[-\frac{\lfloor 2NW \rfloor - k - 2}{\frac{2}{\pi^2}\log(4N)}\right] \\
&= \frac{8\exp\left[-\frac{\lfloor 2NW \rfloor - K - 1}{\frac{2}{\pi^2}\log(4N)}\right]}{1-\exp\left[-\frac{1}{\frac{2}{\pi^2}\log(4N)}\right]} \\
&\leq \frac{16}{\pi^2}\log(4N)\exp\left[-\frac{\lfloor 2NW \rfloor - K - 2}{\frac{2}{\pi^2}\log(4N)}\right].
\end{aligned}$$

In a similar manner, we can apply the second part of the lower bound for λ_k in Corollary 1 instead of the first part of the lower bound to obtain

$$\begin{aligned}
\sum_{k=0}^{K-1}(1-\lambda_k) &\leq \sum_{k=0}^{K-1} 10\exp\left[-\frac{\lfloor 2NW \rfloor - k - 7}{\frac{2}{\pi^2}\log(100NW+25)}\right] \\
&\leq \sum_{k=-\infty}^{K-1} 8\exp\left[-\frac{\lfloor 2NW \rfloor - k - 7}{\frac{2}{\pi^2}\log(100NW+25)}\right] \\
&= \frac{8\exp\left[-\frac{\lfloor 2NW \rfloor - K - 6}{\frac{2}{\pi^2}\log(100NW+25)}\right]}{1-\exp\left[-\frac{1}{\frac{2}{\pi^2}\log(100NW+25)}\right]} \\
&\leq \frac{20}{\pi^2}\log(100NW+25)\exp\left[-\frac{\lfloor 2NW \rfloor - K - 7}{\frac{2}{\pi^2}\log(100NW+25)}\right].
\end{aligned}$$

Combining these two bounds establishes the first part of Corollary 2.

A.2.4 Bounds on $\sum_{k=K}^{N-1} \lambda_k$ for $K \geq \lceil 2NW \rceil$

For any integer K such that $\lceil 2NW \rceil \leq K \leq N-1$, we can apply the first part of the upper bound for λ_k in Corollary 1 along with the inequality $\frac{e^{-x}}{1-e^{-x}} \leq \frac{1}{x}$ for $x > 0$ to obtain

$$\begin{aligned}
\sum_{k=K}^{N-1} \lambda_k &\leq \sum_{k=K}^{N-1} 8 \exp\left[-\frac{k - \lceil 2NW \rceil - 1}{\frac{2}{\pi^2}\log(4N)} \right] \\
&\leq \sum_{k=K}^{\infty} 8 \exp\left[-\frac{k - \lceil 2NW \rceil - 1}{\frac{2}{\pi^2}\log(4N)} \right] \\
&= \frac{8 \exp\left[-\frac{K - \lceil 2NW \rceil - 1}{\frac{2}{\pi^2}\log(4N)} \right]}{1 - \exp\left[-\frac{1}{\frac{2}{\pi^2}\log(4N)} \right]} \\
&\leq \frac{16}{\pi^2} \log(4N) \exp\left[-\frac{K - \lceil 2NW \rceil - 2}{\frac{2}{\pi^2}\log(4N)} \right].
\end{aligned}$$

In a similar manner, we can apply the second part of the upper bound for λ_k in Corollary 1 instead of the first part of the upper bound to obtain

$$\begin{aligned}
\sum_{k=K}^{N-1} \lambda_k &\leq \sum_{k=K}^{N-1} 10 \exp\left[-\frac{k - \lceil 2NW \rceil - 6}{\frac{2}{\pi^2}\log(100NW + 25)} \right] \\
&\leq \sum_{k=K}^{\infty} 10 \exp\left[-\frac{k - \lceil 2NW \rceil - 6}{\frac{2}{\pi^2}\log(100NW + 25)} \right] \\
&= \frac{10 \exp\left[-\frac{K - \lceil 2NW \rceil - 6}{\frac{2}{\pi^2}\log(100NW + 25)} \right]}{1 - \exp\left[-\frac{1}{\frac{2}{\pi^2}\log(100NW + 25)} \right]} \\
&\leq \frac{20}{\pi^2} \log(100NW + 25) \exp\left[-\frac{K - \lceil 2NW \rceil - 7}{\frac{2}{\pi^2}\log(100NW + 25)} \right].
\end{aligned}$$

Combining these two bounds establishes the second part of Corollary 2.

A.3 Proof of PSWF Eigenvalue Bounds

First, we state a result by Boulsane, Bourguiba, and Karoui [88] which quantifies how close the PSWF eigenvalues are to DPSS eigenvalues with the same time-bandwidth product.

Lemma 5. *For any $N \in \mathbb{N}$ and $W \in (0, \frac{1}{2})$,*

$$\left(\sum_{k=0}^{\infty} \left|\lambda_k(N,W) - \widetilde{\lambda}_k(\pi NW)\right|^2\right)^{1/2} \leq \frac{4\pi^2 W^3}{3\sin(2\pi W)},$$

where we define $\lambda_k(N,W) = 0$ for $k \geq N$ for ease of notation.

In particular, we note that this implies

$$\left|\lambda_k\left(N, \frac{c}{\pi N}\right) - \widetilde{\lambda}_k(c)\right| \leq \left(\sum_{k=0}^{\infty} \left|\lambda_k\left(N, \frac{c}{\pi N}\right) - \widetilde{\lambda}_k(c)\right|^2\right)^{1/2} \leq \delta_{c,N} := \frac{4c^3}{3\pi N^3 \sin(\frac{2c}{N})}$$

for all $c > 0$ and all integers $N > \frac{2c}{\pi}$ and $k \geq 0$. Also, for any $c > 0$, we have $\delta_{c,N} \searrow 0$ as $N \to \infty$, and thus,

$$\lim_{N\to\infty} \lambda_k(N, \frac{c}{\pi N}) = \widetilde{\lambda}_k(c).$$

A.3.1 Proof of Theorem 3

Since $\left|\lambda_k\left(N, \frac{c}{\pi N}\right) - \widetilde{\lambda}_k(c)\right| \leq \delta_{c,N}$, we have

$$\epsilon < \widetilde{\lambda}_k(c) < 1 - \epsilon \implies \epsilon - \delta_{c,N} < \lambda_k\left(N, \frac{c}{\pi N}\right) < 1 - \epsilon + \delta_{c,N}$$

for all integers $k \geq 0$. For sufficiently large N, $\delta_{c,N} < \epsilon$ and so, we may apply Theorem 2 for $W = \frac{c}{\pi N}$ to obtain

$$\begin{aligned}\#\left\{k : \epsilon < \widetilde{\lambda}_k(c) < 1 - \epsilon\right\} &\leq \#\left\{k : \epsilon - \delta_{c,N} < \lambda_k\left(N, \frac{c}{\pi N}\right) < 1 - \epsilon + \delta_{c,N}\right\} \\ &\leq \frac{2}{\pi^2}\log\left(\frac{100c}{\pi} + 25\right)\log\left(\frac{5}{(\epsilon - \delta_{c,N})(1 - \epsilon + \delta_{c,N})}\right) + 7.\end{aligned}$$

Since this bound holds for all sufficiently large N, we may take the limit as $N \to \infty$ to obtain

$$\begin{aligned}
&\#\left\{k : \epsilon < \widetilde{\lambda}_k(c) < 1-\epsilon\right\} \\
&\leq \lim_{N\to\infty} \left[\frac{2}{\pi^2}\log\left(\frac{100c}{\pi}+25\right)\log\left(\frac{5}{(\epsilon-\delta_{c,N})(1-\epsilon+\delta_{c,N})}\right)+7\right] \\
&\leq \frac{2}{\pi^2}\log\left(\frac{100c}{\pi}+25\right)\log\left(\frac{5}{\epsilon(1-\epsilon)}\right)+7.
\end{aligned}$$

A.3.2 Proof of PSWF eigenvalue bounds (Corollary 3)

For any $0 \leq k \leq \left\lfloor \frac{2c}{\pi} \right\rfloor - 1$, we can apply Corollary 1 for any $N > \frac{2c}{\pi}$ and $W = \frac{c}{\pi N}$ to obtain

$$\lambda_k\left(N, \frac{c}{\pi N}\right) \geq 1 - 10\exp\left[-\frac{\left\lfloor \frac{2c}{\pi} \right\rfloor - k - 7}{\frac{2}{\pi^2}\log\left(\frac{100c}{\pi}+25\right)}\right].$$

Since this holds for all $N > \frac{2c}{\pi}$, we have

$$\widetilde{\lambda}_k(c) = \lim_{N\to\infty} \lambda_k\left(N, \frac{c}{\pi N}\right) \geq 1 - 10\exp\left[-\frac{\left\lfloor \frac{2c}{\pi} \right\rfloor - k - 7}{\frac{2}{\pi^2}\log\left(\frac{100c}{\pi}+25\right)}\right].$$

Similarly, for any $k \geq \left\lceil \frac{2c}{\pi} \right\rceil$, we can apply Corollary 1 for any $N > k$ and $W = \frac{c}{\pi N}$ to obtain and

$$\lambda_k\left(N, \frac{c}{\pi N}\right) \leq 10\exp\left[-\frac{k - \left\lceil \frac{2c}{\pi} \right\rceil - 6}{\frac{2}{\pi^2}\log\left(\frac{100c}{\pi}+25\right)}\right].$$

Since this holds for all $N > k$, we have

$$\widetilde{\lambda}_k(c) = \lim_{N\to\infty} \lambda_k\left(N, \frac{c}{\pi N}\right) \leq 10\exp\left[-\frac{k - \left\lceil \frac{2c}{\pi} \right\rceil - 6}{\frac{2}{\pi^2}\log\left(\frac{100c}{\pi}+25\right)}\right].$$

A.3.3 Proof of PSWF eigenvalue sum bounds (Corollary 4)

For any integer K such that $1 \leq K \leq \left\lfloor \frac{2c}{\pi} \right\rfloor$, we can apply the lower bound for $\widetilde{\lambda}_k(c)$ in Corollary 3 along with the inequality $\frac{e^{-x}}{1-e^{-x}} \leq \frac{1}{x}$ for $x > 0$ to obtain

$$\begin{aligned}
\sum_{k=0}^{K-1} \left(1 - \widetilde{\lambda}_k(c)\right) &\leq \sum_{k=0}^{K-1} 10 \exp\left[-\frac{\left\lfloor \frac{2c}{\pi} \right\rfloor - k - 7}{\frac{2}{\pi^2}\log\left(\frac{100c}{\pi} + 25\right)}\right] \\
&\leq \sum_{k=-\infty}^{K-1} 10 \exp\left[-\frac{\left\lfloor \frac{2c}{\pi} \right\rfloor - k - 7}{\frac{2}{\pi^2}\log\left(\frac{100c}{\pi} + 25\right)}\right] \\
&= \frac{10 \exp\left[-\frac{\left\lfloor \frac{2c}{\pi} \right\rfloor - k - 6}{\frac{2}{\pi^2}\log\left(\frac{100c}{\pi} + 25\right)}\right]}{1 - \exp\left[-\frac{1}{\frac{2}{\pi^2}\log\left(\frac{100c}{\pi} + 25\right)}\right]} \\
&\leq \frac{20}{\pi^2}\log\left(\frac{100c}{\pi} + 25\right) \exp\left[-\frac{\left\lfloor \frac{2c}{\pi} \right\rfloor - K - 7}{\frac{2}{\pi^2}\log\left(\frac{100c}{\pi} + 25\right)}\right].
\end{aligned}$$

Similarly, for any integer $K \geq \left\lceil \frac{2c}{\pi} \right\rceil$, we can apply the upper bound for $\widetilde{\lambda}_k(c)$ in Corollary 3 along with the inequality $\frac{e^{-x}}{1-e^{-x}} \leq \frac{1}{x}$ for $x > 0$ to obtain

$$\begin{aligned}
\sum_{k=K}^{\infty} \widetilde{\lambda}_k(c) &\leq \sum_{k=K}^{\infty} 10 \exp\left[-\frac{k - \left\lceil \frac{2c}{\pi} \right\rceil - 6}{\frac{2}{\pi^2}\log\left(\frac{100c}{\pi} + 25\right)}\right] \\
&= \frac{10 \exp\left[-\frac{k - \left\lceil \frac{2c}{\pi} \right\rceil - 6}{\frac{2}{\pi^2}\log\left(\frac{100c}{\pi} + 25\right)}\right]}{1 - \exp\left[-\frac{1}{\frac{2}{\pi^2}\log\left(\frac{100c}{\pi} + 25\right)}\right]} \\
&\leq \frac{20}{\pi^2}\log\left(\frac{100c}{\pi} + 25\right) \exp\left[-\frac{K - \left\lceil \frac{2c}{\pi} \right\rceil - 7}{\frac{2}{\pi^2}\log\left(\frac{100c}{\pi} + 25\right)}\right].
\end{aligned}$$

APPENDIX B

PROOFS FOR CHAPTER 4

B.1 Proof of Theorem 4

Denote the eigendecomposition of the prolate matrix to be $\boldsymbol{B} = \boldsymbol{S}\boldsymbol{\Lambda}\boldsymbol{S}^*$ where

$$\boldsymbol{S} = \begin{bmatrix} \boldsymbol{s}_0 & \boldsymbol{s}_1 & \cdots & \boldsymbol{s}_{N-1} \end{bmatrix} \in \mathbb{R}^{N \times N}$$

is the matrix containing the Slepian basis eigenvectors and

$$\boldsymbol{\Lambda} = \mathrm{diag}(\lambda_0, \lambda_1, \ldots, \lambda_{N-1}) \in \mathbb{R}^{N \times N}$$

is the diagonal matrix containing the Slepian basis eigenvalues. For any set $\mathcal{I} \subseteq [N]$, we will define $\boldsymbol{S}_{\mathcal{I}} \in \mathbb{R}^{N \times \#(\mathcal{I})}$ to be the submatrix of $\boldsymbol{S}$ which contains the columns $\boldsymbol{s}_k$ for $k \in \mathcal{I}$ sorted in ascending order of k, and we will define $\boldsymbol{\Lambda}_{\mathcal{I}} \in \mathbb{R}^{\#(\mathcal{I}) \times \#(\mathcal{I})}$ to be the diagonal submatrix of $\boldsymbol{\Lambda}$ which contains the eigenvalues λ_k for $k \in \mathcal{I}$ sorted in ascending order of k.

B.1.1 Proof of Theorem 4a

Since $K \in [N]$ satisfies $\lambda_{K-1} > \epsilon$ and $\lambda_K < 1 - \epsilon$, we can partition the indices $[N]$ as follows:

$$\mathcal{I}_1 = \{k \in [K] : \lambda_k \geq 1 - \epsilon\}$$

$$\mathcal{I}_2 = \{k \in [K] : \epsilon < \lambda_k < 1 - \epsilon\}$$

$$\mathcal{I}_3 = \{k \in [N] \setminus [K] : \epsilon < \lambda_k < 1 - \epsilon\}$$

$$\mathcal{I}_4 = \{k \in [N] \setminus [K] : \lambda_k \leq \epsilon\}.$$

Then, we can write

$$\boldsymbol{B} = \boldsymbol{S}\boldsymbol{\Lambda}\boldsymbol{S}^* = \boldsymbol{S}_{\mathcal{I}_1}\boldsymbol{\Lambda}_{\mathcal{I}_1}\boldsymbol{S}_{\mathcal{I}_1}^* + \boldsymbol{S}_{\mathcal{I}_2}\boldsymbol{\Lambda}_{\mathcal{I}_2}\boldsymbol{S}_{\mathcal{I}_2}^* + \boldsymbol{S}_{\mathcal{I}_3}\boldsymbol{\Lambda}_{\mathcal{I}_3}\boldsymbol{S}_{\mathcal{I}_3}^* + \boldsymbol{S}_{\mathcal{I}_4}\boldsymbol{\Lambda}_{\mathcal{I}_4}\boldsymbol{S}_{\mathcal{I}_4}^*,$$

$$\boldsymbol{S}_K\boldsymbol{S}_K^* = \boldsymbol{S}_{\mathcal{I}_1}\boldsymbol{S}_{\mathcal{I}_1}^* + \boldsymbol{S}_{\mathcal{I}_2}\boldsymbol{S}_{\mathcal{I}_2}^*,$$

$$\boldsymbol{S}_\epsilon = \begin{bmatrix} \boldsymbol{S}_{\mathcal{I}_2} & \boldsymbol{S}_{\mathcal{I}_3} \end{bmatrix}.$$

By defining

$$\boldsymbol{D}_1 = \begin{bmatrix} \mathbf{I} - \boldsymbol{\Lambda}_{\mathcal{I}_2} & \mathbf{0} \\ \mathbf{0} & -\boldsymbol{\Lambda}_{\mathcal{I}_3} \end{bmatrix},$$

we have,

$$\boldsymbol{S}_\epsilon\boldsymbol{D}_1\boldsymbol{S}_\epsilon^* = \boldsymbol{S}_{\mathcal{I}_2}\left(\mathbf{I} - \boldsymbol{\Lambda}_{\mathcal{I}_2}\right)\boldsymbol{S}_{\mathcal{I}_2}^* - \boldsymbol{S}_{\mathcal{I}_3}\boldsymbol{\Lambda}_{\mathcal{I}_3}\boldsymbol{S}_{\mathcal{I}_3}^*.$$

Hence,

$$\begin{aligned}
\boldsymbol{S}_K\boldsymbol{S}_K^* - \left(\boldsymbol{B} + \boldsymbol{S}_\epsilon\boldsymbol{D}_1\boldsymbol{S}_\epsilon^*\right) &= \left(\boldsymbol{S}_{\mathcal{I}_1}\boldsymbol{S}_{\mathcal{I}_1}^* + \boldsymbol{S}_{\mathcal{I}_2}\boldsymbol{S}_{\mathcal{I}_2}^*\right) \\
&\quad - \left(\boldsymbol{S}_{\mathcal{I}_1}\boldsymbol{\Lambda}_{\mathcal{I}_1}\boldsymbol{S}_{\mathcal{I}_1}^* + \boldsymbol{S}_{\mathcal{I}_2}\boldsymbol{\Lambda}_{\mathcal{I}_2}\boldsymbol{S}_{\mathcal{I}_2}^* + \boldsymbol{S}_{\mathcal{I}_3}\boldsymbol{\Lambda}_{\mathcal{I}_3}\boldsymbol{S}_{\mathcal{I}_3}^* + \boldsymbol{S}_{\mathcal{I}_4}\boldsymbol{\Lambda}_{\mathcal{I}_4}\boldsymbol{S}_{\mathcal{I}_4}^*\right) \\
&\quad - \left(\boldsymbol{S}_{\mathcal{I}_2}\left(\mathbf{I} - \boldsymbol{\Lambda}_{\mathcal{I}_2}\right)\boldsymbol{S}_{\mathcal{I}_2}^* - \boldsymbol{S}_{\mathcal{I}_3}\boldsymbol{\Lambda}_{\mathcal{I}_3}\boldsymbol{S}_{\mathcal{I}_3}^*\right) \\
&= \boldsymbol{S}_{\mathcal{I}_1}\left(\mathbf{I} - \boldsymbol{\Lambda}_{\mathcal{I}_1}\right)\boldsymbol{S}_{\mathcal{I}_1}^* - \boldsymbol{S}_{\mathcal{I}_4}\boldsymbol{\Lambda}_{\mathcal{I}_4}\boldsymbol{S}_{\mathcal{I}_4}^*
\end{aligned}$$

For all $k \in \mathcal{I}_1$, we have $1 - \epsilon \leq \lambda_k \leq 1$, and thus $0 \leq 1 - \lambda_k \leq \epsilon$. Hence, $\|\mathbf{I} - \boldsymbol{\Lambda}_{\mathcal{I}_1}\| \leq \epsilon$. For all $k \in \mathcal{I}_4$, we have $0 \leq \lambda_k \leq \epsilon$. Hence, $\|\boldsymbol{\Lambda}_{\mathcal{I}_4}\| \leq \epsilon$. Then, since $\begin{bmatrix} \boldsymbol{S}_{\mathcal{I}_1} & \boldsymbol{S}_{\mathcal{I}_4} \end{bmatrix}$ has orthonormal columns, we have that

$$\begin{aligned}
\|\boldsymbol{S}_K\boldsymbol{S}_K^* - \left(\boldsymbol{B} + \boldsymbol{S}_\epsilon\boldsymbol{D}_1\boldsymbol{S}_\epsilon^*\right)\| &= \|\boldsymbol{S}_{\mathcal{I}_1}\left(\mathbf{I} - \boldsymbol{\Lambda}_{\mathcal{I}_1}\right)\boldsymbol{S}_{\mathcal{I}_1}^* - \boldsymbol{S}_{\mathcal{I}_4}\boldsymbol{\Lambda}_{\mathcal{I}_4}\boldsymbol{S}_{\mathcal{I}_4}^*\| \\
&= \max\{\|\mathbf{I} - \boldsymbol{\Lambda}_{\mathcal{I}_1}\|, \|\boldsymbol{\Lambda}_{\mathcal{I}_4}\|\} \\
&\leq \epsilon.
\end{aligned}$$

B.1.2 Proof of Theorem 4b

Partition $[N]$ into $\mathcal{I}_1, \mathcal{I}_2, \mathcal{I}_3, \mathcal{I}_4$ as done in the previous subsection. Then, we can write

$$\boldsymbol{B} = \boldsymbol{S}\boldsymbol{\Lambda}\boldsymbol{S}^* = \boldsymbol{S}_{\mathcal{I}_1}\boldsymbol{\Lambda}_{\mathcal{I}_1}\boldsymbol{S}_{\mathcal{I}_1}^* + \boldsymbol{S}_{\mathcal{I}_2}\boldsymbol{\Lambda}_{\mathcal{I}_2}\boldsymbol{S}_{\mathcal{I}_2}^* + \boldsymbol{S}_{\mathcal{I}_3}\boldsymbol{\Lambda}_{\mathcal{I}_3}\boldsymbol{S}_{\mathcal{I}_3}^* + \boldsymbol{S}_{\mathcal{I}_4}\boldsymbol{\Lambda}_{\mathcal{I}_4}\boldsymbol{S}_{\mathcal{I}_4}^*,$$

$$\boldsymbol{S}_K\boldsymbol{\Lambda}_K^{-1}\boldsymbol{S}_K^* = \boldsymbol{S}_{\mathcal{I}_1}\boldsymbol{\Lambda}_{\mathcal{I}_1}^{-1}\boldsymbol{S}_{\mathcal{I}_1}^* + \boldsymbol{S}_{\mathcal{I}_2}\boldsymbol{\Lambda}_{\mathcal{I}_2}^{-1}\boldsymbol{S}_{\mathcal{I}_2}^*$$

$$\boldsymbol{S}_\epsilon = \begin{bmatrix} \boldsymbol{S}_{\mathcal{I}_2} & \boldsymbol{S}_{\mathcal{I}_3} \end{bmatrix}.$$

By defining

$$\boldsymbol{D}_2 = \begin{bmatrix} \boldsymbol{\Lambda}_{\mathcal{I}_2}^{-1} - \boldsymbol{\Lambda}_{\mathcal{I}_2} & \boldsymbol{0} \\ \boldsymbol{0} & -\boldsymbol{\Lambda}_{\mathcal{I}_3} \end{bmatrix},$$

we have,

$$\boldsymbol{S}_\epsilon\boldsymbol{D}_2\boldsymbol{S}_\epsilon^* = \boldsymbol{S}_{\mathcal{I}_2}\left(\boldsymbol{\Lambda}_{\mathcal{I}_2}^{-1} - \boldsymbol{\Lambda}_{\mathcal{I}_2}\right)\boldsymbol{S}_{\mathcal{I}_2}^* - \boldsymbol{S}_{\mathcal{I}_3}\boldsymbol{\Lambda}_{\mathcal{I}_3}\boldsymbol{S}_{\mathcal{I}_3}^*.$$

Hence,

$$\begin{aligned}
&\boldsymbol{S}_K\boldsymbol{\Lambda}_K^{-1}\boldsymbol{S}_K^* - (\boldsymbol{B} + \boldsymbol{S}_\epsilon\boldsymbol{D}_2\boldsymbol{S}_\epsilon^*) \\
&= \left(\boldsymbol{S}_{\mathcal{I}_1}\boldsymbol{\Lambda}_{\mathcal{I}_1}^{-1}\boldsymbol{S}_{\mathcal{I}_1}^* + \boldsymbol{S}_{\mathcal{I}_2}\boldsymbol{\Lambda}_{\mathcal{I}_2}^{-1}\boldsymbol{S}_{\mathcal{I}_2}^*\right) \\
&\quad - \left(\boldsymbol{S}_{\mathcal{I}_1}\boldsymbol{\Lambda}_{\mathcal{I}_1}\boldsymbol{S}_{\mathcal{I}_1}^* + \boldsymbol{S}_{\mathcal{I}_2}\boldsymbol{\Lambda}_{\mathcal{I}_2}\boldsymbol{S}_{\mathcal{I}_2}^* + \boldsymbol{S}_{\mathcal{I}_3}\boldsymbol{\Lambda}_{\mathcal{I}_3}\boldsymbol{S}_{\mathcal{I}_3}^* + \boldsymbol{S}_{\mathcal{I}_4}\boldsymbol{\Lambda}_{\mathcal{I}_4}\boldsymbol{S}_{\mathcal{I}_4}^*\right) \\
&\quad - \left(\boldsymbol{S}_{\mathcal{I}_2}\left(\boldsymbol{\Lambda}_{\mathcal{I}_2}^{-1} - \boldsymbol{\Lambda}_{\mathcal{I}_2}\right)\boldsymbol{S}_{\mathcal{I}_2}^* - \boldsymbol{S}_{\mathcal{I}_3}\boldsymbol{\Lambda}_{\mathcal{I}_3}\boldsymbol{S}_{\mathcal{I}_3}^*\right) \\
&= \boldsymbol{S}_{\mathcal{I}_1}\left(\boldsymbol{\Lambda}_{\mathcal{I}_1}^{-1} - \boldsymbol{\Lambda}_{\mathcal{I}_1}\right)\boldsymbol{S}_{\mathcal{I}_1}^* - \boldsymbol{S}_{\mathcal{I}_4}\boldsymbol{\Lambda}_{\mathcal{I}_4}\boldsymbol{S}_{\mathcal{I}_4}^*
\end{aligned}$$

For all $k \in \mathcal{I}_1$, we have $1 - \epsilon \leq \lambda_k \leq 1$, and so $1 \leq \frac{1}{\lambda_k} \leq \frac{1}{1-\epsilon}$. Hence, $0 \leq \frac{1}{\lambda_k} - \lambda_k \leq \frac{1}{1-\epsilon} - (1-\epsilon) \leq \frac{\epsilon}{1-\epsilon} + \epsilon \leq 2\epsilon + \epsilon = 3\epsilon$ (because $0 < \epsilon < \frac{1}{2}$), and thus, $\|\boldsymbol{\Lambda}_{\mathcal{I}_1}^{-1} - \boldsymbol{\Lambda}_{\mathcal{I}_1}\| \leq 3\epsilon$. For all $k \in \mathcal{I}_4$, we have $0 \leq \lambda_k \leq \epsilon$. Hence, $\|\boldsymbol{\Lambda}_{\mathcal{I}_4}\| \leq \epsilon$. Then, since $\begin{bmatrix} \boldsymbol{S}_{\mathcal{I}_1} & \boldsymbol{S}_{\mathcal{I}_4} \end{bmatrix}$ has

orthonormal columns, we have that

$$\begin{aligned}\|\boldsymbol{S}_K\boldsymbol{S}_K^* - (\boldsymbol{B} + \boldsymbol{S}_\epsilon\boldsymbol{D}_2\boldsymbol{S}_\epsilon^*)\| &= \|\boldsymbol{S}_{\mathcal{I}_1}\left(\boldsymbol{\Lambda}_{\mathcal{I}_1}^{-1} - \boldsymbol{\Lambda}_{\mathcal{I}_1}\right)\boldsymbol{S}_{\mathcal{I}_1}^* - \boldsymbol{S}_{\mathcal{I}_4}\boldsymbol{\Lambda}_{\mathcal{I}_4}\boldsymbol{S}_{\mathcal{I}_4}^*\| \\ &= \max\{\|\boldsymbol{\Lambda}_{\mathcal{I}_1}^{-1} - \boldsymbol{\Lambda}_{\mathcal{I}_1}\|, \|\boldsymbol{\Lambda}_{\mathcal{I}_4}\|\} \\ &\leq 3\epsilon.\end{aligned}$$

B.1.3 Proof of Theorem 4c

Partition $[N]$ into two sets as follows:

$$\begin{aligned}\mathcal{I}_1 &= \{k \in [N] : \lambda_k \geq 1 - \epsilon \text{ or } \lambda_k \leq \epsilon\} \\ \mathcal{I}_2 &= \{k \in [N] : \epsilon < \lambda_k < 1 - \epsilon\}\end{aligned}$$

Then, we can write

$$\begin{aligned}\boldsymbol{B} = \boldsymbol{S}\boldsymbol{\Lambda}\boldsymbol{S}^* &= \boldsymbol{S}_{\mathcal{I}_1}\boldsymbol{\Lambda}_{\mathcal{I}_1}\boldsymbol{S}_{\mathcal{I}_1}^* + \boldsymbol{S}_{\mathcal{I}_2}\boldsymbol{\Lambda}_{\mathcal{I}_2}\boldsymbol{S}_{\mathcal{I}_2}^*, \\ (\boldsymbol{B}^2 + \alpha\mathbf{I})^{-1}\boldsymbol{B} &= \boldsymbol{S}_{\mathcal{I}_1}\left(\boldsymbol{\Lambda}_{\mathcal{I}_1}^2 + \alpha\mathbf{I}\right)^{-1}\boldsymbol{\Lambda}_{\mathcal{I}_1}\boldsymbol{S}_{\mathcal{I}_1}^* + \boldsymbol{S}_{\mathcal{I}_2}\left(\boldsymbol{\Lambda}_{\mathcal{I}_2}^2 + \alpha\mathbf{I}\right)^{-1}\boldsymbol{\Lambda}_{\mathcal{I}_2}\boldsymbol{S}_{\mathcal{I}_2}^*, \\ \boldsymbol{S}_\epsilon &= \boldsymbol{S}_{\mathcal{I}_2}.\end{aligned}$$

By defining

$$\boldsymbol{D}_3 = \left(\boldsymbol{\Lambda}_{\mathcal{I}_2}^2 + \alpha\mathbf{I}\right)^{-1}\boldsymbol{\Lambda}_{\mathcal{I}_2} - \frac{1}{1+\alpha}\boldsymbol{\Lambda}_{\mathcal{I}_2}$$

we have,

$$\boldsymbol{S}_\epsilon\boldsymbol{D}_3\boldsymbol{S}_\epsilon^* = \boldsymbol{S}_{\mathcal{I}_2}\left(\left(\boldsymbol{\Lambda}_{\mathcal{I}_2}^2 + \alpha\mathbf{I}\right)^{-1}\boldsymbol{\Lambda}_{\mathcal{I}_2} - \frac{1}{1+\alpha}\boldsymbol{\Lambda}_{\mathcal{I}_2}\right)\boldsymbol{S}_{\mathcal{I}_2}^*$$

Hence,

$$\begin{aligned}
&(\boldsymbol{B}^2+\alpha\mathbf{I})^{-1}\boldsymbol{B}-\left(\frac{1}{1+\alpha}\boldsymbol{B}+\boldsymbol{S}_\epsilon\boldsymbol{D}_3\boldsymbol{S}_\epsilon^*\right)\\
&=\left(\boldsymbol{S}_{\mathcal{I}_1}\left(\boldsymbol{\Lambda}_{\mathcal{I}_1}^2+\alpha\mathbf{I}\right)^{-1}\boldsymbol{\Lambda}_{\mathcal{I}_1}\boldsymbol{S}_{\mathcal{I}_1}^*+\boldsymbol{S}_{\mathcal{I}_2}\left(\boldsymbol{\Lambda}_{\mathcal{I}_2}^2+\alpha\mathbf{I}\right)^{-1}\boldsymbol{\Lambda}_{\mathcal{I}_2}\boldsymbol{S}_{\mathcal{I}_2}^*\right)\\
&\quad-\frac{1}{1+\alpha}\left(\boldsymbol{S}_{\mathcal{I}_1}\boldsymbol{\Lambda}_{\mathcal{I}_1}\boldsymbol{S}_{\mathcal{I}_1}^*+\boldsymbol{S}_{\mathcal{I}_2}\boldsymbol{\Lambda}_{\mathcal{I}_2}\boldsymbol{S}_{\mathcal{I}_2}^*\right)\\
&\quad-\left(\boldsymbol{S}_{\mathcal{I}_2}\left(\left(\boldsymbol{\Lambda}_{\mathcal{I}_2}^2+\alpha\mathbf{I}\right)^{-1}\boldsymbol{\Lambda}_{\mathcal{I}_2}-\frac{1}{1+\alpha}\boldsymbol{\Lambda}_{\mathcal{I}_2}\right)\boldsymbol{S}_{\mathcal{I}_2}^*\right)\\
&=\boldsymbol{S}_{\mathcal{I}_1}\left(\left(\boldsymbol{\Lambda}_{\mathcal{I}_1}^2+\alpha\mathbf{I}\right)^{-1}\boldsymbol{\Lambda}_{\mathcal{I}_1}-\frac{1}{1+\alpha}\boldsymbol{\Lambda}_{\mathcal{I}_1}\right)\boldsymbol{S}_{\mathcal{I}_1}^*
\end{aligned}$$

The matrix $\left(\boldsymbol{\Lambda}_{\mathcal{I}_1}^2+\alpha\mathbf{I}\right)^{-1}\boldsymbol{\Lambda}_{\mathcal{I}_1}-\frac{1}{1+\alpha}\boldsymbol{\Lambda}_{\mathcal{I}_1}$ is diagonal with entries of the form

$$\frac{\lambda_k}{\lambda_k^2+\alpha}-\frac{\lambda_k}{1+\alpha}=\frac{\lambda_k-\lambda_k^3}{(1+\alpha)(\lambda_k^2+\alpha)}.$$

For $k\in\mathcal{I}_1$ such that $1-\epsilon\le\lambda_k\le 1$, we have

$$0\le\frac{\lambda_k-\lambda_k^3}{(1+\alpha)(\lambda_k^2+\alpha)}=\frac{(1-\lambda_k)(\lambda_k^2+\lambda_k)}{(1+\alpha)(\lambda_k^2+\alpha)}\le\frac{1-\lambda_k}{1+\alpha}\cdot\frac{\lambda_k^2+\lambda_k}{\alpha\lambda_k^2+\alpha\lambda_k}\le\frac{\epsilon}{1+\alpha}\cdot\frac{1}{\alpha}\le\frac{\epsilon}{\alpha}.$$

For $k\in\mathcal{I}_1$ such that $0\le\lambda_k\le\epsilon$, we have

$$0\le\frac{\lambda_k-\lambda_k^3}{(1+\alpha)(\lambda_k^2+\alpha)}=\frac{\lambda_k(1-\lambda_k^2)}{(1+\alpha)(\lambda_k^2+\alpha)}\le\frac{\epsilon\cdot 1}{(1+\alpha)\cdot\alpha}\le\frac{\epsilon}{\alpha}.$$

Hence, all the diagonal entries are between 0 and $\frac{\epsilon}{\alpha}$, and thus,

$$\left\|\left(\boldsymbol{\Lambda}_{\mathcal{I}_1}^2+\alpha\mathbf{I}\right)^{-1}\boldsymbol{\Lambda}_{\mathcal{I}_1}-\tfrac{1}{1+\alpha}\boldsymbol{\Lambda}_{\mathcal{I}_1}\right\|\le\frac{\epsilon}{\alpha}.$$

Finally,

$$\begin{aligned}
&\left\|(\boldsymbol{B}^2+\alpha\mathbf{I})^{-1}\boldsymbol{B}-\left(\frac{1}{1+\alpha}\boldsymbol{B}+\boldsymbol{S}_\epsilon\boldsymbol{D}_3\boldsymbol{S}_\epsilon^*\right)\right\| \\
&=\left\|\boldsymbol{S}_{\mathcal{I}_1}\left(\left(\boldsymbol{\Lambda}_{\mathcal{I}_1}^2+\alpha\mathbf{I}\right)^{-1}\boldsymbol{\Lambda}_{\mathcal{I}_1}-\frac{1}{1+\alpha}\boldsymbol{\Lambda}_{\mathcal{I}_1}\right)\boldsymbol{S}_{\mathcal{I}_1}^*\right\| \\
&=\left\|\left(\boldsymbol{\Lambda}_{\mathcal{I}_1}^2+\alpha\mathbf{I}\right)^{-1}\boldsymbol{\Lambda}_{\mathcal{I}_1}-\tfrac{1}{1+\alpha}\boldsymbol{\Lambda}_{\mathcal{I}_1}\right\| \\
&\leq\frac{\epsilon}{\alpha}.
\end{aligned}$$

B.2 Proof of Theorem 5

Our goal is to show that $\boldsymbol{B}-\boldsymbol{F}_W\boldsymbol{F}_W^*$ is well-approximated as a factored low rank matrix. To do this, we will express $\boldsymbol{B}-\boldsymbol{F}_W\boldsymbol{F}_W^*$ in terms of other matrices, whose entries also have a closed form. We will then derive a factored low rank approximation for each of these other matrices. Finally, we will combine these low rank approximations to get a factored low rank approximation for $\boldsymbol{B}-\boldsymbol{F}_W\boldsymbol{F}_W^*$.

For convenience, set $W'=\frac{2\lfloor NW\rfloor+1}{2N}$. We let $\boldsymbol{A}_0,\boldsymbol{B}_0\in\mathbb{R}^{N\times N}$ be defined by

$$\boldsymbol{A}_0[m,n]=\begin{cases}\dfrac{1}{\pi(m-n)}-\dfrac{1}{N\sin\left(\pi\frac{m-n}{N}\right)} & \text{if } m\neq n,\\ 0 & \text{if } m=n,\end{cases}$$

and

$$\boldsymbol{B}_0[m,n]=\frac{2\sin(\pi(W-W')(m-n))}{\pi(m-n)}\quad\text{for}\quad m,n\in[N].$$

Also, we let $\boldsymbol{D}_A\in\mathbb{C}^{N\times N}$ and $\boldsymbol{D}_B\in\mathbb{C}^{N\times N}$ be diagonal matrices with diagonal entries $\boldsymbol{D}_A[n,n]=e^{j2\pi W'n}$ and $\boldsymbol{D}_B[n,n]=e^{j(W+W')n}$ for $n\in[N]$.

With these definitions, we can write the (m,n)-th entry of $\boldsymbol{B} - \boldsymbol{F}_W \boldsymbol{F}_W^*$ as

$$
\begin{aligned}
&(\boldsymbol{B} - \boldsymbol{F}_W \boldsymbol{F}_W^*)[m,n] \\
&= \frac{\sin(2\pi W(m-n))}{\pi(m-n)} - \frac{\sin(2\pi W'(m-n))}{N\sin(\pi\frac{m-n}{N})} \\
&= \frac{\sin(2\pi W(m-n))}{\pi(m-n)} - \frac{\sin(2\pi W'(m-n))}{\pi(m-n)} + \frac{\sin(2\pi W'(m-n))}{\pi(m-n)} - \frac{\sin(2\pi W'(m-n))}{N\sin(\pi\frac{m-n}{N})} \\
&= \frac{2\sin(\pi(W-W')(m-n))\cos(\pi(W+W')(m-n))}{\pi(m-n)} \\
&\quad + \frac{\sin(2\pi W'(m-n))}{\pi(m-n)} - \frac{\sin(2\pi W'(m-n))}{N\sin(\pi\frac{m-n}{N})} \\
&= \boldsymbol{B}_0[m,n]\cos(\pi(W+W')(m-n)) + \boldsymbol{A}_0[m,n]\sin(2\pi W'(m-n)) \\
&= \frac{1}{2}e^{j\pi(W+W')m}\boldsymbol{B}_0[m,n]e^{-j\pi(W+W')n} + \frac{1}{2}e^{-j\pi(W+W')m}\boldsymbol{B}_0[m,n]e^{j\pi(W+W')n} \\
&\quad + \frac{1}{2j}e^{j2\pi W'm}\boldsymbol{A}_0[m,n]e^{-j2\pi W'n} - \frac{1}{2j}e^{-j2\pi W'm}\boldsymbol{A}_0[m,n]e^{j2\pi W'n} \\
&= \frac{1}{2}\boldsymbol{D}_B[m,m]\boldsymbol{B}_0[m,n]\overline{\boldsymbol{D}_B[n,n]} + \frac{1}{2}\overline{\boldsymbol{D}_B[m,m]}\boldsymbol{B}_0[m,n]\boldsymbol{D}_B[n,n] \\
&\quad + \frac{1}{2j}\boldsymbol{D}_A[m,m]\boldsymbol{A}_0[m,n]\overline{\boldsymbol{D}_A[n,n]} - \frac{1}{2j}\overline{\boldsymbol{D}_A[m,m]}\boldsymbol{A}_0[m,n]\boldsymbol{D}_A[n,n] \\
&= \left[\frac{1}{2}\boldsymbol{D}_B\boldsymbol{B}_0\boldsymbol{D}_B^* + \frac{1}{2}\boldsymbol{D}_B^*\boldsymbol{B}_0\boldsymbol{D}_B + \frac{1}{2j}\boldsymbol{D}_A\boldsymbol{A}_0\boldsymbol{D}_A^* - \frac{1}{2j}\boldsymbol{D}_A^*\boldsymbol{A}_0\boldsymbol{D}_A\right][m,n].
\end{aligned}
$$

Hence,

$$
\boldsymbol{B} - \boldsymbol{F}_W \boldsymbol{F}_W^* = \frac{1}{2j}\boldsymbol{D}_A\boldsymbol{A}_0\boldsymbol{D}_A^* - \frac{1}{2j}\boldsymbol{D}_A^*\boldsymbol{A}_0\boldsymbol{D}_A + \frac{1}{2}\boldsymbol{D}_B\boldsymbol{B}_0\boldsymbol{D}_B^* + \frac{1}{2}\boldsymbol{D}_B^*\boldsymbol{B}_0\boldsymbol{D}_B. \quad \text{(B.1)}
$$

Thus, we can find a low-rank approximation for $\boldsymbol{B} - \boldsymbol{F}_W \boldsymbol{F}_W^*$ by finding low-rank approximations for $\boldsymbol{A}_0$ and $\boldsymbol{B}_0$.

In order to do so, we now define $\boldsymbol{A}_1 \in \mathbb{R}^{N\times N}$ by

$$
\boldsymbol{A}_1[m,n] = \begin{cases} \boldsymbol{A}_0[m,n] - \dfrac{1}{\pi(m-n+N)} - \dfrac{1}{\pi(m-n-N)} & \text{if } m \neq n, \\ 0 & \text{if } m = n. \end{cases}
$$

Next, we let $\boldsymbol{H} \in \mathbb{R}^{N \times N}$ denote the *Hilbert matrix*, which has entries

$$\boldsymbol{H}[m,n] = \frac{1}{m+n+1} \quad \text{for} \quad m,n \in [N],$$

and let $\boldsymbol{J} \in \mathbb{R}^{N \times N}$ be the so-called *exchange matrix*, i.e.

$$\boldsymbol{J}[m,n] = \begin{cases} 1 & \text{if } m+n = N-1 \\ 0 & \text{otherwise.} \end{cases}$$

Note that for an arbitrary $\boldsymbol{X} \in \mathbb{R}^{N \times N}$, $\boldsymbol{JX}$ is simply $\boldsymbol{X}$ flipped vertically and $\boldsymbol{XJ}$ is $\boldsymbol{X}$ flipped horizontally. Using these definitions, we can write $\boldsymbol{A}_0$ as

$$\boldsymbol{A}_0 = \frac{1}{\pi}(\boldsymbol{HJ} - \boldsymbol{JH}) + \boldsymbol{A}_1. \tag{B.2}$$

By combining (B.1) and (B.2), we get

$$\begin{aligned} &\boldsymbol{B}_{N,W} - \boldsymbol{F}_{N,W}\boldsymbol{F}_{N,W}^* \\ &= \frac{1}{2j}\boldsymbol{D}_A \left[\frac{1}{\pi}(\boldsymbol{HJ} - \boldsymbol{JH}) + \boldsymbol{A}_1\right] \boldsymbol{D}_A^* - \frac{1}{2j}\boldsymbol{D}_A^* \left[\frac{1}{\pi}(\boldsymbol{HJ} - \boldsymbol{JH}) + \boldsymbol{A}_1\right] \boldsymbol{D}_A \\ &\quad + \frac{1}{2}\boldsymbol{D}_B\boldsymbol{B}_0\boldsymbol{D}_B^* + \frac{1}{2}\boldsymbol{D}_B^*\boldsymbol{B}_0\boldsymbol{D}_B. \end{aligned} \tag{B.3}$$

Therefore, we can come up with a factored low rank approximation for $\boldsymbol{B} - \boldsymbol{F}_W\boldsymbol{F}_W^*$ by first deriving factored low rank approximations for each of the matrices $\boldsymbol{H}$, $\boldsymbol{A}_1$, and $\boldsymbol{B}_0$.

Low rank approximation of $\boldsymbol{H}$

Our goal is to construct a factored low-rank matrix $\widetilde{\boldsymbol{H}} \in \mathbb{R}^{N \times N}$ such that $\|\boldsymbol{H} - \widetilde{\boldsymbol{H}}\| \leq \delta_H$ for some desired $\delta_H > 0$. To do this, we show that the Hilbert matrix $\boldsymbol{H}$ is the solution to a Lyapunov equation. Then, we use Lemma 20 (proven in Section E.4) to construct a low-rank approximation to $\boldsymbol{H}$.

Let $\boldsymbol{A} \in \mathbb{R}^{N\times N}$ be the diagonal matrix with diagonal entries $\boldsymbol{A}[n,n] = n + \frac{1}{2}$ for $n \in [N]$, and let $\boldsymbol{U} \in \mathbb{R}^N$ be a vector of all ones. It is easy to verify that the positive definite solution $\boldsymbol{X}$ to $\boldsymbol{A}\boldsymbol{X} + \boldsymbol{X}\boldsymbol{A}^* = \boldsymbol{U}\boldsymbol{U}^*$ is simply $\boldsymbol{X} = \boldsymbol{H}$. The minimum and maximum eigenvalues of $\boldsymbol{A}$ are $\lambda_{\min}(\boldsymbol{A}) = \frac{1}{2}$ and $\lambda_{\max}(\boldsymbol{A}) = N - \frac{1}{2}$, and thus the condition number for $\boldsymbol{A}$ is $\kappa = 2N - 1$. Thus, by applying Lemma 20 with $\delta = \frac{\delta_H}{\pi}$, we can construct $\boldsymbol{Z} \in \mathbb{R}^{N\times r_H}$ with

$$r_H = \left\lceil \frac{1}{\pi^2} \log(8N-4) \log\left(\frac{4\pi}{\delta_H}\right) \right\rceil$$

such that

$$\|\boldsymbol{H} - \boldsymbol{Z}\boldsymbol{Z}^*\| \leq \frac{\delta_H}{\pi}\|\boldsymbol{H}\|.$$

It is shown in [116] that the operator norm of the infinite Hilbert matrix is bounded above by π, and thus, the finite dimensional matrix $\boldsymbol{H}$ satisfies $\|\boldsymbol{H}\| \leq \pi$. Therefore, $\|\boldsymbol{H} - \boldsymbol{Z}\boldsymbol{Z}^*\| \leq \delta_H$, as desired.

Low rank approximation of $\boldsymbol{A}_1$

Next, we construct a factored low-rank matrix $\widetilde{\boldsymbol{A}}_1 \in \mathbb{R}^{N\times N}$ such that $\|\boldsymbol{A}_1 - \widetilde{\boldsymbol{A}}_1\| \leq \delta_A$ for some desired $\delta_A > 0$. In this case we will require a different approach. We begin by noting that by using the Taylor series expansions [1]

$$\frac{1}{\sin \pi x} - \frac{1}{\pi x} = \frac{2}{\pi}\sum_{k=1}^{\infty}(1 - 2^{-(2k-1)})\zeta(2k)x^{2k-1},$$

and

$$\frac{1}{\pi(x+1)} + \frac{1}{\pi(x-1)} = -\frac{2x}{\pi(1-x^2)} = -\frac{2}{\pi}\sum_{k=1}^{\infty} x^{2k-1},$$

[1] Here, $\zeta(s) := \sum_{n=1}^{\infty} n^{-s}$ is the Riemann-Zeta function.

we can write

$$\begin{aligned}\boldsymbol{A}_1[m,n] &= \frac{1}{\pi(m-n)} - \frac{1}{N\sin\left(\pi\frac{m-n}{N}\right)} - \frac{1}{\pi(m-n+N)} - \frac{1}{\pi(m-n-N)} \\ &= \frac{2}{N\pi}\sum_{k=1}^{\infty}\left[1-(1-2^{-(2k-1)})\zeta(2k)\right]\left(\frac{m-n}{N}\right)^{2k-1}.\end{aligned}$$

We can then define an approximation $\widetilde{\boldsymbol{A}}_1 \in \mathbb{R}^{N\times N}$ to $\boldsymbol{A}_1$ by truncating the series to r_A terms:

$$\widetilde{\boldsymbol{A}}_1[m,n] := \frac{2}{N\pi}\sum_{k=1}^{r_A}\left[1-(1-2^{-(2k-1)})\zeta(2k)\right]\left(\frac{m-n}{N}\right)^{2k-1}.$$

Note that each entry of $\widetilde{\boldsymbol{A}}_1$ is a polynomial of degree $2r_A-1$ in both m and n. Thus, we can also write

$$\widetilde{\boldsymbol{A}}_1[m,n] = \sum_{k=0}^{2r_A-1}\sum_{\ell=0}^{2r_A-1} c_{k,\ell}m^k n^\ell,$$

for some set of coefficients $c_{k,\ell} \in \mathbb{R}$. If we define $\boldsymbol{V}_A \in \mathbb{R}^{N\times 2r_A}$ by $\boldsymbol{V}_A[m,k] = m^k$ and define $\boldsymbol{C}_A \in \mathbb{R}^{2r_A\times 2r_A}$ by $\boldsymbol{C}_A[k,\ell] = c_{k,\ell}$, then it is easy to see that we can write $\widetilde{\boldsymbol{A}}_1 = \boldsymbol{V}_A\boldsymbol{C}_A\boldsymbol{V}_A^*$. Thus, $\operatorname{rank}(\widetilde{\boldsymbol{A}}_1) \le 2r_A$.

Next, we note that by using the identity $(1-2^{1-s})\zeta(s) = \sum_{n=1}^{\infty}\frac{(-1)^{n+1}}{n^s}$ for $s>1$, we have

$$0 \le 1-(1-2^{-(2k-1)})\zeta(2k) = \sum_{n=2}^{\infty}\frac{(-1)^n}{n^{2k}} \le \frac{1}{2^{2k}},$$

where the inequality follows from the fact that this is an alternating series whose terms decrease in magnitude. Hence, we can bound the truncation error $|\boldsymbol{A}_1[m,n] - \widetilde{\boldsymbol{A}}_1[m,n]|$

by

$$
\begin{aligned}
|\boldsymbol{A}_1[m,n] - \widetilde{\boldsymbol{A}}_1[m,n]| &= \left| \frac{2}{N\pi} \sum_{k=r_A+1}^{\infty} \left[1 - (1 - 2^{-(2k-1)})\zeta(2k)\right] \left(\frac{m-n}{N}\right)^{2k-1} \right| \\
&\leq \frac{2}{N\pi} \sum_{k=r_A+1}^{\infty} \left[1 - (1 - 2^{-(2k-1)})\zeta(2k)\right] \left|\frac{m-n}{N}\right|^{2k-1} \\
&\leq \frac{2}{N\pi} \sum_{k=r_A+1}^{\infty} \frac{1}{2^{2k}} \cdot 1 \\
&= \frac{2}{3N\pi} \left(\frac{1}{2}\right)^{2r_A}.
\end{aligned}
$$

Therefore, the error $\|\boldsymbol{A}_1 - \widetilde{\boldsymbol{A}}_1\|_F^2$ is bounded by:

$$
\|\boldsymbol{A}_1 - \widetilde{\boldsymbol{A}}_1\|_F^2 = \sum_{m=0}^{N-1} \sum_{n=0}^{N-1} |\boldsymbol{A}_1[m,n] - \widetilde{\boldsymbol{A}}_1[m,n]|^2 \leq N \cdot N \cdot \left[\frac{2}{3N\pi} \left(\frac{1}{2}\right)^{2r_A}\right]^2 = \frac{4}{9\pi^2} \left(\frac{1}{2}\right)^{4r_A}.
$$

Hence,

$$
\|\boldsymbol{A}_1 - \widetilde{\boldsymbol{A}}_1\| \leq \|\boldsymbol{A}_1 - \widetilde{\boldsymbol{A}}_1\|_F \leq \frac{2}{3\pi} \left(\frac{1}{2}\right)^{2r_A}.
$$

So for any $\delta_A \in (0, \frac{8}{3\pi})$, we can set $r_A = \left\lceil \frac{1}{2\log 2} \log\left(\frac{2}{3\pi\delta_A}\right) \right\rceil$ to ensure $\|\boldsymbol{A}_1 - \widetilde{\boldsymbol{A}}_1\| \leq \delta_A$ and

$$
\operatorname{rank}(\widetilde{\boldsymbol{A}}_1) \leq 2 \left\lceil \frac{1}{2\log 2} \log\left(\frac{2}{3\pi\delta_A}\right) \right\rceil.
$$

Low rank approximation of $\boldsymbol{B}_0$

To construct a factored low-rank matrix $\widetilde{\boldsymbol{B}}_0 \in \mathbb{R}^{N \times N}$ such that $\|\boldsymbol{B}_0 - \widetilde{\boldsymbol{B}}_0\| \leq \delta_B$ for some desired $\delta_B > 0$, we use a similar approach as above. Using the Taylor series

$$
\sin x = \sum_{k=0}^{\infty} \frac{(-1)^k x^{2k+1}}{(2k+1)!},
$$

we can write

$$\begin{aligned}\boldsymbol{B}_0[m,n] &= \frac{2\sin(\pi(W-W')(m-n))}{\pi(m-n)} \\ &= \sum_{k=0}^{\infty} \frac{2(-1)^k[\pi(W-W')(m-n)]^{2k+1}}{(2k+1)!\pi(m-n)} \\ &= \frac{2}{N\pi}\sum_{k=0}^{\infty} \frac{(-1)^k[\pi(W-W')N]^{2k+1}}{(2k+1)!}\left(\frac{m-n}{N}\right)^{2k}.\end{aligned}$$

We can then define a new matrix $\widetilde{\boldsymbol{B}}_0 \in \mathbb{R}^{N\times N}$ by truncating the series to r_B terms:

$$\widetilde{\boldsymbol{B}}_0[m,n] := \frac{2}{N\pi}\sum_{k=0}^{r_B-1} \frac{(-1)^k[\pi(W-W')N]^{2k+1}}{(2k+1)!}\left(\frac{m-n}{N}\right)^{2k}.$$

Note that each entry of $\widetilde{\boldsymbol{B}}_0$ is a polynomial of degree $2r_B-2$ in both m and n. Thus, we could also write

$$\widetilde{\boldsymbol{B}}_0[m,n] = \sum_{k=0}^{2r_B-2}\sum_{\ell=0}^{2r_B-2} c'_{k,\ell} m^k n^\ell,$$

for a set of scalars $c'_{k,\ell} \in \mathbb{R}$. If we define $\boldsymbol{V}_B \in \mathbb{R}^{N\times(2r_B-1)}$ by $\boldsymbol{V}_B[m,k] = m^k$ and define $\boldsymbol{C}_B \in \mathbb{R}^{(2r_B-1)\times(2r_B-1)}$ by $\boldsymbol{C}_B[k,\ell] = c'_{k,\ell}$, then it is easy to see that we can write $\widetilde{\boldsymbol{B}}_0 = \boldsymbol{V}_B\boldsymbol{C}_B\boldsymbol{V}_B^*$. Thus, $\operatorname{rank}(\widetilde{\boldsymbol{B}}_0) \le 2r_B-1$.

Since $|\pi(W-W')N| = \left|\pi\left(W - \frac{2\lfloor NW\rfloor+1}{2N}\right)N\right| = \frac{\pi}{2}\left|2NW - 2\lfloor NW\rfloor - 1\right| \le \frac{\pi}{2}$, and $(2k+1)! \ge \frac{2}{9}\cdot 3^{2k+1}$ for all integers $k \ge 0$, we can bound the truncation error $|\boldsymbol{B}_0[m,n] - \widetilde{\boldsymbol{B}}_0[m,n]|$ by:

$$\begin{aligned}|\boldsymbol{B}_0[m,n] - \widetilde{\boldsymbol{B}}_0[m,n]| &\le \left|\frac{2}{N\pi}\sum_{k=r_B}^{\infty}\frac{(-1)^k[\pi(W-W')N]^{2k+1}}{(2k+1)!}\left(\frac{m-n}{N}\right)^{2k}\right| \\ &\le \frac{2}{N\pi}\left|\frac{(-1)^{r_B}[\pi(W-W')N]^{2r_b+1}}{(2K+1)!}\left(\frac{m-n}{N}\right)^{2K}\right| \\ &\le \frac{2}{N\pi}\frac{\left(\frac{\pi}{2}\right)^{2r_B+1}}{\frac{2}{9}\cdot 3^{2r_B+1}}\cdot 1 \\ &= \frac{3}{2N}\left(\frac{\pi}{6}\right)^{2r_B},\end{aligned}$$

where we have used the fact that an alternating series whose terms decrease in magnitude can be bounded by the magnitude of the first term. Thus, the error $\|\boldsymbol{B}_0 - \widetilde{\boldsymbol{B}}_0\|_F^2$ is bounded by:

$$\|\boldsymbol{B}_0 - \widetilde{\boldsymbol{B}}_0\|_F^2 = \sum_{m=0}^{N-1}\sum_{n=0}^{N-1} |\boldsymbol{B}_0[m,n] - \widetilde{\boldsymbol{B}}_0[m,n]|^2 \leq N \cdot N \cdot \left[\frac{3}{2N}\left(\frac{\pi}{6}\right)^{2r_B}\right]^2 = \frac{9}{4}\left(\frac{\pi}{6}\right)^{4r_B}.$$

Hence,

$$\|\boldsymbol{B}_0 - \widetilde{\boldsymbol{B}}_0\| \leq \|\boldsymbol{B}_0 - \widetilde{\boldsymbol{B}}_0\|_F \leq \frac{3}{2}\left(\frac{\pi}{6}\right)^{2r_B}.$$

So for any $\delta_B \in (0, \frac{3}{2})$, we can set $r_B = \left\lceil \frac{1}{2\log\frac{6}{\pi}} \log\left(\frac{3}{2\delta_B}\right)\right\rceil$ to ensure $\|\boldsymbol{B}_0 - \widetilde{\boldsymbol{B}}_0\| \leq \delta_B$ and

$$\operatorname{rank}(\widetilde{\boldsymbol{B}}_0) \leq 2\left\lceil \frac{1}{2\log\frac{6}{\pi}} \log\left(\frac{3}{2\delta_B}\right)\right\rceil - 1.$$

Putting it all together

Now that we have a way to construct a factored low rank approximation of $\boldsymbol{H}$, $\boldsymbol{A}_1$, and $\boldsymbol{B}_0$, we will combine those results to derive a factored low rank approximation for $\boldsymbol{B} - \boldsymbol{F}_W\boldsymbol{F}_W^*$. For any $\epsilon \in (0, \frac{1}{2})$, set[2] $\delta_H = \frac{4\pi}{15}\epsilon$ and $\delta_A = \delta_B = \frac{7}{30}\epsilon$. Then, let $\widetilde{\boldsymbol{H}} = \boldsymbol{Z}\boldsymbol{Z}^*$, $\widetilde{\boldsymbol{A}}_1 = \boldsymbol{V}_A\boldsymbol{C}_A\boldsymbol{V}_A^*$, and $\widetilde{\boldsymbol{B}}_0 = \boldsymbol{V}_B\boldsymbol{C}_B\boldsymbol{V}_B^*$ be defined as in the previous subsections. Also, define $\boldsymbol{\Delta}_H = \boldsymbol{H} - \widetilde{\boldsymbol{H}}$, $\boldsymbol{\Delta}_A = \boldsymbol{A}_1 - \widetilde{\boldsymbol{A}}_1$, $\boldsymbol{\Delta}_B = \boldsymbol{B}_0 - \widetilde{\boldsymbol{B}}_0$. By using these definitions along with (B.3), we can write

$$\boldsymbol{B} - \boldsymbol{F}_W\boldsymbol{F}_W^* = \boldsymbol{L} + \boldsymbol{\Delta},$$

[2]It may be possible to obtain a slightly better bound via a more careful selection of δ_A, δ_B, and δ_H. We have not pursued such refinements here as there is not much room for significant improvement.

where

$$\begin{aligned}\boldsymbol{L} &= \frac{1}{2j}\boldsymbol{D}_A\left[\frac{1}{\pi}(\widetilde{\boldsymbol{H}}\boldsymbol{J}-\boldsymbol{J}\widetilde{\boldsymbol{H}})+\widetilde{\boldsymbol{A}}_1\right]\boldsymbol{D}_A^* - \frac{1}{2j}\boldsymbol{D}_A^*\left[\frac{1}{\pi}(\widetilde{\boldsymbol{H}}\boldsymbol{J}-\boldsymbol{J}\widetilde{\boldsymbol{H}})+\widetilde{\boldsymbol{A}}_1\right]\boldsymbol{D}_A \\ &\quad + \frac{1}{2}\boldsymbol{D}_B\widetilde{\boldsymbol{B}}_0\boldsymbol{D}_B^* + \frac{1}{2}\boldsymbol{D}_B^*\widetilde{\boldsymbol{B}}_0\boldsymbol{D}_B \\ &= \frac{1}{2\pi j}(\boldsymbol{D}_A\boldsymbol{Z}\boldsymbol{Z}^*\boldsymbol{J}\boldsymbol{D}_A^* - \boldsymbol{D}_A\boldsymbol{J}\boldsymbol{Z}\boldsymbol{Z}^*\boldsymbol{D}_A^* - \boldsymbol{D}_A^*\boldsymbol{Z}\boldsymbol{Z}^*\boldsymbol{J}\boldsymbol{D}_A - \boldsymbol{D}_A^*\boldsymbol{J}\boldsymbol{Z}\boldsymbol{Z}^*\boldsymbol{D}_A) \\ &\quad + \frac{1}{2j}(\boldsymbol{D}_A\boldsymbol{V}_A\boldsymbol{C}_A\boldsymbol{V}_A^*\boldsymbol{D}_A^* - \boldsymbol{D}_A^*\boldsymbol{V}_A\boldsymbol{C}_A\boldsymbol{V}_A^*\boldsymbol{D}_A) \\ &\quad + \frac{1}{2}(\boldsymbol{D}_B\boldsymbol{V}_B\boldsymbol{C}_B\boldsymbol{V}_B^*\boldsymbol{D}_B^* + \boldsymbol{D}_B^*\boldsymbol{V}_B\boldsymbol{C}_B\boldsymbol{V}_B^*\boldsymbol{D}_B)\end{aligned}$$

and

$$\begin{aligned}\boldsymbol{\Delta} &= \frac{1}{2j}\boldsymbol{D}_A\left[\frac{1}{\pi}(\boldsymbol{\Delta}_H\boldsymbol{J}-\boldsymbol{J}\boldsymbol{\Delta}_H)+\boldsymbol{\Delta}_A\right]\boldsymbol{D}_A^* - \frac{1}{2j}\boldsymbol{D}_A^*\left[\frac{1}{\pi}(\boldsymbol{\Delta}_H\boldsymbol{J}-\boldsymbol{J}\boldsymbol{\Delta}_H)+\boldsymbol{\Delta}_A\right]\boldsymbol{D}_A \\ &\quad + \frac{1}{2}\boldsymbol{D}_B\boldsymbol{\Delta}_B\boldsymbol{D}_B^* + \frac{1}{2}\boldsymbol{D}_B^*\boldsymbol{\Delta}_B\boldsymbol{D}_B.\end{aligned}$$

If we define

$$\begin{aligned}\boldsymbol{L}_1 = \Bigg[&\frac{1}{2\pi j}\boldsymbol{D}_A\boldsymbol{Z} \quad -\frac{1}{2\pi j}\boldsymbol{D}_A\boldsymbol{J}\boldsymbol{Z} \quad -\frac{1}{2\pi j}\boldsymbol{D}_A^*\boldsymbol{Z} \quad \frac{1}{2\pi j}\boldsymbol{D}_A^*\boldsymbol{J}\boldsymbol{Z} \quad \cdots \\ &\cdots \quad \frac{1}{2j}\boldsymbol{D}_A\boldsymbol{V}_A \quad -\frac{1}{2j}\boldsymbol{D}_A^*\boldsymbol{V}_A \quad \frac{1}{2}\boldsymbol{D}_B\boldsymbol{V}_B \quad \frac{1}{2}\boldsymbol{D}_B^*\boldsymbol{V}_B\Bigg],\end{aligned}$$

and

$$\begin{aligned}\boldsymbol{L}_2 = [&\boldsymbol{D}_A\boldsymbol{J}\boldsymbol{Z} \quad \boldsymbol{D}_A\boldsymbol{Z} \quad \boldsymbol{D}_A^*\boldsymbol{J}\boldsymbol{Z} \quad \boldsymbol{D}_A^*\boldsymbol{Z} \quad \cdots \\ &\cdots \quad \boldsymbol{D}_A\boldsymbol{V}_A\boldsymbol{C}_A^* \quad \boldsymbol{D}_A^*\boldsymbol{V}_A\boldsymbol{C}_A^* \quad \boldsymbol{D}_B\boldsymbol{V}_B\boldsymbol{C}_B^* \quad \boldsymbol{D}_B^*\boldsymbol{V}_B\boldsymbol{C}_B^*],\end{aligned}$$

then $\boldsymbol{L} = \boldsymbol{L}_1 \boldsymbol{L}_2^*$ and $\boldsymbol{L}_1, \boldsymbol{L}_2 \in \mathbb{C}^{N \times r'}$, where

$$\begin{aligned}
r' &= 4 \cdot r_H + 2 \cdot 2r_A + 2 \cdot (2r_B - 1) \\
&= 4 \left\lceil \frac{1}{\pi^2} \log(8N-4) \log \frac{4\pi}{\delta_H} \right\rceil + 4 \left\lceil \frac{1}{2 \log 2} \log \frac{2}{3\pi\delta_A} \right\rceil + 4 \left\lceil \frac{1}{2 \log \frac{6}{\pi}} \log \frac{3}{2\delta_B} \right\rceil - 2 \\
&\leq \frac{4}{\pi^2} \log(8N-4) \log \frac{4\pi}{\delta_H} + \frac{2}{\log 2} \log \frac{2}{3\pi\delta_A} + \frac{2}{\log \frac{6}{\pi}} \log \frac{3}{2\delta_B} + 10 \\
&= \frac{4}{\pi^2} \log(8N-4) \log \frac{15}{\epsilon} + \frac{2}{\log 2} \log \frac{20}{7\pi\epsilon} + \frac{2}{\log \frac{6}{\pi}} \log \frac{45}{7\epsilon} + 10 \\
&= \left(\frac{4}{\pi^2} \log(8N-4) + \frac{2}{\log 2} + \frac{2}{\log \frac{6}{\pi}} \right) \log \frac{15}{\epsilon} + \frac{2}{\log 2} \log \frac{4}{21\pi} + \frac{2}{\log \frac{6}{\pi}} \log \frac{3}{7} + 10 \\
&\leq \left(\frac{4}{\pi^2} \log(8N) + 6 \right) \log \left(\frac{15}{\epsilon} \right).
\end{aligned}$$

Also, by applying the triangle inequality and the fact that $\|\boldsymbol{D}_A\| = \|\boldsymbol{D}_B\| = \|\boldsymbol{J}\| = 1$, we see that

$$\begin{aligned}
\|\boldsymbol{B} - (\boldsymbol{F}_W \boldsymbol{F}_W^* + \boldsymbol{L}_1 \boldsymbol{L}_2^*)\| &= \|\boldsymbol{\Delta}\| \\
&\leq \frac{2}{\pi} \|\boldsymbol{\Delta}_H\| + \|\boldsymbol{\Delta}_A\| + \|\boldsymbol{\Delta}_B\| \\
&\leq \frac{2}{\pi} \delta_H + \delta_A + \delta_B \\
&= \frac{2}{\pi} \cdot \frac{4\pi\epsilon}{15} + \frac{7\epsilon}{30} + \frac{7\epsilon}{30} \\
&= \epsilon.
\end{aligned}$$

Together, these two facts establish the theorem.

APPENDIX C

PROOFS FOR CHAPTER 5

C.1 Proof of Results in Section 5.1

C.1.1 Norms of Gaussian random variables

In this subsection, we develop results on the 2-norm of linear combinations of Gaussian random variables, which will be critical to our proofs of the theorems in Section 5.1.

First, we state a result from [117] regarding the product of four jointly complex Gaussian vectors.

Lemma 6. *[117] Suppose $\boldsymbol{a}, \boldsymbol{b}, \boldsymbol{c}, \boldsymbol{d} \in \mathbb{C}^K$ have a joint complex Gaussian distribution. Then*

$$\mathbb{E}[\boldsymbol{a}^*\boldsymbol{b}\boldsymbol{c}^*\boldsymbol{d}] = \mathbb{E}[\boldsymbol{a}^*\boldsymbol{b}]\mathbb{E}[\boldsymbol{c}^*\boldsymbol{d}] + \mathbb{E}[\boldsymbol{c}^* \otimes \boldsymbol{a}^*]\mathbb{E}[\boldsymbol{d} \otimes \boldsymbol{b}] + \mathbb{E}[\boldsymbol{a}^*\mathbb{E}[\boldsymbol{b}\boldsymbol{c}^*]\boldsymbol{d}] + 2\mathbb{E}[\boldsymbol{a}^*]\mathbb{E}[\boldsymbol{b}]\mathbb{E}[\boldsymbol{c}^*]\mathbb{E}[\boldsymbol{d}],$$

where $\otimes$ denotes the Kronecker product.

It should be noted that [117] proves a more general result for the product of four joint complex Gaussian matrices, but this is a bit harder to state. So we give the result for vectors.

We now prove a result regarding the norm-squared of linear combinations of complex Gaussians.

Lemma 7. *Let $\boldsymbol{x} \sim \mathcal{CN}(\boldsymbol{0}, \boldsymbol{R})$ for some positive semidefinite $\boldsymbol{R} \in \mathbb{C}^{N\times N}$ and let $\boldsymbol{U}, \boldsymbol{V} \in \mathbb{C}^{K\times N}$. Then, we have:*

$$\mathbb{E}\left[\|\boldsymbol{U}\boldsymbol{x}\|_2^2\right] = \mathrm{tr}[\boldsymbol{U}\boldsymbol{R}\boldsymbol{U}^*] \quad \textit{and} \quad \mathrm{Cov}\left[\|\boldsymbol{U}\boldsymbol{x}\|_2^2, \|\boldsymbol{V}\boldsymbol{x}\|_2^2\right] = \|\boldsymbol{U}\boldsymbol{R}\boldsymbol{V}^*\|_F^2.$$

Proof. The expectation of $\|\boldsymbol{U}\boldsymbol{x}\|_2^2$ can be computed as follows

$$\mathbb{E}\left[\|\boldsymbol{U}\boldsymbol{x}\|_2^2\right] = \mathbb{E}\left[\mathrm{tr}\left[\boldsymbol{U}\boldsymbol{x}\boldsymbol{x}^*\boldsymbol{U}^*\right]\right] = \mathrm{tr}\left[\mathbb{E}\left[\boldsymbol{U}\boldsymbol{x}\boldsymbol{x}^*\boldsymbol{U}^*\right]\right] = \mathrm{tr}\left[\boldsymbol{U}\mathbb{E}\left[\boldsymbol{x}\boldsymbol{x}^*\right]\boldsymbol{U}^*\right] = \mathrm{tr}\left[\boldsymbol{U}\boldsymbol{R}\boldsymbol{U}^*\right].$$

Since the entries of $\boldsymbol{x}$ are jointly Gaussian with mean 0, the entries of $\boldsymbol{U}\boldsymbol{x}$ and $\boldsymbol{V}\boldsymbol{x}$ are also jointly Gaussian with mean 0. Then, by applying Lemma 6 (with $\boldsymbol{a} = \boldsymbol{b} = \boldsymbol{U}\boldsymbol{x}$ and $\boldsymbol{c} = \boldsymbol{d} = \boldsymbol{V}\boldsymbol{x}$), we find that

$$\begin{aligned}
\mathrm{Cov}\left[\|\boldsymbol{U}\boldsymbol{x}\|_2^2, \|\boldsymbol{V}\boldsymbol{x}\|_2^2\right] &= \mathbb{E}\left[\|\boldsymbol{U}\boldsymbol{x}\|_2^2 \cdot \|\boldsymbol{V}\boldsymbol{x}\|_2^2\right] - \mathbb{E}\left[\|\boldsymbol{U}\boldsymbol{x}\|_2^2\right]\mathbb{E}\left[\|\boldsymbol{V}\boldsymbol{x}\|_2^2\right] \\
&= \mathbb{E}\left[\boldsymbol{x}^*\boldsymbol{U}^*\boldsymbol{U}\boldsymbol{x}\boldsymbol{x}^*\boldsymbol{V}^*\boldsymbol{V}\boldsymbol{x}\right] - \mathbb{E}\left[\boldsymbol{x}^*\boldsymbol{U}^*\boldsymbol{U}\boldsymbol{x}\right]\mathbb{E}\left[\boldsymbol{x}^*\boldsymbol{V}^*\boldsymbol{V}\boldsymbol{x}\right] \\
&= \mathbb{E}\left[\boldsymbol{x}^*\boldsymbol{V}^* \otimes \boldsymbol{x}^*\boldsymbol{U}^*\right]\mathbb{E}\left[\boldsymbol{V}\boldsymbol{x} \otimes \boldsymbol{U}\boldsymbol{x}\right] + \mathbb{E}\left[\boldsymbol{x}^*\boldsymbol{U}^*\mathbb{E}\left[\boldsymbol{U}\boldsymbol{x}\boldsymbol{x}^*\boldsymbol{V}^*\right]\boldsymbol{V}\boldsymbol{x}\right] \\
&\quad + 2\mathbb{E}[\boldsymbol{x}^*\boldsymbol{U}^*]\mathbb{E}[\boldsymbol{U}\boldsymbol{x}]\mathbb{E}[\boldsymbol{x}^*\boldsymbol{V}^*]\mathbb{E}[\boldsymbol{V}\boldsymbol{x}].
\end{aligned}$$

We proceed to evaluate each of these three terms.

Since $\boldsymbol{x} \sim \mathcal{CN}(\boldsymbol{0}, \boldsymbol{R})$, we can write $\boldsymbol{x} = \boldsymbol{R}^{1/2}\boldsymbol{y}$ where $\boldsymbol{y} \sim \mathcal{CN}(\boldsymbol{0}, \mathbf{I})$ and $\boldsymbol{R}^{1/2}$ is the unique positive semidefinite squareroot of $\boldsymbol{R}$. Then, by using the identity $\boldsymbol{X}_1\boldsymbol{X}_2 \otimes \boldsymbol{X}_3\boldsymbol{X}_4 = (\boldsymbol{X}_1 \otimes \boldsymbol{X}_3)(\boldsymbol{X}_2 \otimes \boldsymbol{X}_4)$ for appropriately sized matrices $\boldsymbol{X}_1, \boldsymbol{X}_2, \boldsymbol{X}_3, \boldsymbol{X}_4$, we obtain

$$\begin{aligned}
\mathbb{E}[\boldsymbol{V}\boldsymbol{x} \otimes \boldsymbol{U}\boldsymbol{x}] &= \mathbb{E}\left[\boldsymbol{V}\boldsymbol{R}^{1/2}\boldsymbol{y} \otimes \boldsymbol{U}\boldsymbol{R}^{1/2}\boldsymbol{y}\right] \\
&= \mathbb{E}\left[\left(\boldsymbol{V}\boldsymbol{R}^{1/2} \otimes \boldsymbol{U}\boldsymbol{R}^{1/2}\right)(\boldsymbol{y} \otimes \boldsymbol{y})\right] \\
&= \left(\boldsymbol{V}\boldsymbol{R}^{1/2} \otimes \boldsymbol{U}\boldsymbol{R}^{1/2}\right)\mathbb{E}[\boldsymbol{y} \otimes \boldsymbol{y}]
\end{aligned}$$

Since the entries of $\boldsymbol{y}$ are i.i.d. $\mathcal{CN}(0,1)$, $\mathbb{E}\left[\boldsymbol{y}[n]\boldsymbol{y}[n']\right] = 0$ for all indices $n, n' \in [N]$. (Note that $\mathbb{E}[\boldsymbol{y}[n]^2] \neq 0$ if the entries of $\boldsymbol{y}$ were i.i.d. $\mathcal{N}(0,1)$ instead of $\mathcal{CN}(0,1)$.) Hence, $\mathbb{E}[\boldsymbol{y} \otimes \boldsymbol{y}] = \boldsymbol{0}$, and thus, $\mathbb{E}[\boldsymbol{V}\boldsymbol{x} \otimes \boldsymbol{U}\boldsymbol{x}] = (\boldsymbol{V}\boldsymbol{R}^{1/2} \otimes \boldsymbol{U}\boldsymbol{R}^{1/2})\mathbb{E}[\boldsymbol{y} \otimes \boldsymbol{y}] = \boldsymbol{0}$. Similarly, $\mathbb{E}[\boldsymbol{x}^*\boldsymbol{V}^* \otimes \boldsymbol{x}^*\boldsymbol{U}^*] = \boldsymbol{0}^*$, and so, $\mathbb{E}\left[\boldsymbol{x}^*\boldsymbol{V}^* \otimes \boldsymbol{x}^*\boldsymbol{U}^*\right]\mathbb{E}\left[\boldsymbol{V}\boldsymbol{x} \otimes \boldsymbol{U}\boldsymbol{x}\right] = 0$.

Using the cyclic property of the trace operator, linearity of the trace and expectation operators, and the fact that $\mathbb{E}[\boldsymbol{x}\boldsymbol{x}^*] = \boldsymbol{R}$, we find that

$$\begin{aligned} E\left[\boldsymbol{x}^*\boldsymbol{U}^*\mathbb{E}\left[\boldsymbol{U}\boldsymbol{x}\boldsymbol{x}^*\boldsymbol{V}^*\right]\boldsymbol{V}\boldsymbol{x}\right] &= \mathbb{E}\left[\operatorname{tr}\left[\mathbb{E}\left[\boldsymbol{U}\boldsymbol{x}\boldsymbol{x}^*\boldsymbol{V}^*\right]\boldsymbol{V}\boldsymbol{x}\boldsymbol{x}^*\boldsymbol{U}^*\right]\right] \\ &= \operatorname{tr}\left[\mathbb{E}\left[\mathbb{E}\left[\boldsymbol{U}\boldsymbol{x}\boldsymbol{x}^*\boldsymbol{V}^*\right]\boldsymbol{V}\boldsymbol{x}\boldsymbol{x}^*\boldsymbol{U}^*\right]\right] \\ &= \operatorname{tr}\left[\boldsymbol{U}\mathbb{E}\left[\boldsymbol{x}\boldsymbol{x}^*\right]\boldsymbol{V}^*\boldsymbol{V}\mathbb{E}\left[\boldsymbol{x}\boldsymbol{x}^*\right]\boldsymbol{U}^*\right] \\ &= \operatorname{tr}\left[\boldsymbol{U}\boldsymbol{R}\boldsymbol{V}^*\boldsymbol{V}\boldsymbol{R}\boldsymbol{U}^*\right] \\ &= \left\|\boldsymbol{U}\boldsymbol{R}\boldsymbol{V}^*\right\|_F^2. \end{aligned}$$

Finally, since $\mathbb{E}[\boldsymbol{x}] = \boldsymbol{0}$, we have $\mathbb{E}[\boldsymbol{U}\boldsymbol{x}] = \mathbb{E}[\boldsymbol{V}\boldsymbol{x}] = \boldsymbol{0}$ and $\mathbb{E}[\boldsymbol{x}^*\boldsymbol{U}^*] = \mathbb{E}[\boldsymbol{x}^*\boldsymbol{V}^*] = \boldsymbol{0}^*$. Hence,

$$2\mathbb{E}[\boldsymbol{x}^*\boldsymbol{U}^*]\mathbb{E}[\boldsymbol{U}\boldsymbol{x}]\mathbb{E}[\boldsymbol{x}^*\boldsymbol{V}^*]\mathbb{E}[\boldsymbol{V}\boldsymbol{x}] = 0.$$

Adding these three terms yields,

$$\begin{aligned} \operatorname{Cov}\left[\left\|\boldsymbol{U}\boldsymbol{x}\right\|_2^2, \left\|\boldsymbol{V}\boldsymbol{x}\right\|_2^2\right] &= \mathbb{E}\left[\boldsymbol{x}^*\boldsymbol{V}^* \otimes \boldsymbol{x}^*\boldsymbol{U}^*\right]\mathbb{E}\left[\boldsymbol{V}\boldsymbol{x} \otimes \boldsymbol{U}\boldsymbol{x}\right] + \mathbb{E}\left[\boldsymbol{x}^*\boldsymbol{U}^*\mathbb{E}\left[\boldsymbol{U}\boldsymbol{x}\boldsymbol{x}^*\boldsymbol{V}^*\right]\boldsymbol{V}\boldsymbol{x}\right] \\ &\quad + 2\mathbb{E}[\boldsymbol{x}^*\boldsymbol{U}^*]\mathbb{E}[\boldsymbol{U}\boldsymbol{x}]\mathbb{E}[\boldsymbol{x}^*\boldsymbol{V}^*]\mathbb{E}[\boldsymbol{V}\boldsymbol{x}]. \\ &= \left\|\boldsymbol{U}\boldsymbol{R}\boldsymbol{V}^*\right\|_F^2. \end{aligned}$$

□

C.1.2 Concentration of norms of Gaussian random variables

Next, we state a result from [118] regarding concentration bounds for sums of independent exponential random variables.

Lemma 8. *[118] Let $Z_0, \ldots, Z_{N-1}$ be independent exponential random variables with $\mathbb{E}[Z_n] = \mu_n$. Then, the sum*

$$Z := \sum_{n=0}^{N-1} Z_n$$

satisfies

$$\mathbb{P}\left\{Z \geq \beta \mathbb{E}[Z]\right\} \leq \beta^{-1} e^{-\kappa(\beta - 1 - \ln \beta)} \quad \textit{for} \quad \beta > 1,$$

and

$$\mathbb{P}\left\{Z \leq \beta \mathbb{E}[Z]\right\} \leq e^{-\kappa(\beta - 1 - \ln \beta)} \quad \textit{for} \quad 0 < \beta < 1,$$

where

$$\kappa = \frac{\sum_{n=0}^{N-1} \mu_n}{\max_{n=0,\ldots,N-1} \mu_n}.$$

We now apply this lemma to derive concentration bounds for $\|\boldsymbol{A}\boldsymbol{x}\|_2^2$, where $\boldsymbol{x}$ is a vector of Gaussian random variables and $\boldsymbol{A}$ is a matrix.

Lemma 9. *Let $\boldsymbol{x} \sim \mathcal{CN}(\boldsymbol{0}, \boldsymbol{R})$ for some positive semidefinite $\boldsymbol{R} \in \mathbb{C}^{N \times N}$. Also, let $\boldsymbol{A} \in \mathbb{C}^{K \times N}$. Then, the random variable $\|\boldsymbol{A}\boldsymbol{x}\|_2^2$ satisfies*

$$\mathbb{P}\left\{\|\boldsymbol{A}\boldsymbol{x}\|_2^2 \geq \beta \mathbb{E}\left[\|\boldsymbol{A}\boldsymbol{x}\|_2^2\right]\right\} \leq \beta^{-1} e^{-\kappa(\beta - 1 - \ln \beta)} \quad \textit{for} \quad \beta > 1,$$

and

$$\mathbb{P}\left\{\|\boldsymbol{A}\boldsymbol{x}\|_2^2 \leq \beta \mathbb{E}\left[\|\boldsymbol{A}\boldsymbol{x}\|_2^2\right]\right\} \leq e^{-\kappa(\beta - 1 - \ln \beta)} \quad \textit{for} \quad 0 < \beta < 1,$$

where

$$\kappa = \frac{\mathrm{tr}\left[\boldsymbol{A}\boldsymbol{R}\boldsymbol{A}^*\right]}{\|\boldsymbol{A}\boldsymbol{R}\boldsymbol{A}^*\|}.$$

Proof. Since $\boldsymbol{x} \sim \mathcal{CN}(\boldsymbol{0}, \boldsymbol{R})$, we can write $\boldsymbol{x} = \boldsymbol{R}^{1/2}\boldsymbol{y}$ where $\boldsymbol{y} \sim \mathcal{CN}(\boldsymbol{0}, \mathbf{I})$ and $\boldsymbol{R}^{1/2}$ is the unique positive semidefinite squareroot of $\boldsymbol{R}$. Then, using eigendecomposition, we can write $\boldsymbol{R}^{1/2}\boldsymbol{A}^*\boldsymbol{A}\boldsymbol{R}^{1/2} = \boldsymbol{W}\boldsymbol{D}\boldsymbol{W}^*$ where $\boldsymbol{W}$ is unitary and $\boldsymbol{D} = \mathrm{diag}(d_1, \ldots, \mathrm{d}_n)$. Since $\boldsymbol{W}$ is unitary, $\boldsymbol{z} := \boldsymbol{W}^*\boldsymbol{y} \sim \mathcal{CN}(\boldsymbol{0}, \mathbf{I}_N)$. Then, we have:

$$\|\boldsymbol{A}\boldsymbol{x}\|_2^2 = \boldsymbol{x}^*\boldsymbol{A}^*\boldsymbol{A}\boldsymbol{x} = \boldsymbol{y}^*\boldsymbol{R}^{1/2}\boldsymbol{A}^*\boldsymbol{A}\boldsymbol{R}^{1/2}\boldsymbol{y} = \boldsymbol{y}^*\boldsymbol{W}\boldsymbol{D}\boldsymbol{W}^*\boldsymbol{y} = \boldsymbol{z}^*\boldsymbol{D}\boldsymbol{z} = \sum_{n=0}^{N-1} d_n \left|\boldsymbol{z}[n]\right|^2.$$

Since $\boldsymbol{z} \sim \mathcal{CN}(\boldsymbol{0}, \mathbf{I}_N)$, we have that $\boldsymbol{z}[0], \ldots, \boldsymbol{z}[N-1]$ are i.i.d. $\mathcal{CN}(0, 1)$. Hence,

$d_n|\boldsymbol{z}[n]|^2 \sim \text{Exp}(d_n)$, and are independent. If we apply Lemma 8, the fact that the trace and operator norm are invariant under unitary similarity transforms, and the matrix identities $\text{tr}[\boldsymbol{X}\boldsymbol{X}^*] = \text{tr}[\boldsymbol{X}^*\boldsymbol{X}]$ and $\|\boldsymbol{X}\boldsymbol{X}^*\| = \|\boldsymbol{X}^*\boldsymbol{X}\|$, we obtain

$$\mathbb{P}\left\{\|\boldsymbol{A}\boldsymbol{x}\|_2^2 \geq \beta\mathbb{E}\left[\|\boldsymbol{A}\boldsymbol{x}\|_2^2\right]\right\} \leq \beta^{-1}e^{-\kappa(\beta-1-\ln\beta)} \quad \text{for} \quad \beta > 1,$$

and

$$\mathbb{P}\left\{\|\boldsymbol{A}\boldsymbol{x}\|_2^2 \leq \beta\mathbb{E}\left[\|\boldsymbol{A}\boldsymbol{x}\|_2^2\right]\right\} \leq e^{-\kappa(\beta-1-\ln\beta)} \quad \text{for} \quad 0 < \beta < 1,$$

where

$$\kappa = \frac{\sum_{n=0}^{N-1} d_n}{\max\limits_{n=0,\ldots,N-1} d_n} = \frac{\text{tr}[\boldsymbol{D}]}{\|\boldsymbol{D}\|} = \frac{\text{tr}[\boldsymbol{W}\boldsymbol{D}\boldsymbol{W}^*]}{\|\boldsymbol{W}\boldsymbol{D}\boldsymbol{W}^*\|} = \frac{\text{tr}\left[\boldsymbol{R}^{1/2}\boldsymbol{A}^*\boldsymbol{A}\boldsymbol{R}^{1/2}\right]}{\left\|\boldsymbol{R}^{1/2}\boldsymbol{A}^*\boldsymbol{A}\boldsymbol{R}^{1/2}\right\|} = \frac{\text{tr}\left[\boldsymbol{A}\boldsymbol{R}\boldsymbol{A}^*\right]}{\|\boldsymbol{A}\boldsymbol{R}\boldsymbol{A}^*\|}.$$

□

We note that similar bounds can be obtained by applying the Hanson-Wright Inequality [119, 120].

C.1.3 Intermediate results

We continue by presenting a lemma showing that certain matrices have a spectral representation as an integral of a frequency dependent rank-1 matrix.

Lemma 10. *For any frequency $f \in \mathbb{R}$, define a complex sinusoid $\boldsymbol{e}_f \in \mathbb{C}^N$ by $\boldsymbol{e}_f[n] = e^{j2\pi fn}$ for $n \in [N]$. Then, we have:*

$$\boldsymbol{B} = \int_{-W}^{W} \boldsymbol{e}_f\boldsymbol{e}_f^*\, df, \quad \mathbf{I} = \int_{-1/2}^{1/2} \boldsymbol{e}_f\boldsymbol{e}_f^*\, df, \quad \textit{and} \quad \int_{\Omega} \boldsymbol{e}_f\boldsymbol{e}_f^*\, df = \mathbf{I} - \boldsymbol{B},$$

where $\Omega = [-\frac{1}{2}, \frac{1}{2}] \setminus [-W, W]$. Furthermore, if $x(t)$ is a stationary, ergodic, zero-mean, Gaussian stochastic process $x(t)$ with power spectral density $S(f)$, and $\boldsymbol{x} \in \mathbb{C}^N$ is a vector

of equispaced samples $\boldsymbol{x}[n] = x(n)$ for $n \in [N]$, then the covariance matrix of $\boldsymbol{x}$ can be written as

$$\boldsymbol{R} := \mathbb{E}[\boldsymbol{x}\boldsymbol{x}^*] = \int_{-1/2}^{1/2} S(f)\boldsymbol{e}_f\boldsymbol{e}_f^*\, df.$$

Proof. For any $m, n \in [N]$, we have

$$\int_{-W}^{W} \boldsymbol{e}_f[m]\overline{\boldsymbol{e}_f[n]}\, df = \int_{-W}^{W} e^{j2\pi f(m-n)}\, df = \frac{\sin[2\pi W(m-n)]}{\pi(m-n)} = \boldsymbol{B}[m,n],$$

and

$$\int_{-1/2}^{1/2} \boldsymbol{e}_f[m]\overline{\boldsymbol{e}_f[n]}\, df = \int_{-1/2}^{1/2} e^{j2\pi f(m-n)}\, df = \begin{cases} 1 & \text{if } m = n \\ 0 & \text{if } m \neq n \end{cases} = \mathbf{I}[m,n].$$

We can put these into matrix form as

$$\int_{-W}^{W} \boldsymbol{e}_f\boldsymbol{e}_f^*\, df = \boldsymbol{B} \quad \text{and} \quad \int_{-1/2}^{1/2} \boldsymbol{e}_f\boldsymbol{e}_f^*\, df = \mathbf{I}.$$

From this, it follows that

$$\int_{\Omega} \boldsymbol{e}_f\boldsymbol{e}_f^*\, df = \int_{-1/2}^{1/2} \boldsymbol{e}_f\boldsymbol{e}_f^*\, df - \int_{-W}^{W} \boldsymbol{e}_f\boldsymbol{e}_f^*\, df = \mathbf{I} - \boldsymbol{B}.$$

Finally, using the definition of the power spectral density, we have

$$\boldsymbol{R}[m,n] = \mathbb{E}[\boldsymbol{x}[m]\overline{\boldsymbol{x}[n]}] = \int_{-1/2}^{1/2} S(f)e^{j2\pi f(m-n)}\, df = \int_{-1/2}^{1/2} S(f)\boldsymbol{e}_f[m]\overline{\boldsymbol{e}_f[n]}\, df$$

for $m, n \in [N]$. Again, we can put this into matrix form as

$$\boldsymbol{R} := \mathbb{E}[\boldsymbol{x}\boldsymbol{x}^*] = \int_{-1/2}^{1/2} S(f)\boldsymbol{e}_f\boldsymbol{e}_f^*\, df.$$

□

Next, we show that the expectation of the multitaper spectral estimate is the convolution

of the power spectral density $S(f)$ with the spectral window $\psi(f)$.

Lemma 11. *The expectation of the multitaper spectral estimate can be written as*

$$\mathbb{E}\left[\widehat{S}_K^{mt}(f)\right] = \int_{-1/2}^{1/2} S(f-f')\psi(f')\,df'$$

where

$$\psi(f) := \frac{1}{K}\operatorname{tr}\left[\boldsymbol{S}_K^* \boldsymbol{e}_{-f}\boldsymbol{e}_{-f}^* \boldsymbol{S}_K\right] = \frac{1}{K}\left\|\boldsymbol{S}_K^*\boldsymbol{e}_{-f}\right\|_2^2 = \frac{1}{K}\sum_{k=0}^{K-1}\left|\sum_{n=0}^{N-1} \boldsymbol{s}_k[n]e^{-j2\pi fn}\right|^2$$

is the spectral window of the multitaper estimate.

Proof. Since $\widehat{S}_K^{\text{mt}}(f) = \frac{1}{K}\left\|\boldsymbol{S}_K^*\boldsymbol{E}_f^*\boldsymbol{x}\right\|_2^2$ where $\boldsymbol{x} \sim \mathcal{CN}(\boldsymbol{0}, \boldsymbol{R})$, by Lemma 7, we have

$$\mathbb{E}\left[\widehat{S}_K^{\text{mt}}(f)\right] = \frac{1}{K}\operatorname{tr}\left[\boldsymbol{S}_K^*\boldsymbol{E}_f^*\boldsymbol{R}\boldsymbol{E}_f\boldsymbol{S}_K\right].$$

We can rewrite this expression as follows:

$$\begin{aligned}
\mathbb{E}\left[\widehat{S}_K^{\text{mt}}(f)\right] &= \frac{1}{K}\operatorname{tr}\left[\boldsymbol{S}_K^*\boldsymbol{E}_f^*\boldsymbol{R}\boldsymbol{E}_f\boldsymbol{S}_K\right] \\
&= \frac{1}{K}\operatorname{tr}\left[\boldsymbol{S}_K^*\boldsymbol{E}_f^*\left(\int_{-1/2}^{1/2} S(f')\boldsymbol{e}_{f'}\boldsymbol{e}_{f'}^*\,df'\right)\boldsymbol{E}_f\boldsymbol{S}_K\right] \\
&= \frac{1}{K}\int_{-1/2}^{1/2} S(f')\operatorname{tr}\left[\boldsymbol{S}_K^*\boldsymbol{E}_f^*\boldsymbol{e}_{f'}\boldsymbol{e}_{f'}^*\boldsymbol{E}_f\boldsymbol{S}_K\right]\,df' \\
&= \frac{1}{K}\int_{-1/2}^{1/2} S(f')\operatorname{tr}\left[\boldsymbol{S}_K^*\boldsymbol{e}_{f'-f}\boldsymbol{e}_{f'-f}^*\boldsymbol{S}_K\right]\,df' \\
&= \int_{-1/2}^{1/2} S(f')\psi(f-f')\,df', \\
&= \int_{f-1/2}^{f+1/2} S(f-f')\psi(f')\,df' \\
&= \int_{-1/2}^{1/2} S(f-f')\psi(f')\,df',
\end{aligned}$$

where the last line follows since $S(f)$ is 1-periodic (by definition) and $\psi(f) = \frac{1}{K}\|\boldsymbol{S}_K^* \boldsymbol{e}_{-f}\|_2^2$ is 1-periodic (because $\boldsymbol{e}_{-f}[n] = e^{-2\pi f n}$ is 1-periodic for all $n \in [N]$).

Finally, it's easy to check that $\psi(f)$ can be written in the following alternate forms:

$$\psi(f) = \frac{1}{K}\operatorname{tr}\left[\boldsymbol{S}_K^* \boldsymbol{e}_{-f}\boldsymbol{e}_{-f}^* \boldsymbol{S}_K\right] = \frac{1}{K}\|\boldsymbol{S}_K^* \boldsymbol{e}_{-f}\|_2^2 = \frac{1}{K}\sum_{k=0}^{K-1}\left|\sum_{n=0}^{N-1} \boldsymbol{s}_k[n] e^{-j2\pi f n}\right|^2.$$

□

Lemma 12. *The spectral window $\psi(f)$ defined in Lemma 11, satisfies the following properties:*

- $\psi(f) = \psi(-f)$ *for all* $f \in \mathbb{R}$
- $\displaystyle\int_{-W}^{W} \psi(f)\, df = 1 - \Sigma_K^{(1)}$ *and* $\displaystyle\int_{\Omega} \psi(f)\, df = \Sigma_K^{(1)}$ *where* $\Omega = [-\tfrac{1}{2}, \tfrac{1}{2}] \setminus [-W, W]$
- $0 \le \psi(f) \le \dfrac{N}{K}$

Proof. First, the spectral window is an even function since

$$\psi(-f) = \frac{1}{K}\sum_{k=0}^{K-1}\left|\sum_{n=0}^{N-1} \boldsymbol{s}_k[n] e^{j2\pi f n}\right|^2 = \frac{1}{K}\sum_{k=0}^{K-1}\left|\sum_{n=0}^{N-1} \boldsymbol{s}_k[n] e^{-j2\pi f n}\right|^2 = \psi(f)$$

for all $f \in \mathbb{R}$.

As a consequence, we can set $\boldsymbol{S}_K = \begin{bmatrix} \boldsymbol{s}_0 & \boldsymbol{s}_1 & \cdots & \boldsymbol{s}_{K-1} \end{bmatrix} \in \mathbb{R}^{N\times K}$ and write $\psi(f) = \psi(-f) = \frac{1}{K}\operatorname{tr}\left[\boldsymbol{S}_K^* \boldsymbol{e}_f \boldsymbol{e}_f^* \boldsymbol{S}_K\right] = \frac{1}{K}\|\boldsymbol{S}_K^* \boldsymbol{e}_f\|_2^2$. Then, the integral of the spectral window

$\psi(f)$ over $[-W, W]$ is

$$\begin{aligned}
\int_{-W}^{W} \psi(f)\, df &= \int_{-W}^{W} \frac{1}{K} \operatorname{tr}\left[\boldsymbol{S}_K^* \boldsymbol{e}_f \boldsymbol{e}_f^* \boldsymbol{S}_K\right]\, df \\
&= \frac{1}{K} \operatorname{tr}\left[\boldsymbol{S}_K^* \left(\int_{-W}^{W} \boldsymbol{e}_f \boldsymbol{e}_f^*\, df\right) \boldsymbol{S}_K\right] \\
&= \frac{1}{K} \operatorname{tr}\left[\boldsymbol{S}_K^* \boldsymbol{B} \boldsymbol{S}_K\right] \\
&= \frac{1}{K} \operatorname{tr}\left[\boldsymbol{\Lambda}_K\right] \\
&= \frac{1}{K} \sum_{k=0}^{K-1} \lambda_k \\
&= 1 - \frac{1}{K} \sum_{k=0}^{K-1} (1 - \lambda_k) \\
&= 1 - \Sigma_K^{(1)},
\end{aligned}$$

where we have used the notation $\boldsymbol{\Lambda}_K = \operatorname{diag}(\lambda_0, \ldots, \lambda_{K-1})$. Similarly, the integral of the spectral window $\psi(f)$ over $\Omega = [-\frac{1}{2}, -W) \cup (W, \frac{1}{2}]$ is

$$\begin{aligned}
\int_{\Omega} \psi(f)\, df &= \int_{\Omega} \frac{1}{K} \operatorname{tr}\left[\boldsymbol{S}_K^* \boldsymbol{e}_f \boldsymbol{e}_f^* \boldsymbol{S}_K\right]\, df \\
&= \frac{1}{K} \operatorname{tr}\left[\boldsymbol{S}_K^* \left(\int_{\Omega} \boldsymbol{e}_f \boldsymbol{e}_f^*\, df\right) \boldsymbol{S}_K\right] \\
&= \frac{1}{K} \operatorname{tr}\left[\boldsymbol{S}_K^* (\mathbf{I} - \boldsymbol{B}) \boldsymbol{S}_K\right] \\
&= \frac{1}{K} \operatorname{tr}\left[\mathbf{I} - \boldsymbol{\Lambda}_K\right] \\
&= \frac{1}{K} \sum_{k=0}^{K-1} (1 - \lambda_k) \\
&= \Sigma_K^{(1)}.
\end{aligned}$$

Finally, the spectral window is bounded by

$$0 \le \psi(f) = \frac{1}{K} \left\|\boldsymbol{S}_K^* \boldsymbol{e}_f\right\|_2^2 \le \frac{1}{K} \left\|\boldsymbol{S}_K^*\right\|^2 \left\|\boldsymbol{e}_f\right\|_2^2 = \frac{N}{K},$$

where we have used $\|\boldsymbol{S}_K^*\| = 1$ (because $\boldsymbol{S}_K$ is orthonormal) and $\|\boldsymbol{e}_f\|_2^2 = N$. $\square$

C.1.4 Proof of Theorem 6

By Lemma 11, we have

$$\mathbb{E}\left[\widehat{S}_K^{\text{mt}}(f)\right] = \int_{-1/2}^{1/2} S(f-f')\psi(f')\,df'.$$

We now split the expression for the bias into two pieces as follows:

$$\begin{aligned}
\text{Bias}\left[\widehat{S}_K^{\text{mt}}(f)\right] &= \left|\mathbb{E}\widehat{S}_K^{\text{mt}}(f) - S(f)\right| \\
&= \left|\int_{-1/2}^{1/2} S(f-f')\psi(f')\,df' - S(f)\right| \\
&= \left|\int_{-W}^{W} S(f-f')\psi(f')\,df' + \int_{\Omega} S(f-f')\psi(f')\,df' - S(f)\right| \\
&\leq \underbrace{\left|\int_{-W}^{W} S(f-f')\psi(f')\,df' - S(f)\right|}_{\text{local bias}} + \underbrace{\left|\int_{\Omega} S(f-f')\psi(f')\,df'\right|}_{\text{broadband bias}}.
\end{aligned}$$

Since $S(f)$ is twice continuously differentiable, for any $f' \in [-W, W]$, there exists a $\xi_{f'}$ between $f - f'$ and f such that

$$S(f-f') = S(f) - S'(f)f' + \frac{1}{2}S''(\xi_{f'})f'^2.$$

Then, since $|S''(\xi_{f'})| \leq \max_{\xi\in[f-W,f+W]} |S''(\xi)| = M_f''$, $\int_{-W}^{W}\psi(f)\,df = 1 - \Sigma_K^{(1)}$, and $0 \leq$

$\psi(f') \leq \frac{N}{K}$ for all $f' \in \mathbb{R}$, we can bound the local bias as follows:

$$
\begin{aligned}
&\left| \int_{-W}^{W} S(f-f')\psi(f')\,df' - S(f) \right| \\
&= \left| \int_{-W}^{W} \left(S(f) - S'(f)f' + \frac{1}{2}S''(\xi_{f'})f'^2 \right) \psi(f')\,df' - S(f) \right| \\
&= \left| \int_{-W}^{W} S(f)\psi(f')\,df' - S(f) - \int_{-W}^{W} \underbrace{S'(f)f'\psi(f')}_{\text{odd w.r.t. } f'}\,df' + \frac{1}{2}\int_{-W}^{W} S''(\xi_{f'})f'^2\psi(f')\,df' \right| \\
&= \left| \int_{-W}^{W} S(f)\psi(f')\,df' - S(f) - 0 + \frac{1}{2}\int_{-W}^{W} S''(\xi_{f'})f'^2\psi(f')\,df' \right| \\
&\leq \left| \int_{-W}^{W} S(f)\psi(f')\,df' - S(f) \right| + \left| \frac{1}{2}\int_{-W}^{W} S''(\xi_{f'})f'^2\psi(f')\,df' \right| \\
&= \left| S(f)(1-\Sigma_K^{(1)}) - S(f) \right| + \left| \frac{1}{2}\int_{-W}^{W} S''(\xi_{f'})f'^2\psi(f')\,df' \right| \\
&\leq S(f)\Sigma_K^{(1)} + \frac{1}{2}\int_{-W}^{W} |S''(\xi_{f'})||f'|^2\psi(f')\,df' \\
&\leq S(f)\Sigma_K^{(1)} + \frac{1}{2}\int_{-W}^{W} M_f''|f'|^2\frac{N}{K}\,df' \\
&= S(f)\Sigma_K^{(1)} + \frac{M_f''NW^3}{3K} \\
&\leq M_f\Sigma_K^{(1)} + \frac{M_f''NW^3}{3K}
\end{aligned}
$$

Since $S(f') \leq \max_{f' \in \mathbb{R}} S(f') = M$, we can bound the broadband bias as follows:

$$
\begin{aligned}
\left| \int_{\Omega} S(f-f')\psi(f')\,df' \right| &= \int_{\Omega} S(f-f')\psi(f')\,df' \\
&\leq \int_{\Omega} M\psi(f')\,df' \\
&= M\Sigma_K^{(1)}
\end{aligned}
$$

Combining the bounds on the local bias and broadband bias yields

$$\begin{aligned}\text{Bias}\left[\widehat{S}_K^{\text{mt}}(f)\right] &\leq \underbrace{\left|\int_{-W}^{W} S(f-f')\psi(f')\,df' - S(f)\right|}_{\text{local bias}} + \underbrace{\left|\int_{\Omega} S(f-f')\psi(f')\,df'\right|}_{\text{broadband bias}} \\ &\leq M_f\Sigma_K^{(1)} + \frac{M_f'' NW^3}{3K} + M\Sigma_K^{(1)} \\ &= \frac{M_f'' NW^3}{3K} + (M+M_f)\Sigma_K^{(1)},\end{aligned}$$

which establishes Theorem 6.

C.1.5 Proof of Theorem 7

Without the assumption that $S(f)$ is twice differentiable, we can still obtain a bound on the bias. Using the bounds $m_f = \min_{\xi\in[f-W,f+W]} S(\xi) \leq S(f') \leq \max_{\xi\in[f-W,f+W]} S(\xi) = M_f$ and $0 \leq S(f') \leq \max_{\xi\in\mathbb{R}} S(\xi) = M$ along with the integrals $\int_{-W}^{W}\psi(f)\,df = 1-\Sigma_K^{(1)}$ and $\int_{\Omega}\psi(f)\,df = \Sigma_K^{(1)}$, we can obtain the following upper bound on $\mathbb{E}\widehat{S}_K^{\text{mt}}(f) - S(f)$:

$$\begin{aligned}\mathbb{E}\widehat{S}_K^{\text{mt}}(f) - S(f) &= \int_{-1/2}^{1/2} S(f-f')\psi(f')\,df' - S(f') \\ &= \int_{-W}^{W} S(f-f')\psi(f')\,df' + \int_{\Omega} S(f-f')\psi(f')\,df' - S(f') \\ &\leq \int_{-W}^{W} M_f\psi(f')\,df' + \int_{\Omega} M\psi(f')\,df' - m_f \\ &= M_f(1-\Sigma_K^{(1)}) + M\Sigma_K^{(1)} - m_f \\ &= (M_f-m_f)(1-\Sigma_K^{(1)}) + (M-m_f)\Sigma_K^{(1)} \\ &\leq (M_f-m_f)(1-\Sigma_K^{(1)}) + M\Sigma_K^{(1)},\end{aligned}$$

Similarly, we can obtain the following lower bound on $\mathbb{E}\widehat{S}_K^{\text{mt}}(f) - S(f)$:

$$
\begin{aligned}
\mathbb{E}\widehat{S}_K^{\text{mt}}(f) - S(f) &= \int_{-1/2}^{1/2} S(f-f')\psi(f')\,df' - S(f') \\
&= \int_{-W}^{W} S(f-f')\psi(f')\,df' + \int_{\Omega} S(f-f')\psi(f')\,df' - S(f') \\
&\geq \int_{-W}^{W} m_f\psi(f')\,df' + \int_{\Omega} 0\psi(f')\,df' - M_f \\
&= m_f(1-\Sigma_K^{(1)}) + 0 - M_f \\
&= -(M_f - m_f)(1-\Sigma_K^{(1)}) - M_f\Sigma_K^{(1)} \\
&\geq -(M_f - m_f)(1-\Sigma_K^{(1)}) - M\Sigma_K^{(1)}.
\end{aligned}
$$

From the above two bounds, we have

$$
\text{Bias}\left[\widehat{S}_K^{\text{mt}}(f)\right] = \left|\mathbb{E}\widehat{S}_K^{\text{mt}}(f) - S(f)\right| \leq (M_f - m_f)(1-\Sigma_K^{(1)}) + M\Sigma_K^{(1)},
$$

which establishes Theorem 7.

C.1.6 Proof of Theorem 8

Since $\widehat{S}_K^{\text{mt}}(f) = \frac{1}{K}\left\|\boldsymbol{S}_K^*\boldsymbol{E}_f^*\boldsymbol{x}\right\|_2^2$ where $\boldsymbol{x} \sim \mathcal{CN}(\boldsymbol{0}, \boldsymbol{R})$, by Lemma 7, we have

$$
\begin{aligned}
\text{Var}\left[\widehat{S}_K^{\text{mt}}(f)\right] &= \text{Var}\left[\frac{1}{K}\left\|\boldsymbol{S}_K^*\boldsymbol{E}_f^*\boldsymbol{x}\right\|_2^2\right] \\
&= \frac{1}{K^2}\,\text{Cov}\left[\left\|\boldsymbol{S}_K^*\boldsymbol{E}_f^*\boldsymbol{x}\right\|_2^2, \left\|\boldsymbol{S}_K^*\boldsymbol{E}_f^*\boldsymbol{x}\right\|_2^2\right] \\
&= \frac{1}{K^2}\left\|\boldsymbol{S}_K^*\boldsymbol{E}_f^*\boldsymbol{R}\boldsymbol{E}_f\boldsymbol{S}_K\right\|_F^2.
\end{aligned}
$$

We focus on bounding the Frobenius norm of $\boldsymbol{S}_K^*\boldsymbol{E}_f^*\boldsymbol{R}\boldsymbol{E}_f\boldsymbol{S}_K$. To do this, we first split it into two pieces - an integral over $[-W, W]$ and an integral over $\Omega = [-\frac{1}{2}, \frac{1}{2}] \setminus [-W, W]$:

$$
\begin{aligned}
&\boldsymbol{S}_K^* \boldsymbol{E}_f^* \boldsymbol{R} \boldsymbol{E}_f \boldsymbol{S}_K \\
&= \boldsymbol{S}_K^* \boldsymbol{E}_f^* \left(\int_{-1/2}^{1/2} S(f') \boldsymbol{e}_{f'} \boldsymbol{e}_{f'}^* \, df' \right) \boldsymbol{E}_f \boldsymbol{S}_K \\
&= \boldsymbol{S}_K^* \left(\int_{-1/2}^{1/2} S(f') \boldsymbol{E}_f^* \boldsymbol{e}_{f'} \boldsymbol{e}_{f'}^* \boldsymbol{E}_f \, df' \right) \boldsymbol{S}_K \\
&= \boldsymbol{S}_K^* \left(\int_{-1/2}^{1/2} S(f') \boldsymbol{e}_{f'-f} \boldsymbol{e}_{f'-f}^* \, df' \right) \boldsymbol{S}_K \\
&= \boldsymbol{S}_K^* \left(\int_{f-1/2}^{f+1/2} S(f+f') \boldsymbol{e}_{f'} \boldsymbol{e}_{f'}^* \, df' \right) \boldsymbol{S}_K \\
&= \boldsymbol{S}_K^* \left(\int_{-1/2}^{1/2} S(f+f') \boldsymbol{e}_{f'} \boldsymbol{e}_{f'}^* \, df' \right) \boldsymbol{S}_K \\
&= \boldsymbol{S}_K^* \left(\int_{-W}^{W} S(f+f') \boldsymbol{e}_{f'} \boldsymbol{e}_{f'}^* \, df' + \int_{\Omega} S(f+f') \boldsymbol{e}_{f'} \boldsymbol{e}_{f'}^* \, df' \right) \boldsymbol{S}_K \\
&= \boldsymbol{S}_K^* \left(\int_{-W}^{W} S(f+f') \boldsymbol{e}_{f'} \boldsymbol{e}_{f'}^* \, df' \right) \boldsymbol{S}_K + \boldsymbol{S}_K^* \left(\int_{\Omega} S(f+f') \boldsymbol{e}_{f'} \boldsymbol{e}_{f'}^* \, df' \right) \boldsymbol{S}_K.
\end{aligned}
$$

We will proceed by bounding the Frobenius norm of the two pieces above, and then applying the triangle inequality. Since $S(f) \leq \max_{f \in \mathbb{R}} S(f) = M$ for all $f \in \mathbb{R}$, we trivially have

$$
\begin{aligned}
\boldsymbol{S}_K^* \left(\int_{\Omega} S(f+f') \boldsymbol{e}_{f'} \boldsymbol{e}_{f'}^* \, df' \right) \boldsymbol{S}_K &\preceq \boldsymbol{S}_K^* \left(\int_{\Omega} M \boldsymbol{e}_{f'} \boldsymbol{e}_{f'}^* \, df' \right) \boldsymbol{S}_K \\
&= \boldsymbol{S}_K^* [M(\mathbf{I} - \boldsymbol{B})] \boldsymbol{S}_K \\
&= M(\mathbf{I} - \boldsymbol{\Lambda}_K).
\end{aligned}
$$

Then, since $\boldsymbol{P} \preceq \boldsymbol{Q}$ implies $\|\boldsymbol{P}\|_F \leq \|\boldsymbol{Q}\|_F$, we have

$$\begin{aligned}\left\| \boldsymbol{S}_K^* \left(\int_\Omega S(f+f') \boldsymbol{e}_{f'} \boldsymbol{e}_{f'}^* \, df' \right) \boldsymbol{S}_K \right\|_F &\leq \|M(\mathbf{I} - \boldsymbol{\Lambda}_K)\|_F \\ &= \sqrt{\sum_{k=0}^{K-1} M^2 (1-\lambda_k)^2} \\ &= M\sqrt{K}\Sigma_K^{(2)}.\end{aligned}$$

Obtaining a good bound on the first piece requires a more intricate argument. We define $\mathbb{1}_W(f) = 1$ if $f \in [-W, W]$ and $\mathbb{1}_W(f) = 0$ if $f \in [-\frac{1}{2}, \frac{1}{2}] \setminus [-W, W]$. For convenience, we also extend $\mathbb{1}_W(f)$ to $f \in \mathbb{R}$ such that $\mathbb{1}_W(f)$ is 1-periodic. With this definition, we can write

$$\begin{aligned}\int_{-W}^{W} S(f+f') \boldsymbol{e}_{f'} \boldsymbol{e}_{f'}^* \, df' &= \int_{-1/2}^{1/2} S(f+f') \mathbb{1}_W(f') \boldsymbol{e}_{f'} \boldsymbol{e}_{f'}^* \, df' \\ &= \int_0^1 S(f+f') \mathbb{1}_W(f') \boldsymbol{e}_{f'} \boldsymbol{e}_{f'}^* \, df' \\ &= \sum_{\ell=0}^{N-1} \int_{\frac{\ell}{N}}^{\frac{\ell+1}{N}} S(f+f') \mathbb{1}_W(f') \boldsymbol{e}_{f'} \boldsymbol{e}_{f'}^* \, df' \\ &= \sum_{\ell=0}^{N-1} \int_0^{\frac{1}{N}} S(f+f'+\tfrac{\ell}{N}) \mathbb{1}_W(f'+\tfrac{\ell}{N}) \boldsymbol{e}_{f'+\frac{\ell}{N}} \boldsymbol{e}_{f'+\frac{\ell}{N}}^* \, df' \\ &= \int_0^{\frac{1}{N}} \sum_{\ell=0}^{N-1} S(f+f'+\tfrac{\ell}{N}) \mathbb{1}_W(f'+\tfrac{\ell}{N}) \boldsymbol{e}_{f'+\frac{\ell}{N}} \boldsymbol{e}_{f'+\frac{\ell}{N}}^* \, df',\end{aligned}$$

where the second line holds since $S(f)$, $\mathbb{1}_W(f)$, and $\boldsymbol{e}_f$ are 1-periodic. Now, for any $f' \in \mathbb{R}$, the vectors $\left\{ \frac{1}{\sqrt{N}} \boldsymbol{e}_{f'+\frac{\ell}{N}} \right\}_{\ell=0}^{N-1}$ form an orthonormal basis of $\mathbb{C}^N$. Hence, we have

$$\left\| \sum_{\ell=0}^{N-1} a_\ell \boldsymbol{e}_{f'+\frac{\ell}{N}} \boldsymbol{e}_{f'+\frac{\ell}{N}}^* \right\|_F^2 = N^2 \sum_{\ell=0}^{N-1} |a_\ell|^2$$

for any choice of coefficients $\{a_\ell\}_{\ell=0}^{N-1}$ and offset frequency $f' \in \mathbb{R}$. By applying this

formula, along with the triangle inequality and the Cauchy-Shwarz Integral inequality, we obtain

$$
\begin{aligned}
&\left\| \int_{-W}^{W} S(f+f') \boldsymbol{e}_{f'} \boldsymbol{e}_{f'}^{*} \, df' \right\|_F^2 \\
&= \left\| \int_{0}^{\frac{1}{N}} \sum_{\ell=0}^{N-1} S(f+f'+\tfrac{\ell}{N}) \mathbb{1}_W(f'+\tfrac{\ell}{N}) \boldsymbol{e}_{f'+\frac{\ell}{N}} \boldsymbol{e}_{f'+\frac{\ell}{N}}^{*} \, df' \right\|_F^2 \\
&\leq \left(\int_{0}^{\frac{1}{N}} \left\| \sum_{\ell=0}^{N-1} S(f+f'+\tfrac{\ell}{N}) \mathbb{1}_W(f'+\tfrac{\ell}{N}) \boldsymbol{e}_{f'+\frac{\ell}{N}} \boldsymbol{e}_{f'+\frac{\ell}{N}}^{*} \right\|_F df' \right)^2 \\
&= \left(\int_{0}^{\frac{1}{N}} N \left(\sum_{\ell=0}^{N-1} S(f+f'+\tfrac{\ell}{N})^2 \mathbb{1}_W(f'+\tfrac{\ell}{N})^2 \right)^{1/2} df' \right)^2 \\
&\leq \left(\int_{0}^{\frac{1}{N}} N^2 \, df' \right) \left(\int_{0}^{\frac{1}{N}} \sum_{\ell=0}^{N-1} S(f+f'+\tfrac{\ell}{N})^2 \mathbb{1}_W(f'+\tfrac{\ell}{N})^2 \, df' \right) \\
&= N \sum_{\ell=0}^{N-1} \int_{0}^{\frac{1}{N}} S(f+f'+\tfrac{\ell}{N})^2 \mathbb{1}_W(f'+\tfrac{\ell}{N})^2 \, df' \\
&= N \sum_{\ell=0}^{N-1} \int_{\frac{\ell}{N}}^{\frac{\ell+1}{N}} S(f+f')^2 \mathbb{1}_W(f')^2 \, df' \\
&= N \int_{0}^{1} S(f+f')^2 \mathbb{1}_W(f')^2 \, df' \\
&= N \int_{-1/2}^{1/2} S(f+f')^2 \mathbb{1}_W(f')^2 \, df' \\
&= N \int_{-W}^{W} S(f+f')^2 \, df' \\
&= 2NWR_f^2
\end{aligned}
$$

Since $\boldsymbol{S}_K \in \mathbb{R}^{N \times K}$ is orthonormal, $\|\boldsymbol{S}_K^* \boldsymbol{X} \boldsymbol{S}_K\|_F \leq \|\boldsymbol{X}\|_F$ for any Hermitian matrix $\boldsymbol{X} \in \mathbb{C}^{N \times N}$. Hence,

$$
\left\| \boldsymbol{S}_K^* \int_{-W}^{W} S(f+f') \boldsymbol{e}_{f'} \boldsymbol{e}_{f'}^{*} \, df' \boldsymbol{S}_K \right\|_F \leq \left\| \int_{-W}^{W} S(f+f') \boldsymbol{e}_{f'} \boldsymbol{e}_{f'}^{*} \, df' \right\|_F \leq R_f \sqrt{2NW}.
$$

Finally, by applying the two bounds we've derived, we obtain

$$
\begin{aligned}
&\left\|\boldsymbol{S}_K^*\boldsymbol{E}_f^*\boldsymbol{R}\boldsymbol{E}_f\boldsymbol{S}_K\right\|_F \\
&= \left\|\boldsymbol{S}_K^*\left(\int_{-W}^{W} S(f+f')\boldsymbol{e}_{f'}\boldsymbol{e}_{f'}^*\,df'\right)\boldsymbol{S}_K + \boldsymbol{S}_K^*\left(\int_{\Omega} S(f+f')\boldsymbol{e}_{f'}\boldsymbol{e}_{f'}^*\,df'\right)\boldsymbol{S}_K\right\|_F \\
&\leq \left\|\boldsymbol{S}_K^*\left(\int_{-W}^{W} S(f+f')\boldsymbol{e}_{f'}\boldsymbol{e}_{f'}^*\,df'\right)\boldsymbol{S}_K\right\|_F + \left\|\boldsymbol{S}_K^*\left(\int_{\Omega} S(f+f')\boldsymbol{e}_{f'}\boldsymbol{e}_{f'}^*\,df'\right)\boldsymbol{S}_K\right\|_F \\
&\leq R_f\sqrt{2NW} + M\sqrt{K}\Sigma_K^{(2)},
\end{aligned}
$$

and thus,

$$
\mathrm{Var}\left[\widehat{S}_K^{\mathrm{mt}}(f)\right] = \frac{1}{K^2}\left\|\boldsymbol{S}_K^*\boldsymbol{E}_f^*\boldsymbol{R}\boldsymbol{E}_f\boldsymbol{S}_K\right\|_F^2 \leq \frac{1}{K}\left(R_f\sqrt{\frac{2NW}{K}} + M\Sigma_K^{(2)}\right)^2.
$$

C.1.7 Proof of Theorem 9

Since $\widehat{S}_K^{\mathrm{mt}}(f) = \frac{1}{K}\left\|\boldsymbol{S}_K^*\boldsymbol{E}_f^*\boldsymbol{x}\right\|_2^2$ where $\boldsymbol{x} \sim \mathcal{CN}(\boldsymbol{0}, \boldsymbol{R})$, by Lemma 7, we have

$$
\begin{aligned}
\mathrm{Cov}\left[\widehat{S}_K^{\mathrm{mt}}(f_1), \widehat{S}_K^{\mathrm{mt}}(f_2)\right] &= \mathrm{Cov}\left[\frac{1}{K}\left\|\boldsymbol{S}_K^*\boldsymbol{E}_{f_1}^*\boldsymbol{x}\right\|_2^2, \frac{1}{K}\left\|\boldsymbol{S}_K^*\boldsymbol{E}_{f_2}^*\boldsymbol{x}\right\|_2^2\right] \\
&= \frac{1}{K^2}\left\|\boldsymbol{S}_K^*\boldsymbol{E}_{f_1}^*\boldsymbol{R}\boldsymbol{E}_{f_2}\boldsymbol{S}_K\right\|_F^2.
\end{aligned}
$$

It's trivial to conclude that $\mathrm{Cov}\left[\widehat{S}_K^{\mathrm{mt}}(f_1), \widehat{S}_K^{\mathrm{mt}}(f_2)\right] \geq 0$. We now focus on obtaining an upper bound on the Frobenius norm of $\boldsymbol{S}_K^*\boldsymbol{E}_{f_1}^*\boldsymbol{R}\boldsymbol{E}_{f_2}\boldsymbol{S}_K$. To do this, we first split it into three pieces - an integral over $[f_1 - W, f_1 + W]$, an integral over $[f_2 - W, f_2 + W]$, and an

integral over $\Omega' = [-\frac{1}{2}, \frac{1}{2}] \setminus ([f_1 - W, f_1 + W] \cup [f_2 - W, f_2 + W])$:

$$
\begin{aligned}
&\boldsymbol{S}_K^* \boldsymbol{E}_{f_1}^* \boldsymbol{R} \boldsymbol{E}_{f_2} \boldsymbol{S}_K \\
&= \boldsymbol{S}_K^* \boldsymbol{E}_{f_1}^* \left(\int_{-1/2}^{1/2} S(f) \boldsymbol{e}_f \boldsymbol{e}_f^* \, df \right) \boldsymbol{E}_{f_2} \boldsymbol{S}_K \\
&= \int_{-1/2}^{1/2} S(f) \boldsymbol{S}_K^* \boldsymbol{E}_{f_1}^* \boldsymbol{e}_f \boldsymbol{e}_f^* \boldsymbol{E}_{f_2} \boldsymbol{S}_K \, df \\
&= \int_{-1/2}^{1/2} S(f) \boldsymbol{S}_K^* \boldsymbol{e}_{f-f_1} \boldsymbol{e}_{f-f_2}^* \boldsymbol{S}_K \, df \\
&= \int_{f_1-W}^{f_1+W} S(f) \boldsymbol{S}_K^* \boldsymbol{e}_{f-f_1} \boldsymbol{e}_{f-f_2}^* \boldsymbol{S}_K \, df + \int_{f_2-W}^{f_2+W} S(f) \boldsymbol{S}_K^* \boldsymbol{e}_{f-f_1} \boldsymbol{e}_{f-f_2}^* \boldsymbol{S}_K \, df \\
&\quad + \int_{\Omega'} S(f) \boldsymbol{S}_K^* \boldsymbol{e}_{f-f_1} \boldsymbol{e}_{f-f_2}^* \boldsymbol{S}_K \, df.
\end{aligned}
$$

By using the triangle inequality, the identity $\|\boldsymbol{x}\boldsymbol{y}^*\|_F = \|\boldsymbol{x}\|_2 \|\boldsymbol{y}\|_2$ for vectors $\boldsymbol{x}, \boldsymbol{y}$, the Cauchy-Shwarz Inequality, and the facts that $\psi(f) \leq \frac{N}{K}$ and $\int_\Omega \psi(f) \, df = \Sigma_K^{(1)}$, we can bound the Frobenius norm of the first piece by

$$
\begin{aligned}
&\left\| \int_{f_1-W}^{f_1+W} S(f) \boldsymbol{S}_K^* \boldsymbol{e}_{f-f_1} \boldsymbol{e}_{f-f_2}^* \boldsymbol{S}_K \, df \right\|_F^2 \\
&\leq \left(\int_{f_1-W}^{f_1+W} \left\| S(f) \boldsymbol{S}_K^* \boldsymbol{e}_{f-f_1} \boldsymbol{e}_{f-f_2}^* \boldsymbol{S}_K \right\|_F \, df \right)^2 \\
&\leq \left(\int_{f_1-W}^{f_1+W} S(f) \left\| \boldsymbol{S}_K^* \boldsymbol{e}_{f-f_1} \right\|_2 \left\| \boldsymbol{S}_K^* \boldsymbol{e}_{f-f_2} \right\|_2 \, df \right)^2 \\
&\leq \left(\int_{f_1-W}^{f_1+W} S(f)^2 \left\| \boldsymbol{S}_K^* \boldsymbol{e}_{f-f_1} \right\|_2^2 \, df \right) \left(\int_{f_1-W}^{f_1+W} \left\| \boldsymbol{S}_K^* \boldsymbol{e}_{f-f_2} \right\|_2^2 \, df \right) \\
&= \left(\int_{-W}^{W} S(f+f_1)^2 \left\| \boldsymbol{S}_K^* \boldsymbol{e}_f \right\|_2^2 \, df \right) \left(\int_{f_1-f_2-W}^{f_1-f_2+W} \left\| \boldsymbol{S}_K^* \boldsymbol{e}_f \right\|_2^2 \, df \right) \\
&= \left(\int_{-W}^{W} S(f+f_1)^2 K \psi(f) \, df \right) \left(\int_{f_1-f_2-W}^{f_1-f_2+W} K \psi(f) \, df \right) \\
&\leq \left(\int_{-W}^{W} S(f+f_1)^2 \cdot N \, df \right) \left(\int_{\Omega} K \psi(f) \, df \right) \\
&= 2NW R_{f_1}^2 \cdot K \Sigma_K^{(1)} \\
&= R_{f_1}^2 \cdot 2NWK \Sigma_K^{(1)}
\end{aligned}
$$

In a nearly identical manner, we can bound the second piece by

$$\left\| \int_{f_2-W}^{f_2+W} S(f) \boldsymbol{S}_K^* \boldsymbol{e}_{f-f_1} \boldsymbol{e}_{f-f_2}^* \boldsymbol{S}_K \, df \right\|_F^2 \leq R_{f_2}^2 \cdot 2NWK\Sigma_K^{(1)}.$$

The third piece can also be bounded in a similar manner, but the details are noticeably different, so we show the derivation:

$$\begin{aligned}
\left\| \int_{\Omega'} S(f) \boldsymbol{S}_K^* \boldsymbol{e}_{f-f_1} \boldsymbol{e}_{f-f_2}^* \boldsymbol{S}_K \, df \right\|_F^2 &\leq \left(\int_{\Omega'} \left\| S(f) \boldsymbol{S}_K^* \boldsymbol{e}_{f-f_1} \boldsymbol{e}_{f-f_2}^* \boldsymbol{S}_K \right\|_F \, df \right)^2 \\
&\leq \left(\int_{\Omega'} S(f) \left\| \boldsymbol{S}_K^* \boldsymbol{e}_{f-f_1} \right\|_2 \left\| \boldsymbol{S}_K^* \boldsymbol{e}_{f-f_2} \right\|_2 \, df \right)^2 \\
&\leq \left(\int_{\Omega'} M \left\| \boldsymbol{S}_K^* \boldsymbol{e}_{f-f_1} \right\|_2 \left\| \boldsymbol{S}_K^* \boldsymbol{e}_{f-f_2} \right\|_2 \, df \right)^2 \\
&\leq M^2 \left(\int_{\Omega'} \left\| \boldsymbol{S}_K^* \boldsymbol{e}_{f-f_1} \right\|_2^2 \, df \right) \left(\int_{\Omega'} \left\| \boldsymbol{S}_K^* \boldsymbol{e}_{f-f_2} \right\|_2^2 \, df \right) \\
&= M^2 \left(\int_{\Omega'} K\psi(f-f_1) \, df \right) \left(\int_{\Omega'} K\psi(f-f_2) \, df \right) \\
&\leq M^2 \left(\int_{\Omega_1'} K\psi(f-f_1) \, df \right) \left(\int_{\Omega_2'} K\psi(f-f_2) \, df \right) \\
&= M^2 \left(\int_{\Omega} K\psi(f) \, df \right) \left(\int_{\Omega} K\psi(f) \, df \right) \\
&= M^2 \left(K\Sigma_K^{(1)} \right)^2
\end{aligned}$$

where $\Omega_1' = [-\frac{1}{2}, \frac{1}{2}] \setminus [f_1 - W, f_1 + W]$ and $\Omega_2' = [-\frac{1}{2}, \frac{1}{2}] \setminus [f_2 - W, f_2 + W]$.

Finally, by applying the three bounds we've derived, we obtain

$$\begin{aligned}
&\left\| \boldsymbol{S}_K^* \boldsymbol{E}_{f_1}^* \boldsymbol{R} \boldsymbol{E}_{f_2} \boldsymbol{S}_K \right\|_F \\
&\leq \left\| \int_{f_1-W}^{f_1+W} S(f) \boldsymbol{S}_K^* \boldsymbol{e}_{f-f_1} \boldsymbol{e}_{f-f_2}^* \boldsymbol{S}_K \, df \right\|_F + \left\| \int_{f_2-W}^{f_2+W} S(f) \boldsymbol{S}_K^* \boldsymbol{e}_{f-f_1} \boldsymbol{e}_{f-f_2}^* \boldsymbol{S}_K \, df \right\|_F \\
&\quad + \left\| \int_{\Omega'} S(f) \boldsymbol{S}_K^* \boldsymbol{e}_{f-f_1} \boldsymbol{e}_{f-f_2}^* \boldsymbol{S}_K \, df \right\|_F \\
&\leq R_{f_1} \sqrt{2NWK\Sigma_K^{(1)}} + R_{f_2} \sqrt{2NWK\Sigma_K^{(1)}} + MK\Sigma_K^{(1)},
\end{aligned}$$

and thus,

$$\begin{aligned}\operatorname{Cov}\left[\widehat{S}_K^{\text{mt}}(f_1), \widehat{S}_K^{\text{mt}}(f_2)\right] &= \frac{1}{K^2}\left\|\boldsymbol{S}_K^*\boldsymbol{E}_{f_1}^*\boldsymbol{R}\boldsymbol{E}_{f_2}\boldsymbol{S}_K\right\|_F^2 \\ &\leq \left((R_{f_1}+R_{f_2})\sqrt{\frac{2NW}{K}\Sigma_K^{(1)}} + M\Sigma_K^{(1)}\right)^2.\end{aligned}$$

C.1.8 Proof of Theorem 10

Since $\widehat{S}_K^{\text{mt}}(f) = \frac{1}{K}\left\|\boldsymbol{S}_K^*\boldsymbol{E}_f^*\boldsymbol{x}\right\|_2^2$ where $\boldsymbol{x} \sim \mathcal{CN}(\boldsymbol{0}, \boldsymbol{R})$, by Lemma 9, we have

$$\mathbb{P}\left\{\widehat{S}_K^{\text{mt}}(f) \geq \beta\mathbb{E}\widehat{S}_K^{\text{mt}}(f)\right\} \leq \beta^{-1}\mathrm{e}^{-\kappa_f(\beta-1-\ln\beta)} \quad \text{for} \quad \beta > 1,$$

and

$$\mathbb{P}\left\{\widehat{S}_K^{\text{mt}}(f) \leq \beta\mathbb{E}\widehat{S}_K^{\text{mt}}(f)\right\} \leq \mathrm{e}^{-\kappa_f(\beta-1-\ln\beta)} \quad \text{for} \quad 0 < \beta < 1,$$

where

$$\kappa_f = \frac{\operatorname{tr}\left[\boldsymbol{S}_K^*\boldsymbol{E}_f^*\boldsymbol{R}\boldsymbol{E}_f\boldsymbol{S}_K\right]}{\left\|\boldsymbol{S}_K^*\boldsymbol{E}_f^*\boldsymbol{R}\boldsymbol{E}_f\boldsymbol{S}_K\right\|}.$$

We can get an upper bound on $\boldsymbol{S}_K^*\boldsymbol{E}_f^*\boldsymbol{R}\boldsymbol{E}_f\boldsymbol{S}_K$ in the Loewner ordering by splitting it into two pieces as done in the proof of Theorem 8, and then bounding each piece:

$$\begin{aligned}&\boldsymbol{S}_K^*\boldsymbol{E}_f^*\boldsymbol{R}\boldsymbol{E}_f\boldsymbol{S}_K \\ &= \boldsymbol{S}_K^*\left(\int_{-W}^{W} S(f+f')\boldsymbol{e}_{f'}\boldsymbol{e}_{f'}^*\,df'\right)\boldsymbol{S}_K + \boldsymbol{S}_K^*\left(\int_{\Omega} S(f+f')\boldsymbol{e}_{f'}\boldsymbol{e}_{f'}^*\,df'\right)\boldsymbol{S}_K \\ &\preceq \boldsymbol{S}_K^*\left(\int_{-W}^{W} M_f\boldsymbol{e}_{f'}\boldsymbol{e}_{f'}^*\,df'\right)\boldsymbol{S}_K + \boldsymbol{S}_K^*\left(\int_{\Omega} M\boldsymbol{e}_{f'}\boldsymbol{e}_{f'}^*\,df'\right)\boldsymbol{S}_K \\ &= \boldsymbol{S}_K^*\left(M_f\boldsymbol{B}\right)\boldsymbol{S}_K + \boldsymbol{S}_K^*\left(M(\mathbf{I}-\boldsymbol{B})\right)\boldsymbol{S}_K \\ &= M_f\boldsymbol{\Lambda}_K + M(\mathbf{I}-\boldsymbol{\Lambda}_K) \\ &= M_f\mathbf{I} + (M-M_f)(\mathbf{I}-\boldsymbol{\Lambda}_K).\end{aligned}$$

Then, by using the fact that $\boldsymbol{P} \preceq \boldsymbol{Q} \implies \|\boldsymbol{P}\| \leq \|\boldsymbol{Q}\|$ for PSD matrices $\boldsymbol{P}$ and $\boldsymbol{Q}$, we

can bound,

$$\left\|\boldsymbol{S}_K^*\boldsymbol{E}_f^*\boldsymbol{R}\boldsymbol{E}_f\boldsymbol{S}_K\right\| \leq \|M_f\mathbf{I} + (M - M_f)(\mathbf{I} - \boldsymbol{\Lambda}_K)\| = M_f + (M - M_f)(1 - \lambda_{K-1}).$$

We can also get a lower bound on $\mathrm{tr}[\boldsymbol{S}_K^*\boldsymbol{E}_f^*\boldsymbol{R}\boldsymbol{E}_f\boldsymbol{S}_K] = K\mathbb{E}\left[\widehat{S}_K^{\mathrm{mt}}(f)\right]$ by using the formula for $E\left[\widehat{S}_K^{\mathrm{mt}}(f)\right]$ from Lemma 11 along with the properties of the spectral window derived in Lemma 12 as follows:

$$\begin{aligned}
\mathrm{tr}[\boldsymbol{S}_K^*\boldsymbol{E}_f^*\boldsymbol{R}\boldsymbol{E}_f\boldsymbol{S}_K] &= K\mathbb{E}\left[\widehat{S}_K^{\mathrm{mt}}(f)\right] \\
&= K\int_{-1/2}^{1/2} S(f - f')\psi(f')\,df' \\
&\geq K\int_{-W}^{W} S(f - f')\psi(f')\,df' \\
&= K\int_{-W}^{W} S(f - f')\left[\frac{N}{K} - \left(\frac{N}{K} - \psi(f')\right)\right]\,df' \\
&= K\int_{-W}^{W} S(f - f')\frac{N}{K}\,df' - K\int_{-W}^{W} S(f - f')\left(\frac{N}{K} - \psi(f')\right)\,df' \\
&= N\int_{f-W}^{f+W} S(f')\,df' - \int_{-W}^{W} S(f - f')(N - K\psi(f'))\,df' \\
&\geq N\int_{f-W}^{f+W} S(f')\,df' - \int_{-W}^{W} M_f(N - K\psi(f'))\,df' \\
&= 2NWA_f - \left(2NW - K\left(1 - \Sigma_K^{(1)}\right)\right)M_f \\
&= K\left(1 - \Sigma_K^{(1)}\right)M_f - 2NW(M_f - A_f)
\end{aligned}$$

Combining the upper bound on $\left\|\boldsymbol{S}_K^*\boldsymbol{E}_f^*\boldsymbol{R}\boldsymbol{E}_f\boldsymbol{S}_K\right\|$ with the lower bound on $\mathrm{tr}[\boldsymbol{S}_K^*\boldsymbol{E}_f^*\boldsymbol{R}\boldsymbol{E}_f\boldsymbol{S}_K]$, yields

$$\kappa_f = \frac{\mathrm{tr}\left[\boldsymbol{S}_K^*\boldsymbol{E}_f^*\boldsymbol{R}\boldsymbol{E}_f\boldsymbol{S}_K\right]}{\left\|\boldsymbol{S}_K^*\boldsymbol{E}_f^*\boldsymbol{R}\boldsymbol{E}_f\boldsymbol{S}_K\right\|} \geq \frac{K\left(1 - \Sigma_K^{(1)}\right)M_f - 2NW(M_f - A_f)}{M_f + (M - M_f)\,(1 - \lambda_{K-1})}.$$

C.2 Proof of Results in Section 5.2

C.2.1 Fast algorithm for computing $\Psi(f)$ at grid frequencies

To begin developing our fast approximations for $\widehat{S}_K^{\text{mt}}(f)$, we first show that an eigenvalue weighted sum of N tapered spectral estimates can be evaluated at a grid of frequencies $f \in [L]/L$ where $L \geq 2N$ in $O(L \log L)$ operations and using $O(L)$ memory.

Lemma 13. *For any vector $\boldsymbol{x} \in \mathbb{C}^N$ and any integer $L \geq 2N$, the quantity*

$$\Psi(f) := \sum_{k=0}^{N-1} \lambda_k \widehat{S}_k(f) \quad \textit{where} \quad \widehat{S}_k(f) = \left| \sum_{n=0}^{N-1} \boldsymbol{s}_k[n] \boldsymbol{x}[n] e^{-j2\pi f n} \right|^2$$

can be evaluated at the grid frequencies $f \in [L]/L$ in $O(L \log L)$ operations and using $O(L)$ memory.

Proof. Using eigendecomposition, we can write $\boldsymbol{B} = \boldsymbol{S}\boldsymbol{\Lambda}\boldsymbol{S}^*$, where

$$\boldsymbol{S} = \begin{bmatrix} \boldsymbol{s}_0 & \boldsymbol{s}_1 & \cdots & \boldsymbol{s}_{N-1} \end{bmatrix}$$

and

$$\boldsymbol{\Lambda} = \operatorname{diag}(\lambda_0, \lambda_1, \ldots, \lambda_{N-1}).$$

For any $f \in \mathbb{R}$, we let $\boldsymbol{E}_f \in \mathbb{C}^{N \times N}$ be a diagonal matrix with diagonal entries

$$\boldsymbol{E}_f[n, n] = e^{j2\pi f n} \quad \text{for} \quad n \in [N].$$

With this definition, $\Psi(f)$ can be written as

$$\begin{aligned}
\Psi(f) &= \sum_{k=0}^{N-1} \lambda_k \widehat{S}_k(f) \\
&= \sum_{k=0}^{N-1} \lambda_k \left| \sum_{n=0}^{N-1} \boldsymbol{s}_k[n] \boldsymbol{x}[n] e^{-j2\pi f n} \right|^2 \\
&= \sum_{k=0}^{N-1} \lambda_k \left| \boldsymbol{s}_k^* \boldsymbol{E}_f^* \boldsymbol{x} \right|^2 \\
&= \sum_{k=0}^{N-1} \boldsymbol{\Lambda}[k,k] \left| (\boldsymbol{S}^* \boldsymbol{E}_f^* \boldsymbol{x})[k] \right|^2 \\
&= \boldsymbol{x}^* \boldsymbol{E}_f \boldsymbol{S} \boldsymbol{\Lambda} \boldsymbol{S}^* \boldsymbol{E}_f^* \boldsymbol{x} \\
&= \boldsymbol{x}^* \boldsymbol{E}_f \boldsymbol{B} \boldsymbol{E}_f^* \boldsymbol{x}
\end{aligned}$$

This gives us a a formula for $\Psi(f) = \sum_{k=0}^{N-1} \lambda_k \widehat{S}_k(f)$ which does not require computing any of the Slepian tapers. We will now use the fact that $\boldsymbol{B}$ is a Toeplitz matrix to efficiently compute $\Psi(\frac{\ell}{L})$ for all $\ell \in [L]/L$.

First, note that we can "extend" $\boldsymbol{B}$ to a larger circulant matrix, which is diagonalized by a Fourier Transform matrix. Specifically, define a vector of sinc samples $\boldsymbol{b} \in \mathbb{R}^L$ by

$$\boldsymbol{b}[\ell] = \begin{cases} \dfrac{\sin[2\pi W \ell]}{\pi \ell} & \text{if } \ell \in \{0, \ldots, N-1\} \\ 0 & \text{if } \ell \in \{N, \ldots, L-N\} \\ \dfrac{\sin[2\pi W (L-\ell)]}{\pi (L-\ell)} & \text{if } \ell \in \{L-N+1, \ldots, L-1\} \end{cases},$$

and let $\boldsymbol{B}_{\text{ext}} \in \mathbb{R}^{L \times L}$ be defined by

$$\boldsymbol{B}_{\text{ext}}[m,n] = \boldsymbol{b}[m-n \pmod L] \text{ for } m,n \in [L].$$

It is easy to check that $\boldsymbol{B}_{\text{ext}}[m,n] = \boldsymbol{B}[m,n]$ for all $m,n \in [N]$, i.e., the upper-left $N \times N$ submatrix of $\boldsymbol{B}_{\text{ext}}$ is $\boldsymbol{B}$. Hence, we can write

$$\boldsymbol{B} = \boldsymbol{Z}^* \boldsymbol{B}_{\text{ext}} \boldsymbol{Z},$$

where

$$\boldsymbol{Z} = \begin{bmatrix} \mathbf{I}_{N\times N} \\ \mathbf{0}_{(L-N)\times N} \end{bmatrix} \in \mathbb{R}^{L\times N}$$

is a zeropadding matrix. Since $\boldsymbol{B}_{\text{ext}}$ is a circulant matrix whose first column is $\boldsymbol{b}$, we can write

$$\boldsymbol{B}_{\text{ext}} = \boldsymbol{F}^{-1} \operatorname{diag}(\boldsymbol{F}\boldsymbol{b}) \boldsymbol{F}$$

where $\boldsymbol{F} \in \mathbb{C}^{L\times L}$ is an FFT matrix, i.e.,

$$\boldsymbol{F}[m,n] = e^{-j2\pi mn/L} \text{ for } m,n \in [L].$$

Note that with this normalization, the inverse FFT satisfies

$$\boldsymbol{F}^{-1} = \frac{1}{L}\boldsymbol{F}^*,$$

as well as the conjugation identity

$$\boldsymbol{F}^{-1}\boldsymbol{y} = \frac{1}{L}\overline{\boldsymbol{F}\overline{\boldsymbol{y}}} \quad \text{for all} \quad \boldsymbol{y} \in \mathbb{C}^N.$$

Next, for any $f \in \mathbb{R}$, let $\boldsymbol{D}_f \in \mathbb{C}^{L\times L}$ be a diagonal matrix with diagonal entries

$$\boldsymbol{D}_f[m,m] = e^{j2\pi fm} \quad \text{for} \quad m \in [L],$$

and for each $\ell \in [L]$, let $\boldsymbol{C}_\ell \in \mathbb{C}^{L \times L}$ be a cyclic shift matrix, i.e.,

$$\boldsymbol{C}_\ell[m,n] = \begin{cases} 1 & \text{if } n - m \equiv \ell \pmod{L} \\ 0 & \text{otherwise} \end{cases}.$$

Since $\boldsymbol{E}_f$ and $\boldsymbol{D}_f$ are both diagonal matrices and $\boldsymbol{E}_f[n,n] = \boldsymbol{D}_f[n,n]$ for $n \in [N]$, we have

$$\boldsymbol{Z}\boldsymbol{E}_f^* = \boldsymbol{D}_f^*\boldsymbol{Z} \quad \text{and} \quad \boldsymbol{E}_f\boldsymbol{Z}^* = \boldsymbol{Z}^*\boldsymbol{D}_f$$

for all $f \in \mathbb{R}$. Also, it is easy to check that cyclically shifting each column of $\boldsymbol{F}$ by ℓ indices is equivalent to modulating the rows of $\boldsymbol{F}$, or more specifically

$$\boldsymbol{F}\boldsymbol{D}_{\ell/L}^* = \boldsymbol{C}_\ell\boldsymbol{F} \quad \text{and} \quad \boldsymbol{D}_{\ell/L}\boldsymbol{F}^* = \boldsymbol{F}^*\boldsymbol{C}_\ell^*$$

for all $\ell \in [L]$. Additionally, for any vectors $\boldsymbol{p}, \boldsymbol{q} \in \mathbb{C}^L$, we will denote $\boldsymbol{p} \circ \boldsymbol{q} \in \mathbb{C}^L$ to be the pointwise multiplication of $\boldsymbol{p}$ and $\boldsymbol{q}$, i.e.,

$$(\boldsymbol{p} \circ \boldsymbol{q})[\ell] = \boldsymbol{p}[\ell]\boldsymbol{q}[\ell] \quad \text{for} \quad \ell \in [L],$$

and $\boldsymbol{p} \circledast \boldsymbol{q} \in \mathbb{C}^L$ to be the circluar cross-correlation of $\boldsymbol{p}$ and $\boldsymbol{q}$, i.e.,

$$(\boldsymbol{p} \circledast \boldsymbol{q})[\ell] = \sum_{\ell'=0}^{L-1} \overline{\boldsymbol{p}[\ell']}\boldsymbol{q}[\ell' + \ell \pmod{L}] \quad \text{for} \quad \ell \in [L].$$

Note that the circular cross-correlation of $\boldsymbol{p}$ and $\boldsymbol{q}$ can be computed using FFTs via the formula

$$\boldsymbol{p} \circledast \boldsymbol{q} = \boldsymbol{F}^{-1}(\overline{\boldsymbol{F}\boldsymbol{p}} \circ \boldsymbol{F}\boldsymbol{q}).$$

We will also use the notation $|\boldsymbol{p}|^2 = \overline{\boldsymbol{p}} \circ \boldsymbol{p}$ for convenience.

We can now manipulate our formula for $\Psi(\frac{\ell}{L})$ as follows

$$\begin{aligned}
\Psi(\tfrac{\ell}{L}) &:= \boldsymbol{x}^* \boldsymbol{E}_{\ell/L} \boldsymbol{B} \boldsymbol{E}_{\ell/L}^* \boldsymbol{x} \\
&= \boldsymbol{x}^* \boldsymbol{E}_{\ell/L} \boldsymbol{Z}^* \boldsymbol{B}_{\text{ext}} \boldsymbol{Z} \boldsymbol{E}_{\ell/L}^* \boldsymbol{x} \\
&= \boldsymbol{x}^* \boldsymbol{E}_{\ell/L} \boldsymbol{Z}^* \boldsymbol{F}^{-1} \operatorname{diag}(\boldsymbol{F}\boldsymbol{b}) \boldsymbol{F} \boldsymbol{Z} \boldsymbol{E}_{\ell/L}^* \boldsymbol{x} \\
&= \frac{1}{L} \boldsymbol{x}^* \boldsymbol{E}_{\ell/L} \boldsymbol{Z}^* \boldsymbol{F}^* \operatorname{diag}(\boldsymbol{F}\boldsymbol{b}) \boldsymbol{F} \boldsymbol{Z} \boldsymbol{E}_{\ell/L}^* \boldsymbol{x} \\
&= \frac{1}{L} \boldsymbol{x}^* \boldsymbol{Z}^* \boldsymbol{D}_{\ell/L} \boldsymbol{F}^* \operatorname{diag}(\boldsymbol{F}\boldsymbol{b}) \boldsymbol{F} \boldsymbol{D}_{\ell/L}^* \boldsymbol{Z} \boldsymbol{x} \\
&= \frac{1}{L} \boldsymbol{x}^* \boldsymbol{Z}^* \boldsymbol{F}^* \boldsymbol{C}_\ell^* \operatorname{diag}(\boldsymbol{F}\boldsymbol{b}) \boldsymbol{C}_\ell \boldsymbol{F} \boldsymbol{Z} \boldsymbol{x} \\
&= \frac{1}{L} \sum_{\ell'=0}^{L-1} (\boldsymbol{F}\boldsymbol{b})[\ell'] \cdot \left| (\boldsymbol{C}_\ell \boldsymbol{F} \boldsymbol{Z} \boldsymbol{x})\,[\ell'] \right|^2 \\
&= \frac{1}{L} \sum_{\ell'=0}^{L-1} (\boldsymbol{F}\boldsymbol{b})[\ell'] \cdot \left| (\boldsymbol{F} \boldsymbol{Z} \boldsymbol{x})\,[\ell' + \ell \pmod L] \right|^2 \\
&= \left(\frac{1}{L} \overline{\boldsymbol{F}\boldsymbol{b}} \circledast \left| \boldsymbol{F} \boldsymbol{Z} \boldsymbol{x} \right|^2 \right)[\ell]. \\
&= \left(\boldsymbol{F}^{-1} \left(\frac{1}{L} \overline{\overline{\boldsymbol{F}} \overline{\boldsymbol{F}\boldsymbol{b}}} \circ \boldsymbol{F} \left| \boldsymbol{F} \boldsymbol{Z} \boldsymbol{x} \right|^2 \right) \right)[\ell] \\
&= \left(\boldsymbol{F}^{-1} \left(\boldsymbol{F}^{-1} \boldsymbol{F}\boldsymbol{b} \circ \boldsymbol{F} \left| \boldsymbol{F} \boldsymbol{Z} \boldsymbol{x} \right|^2 \right) \right)[\ell] \\
&= \left(\boldsymbol{F}^{-1} \left(\boldsymbol{b} \circ \boldsymbol{F} \left| \boldsymbol{F} \boldsymbol{Z} \boldsymbol{x} \right|^2 \right) \right)[\ell].
\end{aligned}$$

Therefore,

$$\begin{bmatrix} \Psi(\frac{0}{L}) & \Psi(\frac{1}{L}) & \cdots & \Psi(\frac{L-2}{L}) & \Psi(\frac{L-1}{L}) \end{bmatrix}^T = \boldsymbol{F}^{-1} \left(\boldsymbol{b} \circ \boldsymbol{F} \left| \boldsymbol{F} \boldsymbol{Z} \boldsymbol{x} \right|^2 \right).$$

So to compute $\Psi(f)$ at all grid frequencies $f \in [L]/L$, we only need to compute $\boldsymbol{F}^{-1} \left(\boldsymbol{b} \circ \boldsymbol{F} \left| \boldsymbol{F} \boldsymbol{Z} \boldsymbol{x} \right|^2 \right)$, which can be done in $O(L \log L)$ operations using $O(L)$ memory via three length-L FFTs/IFFTs and a few pointwise operations on vectors of length L. $\square$

C.2.2 Approximations for general multitaper spectral estimates

Next, we present a lemma regarding approximations to spectral estimates which use orthonormal tapers.

Lemma 14. *Let $\boldsymbol{x} \in \mathbb{C}^N$ be a vector of N equispaced samples, and let $\{\boldsymbol{v}_k\}_{k=0}^{N-1}$ be any orthonormal set of tapers in $\mathbb{C}^N$. For each $k \in [N]$, define a tapered spectral estimate*

$$V_k(f) = \left| \sum_{n=0}^{N-1} \boldsymbol{v}_k[n] \boldsymbol{x}[n] e^{-j2\pi f n} \right|^2.$$

Also, let $\{\gamma_k\}_{k=0}^{N-1}$ and $\{\widetilde{\gamma}_k\}_{k=0}^{N-1}$ be real coefficients, and then define a multitaper spectral estimate $\widehat{V}(f)$ and an approximation $\widetilde{V}(f)$ by

$$\widehat{V}(f) = \sum_{k=0}^{N-1} \gamma_k V_k(f) \quad \textit{and} \quad \widetilde{V}(f) = \sum_{k=0}^{N-1} \widetilde{\gamma}_k V_k(f).$$

Then, for any frequency $f \in \mathbb{R}$, we have

$$\left| \widehat{V}(f) - \widetilde{V}(f) \right| \leq \left(\max_k |\gamma_k - \widetilde{\gamma}_k| \right) \|x\|_2^2.$$

Proof. Let $\boldsymbol{V} = \begin{bmatrix} \boldsymbol{v}_0 & \cdots & \boldsymbol{v}_{N-1} \end{bmatrix}$, and let $\boldsymbol{\Gamma}$, $\widetilde{\boldsymbol{\Gamma}} \in \mathbb{R}^{N \times N}$, and $\boldsymbol{E}_f \in \mathbb{C}^{N \times N}$ be diagonal matrices whose diagonal entries are $\boldsymbol{\Gamma}[n,n] = \gamma_n$, $\widetilde{\boldsymbol{\Gamma}}[n,n] = \widetilde{\gamma}_n$, and $\boldsymbol{E}_f[n,n] = e^{j2\pi f n}$ for

$n \in [N]$. Then,

$$\begin{aligned}
\widehat{V}(f) &= \sum_{k=0}^{N-1} \gamma_k V_k(f) \\
&= \sum_{k=0}^{N-1} \gamma_k \left| \sum_{n=0}^{N-1} \boldsymbol{v}_k[n] \boldsymbol{x}[n] e^{-j2\pi f n} \right|^2 \\
&= \sum_{k=0}^{N-1} \gamma_k \left| \boldsymbol{v}_k^* \boldsymbol{E}_f^* \boldsymbol{x} \right|^2 \\
&= \sum_{k=0}^{N-1} \boldsymbol{\Gamma}[k,k] \left| (\boldsymbol{V}^* \boldsymbol{E}_f^* \boldsymbol{x})[k] \right|^2 \\
&= \boldsymbol{x}^* \boldsymbol{E}_f \boldsymbol{V} \boldsymbol{\Gamma} \boldsymbol{V}^* \boldsymbol{E}_f^* \boldsymbol{x}.
\end{aligned}$$

In a nearly identical manner,

$$\widetilde{V}(f) = \boldsymbol{x}^* \boldsymbol{E}_f \boldsymbol{V} \widetilde{\boldsymbol{\Gamma}} \boldsymbol{V}^* \boldsymbol{E}_f^* \boldsymbol{x}.$$

Since $\boldsymbol{V}$ is orthonormal, $\|\boldsymbol{V}\| = \|\boldsymbol{V}^*\| = 1$. Since $\boldsymbol{E}_f$ is diagonal, and all the diagonal entries have modulus 1, $\|\boldsymbol{E}_f\| = \|\boldsymbol{E}_f^*\| = 1$. Hence, for any $f \in \mathbb{R}$, we can bound

$$\begin{aligned}
\left| \widehat{V}(f) - \widetilde{V}(f) \right| &= \left| \boldsymbol{x}^* \boldsymbol{E}_f \boldsymbol{V} \left(\boldsymbol{\Gamma} - \widetilde{\boldsymbol{\Gamma}} \right) \boldsymbol{V}^* \boldsymbol{E}_f^* \boldsymbol{x} \right| \\
&\leq \|\boldsymbol{x}\|_2 \|\boldsymbol{E}_f\| \|\boldsymbol{V}\| \|\boldsymbol{\Gamma} - \widetilde{\boldsymbol{\Gamma}}\| \|\boldsymbol{V}^*\| \|\boldsymbol{E}_f^*\| \|\boldsymbol{x}\|_2 \\
&= \|\boldsymbol{\Gamma} - \widetilde{\boldsymbol{\Gamma}}\| \|\boldsymbol{x}\|_2^2 \\
&= \left(\max_k |\gamma_k - \widetilde{\gamma}_k| \right) \|x\|_2^2,
\end{aligned}$$

as desired. □

C.2.3 Proof of Theorem 11

Recall that the indices $[N]$ are partitioned as follows:

$$\begin{aligned}
\mathcal{I}_1 &= \{k \in [K] : \lambda_k \geq 1 - \epsilon\} \\
\mathcal{I}_2 &= \{k \in [K] : \epsilon < \lambda_k < 1 - \epsilon\} \\
\mathcal{I}_3 &= \{k \in [N] \setminus [K] : \epsilon < \lambda_k < 1 - \epsilon\} \\
\mathcal{I}_4 &= \{k \in [N] \setminus [K] : \lambda_k \leq \epsilon\}.
\end{aligned}$$

Using the partitioning above, the unweighted multitaper spectral estimate $\widehat{S}_K^{\text{mt}}(f)$ can be written as

$$\begin{aligned}
\widehat{S}_K^{\text{mt}}(f) &= \frac{1}{K} \sum_{k=0}^{K-1} \widehat{S}_k(f) \\
&= \sum_{k \in \mathcal{I}_1 \cup \mathcal{I}_2} \frac{1}{K} \widehat{S}_k(f),
\end{aligned}$$

and the approximate estimator $\widetilde{S}_K^{\text{mt}}(f)$ can be written as

$$\begin{aligned}
\widetilde{S}_K^{\text{mt}}(f) &= \frac{1}{K}\Psi(f) + \frac{1}{K} \sum_{k \in \mathcal{I}_2} (1 - \lambda_k) \widehat{S}_k(f) - \frac{1}{K} \sum_{k \in \mathcal{I}_3} \lambda_k \widehat{S}_k(f) \\
&= \sum_{k=0}^{N-1} \frac{\lambda_k}{K} \widehat{S}_k(f) + \sum_{k \in \mathcal{I}_2} \frac{1 - \lambda_k}{K} \widehat{S}_k(f) - \sum_{k \in \mathcal{I}_3} \frac{\lambda_k}{K} \widehat{S}_k(f) \\
&= \sum_{k \in \mathcal{I}_1 \cup \mathcal{I}_4} \frac{\lambda_k}{K} \widehat{S}_k(f) + \sum_{k \in \mathcal{I}_2} \frac{1}{K} \widehat{S}_k(f)
\end{aligned}$$

Thus, $\widehat{S}_K^{\text{mt}}(f)$ and $\widetilde{S}_K^{\text{mt}}(f)$ can be written as

$$\widehat{S}_K^{\text{mt}}(f) = \sum_{k=0}^{N-1} \gamma_k \widehat{S}_k(f) \quad \text{and} \quad \widetilde{S}_K^{\text{mt}}(f) = \sum_{k=0}^{N-1} \widetilde{\gamma}_k \widehat{S}_k(f)$$

where

$$\gamma_k = \begin{cases} 1/K & k \in \mathcal{I}_1 \cup \mathcal{I}_2, \\ 0 & k \in \mathcal{I}_3 \cup \mathcal{I}_4, \end{cases} \quad \text{and} \quad \widetilde{\gamma}_k = \begin{cases} \lambda_k/K & k \in \mathcal{I}_1 \cup \mathcal{I}_4, \\ 1/K & k \in \mathcal{I}_2, \\ 0 & k \in \mathcal{I}_3. \end{cases}$$

We now bound $|\gamma_k - \widetilde{\gamma}_k|$ for all $k \in [N]$. For $k \in \mathcal{I}_1$, we have $\lambda_k \geq 1 - \epsilon$, and thus,

$$|\gamma_k - \widetilde{\gamma}_k| = \left| \frac{1}{K} - \frac{\lambda_k}{K} \right| = \frac{1 - \lambda_k}{K} \leq \frac{\epsilon}{K}.$$

For $k \in \mathcal{I}_2 \cup \mathcal{I}_3$ we have $\gamma_k = \widetilde{\gamma}_k$, i.e., $|\gamma_k - \widetilde{\gamma}_k| = 0$. For $k \in \mathcal{I}_4$, we have $\lambda_k \leq \epsilon$, and thus,

$$|\gamma_k - \widetilde{\gamma}_k| = \left| 0 - \frac{\lambda_k}{K} \right| = \frac{\lambda_k}{K} \leq \frac{\epsilon}{K}.$$

Hence, $|\gamma_k - \widetilde{\gamma}_k| \leq \frac{\epsilon}{K}$ for all $k \in [N]$, and thus by Lemma 14,

$$\left| \widehat{S}^{\text{mt}}_K(f) - \widetilde{S}^{\text{mt}}_K(f) \right| \leq \frac{\epsilon}{K} \|\boldsymbol{x}\|_2^2$$

for all frequencies $f \in \mathbb{R}$.

C.2.4 Proof of Theorem 12

To evaluate the approximate multitaper estimate

$$\widetilde{S}^{\text{mt}}_K(f) = \frac{1}{K}\Psi(f) + \frac{1}{K}\sum_{k \in \mathcal{I}_2} (1 - \lambda_k)\widehat{S}_k(f) - \frac{1}{K}\sum_{k \in \mathcal{I}_3} \lambda_k \widehat{S}_k(f)$$

at the L grid frequencies $f \in [L]/L$ one needs to:

- For each $k \in \mathcal{I}_2 \cup \mathcal{I}_3$, precompute the Slepian basis vectors $\boldsymbol{s}_k$ and eigenvalues λ_k.

  Computing the Slepian basis vector $\boldsymbol{s}_k$ and the corresponding eigenvalue λ_k for a single index k can be done in $O(N \log N)$ operations and $O(N)$ memory via the method described in [94]. This needs to be done for $\#(\mathcal{I}_2 \cup \mathcal{I}_3) = \#\{k : \epsilon <$

$\lambda_k < 1 - \epsilon\} = O(\log(NW) \log \frac{1}{\epsilon})$ values of k, so the total cost of this step is $O(N \log(N) \log(NW) \log \frac{1}{\epsilon})$ operations and $O(N \log(NW) \log \frac{1}{\epsilon})$ memory.

- For $\ell \in [L]$, evaluate $\Psi(\frac{\ell}{L})$.

  If $L \geq 2N$, then evaluating $\Psi(\frac{\ell}{L})$ for $\ell \in [L]$ can be done in $O(L \log L)$ operations and $O(L)$ memory as shown in Lemma 13. If $N \leq L < 2N$, then $2L \geq 2N$, so by Lemma 13, we can evaluate $\Psi(\frac{\ell}{2L})$ for $\ell \in [2L]$ in $O(2L \log 2L) = O(L \log L)$ operations and $O(2L) = O(L)$ memory and then simply downsample the result to obtain $\Psi(\frac{\ell}{L})$ for $\ell \in [L]$.

- For each $k \in \mathcal{I}_2 \cup \mathcal{I}_3$ and each $\ell \in [L]$, evaluate $\widehat{S}_k(\frac{\ell}{L})$.

  Evaluating $\widehat{S}_k(\frac{\ell}{L}) = \left|\sum_{n=0}^{N-1} \boldsymbol{s}_k[n] \boldsymbol{x}[n] e^{-j2\pi n\ell/L}\right|^2$ for all $\ell \in [L]$ can be done by pointwise multiplying $\boldsymbol{s}_k$ and $\boldsymbol{x}$, zeropadding this vector to length L, computing a length-L FFT, and then computing the squared magnitude of each FFT coefficient. This takes $O(L \log L)$ operations and $O(L)$ memory. This needs to be done for $\#(\mathcal{I}_2 \cup \mathcal{I}_3) = O(\log(NW) \log \frac{1}{\epsilon})$ values of k, so the total cost of this step is $O(L \log L \log(NW) \log \frac{1}{\epsilon})$ operations and $O(L \log(NW) \log \frac{1}{\epsilon})$ memory.

- For each $\ell \in [L]$, evaluate the weighted sum above for $\widetilde{S}_K^{\text{mt}}(\frac{\ell}{L})$.

  Once $\Psi(\frac{\ell}{L})$ and $\widehat{S}_k(\frac{\ell}{L})$ for $k \in \mathcal{I}_2 \cup \mathcal{I}_3$ are computed, evaluating $\widetilde{S}_K^{\text{mt}}(\frac{\ell}{L})$ requires $O(\#(\mathcal{I}_2 \cup \mathcal{I}_3)) = O(\log(NW) \log \frac{1}{\epsilon})$ multiplications and additions. This has to be done for each $\ell \in [L]$, so the total cost is $O(L \log(NW) \log \frac{1}{\epsilon})$ operations.

So, the total cost of evaluating the approximate multitaper estimate $\widetilde{S}_K^{\text{mt}}(f)$ at the L grid frequencies $f \in [L]/L$ is $O(L \log L \log(NW) \log \frac{1}{\epsilon})$ operations and $O(L \log(NW) \log \frac{1}{\epsilon})$ memory, where we have used the assumption $L \geq N$.

APPENDIX D

PROOFS FOR CHAPTER 6

D.1 Proof of Lemma 1

Note that $\lambda_k(\boldsymbol{G} + \delta\mathbf{I}) = \lambda_k(\boldsymbol{G}) + \delta = \lambda_k(\mathcal{A}\mathcal{A}^*) + \delta = \lambda_k(\mathcal{A}^*\mathcal{A}) + \delta$. So we can bound the eigenvalues of $\boldsymbol{G} + \delta\mathbf{I}$ by bounding the eigenvalues of

$$\mathcal{A}^*\mathcal{A} = \sum_{n=0}^{N-1} a_{t_n} a_{t_n}^*,$$

which is a sum of independent, self-adjoint, positive semidefinite, rank-1 operators. As such, it will be helpful to note two matrix concentration results from [113]. Furthermore, we will show that $\mathbb{E}[\mathcal{A}^*\mathcal{A}] = \frac{N}{T}\mathcal{B}_\Omega^{\mathrm{c}}\mathcal{T}_T^{\mathrm{c}}\mathcal{B}_\Omega^{\mathrm{c}}$ where $\mathcal{B}_\Omega^{\mathrm{c}}$ is an operator which bandlimits a signal to the frequency bands in Ω, and $\mathcal{T}_T^{\mathrm{c}}$ is an operator which timelimits a signal to $[-\frac{T}{2}, \frac{T}{2}]$. As such, the eigenvalues of $\mathbb{E}[\mathcal{A}^*\mathcal{A}]$ have a very similar behavior to the prolate spheroidal wave functions (PSWFs). Specifically, $\approx |\Omega|T$ eigenvalues will be on the order of $\frac{N}{T}$, and the rest will exponentially decay towards 0, with only the first $|\Omega|T + O(\log(|\Omega|T))$ eigenvalues being significant.

We will split this proof up into a few subsections. First, we will state the necessary matrix concentration results from [113]. Next, we will

D.1.1 Matrix concentration results

The first result gives tail bounds for the minimum and maximum eigenvalues of a sum of finite-dimensional random Hermitian matrices.

Theorem 15. *[113] Consider a finite sequence $\{\boldsymbol{X}_n\}$ of random, Hermitian matrices with*

common dimension d. Assume that

$$0 \leq \lambda_{min}(\boldsymbol{X}_n) \quad \textit{and} \quad \lambda_{max}(\boldsymbol{X}_n) \leq R \quad \textit{for each index } n.$$

Introduce the random matrix

$$\boldsymbol{Y} = \sum_n \boldsymbol{X}_n.$$

Define the minimum eigenvalue μ_{min} and maximum eigenvalue μ_{max} of the expectation $\mathbb{E}\boldsymbol{Y}$:

$$\mu_{min} = \lambda_{min}(\mathbb{E}\boldsymbol{Y}) = \lambda_{min}\left(\sum_n \mathbb{E}\boldsymbol{X}_n\right),$$
$$\mu_{max} = \lambda_{max}(\mathbb{E}\boldsymbol{Y}) = \lambda_{max}\left(\sum_n \mathbb{E}\boldsymbol{X}_n\right).$$

Then,

$$\mathbb{P}\left\{\lambda_{min}(\boldsymbol{Y}) \leq (1-\rho)\mu_{min}\right\} \leq d\left[\frac{e^{-\rho}}{(1-\rho)^{1-\rho}}\right]^{\mu_{min}/R} \quad \textit{for} \quad \rho \in [0,1),$$
$$\mathbb{P}\left\{\lambda_{max}(\boldsymbol{Y}) \geq (1+\rho)\mu_{max}\right\} \leq d\left[\frac{e^{\rho}}{(1+\rho)^{1+\rho}}\right]^{\mu_{max}/R} \quad \textit{for} \quad \rho \geq 0.$$

The second result gives a tail bound for the maximum eigenvalue of a sum of random Hermitian matrices which depends on the intrinsic dimension of their expectation, as opposed to the actual dimension, which may be much larger.

Theorem 16. *[113] Consider a finite sequence $\{\boldsymbol{X}_n\}$ of random, Hermitian matrices of the same size, and assume that*

$$0 \leq \lambda_{min}(\boldsymbol{X}_n) \quad \textit{and} \quad \lambda_{max}(\boldsymbol{X}_n) \leq R \quad \textit{for each index } n.$$

Introduce the random matrix

$$\boldsymbol{Y} = \sum_n \boldsymbol{X}_n.$$

Suppose that we have a semidefinite upper bound $\boldsymbol{M}$ for the expectation $\mathbb{E}\boldsymbol{Y}$:

$$\boldsymbol{M} \succeq \mathbb{E}\boldsymbol{Y} = \sum_n \mathbb{E}\boldsymbol{X}_n.$$

Define an intrinsic dimension bound and a mean bound

$$d = \mathit{intdim}(\boldsymbol{M}) = \frac{\operatorname{tr} \boldsymbol{M}}{\|\boldsymbol{M}\|} \quad \textit{and} \quad \mu_{\mathit{max}} = \lambda_{\mathit{max}}(\boldsymbol{M}).$$

Then,

$$\mathbb{P}\left\{\lambda_{\mathit{max}}(\boldsymbol{Y}) \geq (1+\rho)\mu_{\mathit{max}}\right\} \leq 2d \left[\frac{e^{\rho}}{(1+\rho)^{1+\rho}}\right]^{\mu_{\mathit{max}}/R} \quad \textit{for} \quad \rho \geq R/\mu_{\mathit{max}}.$$

Although this theorem is proved for finite-dimensional Hermitian matrices $\boldsymbol{X}_n$, it easily extends to infinite-dimensional self-adjoint operators by using the techniques in [121].

D.1.2 Modulated Prolate Spheroidal Wave Functions

We construct an orthonormal basis for $\mathrm{PW}_{\Omega}(\mathbb{R})$ by using modulated PSWFs to form an orthonormal basis for each $\mathrm{PW}_{[f_\ell - W_\ell, f_\ell + W_\ell]}(\mathbb{R})$, and then merging these bases.

Recall that for any bandwidth $W > 0$ the bandlimiting operator $\mathcal{B}_W^{\mathrm{c}} : L_2(\mathbb{R}) \to L_2(\mathbb{R})$ is defined by

$$(\mathcal{B}_W^{\mathrm{c}} y)(t) = \int_{-\infty}^{\infty} \frac{\sin[2\pi W(t-t')]}{\pi(t-t')} y(t')\, dt' \quad \text{for} \quad t \in \mathbb{R},$$

and for any duration $T > 0$, the timelimiting operator $\mathcal{T}_T^{\mathrm{c}} : L_2(\mathbb{R}) \to L_2(\mathbb{R})$ is defined by

$$(\mathcal{T}_T^{\mathrm{c}} y)(t) = \begin{cases} y(t) & \text{if } |t| \leq \frac{T}{2} \\ 0 & \text{if } |t| \geq \frac{T}{2} \end{cases}.$$

Also, for any $f \in \mathbb{R}$, we define a modulation operator $\mathcal{E}_f : L_2(\mathbb{R}) \to L_2(\mathbb{R})$ by

$$(\mathcal{E}_f y)(t) = e^{j2\pi ft} y(t) \quad \text{for} \quad t \in \mathbb{R}.$$

Note that the modulation operator satisfies $\widehat{\mathcal{E}_f y}(f') = \widehat{y}(f' - f)$, i.e. the modulation operator shifts the Fourier transform of a function.

For any $W > 0$ and $T > 0$, we will use the notation $\psi_{W,T}^{(0)}, \psi_{W,T}^{(1)}, \ldots \in L_2(\mathbb{R})$ to denote the prolate spheroidal wave functions (PSWFs), i.e. the eigenfunctions of $\mathcal{B}_W^{\mathrm{c}} \mathcal{T}_T^{\mathrm{c}} \mathcal{B}_W^{\mathrm{c}}$, where the PSWF eigenvalues $1 > \lambda_{W,T}^{(0)} > \lambda_{W,T}^{(1)} > \cdots > 0$ are sorted in decreasing order. This notation allows us to distinguish the PSWFs and PSWF eigenvalues for different values of W and T. Since the PSWFs $\left\{\psi_{W,T}^{(k)}\right\}_{k=0}^{\infty}$ form an orthonormal basis for $\mathrm{PW}_{[-W,W]}(\mathbb{R})$, the modulated PSWFs $\left\{\mathcal{E}_f \psi_{W,T}^{(k)}\right\}_{k=0}^{\infty}$ form an orthonormal basis for $\mathrm{PW}_{[f-W,f+W]}(\mathbb{R})$. Note that this holds for any $W > 0$ and $f \in \mathbb{R}$. Then, since

$$\Omega = \bigcup_{\ell=0}^{L-1} [f_\ell - W_\ell, f_\ell + W_\ell]$$

is a union of L non-overlapping intervals, we have that

$$\bigcup_{\ell=0}^{L-1} \left\{\mathcal{E}_{f_\ell} \psi_{W_\ell,T}^{(k)}\right\}_{k=0}^{\infty}$$

forms an orthonormal basis for $\mathrm{PW}_{\Omega}(\mathbb{R})$.

D.1.3 Multiband Prolate Spheroidal Wave Functions

We construct another orthonormal basis for $\mathrm{PW}_{\Omega}(\mathbb{R})$ as follows. First, we define an operator $\mathcal{B}_{\Omega}^{\mathrm{c}} : L_2(\mathbb{R}) \to L_2(\mathbb{R})$ by

$$(\mathcal{B}_{\Omega}^{\mathrm{c}} y)(t) = \int_{-\infty}^{\infty} \phi(t - t') y(t')\, dt' \quad \text{for} \quad t \in \mathbb{R},$$

where, as a reminder, we defined $\phi \in L_2(\mathbb{R})$ by

$$\phi(t) = \int_\Omega e^{j2\pi ft}\,df = \sum_{\ell=0}^{L-1} \frac{\sin(2\pi W_\ell t)}{\pi t} e^{j2\pi f_\ell t}.$$

Note that for any $y \in L_2(\mathbb{R})$, this operator satisfies $\widehat{\mathcal{B}_\Omega^{\mathrm{c}} y}(f) = 1_\Omega(f)\widehat{y}(f)$ for all $f \in \mathbb{R}$, i.e. $\mathcal{B}_\Omega^{\mathrm{c}}$ bandlimits a signal's continuous-time Fourier transform to Ω. Then, we define the multiband PSWFs $\psi_{\Omega,T}^{(0)}, \psi_{\Omega,T}^{(1)}, \ldots \in \mathrm{PW}_\Omega(\mathbb{R})$ to be the orthonormal eigenfunctions of the self-adjoint operator $\mathcal{B}_\Omega^{\mathrm{c}} \mathcal{T}_T^{\mathrm{c}} \mathcal{B}_\Omega^{\mathrm{c}}$, where the eigenvalues $1 > \lambda_{\Omega,T}^{(0)} \geq \lambda_{\Omega,T}^{(1)} \geq \cdots > 0$ are sorted in descending order. Note that $\left\{\psi_{\Omega,T}^{(k)}\right\}_{k=0}^{\infty}$ forms an orthonormal basis for $\mathrm{PW}_\Omega(\mathbb{R})$.

D.1.4 Bound on 1st eigenvalue of $\mathcal{A}^*\mathcal{A}$

With the matrix concentration bounds and the theory on the modulated PSWFs and the multiband PSWFs, we are now ready to bound some of the eigenvalues of $\mathcal{A}^*\mathcal{A}$. First, we show that with high probability, the largest eigenvalue of $\mathcal{A}^*\mathcal{A}$ is a small constant factor larger than $\frac{N}{T}$.

Lemma 15. *For any constant $\rho_0 > \frac{|\Omega|T}{N}$, we have*

$$\mathbb{P}\left[\lambda_1(\mathcal{A}^*\mathcal{A}) \geq (1+\rho_0)\frac{N}{T}\right] \leq (2|\Omega|T+2)\left[\frac{e^{\rho_0}}{(1+\rho_0)^{1+\rho_0}}\right]^{\frac{N}{|\Omega|T}}.$$

Proof. Since

$$\mathcal{A}^*\mathcal{A} = \sum_{n=0}^{N-1} a_{t_n} a_{t_n}^*$$

is the sum of the rank-1 operators which are self-adjoint, positive semidefinite, and independent (because the t_n's are independent), we can apply Theorem 16.

For any $\tau \in [-\frac{T}{2}, \frac{T}{2}]$, the largest eigenvalue of $a_\tau a_\tau^*$ is

$$\lambda_{\max}(a_\tau a_\tau^*) = \|a_\tau\|^2 = \|\widehat{a}_\tau\|^2 = \int_{-\infty}^{\infty} |\widehat{a}_\tau(f)|^2\,df = \int_{-\infty}^{\infty} |e^{-j2\pi f\tau} 1_\Omega(f)|^2\,df = |\Omega| =: R,$$

where we used the fact that the Fourier transform of a_τ is $\widehat{a}_\tau(f) = e^{-j2\pi ft}1_\Omega(f)$.

Next, we compute the expectation $\mathbb{E}[\mathcal{A}^*\mathcal{A}]$. To do this, we note that for any $z \in L_2(\mathbb{R})$ and any $\tau \in \mathbb{R}$, we have

$$\begin{aligned}\langle a_\tau, z\rangle = \langle \widehat{a}_\tau, \widehat{z}\rangle &= \int_{-\infty}^{\infty} \overline{\widehat{a_\tau(f)}}\widehat{z}(f)\,df = \int_{-\infty}^{\infty} e^{j2\pi ft}1_\Omega(f)\widehat{z}(f)\,df \\ &= \int_{-\infty}^{\infty} \widehat{\mathcal{B}_\Omega^{\mathrm{c}} z}(f)e^{j2\pi f\tau}\,df = (\mathcal{B}_\Omega^{\mathrm{c}} z)(\tau).\end{aligned}$$

Hence, if $\tau \sim \text{Uniform}[-\frac{T}{2}, \frac{T}{2}]$, then for any $z_1, z_2 \in L_2(\mathbb{R})$, we have

$$\begin{aligned}&\langle z_1, \mathbb{E}[a_\tau a_\tau^*]z_2\rangle = \mathbb{E}[\langle z_1, a_\tau \langle a_\tau, z_2\rangle\rangle] = \mathbb{E}[\langle z_1, a_\tau\rangle \langle a_\tau, z_2\rangle] = \mathbb{E}\left[\overline{(\mathcal{B}_\Omega^{\mathrm{c}} z_1)(\tau)}(\mathcal{B}_\Omega^{\mathrm{c}} z_2)(\tau)\right] \\ &= \frac{1}{T}\int_{-T/2}^{T/2} \overline{(\mathcal{B}_\Omega^{\mathrm{c}} z_1)(\tau)}(\mathcal{B}_\Omega^{\mathrm{c}} z_2)(\tau)\,dt = \frac{1}{T}\langle \mathcal{B}_\Omega^{\mathrm{c}} z_1, \mathcal{T}_T^{\mathrm{c}}\mathcal{B}_\Omega^{\mathrm{c}} z_2\rangle = \frac{1}{T}\langle z_1, \mathcal{B}_\Omega^{\mathrm{c}}\mathcal{T}_T^{\mathrm{c}}\mathcal{B}_\Omega^{\mathrm{c}} z_2\rangle,\end{aligned}$$

and thus, $\mathbb{E}[a_\tau a_\tau^*] = \frac{1}{T}\mathcal{B}_\Omega^{\mathrm{c}}\mathcal{T}_T^{\mathrm{c}}\mathcal{B}_\Omega^{\mathrm{c}}$. Then, since the t_n's are i.i.d. Uniform$[-\frac{T}{2}, \frac{T}{2}]$, we have

$$\mathbb{E}[\mathcal{A}^*\mathcal{A}] = \mathbb{E}\left[\sum_{n=0}^{N-1} a_{t_n}a_{t_n}^*\right] = \sum_{n=0}^{N-1}\mathbb{E}\left[a_{t_n}a_{t_n}^*\right] = \sum_{n=0}^{N-1}\frac{1}{T}\mathcal{B}_\Omega^{\mathrm{c}}\mathcal{T}_T^{\mathrm{c}}\mathcal{B}_\Omega^{\mathrm{c}} = \frac{N}{T}\mathcal{B}_\Omega^{\mathrm{c}}\mathcal{T}_T^{\mathrm{c}}\mathcal{B}_\Omega^{\mathrm{c}}.$$

Note that since $\mathcal{B}_\Omega^{\mathrm{c}}$ and $\mathcal{T}_T^{\mathrm{c}}$ are orthogonal projections, the eigenvalues of $\mathcal{B}_\Omega^{\mathrm{c}}\mathcal{T}_T^{\mathrm{c}}\mathcal{B}_\Omega^{\mathrm{c}}$ are all between 0 and 1. We now define $\mathcal{Q} : L_2(\mathbb{R}) \to L_2(\mathbb{R})$ to be the operator obtained by increasing the largest eigenvalue of $\mathcal{B}_\Omega^{\mathrm{c}}\mathcal{T}_T^{\mathrm{c}}\mathcal{B}_\Omega^{\mathrm{c}}$ to exactly 1 while leaving the eigenfunctions and the other eigenvalues unchanged. Then, we can use $\frac{N}{T}\mathcal{Q} \succeq \frac{N}{T}\mathcal{B}_\Omega^{\mathrm{c}}\mathcal{T}_T^{\mathrm{c}}\mathcal{B}_\Omega^{\mathrm{c}} = \mathbb{E}[\mathcal{A}^*\mathcal{A}]$ as the semidefinite upper bound required by Theorem 16. By definition, $\|\mathcal{Q}\| = 1$. Also, since $\mathrm{tr}[\mathcal{B}_\Omega^{\mathrm{c}}\mathcal{T}_T^{\mathrm{c}}\mathcal{B}_\Omega^{\mathrm{c}}] = |\Omega|T$, we have

$$\mathrm{tr}[\mathcal{Q}] = \mathrm{tr}[\mathcal{B}_\Omega^{\mathrm{c}}\mathcal{T}_T^{\mathrm{c}}\mathcal{B}_\Omega^{\mathrm{c}}] + \lambda_1(\mathcal{Q}) - \lambda_1(\mathcal{B}_\Omega^{\mathrm{c}}\mathcal{T}_T^{\mathrm{c}}\mathcal{B}_\Omega^{\mathrm{c}}) \le |\Omega|T + 1.$$

Therefore, the intrinsic dimension bound satisfies

$$d := \text{intdim}\left(\frac{N}{T}\mathcal{Q}\right) = \frac{\mathrm{tr}\left[\frac{N}{T}\mathcal{Q}\right]}{\left\|\frac{N}{T}\mathcal{Q}\right\|} = \frac{\mathrm{tr}\left[\mathcal{Q}\right]}{\|\mathcal{Q}\|} \le \frac{|\Omega|T + 1}{1} = |\Omega|T + 1.$$

Also, the mean bound is

$$\mu_{\max} := \lambda_{\max}\left(\frac{N}{T}\mathcal{Q}\right) = \frac{N}{T}\|\mathcal{Q}\| = \frac{N}{T}.$$

So by applying Theorem 16 with $\boldsymbol{Y} = \mathcal{A}^*\mathcal{A}$, $R = |\Omega|$, $d \leq |\Omega|T + 1$, and $\mu_{\max} = \frac{N}{T}$, we obtain

$$\mathbb{P}\left\{\lambda_1(\mathcal{A}^*\mathcal{A}) \geq (1+\rho_0)\frac{N}{T}\right\} \leq (2|\Omega|T + 2)\left[\frac{e^{\rho_0}}{(1+\rho_0)^{1+\rho_0}}\right]^{\frac{N}{|\Omega|T}} \quad \text{for} \quad \rho_0 \geq \frac{|\Omega|T}{N}.$$

□

D.1.5 Bound on K_1-th eigenvalue of $\mathcal{A}^*\mathcal{A}$

Next, we shall derive a probabilistic lower bound on $\lambda_{K_1}(\mathcal{A}^*\mathcal{A})$ where $K_1 = |\Omega|T - O(L\log(|\Omega|T))$.

Lemma 16. *For any constant $\gamma_1 \in (0, \frac{1}{4})$, let*

$$K_1 = \#\left\{k : \lambda_{\Omega,T}^{(k)} \geq 1 - \gamma_1\right\}.$$

Then, for any $\rho_1 \in (0,1)$, we have

$$\mathbb{P}\left[\lambda_{K_1}(\mathcal{A}^*\mathcal{A}) \leq (1-\rho_1)(1-\gamma_1)\frac{N}{T}\right] \leq |\Omega|T\left[\frac{e^{-\rho_1}}{(1-\rho_1)^{1-\rho_1}}\right]^{(1-\gamma_1)\frac{N}{|\Omega|T}}.$$

Proof. We will prove this theorem by looking at the restriction of the operator $\mathcal{A}^*\mathcal{A}$ to the K_1-dimensional subspace $\mathcal{S}_1 = \text{span}\left\{\psi_{\Omega,T}^{(k)}\right\}_{k=0}^{K_1-1}$, and then applying matrix concentration bounds.

First, we define an operator $\mathcal{V}_{K_1} : \mathbb{C}^{K_1} \to L_2(\mathbb{R})$ by

$$\mathcal{V}_{K_1}\boldsymbol{v} = \sum_{k=0}^{K_1-1} \boldsymbol{v}[k]\psi_{\Omega,T}^{(k)}.$$

The adjoint $\mathcal{V}_{K_1}^* : L_2(\mathbb{R}) \to \mathbb{C}^{K_1}$ is defined by

$$(\mathcal{V}_{K_1}^* y)[k] = \left\langle \psi_{\Omega,T}^{(k)}, y \right\rangle \quad \text{for} \quad k \in [K_1].$$

Now, we will seek to bound $\lambda_{\min}(\mathcal{V}_{K_1}^* \mathcal{A}^* \mathcal{A} \mathcal{V}_{K_1})$, and then use this to bound $\lambda_{K_1}(\mathcal{A}^* \mathcal{A})$. We note that the self-adjoint operator $\mathcal{V}_{K_1}^* \mathcal{A}^* \mathcal{A} \mathcal{V}_{K_1} : \mathbb{C}^{K_1} \to \mathbb{C}^{K_1}$ satisfies

$$\mathcal{V}_{K_1}^* \mathcal{A}^* \mathcal{A} \mathcal{V}_{K_1} = \mathcal{V}_{K_1}^* \left(\sum_{n=0}^{N-1} a_{t_n} a_{t_n}^* \right) \mathcal{V}_{K_1} = \sum_{n=0}^{N-1} \mathcal{V}_{K_1}^* a_{t_n} a_{t_n}^* \mathcal{V}_{K_1},$$

and thus, is equivalent to a sum of i.i.d. rank-1 $K_1 \times K_1$ positive semidefinite Hermitian matrices.

For any $\tau \in [-\frac{T}{2}, \frac{T}{2}]$, the largest eigenvalue of $\mathcal{V}_{K_1}^* a_\tau a_\tau^* \mathcal{V}_{K_1}$ is bounded by

$$\lambda_{\max}(\mathcal{V}_{K_1}^* a_\tau a_\tau^* \mathcal{V}_{K_1}) = \left\| \mathcal{V}_{K_1}^* a_\tau \right\|^2 \leq \|a_\tau\|^2 = |\Omega| =: R,$$

where we made use of our earlier calculation that $\|a_\tau\|^2 = |\Omega|$. Also, since $\mathbb{E}[\mathcal{A}^* \mathcal{A}] = \frac{N}{T} \mathcal{B}_\Omega^{\mathrm{c}} \mathcal{T}_T^{\mathrm{c}} \mathcal{B}_\Omega^{\mathrm{c}}$, we have that

$$\mathbb{E}[\mathcal{V}_{K_1}^* \mathcal{A}^* \mathcal{A} \mathcal{V}_{K_1}] = \frac{N}{T} \mathcal{V}_{K_1}^* \mathcal{B}_\Omega^{\mathrm{c}} \mathcal{T}_T^{\mathrm{c}} \mathcal{B}_\Omega^{\mathrm{c}} \mathcal{V}_{K_1} = \frac{N}{T} \operatorname{diag}\left(\lambda_{\Omega,T}^{(0)}, \lambda_{\Omega,T}^{(1)}, \ldots, \lambda_{\Omega,T}^{(K_1-1)} \right),$$

where we have made use of the fact that the multiband PSWFs are the eigenfunctions of $\mathcal{B}_\Omega^{\mathrm{c}} \mathcal{T}_T^{\mathrm{c}} \mathcal{B}_\Omega^{\mathrm{c}}$. Then, by the definition of K_1, we have

$$\mu_{\min} := \lambda_{\min}\left(\mathbb{E}[\mathcal{V}_{K_1}^* \mathcal{A}^* \mathcal{A} \mathcal{V}_{K_1}] \right) = \frac{N}{T} \lambda_{\Omega,T}^{(K_1-1)} \geq (1 - \gamma_1) \frac{N}{T}.$$

So by applying Theorem 15 with $\boldsymbol{Y} = \mathcal{V}_{K_1}^* \mathcal{A}^* \mathcal{A} \mathcal{V}_{K_1}$, $d = K_1$, $R = |\Omega|$, and $\mu_{\min} =$

$\frac{N}{T}\lambda_{\Omega,T}^{(K_1-1)}$, we get that

$$\mathbb{P}\left\{\lambda_{\min}(\mathcal{V}_{K_1}^*\mathcal{A}^*\mathcal{A}\mathcal{V}_{K_1}) \leq (1-\rho_1)\frac{N}{T}\lambda_{\Omega,T}^{(K_1-1)}\right\} \leq K_1\left[\frac{e^{-\rho_1}}{(1-\rho_1)^{1-\rho_1}}\right]^{\frac{N}{|\Omega|T}\lambda_{\Omega,T}^{(K_1-1)}}.$$

Finally, we use the Courant-Weyl-Fischer min-max characterization to obtain

$$\begin{aligned}\lambda_{K_1}(\mathcal{A}^*\mathcal{A}) &= \max_{\substack{\text{subspaces } \mathcal{S} \\ \dim\mathcal{S}=K_1}} \min_{\substack{x\in\mathcal{S} \\ \|x\|=1}} \langle x, \mathcal{A}^*\mathcal{A}x\rangle \geq \min_{\substack{x\in\mathcal{S}_1 \\ \|x\|=1}} \langle x, \mathcal{A}^*\mathcal{A}x\rangle = \min_{\substack{\boldsymbol{v}\in\mathbb{C}^{K_1} \\ \|\boldsymbol{v}\|_2=1}} \langle \mathcal{V}_{K_1}\boldsymbol{v}, \mathcal{A}^*\mathcal{A}\mathcal{V}_{K_1}\boldsymbol{v}\rangle \\ &= \min_{\substack{\boldsymbol{v}\in\mathbb{C}^{K_1} \\ \|\boldsymbol{v}\|_2=1}} \left\langle \boldsymbol{v}, \mathcal{V}_{K_1}^*\mathcal{A}^*\mathcal{A}\mathcal{V}_{K_1}\boldsymbol{v}\right\rangle = \lambda_{\min}(\mathcal{V}_{K_1}^*\mathcal{A}^*\mathcal{A}\mathcal{V}_{K_1})\end{aligned}$$

By applying this inequality along with $K_1 = \#\left\{k : \lambda_{\Omega,T}^{(k)} > 1-\gamma_1\right\} \leq |\Omega|T$ and $\lambda_{\Omega,T}^{(K_1-1)} \geq 1-\gamma_1$, we obtain the bound

$$\begin{aligned}&\mathbb{P}\left\{\lambda_{K_1}(\mathcal{A}^*\mathcal{A}) \leq (1-\rho_1)(1-\gamma_1)\frac{N}{T}\right\} \\ &\leq \mathbb{P}\left\{\lambda_{\min}(\mathcal{V}_{K_1}^*\mathcal{A}^*\mathcal{A}\mathcal{V}_{K_1}) \leq (1-\rho_1)(1-\gamma_1)\frac{N}{T}\right\} \\ &\leq \mathbb{P}\left\{\lambda_{\min}(\mathcal{V}_{K_1}^*\mathcal{A}^*\mathcal{A}\mathcal{V}_{K_1}) \leq (1-\rho_1)\frac{N}{T}\lambda_{\Omega,T}^{(K_1-1)}\right\} \\ &\leq K_1\left[\frac{e^{-\rho_1}}{(1-\rho_1)^{1-\rho_1}}\right]^{\frac{N}{|\Omega|T}\lambda_{\Omega,T}^{(K_1-1)}} \\ &\leq |\Omega|T\left[\frac{e^{-\rho_1}}{(1-\rho_1)^{1-\rho_1}}\right]^{(1-\gamma_1)\frac{N}{|\Omega|T}}.\end{aligned}$$

□

D.1.6 Bound on K_2-th eigenvalue of $\mathcal{A}^*\mathcal{A}$

Next, we shall derive a deterministic upper bound on $\lambda_{K_2+1}(\mathcal{A}^*\mathcal{A})$ where $K_2 = |\Omega|T + O(L\log(|\Omega|T))$.

Lemma 17. *Let $\gamma_2 \in (0, \frac{1}{2})$ be given and set*

$$K_2 = \#\left\{(k,\ell) \ : \ \ell \in [L], \lambda^{(k)}_{W_\ell,T} > \gamma_2\right\}.$$

Then if $2W_\ell T \geq 1$ for all $\ell \in [L]$, we have

$$\lambda_{K_2+1}(\mathcal{A}^*\mathcal{A}) \leq \left(\frac{8\pi^2}{3}\right)^{1/4} N|\Omega|\gamma_2^{1/2}.$$

Proof. Define a subspace

$$\mathcal{S}_2 = \operatorname{span}\left\{\mathcal{E}_{f_\ell}\psi^{(k)}_{W_\ell,T} : \ell \in [L], \lambda^{(k)}_{W_\ell,T} > \gamma_2\right\} \subset \mathrm{PW}_\Omega(\mathbb{R}).$$

Note that $\dim \mathcal{S}_2 = K_2$. Then, by the Courant-Fischer-Weyl min-max theorem, we have

$$\begin{aligned}\lambda_{K_2+1}(\mathcal{A}^*\mathcal{A}) &= \min_{\substack{\text{subspaces } \mathcal{S} \\ \dim \mathcal{S} = K_2}} \max_{\substack{x \perp \mathcal{S} \\ \|x\|=1}} \langle \mathcal{A}^*\mathcal{A}x, x\rangle \leq \max_{\substack{x \perp \mathcal{S}_2 \\ \|x\|=1}} \langle \mathcal{A}^*\mathcal{A}x, x\rangle \\ &= \max_{\substack{x \perp \mathcal{S}_2 \\ \|x\|=1}} \|\mathcal{A}x\|_2^2 = \max_{\substack{x \perp \mathcal{S}_2 \\ \|x\|=1}} \sum_{n=0}^{N-1} |\langle a_{t_n}, x\rangle|^2 = \max_{\substack{x \perp \mathcal{S}_2 \\ \|x\|=1}} \sum_{n=0}^{N-1} |(\mathcal{B}_\Omega^{\mathrm{c}} x)(t_n)|^2,\end{aligned}$$

where we again used the fact that $\langle a_\tau, x\rangle = (\mathcal{B}_\Omega^{\mathrm{c}}x)(\tau)$ for all $\tau \in \mathbb{R}$ and $x \in L_2(\mathbb{R})$. We will bound the $|(\mathcal{B}_\Omega^{\mathrm{c}}x)(t_n)|$'s for a signal $x \perp \mathcal{S}_2$ by exploiting the fact that $\mathcal{B}_\Omega^{\mathrm{c}}x$ lies in the span of the modulated PSWFs whose eigenvalues are small, and thus, have little energy in $[-\frac{T}{2}, \frac{T}{2}]$.

Formally, suppose $x \in L_2(\mathbb{R})$ satisfies $x \perp \mathcal{S}_2$ and $\|x\| = 1$. Since $\mathcal{B}_\Omega^{\mathrm{c}}$ is an orthogonal projection operator onto $\mathrm{PW}_\Omega(\mathbb{R})$, we have $\mathcal{B}_\Omega^{\mathrm{c}}x \in \mathrm{PW}_\Omega(\mathbb{R})$, $\mathcal{B}_\Omega^{\mathrm{c}}x \perp \mathcal{S}_2$, and $\|\mathcal{B}_\Omega^{\mathrm{c}}x\| \leq \|x\| = 1$. Since $\{\mathcal{E}_{f_\ell}\psi^{(k)}_{W_\ell,T} \ : \ \ell \in [L], k \in \mathbb{N}_0\}$ is an orthonormal basis for $\mathrm{PW}_\Omega(\mathbb{R})$, and $\mathcal{B}_\Omega^{\mathrm{c}}x \perp \mathcal{S}_2 = \operatorname{span}\left\{\mathcal{E}_{f_\ell}\psi^{(k)}_{W_\ell,T} : \ell \in [L], \lambda^{(k)}_{W_\ell,T} > \gamma_2\right\}$ we can write

$$\mathcal{B}_\Omega^{\mathrm{c}}x = \sum_{\ell=0}^{L-1} \sum_{\lambda^{(k)}_{W_\ell,T} \leq \gamma_2} c_{\ell,k}\mathcal{E}_{f_\ell}\psi^{(k)}_{W_\ell,T}$$

for some coefficients $c_{\ell,k} \in \mathbb{C}$ which satisfy

$$\sum_{\ell=0}^{L-1} \sum_{\lambda_{W_\ell,T}^{(k)} \leq \gamma_2} |c_{\ell,k}|^2 .$$

We now split the signal $\mathcal{B}_\Omega^{\mathrm{c}} x$ (which is bandlimited to Ω) into each of its single band components, i.e. for each $\ell \in [L]$, define

$$x_\ell = \sum_{\lambda_{W_\ell,T}^{(k)} \leq \gamma_2} c_{\ell,k} \psi_{W_\ell,T}^{(k)},$$

so that

$$\mathcal{B}_\Omega^{\mathrm{c}} x = \sum_{\ell=0}^{L-1} \mathcal{E}_{f_\ell} x_\ell.$$

We pause to make a couple of observations. Since the Fourier transform of $\mathcal{E}_{f_\ell} x_\ell$ is supported on $[f_\ell - W_\ell, f_\ell + W_\ell]$ for each $\ell \in [L]$, these signals are orthogonal, and thus,

$$\|\mathcal{B}_\Omega^{\mathrm{c}} x\|^2 = \left\| \sum_{\ell=0}^{L-1} \mathcal{E}_{f_\ell} x_\ell \right\|^2 = \sum_{\ell=0}^{L-1} \|\mathcal{E}_{f_\ell} x_\ell\|^2 = \sum_{\ell=0}^{L-1} \|x_\ell\|^2 ,$$

where the last equality holds since the modulation operators $\mathcal{E}_{f_\ell}$ are unitary. Also, since the PSWFs $\psi_{W_\ell,T}^{(k)}$ are also orthogonal on $[-\frac{T}{2}, \frac{T}{2}]$, we have

$$\begin{aligned} \int_{-T/2}^{T/2} |x_\ell(t)|^2 \, dt &= \int_{-T/2}^{T/2} \left| \sum_{\lambda_{W_\ell,T}^{(k)} \leq \gamma_2} c_{\ell,k} \psi_{W_\ell,T}^{(k)}(t) \right|^2 dt = \sum_{\lambda_{W_\ell,T}^{(k)} \leq \gamma_2} |c_{\ell,k}|^2 \int_{-T/2}^{T/2} \left| \psi_{W_\ell,T}^{(k)}(t) \right|^2 dt \\ &= \sum_{\lambda_{W_\ell,T}^{(k)} \leq \gamma_2} \lambda_{W_\ell,T}^{(k)} |c_{\ell,k}|^2 \leq \sum_{\lambda_{W_\ell,T}^{(k)} \leq \gamma_2} \gamma_2 |c_{\ell,k}|^2 = \gamma_2 \|x_\ell\|^2, \end{aligned}$$

i.e. the energy of x_ℓ in the time interval $[-\frac{T}{2}, \frac{T}{2}]$ is "small".

Since each x_ℓ is a sum of PSWFs with bandwidth W_ℓ, each x_ℓ is bandlimited to $[-W_\ell, W_\ell]$.

Hence, we can write

$$x_\ell(t) = \int_{-W_\ell}^{W_\ell} \widehat{x}_\ell(f) e^{j2\pi ft}\, df,$$

and thus, the energy $\chi_\ell(t) := |x_\ell(t)|^2$ can be written as

$$\begin{aligned}
\chi_\ell(t) &= x_\ell(t)\overline{x_\ell(t)} \\
&= \left(\int_{-W_\ell}^{W_\ell} \widehat{x}_\ell(f) e^{j2\pi ft}\, df\right)\left(\int_{-W_\ell}^{W_\ell} \overline{\widehat{x}_\ell(f')} e^{-j2\pi f't}\, df'\right) \\
&= \int_{-W_\ell}^{W_\ell}\int_{-W_\ell}^{W_\ell} \widehat{x}_\ell(f)\overline{\widehat{x}_\ell(f')} e^{j2\pi(f-f')t}\, df\, df'.
\end{aligned}$$

Then, the derivative of $\chi_\ell(t)$ can be bounded by

$$\begin{aligned}
|\chi_\ell'(t)|^2 &= \left|\int_{-W_\ell}^{W_\ell}\int_{-W_\ell}^{W_\ell} \widehat{x}_\ell(f)\overline{\widehat{x}_\ell(f')} j2\pi(f-f') e^{j2\pi(f-f')t}\, df\, df'\right|^2 \\
&\le \left[\int_{-W_\ell}^{W_\ell}\int_{-W_\ell}^{W_\ell} \left|\widehat{x}_\ell(f)\overline{\widehat{x}_\ell(f')}\right|^2 df\, df'\right]\left[\int_{-W_\ell}^{W_\ell}\int_{-W_\ell}^{W_\ell} \left|j2\pi(f-f') e^{j2\pi(f-f')t}\right|^2 df\, df'\right] \\
&= \left[\int_{-W_\ell}^{W_\ell}\int_{-W_\ell}^{W_\ell} |\widehat{x}_\ell(f)|^2 |\widehat{x}_\ell(f')|^2\, df\, df'\right]\left[\int_{-W_\ell}^{W_\ell}\int_{-W_\ell}^{W_\ell} 4\pi^2(f-f')^2\, df\, df'\right] \\
&= \|\widehat{x}_\ell\|_{L_2([-W_\ell,W_\ell])}^4 \cdot \frac{32\pi^2}{3} W_\ell^4 \\
&= \frac{32\pi^2}{3} W_\ell^4 \|x_\ell\|^4,
\end{aligned}$$

where we have used the Cauchy-Schwarz inequality along with the Parseval-Plancherel identity. For convenience, set $C = \left(\frac{128\pi^2}{3}\right)^{1/4}$, so that $|\chi_\ell'(t)| \le \frac{1}{2} C^2 W_\ell^2 \|x_\ell\|^2$ for all $t \in \mathbb{R}$. Hence, for any $\tau, t \in \mathbb{R}$, we can use the fundamental theorem of calculus to obtain

$$\chi_\ell(t) = \chi_\ell(\tau) + \int_\tau^t \chi_\ell'(t)\, dt \ge \chi_\ell(\tau) - \int_\tau^t |\chi_\ell'(t)| \cdot |\, dt| \ge \chi_\ell(\tau) - \frac{1}{2} C^2 W_\ell^2 \|x_\ell\|^2 \cdot |t-\tau|,$$

i.e.

$$|x_\ell(t)|^2 \ge |x_\ell(\tau)|^2 - \frac{1}{2} C^2 W_\ell^2 \|x_\ell\|^2 \cdot |t-\tau|.$$

Now, suppose that $|x_\ell(\tau)|^2 > C\gamma_2^{1/2} W_\ell \|x_\ell\|^2$ for some $\tau \in [-\frac{T}{2}, \frac{T}{2}]$.

If $\tau \leq 0$, then since $2W_\ell T \geq 1 \geq \frac{4\gamma_2^{1/2}}{C}$, we have $\frac{2\gamma_2^{1/2}}{CW_\ell} \leq \frac{T}{2}$. Hence, $\left[\tau, \tau + \frac{2\gamma_2^{1/2}}{CW_\ell}\right] \subset [-\frac{T}{2}, \frac{T}{2}]$, and thus,

$$\begin{aligned}
\int_{-T/2}^{T/2} |x(t)|^2\,dt &\geq \int_{\tau}^{\tau+\frac{2\gamma_2^{1/2}}{CW_\ell}} |x(t)|^2\,dt \\
&\geq \int_{\tau}^{\tau+\frac{2\gamma_2^{1/2}}{CW_\ell}} \left[|x(\tau)|^2 - \frac{1}{2}C^2W_\ell^2\|x_\ell\|^2 \cdot |t-\tau|\right] dt \\
&> \int_{\tau}^{\tau+\frac{2\gamma_2^{1/2}}{CW_\ell}} \left[C\gamma_2^{1/2}W_\ell\|x_\ell\|^2 - \frac{1}{2}C^2W_\ell^2\|x_\ell\|^2 \cdot |t-\tau|\right] dt \\
&= C\gamma_2^{1/2}W_\ell\|x_\ell\|^2 \cdot \frac{2\gamma_2^{1/2}}{CW_\ell} - \frac{1}{2}C^2W_\ell^2\|x_\ell\|^2 \cdot \frac{1}{2}\left(\frac{2\gamma_2^{1/2}}{CW_\ell}\right)^2 \\
&= \gamma_2\|x_\ell\|^2.
\end{aligned}$$

Similarly, if $\tau > 0$, then since $2W_\ell T \geq 1 \geq \frac{4\gamma_2^{1/2}}{C}$, we have $\frac{2\gamma_2^{1/2}}{CW_\ell} \leq \frac{T}{2}$. Hence, $\left[\tau - \frac{2\gamma_2^{1/2}}{CW_\ell}, \tau\right] \subset [-\frac{T}{2}, \frac{T}{2}]$, and thus,

$$\begin{aligned}
\int_{-T/2}^{T/2} |x(t)|^2\,dt &\geq \int_{\tau-\frac{2\gamma_2^{1/2}}{CW_\ell}}^{\tau} |x(t)|^2\,dt \\
&\geq \int_{\tau-\frac{2\gamma_2^{1/2}}{CW_\ell}}^{\tau} \left[|x(\tau)|^2 - \frac{1}{2}C^2W_\ell^2\|x_\ell\|^2 \cdot |t-\tau|\right] dt \\
&> \int_{\tau-\frac{2\gamma_2^{1/2}}{CW_\ell}}^{\tau} \left[C\gamma_2^{1/2}W_\ell\|x_\ell\|^2 - \frac{1}{2}C^2W_\ell^2\|x_\ell\|^2 \cdot |t-\tau|\right] dt \\
&= C\gamma_2^{1/2}W_\ell\|x_\ell\|^2 \cdot \frac{2\gamma_2^{1/2}}{CW_\ell} - \frac{1}{2}C^2W_\ell^2\|x_\ell\|^2 \cdot \frac{1}{2}\left(\frac{2\gamma_2^{1/2}}{CW_\ell}\right)^2 \\
&= \gamma_2\|x_\ell\|^2.
\end{aligned}$$

In either case, we obtain $\int_{-T/2}^{T/2} |x(t)|^2\,dt > \gamma_2\|x_\ell\|^2$ which contradicts $\int_{-T/2}^{T/2} |x(t)|^2\,dt \leq \gamma_2\|x_\ell\|^2$ derived earlier. Therefore,

$$|x_\ell(\tau)|^2 \leq C\gamma_2^{1/2}W_\ell\|x_\ell\|^2 \quad \text{for all} \quad \tau \in [-\tfrac{T}{2}, \tfrac{T}{2}].$$

Then, by using the triangle inequality and the Cauchy-Schwarz inequality, we obtain

$$\begin{aligned}
|(\mathcal{B}_\Omega^{\mathrm{c}} x)(\tau)| &= \left| \sum_{\ell=0}^{L-1} (\mathcal{E}_{f_\ell} x_\ell)(\tau) \right| \\
&\leq \sum_{\ell=0}^{L-1} |(\mathcal{E}_{f_\ell} x_\ell)(\tau)| \\
&\leq \sum_{\ell=0}^{L-1} \left| e^{j2\pi f_\ell \tau} x_\ell(\tau) \right| \\
&\leq \sum_{\ell=0}^{L-1} |x_\ell(\tau)| \\
&\leq \sum_{\ell=0}^{L-1} C^{1/2} \gamma_2^{1/4} W_\ell^{1/2} \|x_\ell\| \\
&\leq \left(\sum_{\ell=0}^{L-1} C \gamma_2^{1/2} W_\ell \right)^{1/2} \left(\sum_{\ell=0}^{L-1} \|x_\ell\|^2 \right)^{1/2} \\
&= \frac{C^{1/2} \gamma_2^{1/4}}{2^{1/2}} \left(\sum_{\ell=0}^{L-1} 2 W_\ell \right)^{1/2} \|\mathcal{B}_\Omega^{\mathrm{c}} x\| \\
&\leq \frac{C^{1/2} \gamma_2^{1/4}}{2^{1/2}} |\Omega|^{1/2},
\end{aligned}$$

and thus,

$$|(\mathcal{B}_\Omega^{\mathrm{c}} x)(\tau)|^2 \leq \frac{1}{2} C |\Omega| \gamma_2^{1/2} \quad \text{for all} \quad \tau \in [-\tfrac{T}{2}, \tfrac{T}{2}].$$

Finally, by applying this bound to our earlier derived bound for $\lambda_{K_2+1}(\mathcal{A}^*\mathcal{A})$, we have

$$\lambda_{K_2+1}(\mathcal{A}^*\mathcal{A}) \leq \max_{\substack{x \perp \mathcal{S}_2 \\ \|x\|=1}} \sum_{n=0}^{N-1} |(\mathcal{B}_\Omega^{\mathrm{c}} x)(t_n)|^2 \leq \sum_{n=0}^{N-1} \frac{1}{2} C |\Omega| \gamma_2^{1/2} = \left(\frac{8\pi^2}{3} \right)^{1/4} N |\Omega| \gamma_2^{1/2}.$$

□

We are now ready to prove Lemma 1. First, by applying Lemma 15 with $\rho_0 = 1.3603$ (chosen so that $\frac{e^{\rho_0}}{(1+\rho_0)^{1+\rho_0}} \leq e^{-2/3}$ and $\rho_0 \geq 1 \geq \frac{|\Omega|T}{N}$), we get that

$$\lambda_1(\boldsymbol{G}) = \lambda_1(\mathcal{A}^*\mathcal{A}) \leq (1+\rho_0)\frac{N}{T}$$

fails with probability at most

$$(2|\Omega|T+2)\left[\frac{e^{\rho_0}}{(1+\rho_0)^{1+\rho_0}}\right]^{\frac{N}{|\Omega|T}} \leq (2|\Omega|T+2)e^{-\frac{2N}{3|\Omega|T}}.$$

Next, by applying Lemma 16 with $\gamma_1 = 0.02$ and $\rho_1 = 0.9046$ (chosen such that $\left(\frac{e^{-\rho_1}}{(1-\rho_1)^{1-\rho_1}}\right)^{1-\gamma_1} \leq e^{-2/3}$), we get that

$$\lambda_{K_1}(\boldsymbol{G}) = \lambda_{K_1}(\mathcal{A}^*\mathcal{A}) \geq (1-\rho_1)(1-\gamma_1)\frac{N}{T}$$

fails with probability at most

$$|\Omega|T\left[\frac{e^{-\rho_1}}{(1-\rho_1)^{1-\rho_1}}\right]^{(1-\gamma_1)\frac{N}{|\Omega|T}} \leq |\Omega|Te^{-\frac{2N}{3|\Omega|T}}.$$

Furthermore, by applying Lemma 17 with $\gamma_2 = \dfrac{\sqrt{6}\delta^2\epsilon^{1/4}}{\pi N^2|\Omega|^2}$, we get that $\lambda_{K_2+1}(\boldsymbol{G}) = \lambda_{K_2}(\mathcal{A}^*\mathcal{A}) \leq \left(\dfrac{8\pi^2}{3}\right)^{1/4} N|\Omega|\gamma_2^{1/2} = 2\delta\epsilon^{1/8}$ holds with probability 1. Therefore, the bounds

$$\begin{aligned}\lambda_1(\boldsymbol{G}) &\leq C_1\frac{N}{|\Omega|T},\\ \lambda_{K_1}(\boldsymbol{G}) &\geq C_2\frac{N}{|\Omega|T},\\ \lambda_{K_2+1}(\boldsymbol{G}) &\leq 2\delta\epsilon^{1/8}.\end{aligned}$$

for $C_1 = 1+\rho_1$ and $C_2 = (1-\rho_0)(1-\gamma_1)$ hold with probability at least

$$1-(3|\Omega|T+2)e^{-\frac{2N}{3|\Omega|T}}.$$

Furthermore, using equation (2) in [90], we obtain

$$\begin{aligned} K_1 &= \#\left\{k : \lambda_{\Omega,T}^{(k)} \geq 1-\gamma_1\right\} \\ &= |\Omega|T + \frac{L}{\pi^2}\log\left(\frac{\pi}{2}|\Omega|T\right)\log\left(\frac{\gamma_1}{1-\gamma_1}\right) + o\left(\log\left(\frac{\pi}{2}|\Omega|T\right)\right), \end{aligned}$$

and

$$\begin{aligned} K_2 &= \#\left\{(k,\ell) : \ell \in [L], \lambda_{W_\ell,T}^{(k)} > \gamma_2\right\} \\ &= \sum_{\ell=0}^{L-1} \#\left\{k : \lambda_{W_\ell,T}^{(k)} > \gamma_2\right\} \\ &= \sum_{\ell=0}^{L-1} 2W_\ell T + \frac{1}{\pi^2}\log(\pi W_\ell T)\log\left(\frac{1-\gamma_2}{\gamma_2}\right) + o\left(\log\left(\pi W_\ell T\right)\right) \\ &\leq \sum_{\ell=0}^{L-1} 2W_\ell T + \frac{1}{\pi^2}\log\left(\frac{\pi}{2}|\Omega|T\right)\log\left(\frac{1-\gamma_2}{\gamma_2}\right) + o\left(\log\left(\frac{\pi}{2}|\Omega|T\right)\right) \\ &= |\Omega|T + \frac{L}{\pi^2}\log\left(\frac{\pi}{2}|\Omega|T\right)\log\left(\frac{1-\gamma_2}{\gamma_2}\right) + o\left(\log\left(\frac{\pi}{2}|\Omega|T\right)\right). \end{aligned}$$

Hence,

$$\begin{aligned} K_2 - K_1 &= \frac{L}{\pi^2}\log\left(\frac{\pi}{2}|\Omega|T\right)\left(\log\left(\frac{1-\gamma_2}{\gamma_2}\right) - \log\left(\frac{\gamma_1}{1-\gamma_1}\right)\right) + o\left(\log\left(\frac{\pi}{2}|\Omega|T\right)\right) \\ &\leq \frac{L}{\pi^2}\log\left(\frac{\pi}{2}|\Omega|T\right)\left(\log\left(\frac{1}{\gamma_2}\right) + \log(49)\right) + o\left(\log\left(\frac{\pi}{2}|\Omega|T\right)\right) \\ &= \frac{L}{\pi^2}\log\left(\frac{\pi}{2}|\Omega|T\right)\left(\log\left(\frac{\pi N^2|\Omega|^2}{\sqrt{6}\delta^2\epsilon^{1/4}}\right) + \log(49)\right) + o\left(\log\left(\frac{\pi}{2}|\Omega|T\right)\right) \\ &\leq C_0 L\log\left(\frac{\pi}{2}|\Omega|T\right)\log\left(\frac{N^2|\Omega|^2}{\delta^2\epsilon^{1/4}}\right), \end{aligned}$$

for some constant C_0, as desired.

D.2 Proof of Lemma 2

As mentioned in Section 6.4, error satisfies

$$\left\|\boldsymbol{z}^{(k)} - \boldsymbol{A}^{-1}\boldsymbol{y}\right\|_{\boldsymbol{A}}^2 \leq \left\|\boldsymbol{A}^{-1}\boldsymbol{y}\right\|_{\boldsymbol{A}}^2 \cdot \min_{\substack{\text{polynomials } P \\ \deg P = k \\ P(0)=1}} \left[\max_{\lambda \in \text{Spec}(\boldsymbol{A})} |P(\lambda)|^2\right].$$

Our goal is to construct a low-degree polynomial $Q(\lambda)$ such that $Q(0) = 1$ and $|Q(\lambda)| \leq \epsilon$ for all $\lambda \in \text{Spec}(\boldsymbol{A})$, which allows us to obtain the bound $\left\|\boldsymbol{z}^{(k)} - \boldsymbol{A}^{-1}\boldsymbol{y}\right\|_{\boldsymbol{A}} \leq \epsilon \left\|\boldsymbol{A}^{-1}\boldsymbol{y}\right\|_{\boldsymbol{A}}$.

To construct such a polynomial, we will use the Chebyshev polynomials of the first kind, which are defined by

$$T_d(\lambda) = \frac{1}{2}\left[\left(\lambda + \sqrt{\lambda^2 - 1}\right)^d + \left(\lambda - \sqrt{\lambda^2 - 1}\right)^d\right],$$

for non-negative integers d. These satisfy the following key properties:

$\deg T_d = d$ and all d roots of $T_d(\lambda)$ lie in $[-1, 1]$

$|T_d(\lambda)| \leq 1$ for all $\lambda \in [-1, 1]$

$|T_d(\lambda)|$ is increasing on $[1, \infty)$ and decreasing on $(-\infty, -1]$

$|T_d(\lambda)| \geq \frac{1}{2}\left(|\lambda| + \sqrt{|\lambda|^2 - 1}\right)^d$ for all $|\lambda| \geq 1$.

With these properties in mind, set

$$d = \left\lceil \frac{1}{2}\sqrt{\frac{b}{a}}\left((p+q)\log\frac{b}{\delta} + \log\frac{2}{\epsilon}\right)\right\rceil,$$

and consider the degree $d + p + q$ polynomial

$$Q(\lambda) = \frac{\left(1 + \epsilon^{1/q} - \lambda/\delta\right)^q}{\left(1 + \epsilon^{1/q}\right)^q}\left[\prod_{i=0}^{p-1}\frac{c_i - \lambda}{c_i}\right]\frac{T_d\left(\dfrac{b+a-2\lambda}{b-a}\right)}{T_d\left(\dfrac{b+a}{b-a}\right)}.$$

Clearly, $Q(0) = 1$. We can bound $|Q(\lambda)|$ for $\lambda \in \text{Spec}(\boldsymbol{A})$ in three cases:

Case I: $\delta \leq \lambda \leq \delta(1+2\epsilon^{1/q})$.

Over this range of λ, we have $|1+\epsilon^{1/q}-\lambda/\delta| \leq \epsilon^{1/q}$ and $|c_i-\lambda| \leq c_i$ for all $i \in [p]$. Since $|T_d(\cdot)|$ is increasing on $[1,\infty)$ we have $\left|T_d(\frac{b+a-2\lambda}{b-a})\right| \leq \left|T_d(\frac{b+a}{b-a})\right|$. Therefore,

$$\begin{aligned}
|Q(\lambda)| &= \frac{\left|1+\epsilon^{1/q}-\lambda/\delta\right|^q}{|1+\epsilon^{1/q}|^q}\left[\prod_{i=0}^{p-1}\frac{|c_i-\lambda|}{|c_i|}\right]\frac{\left|T_d\left(\frac{b+a-2\lambda}{b-a}\right)\right|}{\left|T_d\left(\frac{b+a}{b-a}\right)\right|} \\
&\leq \frac{\left(\epsilon^{1/q}\right)^q}{1^q}\left[\prod_{i=0}^{p-1}\frac{c_i}{c_i}\right]\frac{\left|T_d\left(\frac{b+a}{b-a}\right)\right|}{\left|T_d\left(\frac{b+a}{b-a}\right)\right|} \\
&= \epsilon.
\end{aligned}$$

Case II: $\lambda = c_i$ for some $i \in [p]$.

We trivially have $|Q(\lambda)| = 0 \leq \epsilon$.

Case III: $a \leq \lambda \leq b$.

Over this range of λ, we have $|1+\epsilon^{1/q}-\lambda/\delta| \leq b/\delta$ and $|c_i-\lambda| \leq b$ for $i \in [p]$. Also, $c_i \geq \delta$ for all $i \in [p]$. Since $-1 \leq \frac{b+a-2\lambda}{b-a} \leq 1$, we have $|T_d(\frac{b+a-2\lambda}{b-a})| \leq 1$. Also, we can bound

$$\begin{aligned}
\left|T_d\left(\frac{b+a}{b-a}\right)\right| &\geq \frac{1}{2}\left[\left(\frac{b+a}{b-a}\right)+\sqrt{\left(\frac{b+a}{b-a}\right)^2-1}\right]^d \\
&= \frac{1}{2}\left[\left(\frac{1+a/b}{1-a/b}\right)+\sqrt{\left(\frac{1+a/b}{1-a/b}\right)^2-1}\right]^d \\
&= \frac{1}{2}\left(\frac{1+\sqrt{a/b}}{1-\sqrt{a/b}}\right)^d \\
&\geq \frac{1}{2}e^{2d\sqrt{a/b}}
\end{aligned}$$

where we have made use of the identity $\frac{1+c}{1-c}+\sqrt{\left(\frac{1+c}{1-c}\right)^2-1} = \frac{1+\sqrt{c}}{1-\sqrt{c}}$ for $0 \leq c < 1$ and the

inequality $\frac{1+c}{1-c} \geq e^{2c}$ for $0 \leq c < 1$. Therefore, we can bound

$$\begin{aligned}
|Q(\lambda)| &= \frac{|1+\epsilon^{1/q}-\lambda/\delta|^q}{|1+\epsilon^{1/q}|^q}\left[\prod_{i=0}^{p-1}\frac{|c_i-\lambda|}{c_i}\right]\frac{\left|T_n\left(\frac{b+a-2\lambda}{b-a}\right)\right|}{\left|T_n\left(\frac{b+a}{b-a}\right)\right|} \\
&\leq \frac{(b/\delta)^q}{1^q}\left[\prod_{i=0}^{p-1}\frac{b}{\delta}\right]\frac{1}{\frac{1}{2}e^{2d\sqrt{a/b}}} \\
&= 2\left(\frac{b}{\delta}\right)^{p+q}e^{-2d\sqrt{a/b}} \\
&\leq \epsilon,
\end{aligned}$$

where the last inequality holds due to our choice of d.

Therefore, for the integer

$$k = d+p+q = \left\lceil \frac{1}{2}\sqrt{\frac{b}{a}}\left((p+q)\log\frac{b}{\delta}+\log\frac{2}{\epsilon}\right)\right\rceil + p + q,$$

we have

$$\min_{\substack{\text{polynomials } P \\ \deg P = k \\ P(0)=1}}\left[\max_{\lambda\in\text{Spec}(\boldsymbol{A})}|P(\lambda)|^2\right] \leq \max_{\lambda\in\text{Spec}(\boldsymbol{A})}|Q(\lambda)|^2 \leq \epsilon^2.$$

Hence, after at most k iterations, we have

$$\left\|\boldsymbol{z}^{(k)} - \boldsymbol{A}^{-1}\boldsymbol{y}\right\|_{\boldsymbol{A}} \leq \epsilon\left\|\boldsymbol{A}^{-1}\boldsymbol{y}\right\|_{\boldsymbol{A}}.$$

Note that this proves a slightly more general result than Lemma 2. Simply set $q = 8$ to obtain the content of Lemma 2.

D.3 Proof of Theorem 13

From Lemma 1, we have that with probability at least $1-(3|\Omega|T+2)e^{-\frac{2N}{3|\Omega|T}}$, the bounds

$$\lambda_1(\boldsymbol{G}+\delta\mathbf{I}) = \lambda_1(\boldsymbol{G}) + \delta \leq C_1\frac{N}{T} + \delta =: b,$$

$$\lambda_{K_1}(\boldsymbol{G}+\delta\mathbf{I}) = \lambda_{K_1}(\boldsymbol{G}) + \delta \geq C_2\frac{N}{T} + \delta =: a,$$

$$\lambda_{K_2+1}(\boldsymbol{G}+\delta\mathbf{I}) = \lambda_{K_2+1}(\boldsymbol{G}) + \delta \leq \delta + 2\delta\epsilon^{1/8},$$

all hold. Therefore,

$$\mathrm{Spec}(\boldsymbol{G}+\delta\mathbf{I}) \subseteq [\delta, \delta+2\delta\epsilon^{1/8}] \bigcup \{\lambda_k(\boldsymbol{G}+\delta\mathbf{I})\}_{k=K_1+1}^{K_2} \bigcup [a,b].$$

Then, by applying Lemma 2, with $a = C_2\frac{N}{T} + \delta$, $b = C_1\frac{N}{T} + \delta$, $p = K_2 - K_1 \leq C_0 L \log\left(\frac{\pi}{2}|\Omega|T\right)\log\left(\frac{N^2|\Omega|^2}{\delta^2\epsilon^{1/4}}\right)$, and $\{c_i\}_{i=1}^{p} = \{\lambda_k(\boldsymbol{G}+\delta\mathbf{I})\}_{k=K_1+1}^{K_2}$, we have that CGD will need at most

$$k \leq \left\lceil \frac{1}{2}\sqrt{\frac{b}{a}}\left((p+8)\log\frac{b}{\delta} + \log\frac{2}{\epsilon}\right)\right\rceil + p + 8 = L \cdot \mathrm{polylog}\left(|\Omega|T, \frac{N}{|\Omega|T}, \frac{1}{\delta}, \frac{1}{\epsilon}\right)$$

iterations to return a vector $\boldsymbol{z}^{(k)}$ such that

$$\left\|\boldsymbol{z}^{(k)} - (\boldsymbol{G}+\delta\mathbf{I})^{-1}\boldsymbol{y}\right\|_{\boldsymbol{G}+\delta\mathbf{I}} \leq \epsilon\|(\boldsymbol{G}+\delta\mathbf{I})^{-1}\boldsymbol{y}\|_{\boldsymbol{G}+\delta\mathbf{I}},$$

as desired.

APPENDIX E

MISCELLANEOUS RESULTS

E.1 Zolotarev numbers

In this section, we review some properties of Zolotarev numbers, which will be useful in our analysis in Section E.2. With the exception of Corollary 6, all the results here have been proven elsewhere. However, we state these results and outline the proofs for sake of completeness.

For any integer $k \geq 0$, we let $\mathcal{R}_{k,k}$ denote the set of rational functions $\varphi(z) = \frac{p(z)}{q(z)}$ such that $p(z)$ and $q(z)$ are polynomials with degree at most k. For any two disjoint, closed subsets of the Riemann sphere $E, F \subset \mathbb{C} \cup \{\infty\}$, the Zolotarev number $Z_k(E, F)$ is defined as

$$Z_k(E, F) = \inf_{\varphi \in \mathcal{R}_{k,k}} \frac{\sup_{z \in E} |\varphi(z)|}{\inf_{z \in F} |\varphi(z)|}.$$

Note that any rational function $\varphi(z) = \frac{p(z)}{q(z)}$ can be extended to a continuous function on the Riemann sphere $\mathbb{C} \cup \{\infty\}$ by defining $\varphi(\infty) = \lim_{|z| \to \infty} \varphi(z)$ and $\varphi(z) = \infty$ for any z such that $q(z) = 0$.

Beckermann and Townsend [114] proved the following bound on the Zolotarev numbers for the intervals $E = [-b, -a]$ and $F = [a, b]$.

Theorem 17. *[114] For any reals $b > a > 0$, and any integer $k \geq 0$,*

$$Z_k([-b, -a], [a, b]) \leq 4 \exp\left[-\frac{\pi^2 k}{\log(\frac{4b}{a})}\right].$$

The proof of Theorem 17 involves using theory of elliptic functions to construct a rational function $\varphi \in \mathcal{R}_{k,k}$ for which $\frac{\sup_{z \in [-b,-a]} |\varphi(z)|}{\inf_{z \in [a,b]} |\varphi(z)|} \leq 4 \exp\left[-\frac{\pi^2 k}{\log(\frac{4b}{a})}\right]$.

A fact about Zolotarev numbers is that they are invariant under invertible Möbius transforms [122].

Lemma 18. *[122] For any two disjoint, closed subsets of the Riemann sphere* $E, F \subset \mathbb{C} \cup \{\infty\}$ *and any Möbius transform* $\phi(z) = \dfrac{\beta_1 z + \beta_2}{\beta_3 z + \beta_4}$ *such that* $\beta_1\beta_4 \neq \beta_2\beta_3$*, we have* $Z_k(\phi(E), \phi(F)) = Z_k(E, F)$ *for all integers* $k \geq 0$*.*

This fact is easily proved by noting that $\varphi^* \in \mathcal{R}_{k,k}$ is the extremal rational function for $(\phi(E), \phi(F))$ if and only if $\varphi^* \circ \phi \in \mathcal{R}_{k,k}$ is the extremal rational function for (E, F).

Using this fact, Beckermann and Townsend proved the following bound on the Zolotarev numbers for two non-overlapping intervals.

Corollary 5. *[114] For any two intervals* $[c_1, c_2]$ *and* $[d_1, d_2]$ *that are nonoverlapping, and any integer* $k \geq 0$*,*

$$Z_k([c_1, c_2], [d_1, d_2]) \leq 4\exp\left[-\frac{\pi^2 k}{\log(16\gamma)}\right] \quad \textit{where} \quad \gamma = \frac{(d_1 - c_1)(d_2 - c_2)}{(d_2 - c_1)(d_1 - c_2)}.$$

Proof. It is trivial to check that $\gamma > 1$ when $[c_1, c_2]$ and $[d_1, d_2]$ do not overlap. Now, set $\alpha = 2\gamma - 1 + 2\sqrt{\gamma^2 - \gamma}$ and define the Möbius transforms

$$\phi_1(z) = \frac{(d_2 - d_1)(z - c_2)}{(d_2 - c_2)(z - d_1)} \quad \text{and} \quad \phi_2(z) = \frac{(\alpha - 1)(z + 1)}{(\alpha + 1)(z - 1)}.$$

One can check that $\phi_1([c_1, c_2]) = [0, \frac{\gamma-1}{\gamma}] = [0, \frac{(\alpha-1)^2}{(\alpha+1)^2}] = \phi_2([-\alpha, -1])$ and $\phi_1([d_1, d_2]) = [1, \infty] = \phi_2([1, \alpha])$, and that both ϕ_1 and ϕ_2 are bijections. Thus, the Möbius transform $\phi = \phi_2^{-1} \circ \phi_1$ satisfies $\phi([c_1, c_2]) = [-\alpha, -1]$ and $\phi([d_1, d_2]) = [1, \alpha]$. So by applying Theorem 17, Lemma 18, and the bound $\alpha = 2\gamma - 1 + 2\sqrt{\gamma^2 - \gamma} \leq 4\gamma$, we have

$$Z_k([c_1, c_2], [d_1, d_2]) = Z_k([-\alpha, -1], [1, \alpha]) \leq 4\exp\left[-\frac{\pi^2 k}{\log(4\alpha)}\right] \leq 4\exp\left[-\frac{\pi^2 k}{\log(16\gamma)}\right].$$

□

In a nearly identical manner, we can also prove the following bound.

Corollary 6. *For any real numbers $c_1 < d_1 < d_2 < c_2$, and any integer $k \geq 0$,*

$$Z_k([-\infty, c_1] \cup [c_2, \infty], [d_1, d_2]) \leq 4 \exp\left[-\frac{\pi^2 k}{\log(16\gamma)}\right] \quad \textit{where} \quad \gamma = \frac{(c_2 - d_1)(d_2 - c_1)}{(c_2 - d_2)(d_1 - c_1)}.$$

Proof. Again, since $c_1 < d_1 < d_2 < c_2$, we have $\gamma > 1$. Now, set $\alpha = 2\gamma - 1 + 2\sqrt{\gamma^2 - \gamma}$ and define the Möbius transforms

$$\phi_1(z) = \frac{(d_2 - d_1)(z - c_1)}{(d_2 - c_1)(z - d_1)} \quad \text{and} \quad \phi_2(z) = \frac{(\alpha - 1)(z + 1)}{(\alpha + 1)(z - 1)}.$$

One can check that $\phi_1([-\infty, c_1] \cup [c_2, \infty]) = [0, \frac{\gamma-1}{\gamma}] = [0, \frac{(\alpha-1)^2}{(\alpha+1)^2}] = \phi_2([-\alpha, -1])$ and $\phi_1([d_1, d_2]) = [1, \infty] = \phi_2([1, \alpha])$, and that both ϕ_1 and ϕ_2 are bijections. Thus, the Möbius transform $\phi = \phi_2^{-1} \circ \phi_1$ satisfies $\phi([-\infty, c_1] \cup [c_2, \infty]) = [-\alpha, -1]$ and $\phi([d_1, d_2]) = [1, \alpha]$. So by applying Theorem 17, Lemma 18, and the bound $\alpha = 2\gamma - 1 + 2\sqrt{\gamma^2 - \gamma} \leq 4\gamma$, we have

$$\begin{aligned} Z_k([-\infty, c_1] \cup [c_2, \infty], [d_1, d_2]) &= Z_k([-\alpha, -1], [1, \alpha]) \\ &\leq 4 \exp\left[-\frac{\pi^2 k}{\log(4\alpha)}\right] \\ &\leq 4 \exp\left[-\frac{\pi^2 k}{\log(16\gamma)}\right]. \end{aligned}$$

□

E.2 Singular values of matrices with low rank displacement

With the exception of Theorem 14, the results in this section have all been proven elsewhere. Furthermore, the proof of Theorem 14 is very similar to that of Theorem 19. However, we state these results and the proof of Theorem 14 for sake of completeness.

Throughout this section, we suppose that $\boldsymbol{X} \in \mathbb{C}^{M \times N}$ satisfies the displacement equa-

tion

$$\boldsymbol{C}\boldsymbol{X} - \boldsymbol{X}\boldsymbol{D} = \boldsymbol{U}\boldsymbol{V}^*,$$

where $\boldsymbol{C} \in \mathbb{C}^{M\times M}$ and $\boldsymbol{D} \in \mathbb{C}^{N\times N}$ are normal matrices, and $\boldsymbol{U} \in \mathbb{C}^{M\times \nu}$ and $\boldsymbol{V} \in \mathbb{C}^{N\times \nu}$ (where it is understood that $\nu \ll \min\{M, N\}$ for the results in this section to be useful). Our goal is to show that $\boldsymbol{X}$ is approximately low-rank under certain assumptions on $\mathrm{Spec}(\boldsymbol{C})$ and $\mathrm{Spec}(\boldsymbol{D})$.

Beckermann and Townsend [114] showed that the numerical rank of $\boldsymbol{X}$ can be bounded in terms of Zolotarev numbers.

Theorem 18. *[114] If* $\mathrm{Spec}(\boldsymbol{C}) \subset E$ *and* $\mathrm{Spec}(\boldsymbol{D}) \subset F$*, then the singular values of* $\boldsymbol{X}$ *satisfy*

$$\sigma_{\nu k+j}(\boldsymbol{X}) \leq \sigma_j(\boldsymbol{X}) Z_k(E, F)$$

for any integers $j \geq 1$*,* $k \geq 0$*.*

The proof involves showing that for any rational function $\varphi \in \mathcal{R}_{k,k}$, we can construct a rank-$(\nu k + j - 1)$ matrix $\boldsymbol{Y}$ such that

$$\boldsymbol{X} - \boldsymbol{Y} = \varphi(\boldsymbol{C})(\boldsymbol{X} - \boldsymbol{X}_{j-1})\varphi(\boldsymbol{D})^{-1}$$

where $\boldsymbol{X}_{j-1}$ is the best rank-$(j-1)$ approximation to $\boldsymbol{X}$. Then, by applying the facts that

$$\|\varphi(\boldsymbol{C})\| \leq \sup_{z\in E} |\varphi(z)|,$$

$$\|\varphi(\boldsymbol{D})^{-1}\| \leq \sup_{z\in F} |\varphi(z)^{-1}| = \left(\inf_{z\in F} |\varphi(z)|\right)^{-1},$$

$$\|\boldsymbol{X} - \boldsymbol{X}_{j-1}\| = \sigma_j(\boldsymbol{X}),$$

along with the submultiplicativity of the matrix norm, we obtain

$$\sigma_{\nu k+j}(\boldsymbol{X}) \leq \|\boldsymbol{X}-\boldsymbol{Y}\| \leq \|\varphi(\boldsymbol{C})\| \cdot \|\boldsymbol{X}-\boldsymbol{X}_{j-1}\| \cdot \|\varphi(\boldsymbol{D})^{-1}\| \leq \sigma_j(\boldsymbol{X}) \cdot \frac{\sup\limits_{z\in E}|\varphi(z)|}{\inf\limits_{z\in F}|\varphi(z)|}.$$

This bound holds for any $\varphi \in \mathcal{R}_{k,k}$. Taking the infimum over all $\varphi \in \mathcal{R}_{k,k}$ yields $\sigma_{\nu k+j}(\boldsymbol{X}) \leq \sigma_j(\boldsymbol{X}) Z_k(E,F)$.

By combining Theorem 18 (with $j = 1$) along with Corollary 5, Beckermann and Townsend established the following result.

Theorem 19. *[114] If Spec$(\boldsymbol{C}) \subset [c_1,c_2]$ and Spec$(\boldsymbol{D}) \subset [d_1,d_2]$ where $[c_1,c_2]$ and $[d_1,d_2]$ are nonoverlapping, then for any integer $k \geq 0$,*

$$\sigma_{\nu k+1}(\boldsymbol{X}) \leq 4\|\boldsymbol{X}\| \exp\left[-\frac{\pi^2 k}{\log(16\gamma)}\right] \quad \textit{where} \quad \gamma = \frac{(d_1-c_1)(d_2-c_2)}{(d_2-c_1)(d_1-c_2)}.$$

In an identical manner, we can combine Theorem 18 (with $j = 1$) along with Corollary 6 to establish Theorem 14 (stated in Section A.1.3).

E.3 Polynomial approximations of the sinc function

For a bandwidth parameter $W > 0$, we define the sinc function

$$g(t) = \frac{\sin(2\pi W t)}{\pi t} \quad \text{for} \quad t \in \mathbb{R}.$$

First, we prove the following bound on the derivatives of $g(t)$.

Lemma 19. *For any non-negative integer k,*

$$\left|g^{(k)}(t)\right| \leq (2\pi W)^k \min\left\{\frac{2W}{k+1}, \frac{2}{\pi|t|}\right\} \quad \textit{for all} \quad t \in \mathbb{R}.$$

Proof. For $k = 0$, we can apply the inequality $|\sin\theta| \leq \min\{|\theta|, 2\}$ to obtain $|g(t)| \leq \min\{2W, \frac{2}{\pi|t|}\}$. Hence, we can proceed with the case where $k \geq 1$. Note that we can write

the sinc function as

$$g(t) = \frac{\sin(2\pi W t)}{\pi t} = \int_{-W}^{W} e^{j2\pi f t}\, df.$$

By differentiating under the integral sign k times, we obtain

$$g^{(k)}(t) = \frac{d^k}{dt^k}\left[\int_{-W}^{W} e^{j2\pi f t}\, df\right] = \int_{-W}^{W} \frac{d^k}{dt^k}\left[e^{j2\pi f t}\right]\, df = \int_{-W}^{W} (j2\pi f)^k e^{j2\pi f t}\, df.$$

Applying the triangle inequality yields the bound

$$\begin{aligned}
\left|g^{(k)}(t)\right| &= \left|\int_{-W}^{W} (j2\pi f)^k e^{j2\pi f t}\, df\right| \\
&\leq \int_{-W}^{W} \left|(j2\pi f)^k e^{j2\pi f t}\right|\, df \\
&= \int_{-W}^{W} (2\pi|f|)^k\, df \\
&= \frac{(2\pi W)^{k+1}}{\pi(k+1)}.
\end{aligned}$$

Alternatively, using integration by parts before applying the triangle inequality yields

$$\begin{aligned}
\left|g^{(k)}(t)\right| &= \left|\int_{-W}^{W} (j2\pi f)^k e^{j2\pi f t}\, df\right| \\
&= \left|\left[(j2\pi f)^k \frac{e^{j2\pi f t}}{j2\pi t}\right]_{f=-W}^{f=W} - \int_{-W}^{W} j2\pi k (j2\pi f)^{k-1} \frac{e^{j2\pi f t}}{j2\pi t}\, df\right| \\
&= \left|\frac{(j2\pi W)^k e^{j2\pi W t}}{j2\pi t} - \frac{(-j2\pi W)^k e^{-j2\pi W t}}{j2\pi t} - \int_{-W}^{W} j2\pi k (j2\pi f)^{k-1} \frac{e^{j2\pi f t}}{j2\pi t}\, df\right| \\
&\leq \left|\frac{(j2\pi W)^k e^{j2\pi W t}}{j2\pi t}\right| + \left|\frac{(-j2\pi W)^k e^{-j2\pi W t}}{j2\pi t}\right| + \left|\int_{-W}^{W} j2\pi k (j2\pi f)^{k-1} \frac{e^{j2\pi f t}}{j2\pi t}\, df\right| \\
&\leq \left|\frac{(j2\pi W)^k e^{j2\pi W t}}{j2\pi t}\right| + \left|\frac{(-j2\pi W)^k e^{-j2\pi W t}}{j2\pi t}\right| + \int_{-W}^{W} \left|j2\pi k (j2\pi f)^{k-1} \frac{e^{j2\pi f t}}{j2\pi t}\right| df \\
&= \frac{(2\pi W)^k}{2\pi|t|} + \frac{(2\pi W)^k}{2\pi|t|} + \int_{-W}^{W} \frac{k}{|t|}(2\pi|f|)^{k-1}\, df \\
&= \frac{(2\pi W)^k}{\pi|t|} + \frac{(2\pi W)^k}{\pi|t|} \\
&= \frac{2(2\pi W)^k}{\pi|t|}.
\end{aligned}$$

Combining the two bounds yields

$$\left|g^{(k)}(t)\right| \leq \min\left\{\frac{(2\pi W)^{k+1}}{\pi(k+1)}, \frac{2(2\pi W)^k}{\pi|t|}\right\} = (2\pi W)^k \min\left\{\frac{2W}{k+1}, \frac{2}{\pi|t|}\right\}.$$

□

We finish this section by noting a well-known theorem on Chebyshev interpolation.

Theorem 20. *[123] Suppose $g \in C^k[a,b]$ for some positive integer k. Define the Chebyshev interpolating polynomial of degree $k-1$ by*

$$P_k(t) = \sum_{m=1}^{k} g(t_m) \prod_{\substack{m'=1,\ldots,k \\ m' \neq m}} \frac{t - t_{m'}}{t_m - t_{m'}}$$

where

$$t_m = \frac{b+a}{2} + \frac{b-a}{2}\cos\left(\frac{2m-1}{2k}\pi\right) \quad \textit{for} \quad m = 1, \ldots, k$$

are the Chebyshev nodes used for interpolation. Then, for any $t \in [a,b]$, we have

$$|g(t) - P_k(t)| \leq \frac{(b-a)^k}{2^{2k-1}k!} \max_{\xi \in [a,b]} \left|g^{(k)}(\xi)\right|.$$

We will use both Lemma 19 and Theorem 20 in Section A.1.4 to prove Theorem 2.

E.4 Low rank approximation to solutions of Lyapunov equations

Iterative methods for efficiently computing a low-rank approximation to the solution of a Lyapunov system have been well-studied [124, 125]. Here we prove a lemma which shows how to construct a factored low-rank approximation to the solution of a Lyapunov equation where the right side is low-rank.

Lemma 20. *Let $\boldsymbol{A} \in \mathbb{R}^{N \times N}$ be a symmetric positive definite matrix with condition number κ, let $\boldsymbol{U} \in \mathbb{R}^{N \times M}$ with $M \leq N$, and let $\boldsymbol{X} \in \mathbb{R}^{N \times N}$ be the positive definite solution to the*

Lyapunov equation

$$\boldsymbol{A}\boldsymbol{X} + \boldsymbol{X}\boldsymbol{A}^* = \boldsymbol{U}\boldsymbol{U}^*.$$

Then for any $\delta \in (0, 1]$, there exists an $N \times rM$ matrix $\boldsymbol{Z}$ with

$$r = \left\lceil \frac{1}{\pi^2} \log(4\kappa) \log\left(\frac{4}{\delta}\right) \right\rceil, \tag{E.1}$$

such that

$$\|\boldsymbol{X} - \boldsymbol{Z}\boldsymbol{Z}^*\| \leq \delta \|\boldsymbol{X}\|. \tag{E.2}$$

Proof. The CF-ADI algorithm presented in [126] constructs a factor $\boldsymbol{Z} \in \mathbb{R}^{N \times rM}$ by concatenating a series of r $N \times M$ matrices, $\boldsymbol{Z} = \begin{bmatrix} \boldsymbol{Z}_1 & \boldsymbol{Z}_2 & \cdots & \boldsymbol{Z}_r \end{bmatrix}$, where

$$\begin{aligned}
\boldsymbol{Z}_1 &= \sqrt{2p_1}(\boldsymbol{A} + p_1\mathbf{I})^{-1}\boldsymbol{U} \\
\boldsymbol{Z}_k &= \sqrt{\frac{p_k}{p_{k-1}}} \left(\mathbf{I} - (p_k + p_{k-1})(\boldsymbol{A} + p_k\mathbf{I})^{-1}\right) \boldsymbol{Z}_{k-1}, \quad k = 2, \ldots, r,
\end{aligned}$$

for some choice of positive real numbers $p_1, \ldots, p_r$. They show that the matrix $\boldsymbol{Z}\boldsymbol{Z}^*$ produced by this iteration is equivalent to the matrix produced by the ADI iteration given in [124], and thus, $\boldsymbol{Z}\boldsymbol{Z}^*$ satisfies

$$\boldsymbol{X} - \boldsymbol{Z}\boldsymbol{Z}^* = \phi(\boldsymbol{A})\boldsymbol{X}\phi(\boldsymbol{A})^* \text{ where } \phi(x) = \prod_{j=1}^{r} \frac{x - p_j}{x + p_j}.$$

(This is shown in [124] by using induction on r.) Therefore, the error $\|\boldsymbol{X} - \boldsymbol{Z}\boldsymbol{Z}^*\|$ satisfies

$$\|\boldsymbol{X} - \boldsymbol{Z}\boldsymbol{Z}^*\| \leq \|\boldsymbol{X}\| \cdot \|\phi(\boldsymbol{A})\|^2 = \|\boldsymbol{X}\| \cdot \max_{x \in \text{Spec}(\boldsymbol{A})} |\phi(x)|^2 \leq \|\boldsymbol{X}\| \cdot \max_{x \in [a,b]} |\phi(x)|^2,$$

where $a = \lambda_{\min}(\boldsymbol{A})$ and $b = \lambda_{\max}(\boldsymbol{A})$ (so $\kappa = \frac{b}{a}$). In [125], it is shown that for a given interval $[a, b]$ and a number of ADI iterations r, there exists a choice of parameters $p_1, \ldots, p_r$

such that $\max_{x\in[a,b]} |\phi(x)|^2 = \alpha$, where α satisfies

$$\frac{I(\sqrt{1-\alpha^2})}{I(\alpha)} = \frac{4rI(\kappa^{-1})}{I(\sqrt{1-\kappa^{-2}})},$$

where $I(\tau)$ is the complete elliptic integral of the first kind, defined by

$$I(\tau) := \int_0^{\pi/2} (1-\tau^2\sin^2\theta)^{-1/2}\, d\theta.$$

It is shown in [127] that the elliptic nome, defined as

$$q(\tau) := \exp\left[-\pi\frac{I(\sqrt{1-\tau^2})}{I(\tau)}\right]$$

satisfies

$$\tau^2 = 16q(\tau)\prod_{n=1}^{\infty}\left(\frac{1+q(\tau)^{2n}}{1+q(\tau)^{2n-1}}\right)^8.$$

For $0 \le \tau \le 1$, the range of the elliptic nome is $0 \le q(\tau) \le 1$. Hence, the above equation gives us the inequality $\tau^2 \le 16q(\tau)$. By using the definition of the elliptic nome, this inequality becomes

$$\frac{I(\sqrt{1-\tau^2})}{I(\tau)} \le \frac{2}{\pi}\log\frac{4}{\tau} \text{ for } 0 \le \tau \le 1.$$

So, by setting the number of iterations as $r = \left\lceil \frac{1}{\pi^2}\log(4\kappa)\log\left(\frac{4}{\delta}\right)\right\rceil$, we have

$$\frac{2}{\pi}\log\frac{4}{\alpha} \ge \frac{I(\sqrt{1-\alpha^2})}{I(\alpha)} = \frac{4rI(\kappa^{-1})}{I(\sqrt{1-\kappa^{-2}})} \ge \frac{4\cdot\frac{1}{\pi^2}\log(4\kappa)\log(\frac{4}{\delta})}{\frac{2}{\pi}\log(4\kappa)} = \frac{2}{\pi}\log\frac{4}{\delta}.$$

Hence, $\max_{x\in[a,b]} |\phi(x)|^2 = \alpha \le \delta$, and thus, $\|\boldsymbol{X} - \boldsymbol{Z}\boldsymbol{Z}^*\| \le \delta\|\boldsymbol{X}\|$, as desired. □

Note, it is shown in [124] that (E.1) is a good approximation for the number of iterations needed to get the relative error less than δ, provided that $\kappa \gg 1$. It is shown in [125] that (E.1) is a good approximation provided that $r \ge 3$. Here, we have shown that (E.1) is sufficient to guarantee a strict bound on the error.

The choice of parameters $p_1, \ldots, p_r$ which minimizes $\max_{x \in [a,b]} |\phi(x)|^2$ is given by the formula $p_k = b\text{dn}\left[\frac{2k-1}{2r} I(\sqrt{1-\kappa^{-2}}), \sqrt{1-\kappa^{-2}}\right]$, where dn$[z, \tau]$ is the Jacobi elliptic function. This function is defined as dn$[z, \tau] = \sqrt{1 - \tau^2 \sin^2 \varphi}$, where φ satisfies $\int_0^{\varphi} (1 - \tau^2 \sin^2 \theta)^{-1/2} \, d\theta = z$. If the Jacobi elliptic function dn is not available, a suboptimal choice of parameters $p_1, \ldots, p_r$ is given by $p_k = a^{\frac{2k-1}{2r}} b^{\frac{2r-2k+1}{2r}}$, i.e., we can pick the parameters to be evenly spaced on a log scale.

If the matrix $\boldsymbol{A}$ is diagonal, each iteration of the CF-ADI algorithm above will take $O(N)$ operations. Hence, the matrix $\boldsymbol{Z}$ can be computed in $O(rN)$ operations.